UNIVERSITY OF CALIFORNIA

Santa Barbara

Influence of Phytoplankton and Extracellular Polymeric Substances on the Fate of

Engineered Nanomaterials in Natural Aquatic Systems

A dissertation submitted in partial satisfaction of the

requirements for the degree Doctor of Philosophy

in Environmental Science & Management

by

Adeyemi S. Adeleye

Committee in charge:

Professor Arturo A. Keller, Chair

Professor Patricia A. Holden

Professor Hunter S. Lenihan

June 2015

The dissertation of Adeyemi S. Adeleye is approved.

_____

Patricia A. Holden

_____

Hunter S. Lenihan

_____

Arturo A. Keller, Committee Chair

June 2015

Influence of Phytoplankton and Extracellular Polymeric Substances on the Fate of

Engineered Nanomaterials in Natural Aquatic Systems

To my dear wife, Olusola.

ACKNOWLEDGEMENTS

VITA OF ADEYEMI S. ADELEYE

June 2015

Bren School of Environmental Science & Management   Email: adeyemiadeleye@umail.ucsb.edu
2324 Bren Hall, University of California, Santa Barbara   Website: www.aadeleye.com
Santa Barbara, CA 93106-5131   Phone: (805) 893-5352

EDUCATION

PhD   University of California, Santa Barbara   2015
           Bren School of Environmental Science & Management
           Dissertation: The role of phytoplankton and extracellular polymeric substances on
           the fate of engineered nanomaterials in natural aquatic systems

MESM   University of California, Santa Barbara   2011
           Bren School of Environmental Science & Management
           Thesis: CERNS: A Condensed EH&S Reference for Nanotechnology Startups

BSc   Obafemi Awolowo University, Ile-Ife, Nigeria   2006
           Department of Microbiology
           Major: Microbiology (First Class Honors)

PUBLICATIONS

- Su, Y.; **Adeleye, A. S**.; Keller, A. A.; Huang, Y.; Dai, C.; Zhou, X.; Zhang, Y. (2015). Magnetic sulfide-modified nanoscale zerovalent iron (S-nZVI) for dissolved metal ion removal. *Water Research*, 74:47 – 57

- Aceves Bueno, E.; **Adeleye, A. S**.; Bradley, D.; Brandt, W.; Callery, P.; Feraud, M.; Garner, K.; et al. (2015). Citizen science as an approach for overcoming insufficient monitoring and inadequate stakeholder buy-in in adaptive management: Criteria and evidence. *Ecosystems*, 18(3):493 – 506

- Conway, J. R.; **Adeleye, A. S.**; Gardea-Torresday, J.; Keller, A. A. (2015). Aggregation, dissolution and transformation of copper nanoparticles in natural waters. *Environmental Science & Technology*, 49(5):2749 – 2756

- **Adeleye, A. S.**; Conway, J. R.; Perez, T.; Rutten, P.; Keller A. A. (2014). Influence of extracellular polymeric substances on the long-term fate, dissolution and speciation of copper-based nanoparticles. *Environmental Science & Technology*, 48(21):12561 – 12568

- Hong, J.; Rico, C.; Zhao, L.; **Adeleye, A. S.**; Keller, A. A.; Peralta-Videa, J.; Gardea-Torresday, J. (2015). Toxicity effects of seven Cu nanoparticles/compounds to lettuce (*Lactuca sativa*) and alfalfa (*Medicago sativa*). *Environmental Science: Processes & Impacts*, 17(1):177 – 185

- **Adeleye, A. S**.; Keller, A.A. (2014). Long-term colloidal stability and metal leaching of single wall carbon nanotubes: Effect of temperature and extracellular polymeric substances. *Water Research*, 49:236–250

- Priester, J.; Van De Werfhorst, L.; Ge, Y.; **Adeleye, A. S**.; Tomar, S.; Tom, L; M. Piceno, Y.; Andersen, G.; Holden, P. (2014). Effects of TiO2 and Ag nanoparticles on polyhydroxybutyrate biosynthesis by activated sludge bacteria. *Environmental Science & Technology*, 48(24):14712 – 14720

- Su, Y.; **Adeleye, A. S**.; Huang, Y.; Sun, X.; Dai, C.; Zhou, X.; Zhang, Y.; Keller, A. A.. (2014). Simultaneous removal of cadmium and nitrate in aqueous media by nanoscale zerovalent iron (nZVI) and Au doped nZVI particles. *Water Research*, 63:102 – 111

- Su, Y.; **Adeleye, A. S**.; Zhou, X.; Dai, C.; Zhang, W.; Keller, A. A.; Zhang, Y. (2014). Effect of nitrate on the treatment of lead contaminated groundwater nanoscale zerovalent iron. *Journal of Hazardous Materials,* 280:504 – 513

- **Adeleye, A. S.**; Keller A. A.; Miller, R. J.; Lenihan, H. S. (2013). Persistence of commercial nanoscaled zero-valent iron (nZVI) and by-products. *Journal of Nanoparticle Research*, 15:1418

- Bennett, S.; **Adeleye, A. S.**; Ji, Z.; Keller, A. A. (2013). Stability, metal leaching, photoactivity and toxicity in freshwater systems of commercial single wall carbon nanotubes. *Water Research*, 47(12):4074 – 4085

- Wang, H.; **Adeleye, A. A.**; Huang, Y.; Li, F; Keller, A. A. Heteroaggregation of nanoparticles with biocolloids and geocolloids. In review at *Advances in Colloid and Interface Science*

- **Adeleye, A. S.**; Conway, J. R.; Garner, K.; Huang, Y.; Su, Y.; Keller, A. A. Use of engineered nanomaterials for water treatment and remediation: A review of costs, benefits, and applicability. In Review at *Chemical Engineering Journal*

- Torres-Duarte, C.; **Adeleye, A. S.**; Pokhrel, S.; Mädler, L.; Keller, A. A.; Cherr, G. N. Developmental Effects of Two Different Copper Oxide Nanomaterials in Sea Urchin (*Lytechinus pictus*). In Review at *Nanotoxicology*

RESEARCH EXPERIENCE

Graduate Student Researcher   2011 – 2015
Prof. Keller's Lab, University of California's Center for Environmental Implications of Nanotechnology
- Carry out research to meet the goals of the Center and publish findings in peered-reviewed journals
- Provide mentorship for undergraduate and master's student researchers

Research Intern   2010
University of California's Center for Environmental Implications of Nanotechnology
- Synthesized guidance recommendation documents for Environmental Health & Safety (EH&S) of engineered nanomaterials published by academic and government institutions

- Worked with other interns to create a draft of comprehensive matrix of nanomaterial EH&S guidance recommendations for Center for Environmental Implications of Nanotechnology

Laboratory Assistant   2009 – 2010
Prof. Holden's Lab, Bren School, University of California, Santa Barbara
- Literature review on production of polyhydroxyalkanoates (PHA) by activated sludge microbes
- Planned and staged experiments on determining PHA production by *Azotobacter vinelandii* UWD
- Developed staining procedures, and quantification of PHA

TEACHING EXPERIENCE

Invited Lecturer, University of California, Santa Barbara
- Fate & Transport of Pollutants in the Environment (Master's Level)   2015
  - Taught a lecture on "Equilibrium Distribution of Pollutants in the Environment"

Teaching Assistant, University of California, Santa Barbara
- Fate & Transport of Pollutants in the Environment (Master's Level)   2014
  - Lectured when professor was out of town

- Laboratory in Management of Soil and Groundwater Quality (Master's Level)   2013

- Fate & Transport of Pollutants in the Environment (Master's Level)   2012

- Earth System Science (Master's Level)   2012

Tutor, University of California, Santa Barbara
- Fate & Transport of Pollutants in the Environment (Master's Level)   2011

SELECTED CONFERENCES & PRESENTATIONS

- *Invited speaker, 2015 Environmental Nanotechnology Gordon Research Seminar (GRS), West Dover, Vermont, June 2015: "Influence of phytoplankton on fate and effects of iron nanoparticles."

- *Accepted presenter, 2015 Environmental Nanotechnology Gordon Research Conference (GRC), West Dover, Vermont, June 2015: "Long term release of nanoparticulate copper from an antifouling paint."

- Presenter, Society of Environmental Toxicology and Chemistry (SETAC) Europe 25th Annual Meeting, Barcelona, Spain, May 2015: "Effect of freshwater algal growth stage on physicochemical properties, transformations, and toxicity of iron nanoparticles."

- Presenter, 249th American Chemical Society (ACS) National Meeting, Denver, Colorado, March 2015: "Effect of extracellular polymeric substances on the fate and transformation of engineered nanomaterials."

- Presenter, Society of Environmental Toxicology and Chemistry (SETAC) North America 35th Annual Meeting, Vancouver, Canada, November 2014: "Release of nanosized copper particles from an antifouling paint."

- Presenter, 248th ACS National Meeting, San Francisco, California, August 2014: "Long-term dissolution of copper-based nanoparticles in aqueous media: Effects of extracellular polymeric substances, pH, and ionic strength."

- Presenter, American Geophysical Union (AGU) Fall Meeting, San Francisco, California, December 2013: "Influence of extracellular polymeric substances on CuO nanoparticle dissolution and colloidal stability."

- Presenter, 2nd Sustainable Nanotechnology Organization (SNO) Conference, Santa Barbara, California, November 2013: "Extracellular polymeric substances stabilize carbon nanotubes in aqueous phase."

- Presenter, 244th ACS National Meeting, San Diego, California, August 2012: "Persistence of commercial nanoscale zero-valent iron (nZVI) and its by-products."

- Presenter, 1st SNO Conference, Arlington, Virginia, November 2012: "Long-term colloidal stability and metal leachate of carbon nanotubes in natural waters"

- Presenter, International Conference on Environmental Implications of Nanotechnology, Durham, North Carolina, May 2011: "A condensed EH&S reference for nanotechnology startups (CERNS)."

*Upcoming presentations

FELLOWSHIPS, AWARDS & HONORS

- ACS Division of Environmental Chemistry Graduate Student Award	2015
- Dean's Fellowship, University of California, Santa Barbara	2014
- Sustainable Nanotechnology Organization Student Award	2013
- American Geophysical Union Student Travel Grant	2013
- UC Santa Barbara Earth Research Institute Travel Award	2013
- American Chemical Society Symposium Award	2012
- Michael J. Connell Memorial Fellowship	2012
- Sustainable Nanotechnology Organization Student Award	2012
- American Chemical Society Environmental Chemistry Division Certificate of Merit	2012
- Michael J. Connell Memorial Fellowship	2010
- Sustainable Energy Development Fellowship	2009
- Best Graduating Student in Department of Microbiology and Faculty of Science	2006

SERVICES/ACTIVITIES

- Lab supply manager, Prof. Arturo Keller's lab group, UCSB   2012 – Date
- Organizing committee member, Bren School's Faculty-PhD Informal Gathering   2013
- Graduate Student's representative, Sierra Madre Student Housing Building Committee   2012
- Resident coordinator, Apartment Complex & Living (AC&L), UCSB   2010 – 2011

INSTRUMENTATION SKILLS

Dynamic Light Scattering (DLS), Nanoparticle Tracking Analysis (NTA), Inductively Coupled Plasma-Atomic Emission Spectrometry (ICP-AES), Scanning Electron Microscopy (SEM), Transmission Electron Microscopy (TEM), X-ray Diffraction (XRD), Fourier Transform Infrared Spectroscopy (FTIR), UV-Vis Spectrophotometry, Thermogravimetric Analysis (TGA), Brunauer-Emmet-Teller (BET) Porosimetry

JOURNALS REFEREED

- Environmental Science & Technology
- Environmental Science: Nano
- Journal of Hazardous Materials
- Environmental Pollution
- ACS Sustainable Chemistry & Engineering
- Journal of Nanoparticle Research

PROFESSIONAL AFFILIATIONS

- American Chemical Society (ACS)
- American Geophysical Union (AGU)
- Society for Risk Analysis (SRA)
- Society of Environmental Toxicology and Chemistry (SETAC)
- Sustainable Nanotechnology Organization (SNO)

ABSTRACT

Influence of Phytoplankton and Extracellular Polymeric Substances on the Fate of

Engineered Nanomaterials in Natural Aquatic Systems

by

Adeyemi S. Adeleye

Although the risks of engineered nanomaterials (ENMs) to human and the environment are poorly understood, over 1800 consumer products currently on the market contain at least one ENM and the list continues to grow. The use of many of these consumer products will lead to direct release of ENMs into natural aquatic systems and several studies have demonstrated that ENMs can have adverse ecological effects. It is therefore important to understand the fate of ENMs in aquatic systems in order to predict and/or investigate their environmental implications. Microorganisms are abundant in natural waters into which they also release exudates such as soluble extracellular polymeric substance (sEPS). However, studies on how microorganisms and sEPS influence the fate and transformations of ENMs in natural waters are rare. In this doctoral research, sEPS were extracted from freshwater and marine phytoplankton (an important class of microorganisms) and their effects on the environmental fate of a variety of ENMs—including carbon nanotubes, copper and its oxides, iron, and titania nanomaterials—were studied. Interactions between algae, sEPS and ENMs were investigated via electron microscopy with energy dispersive X-ray spectroscopy, electrophoretic and dynamic light scattering, UV-Vis spectroscopy, X-ray diffraction, and

infra-red spectroscopy. Effects of sEPS were investigated by studying changes in physicochemical properties, aggregation and sedimentation kinetics, and transformation of ENMs. The major components of sEPS were polysaccharides and proteins; and the ratio of both components varied with species and age of organism, as well as the nutrient composition of growth media. sEPS contained charged functional groups, such as carboxyl, phosphoryl, carbonyl, hydroxyl, amide, etc. Evidences for direct interactions (physisorption and chemisorption) between algae/sEPS and ENMs, mediated by the various functional groups on proteins and nucleic acids or phospholipids were found. Adsorption of sEPS to ENMs changed the size and surface charge of the particles. In addition, the attachment efficiencies of ENMs decreased in the presence of sEPS due to electrosteric stabilization. Impacts of algae and sEPS were also found on ENMs' dissolution, transformation, and toxicity. This study demonstrated that the presence of phytoplankton and EPS in natural waters will have unique and important impact on the fate, transport, transformation, and effects of ENMs.

TABLE OF CONTENTS

Chapter 1. Introduction

1.1. Nanotechnology and the Environment

Nanotechnology is "the control and restructuring of matter at the nanoscale, at the atomic

and molecular levels in the size range of about 1 to 100 nm, in order to create materials,

devices, and systems with fundamentally new properties and functions due to their small

structure" (Roco *et al.* 2011). Nanotechnology has found applications in fields such as

energy, medicine, material science, information technology, agriculture, and environmental

science (Keller *et al.* 2013; Tsuzuki 2013). Over 1800 consumer products are currently

reported to be enabled with at least one engineered nanomaterial or ENM (PEN 2014).

ENM-enabled products currently on the market include clothing (e.g. socks embedded with

nano-silver), personal care products (e.g. sunscreens based on nano-TiO_2), computer

hardware (e.g. flash memory with nano-silicon), coatings (e.g. antifouling paint with nano-

ZnO as biocide), and thermoplastics (e.g. polycarbonate-carbon nanotube composites).

Revenue from ENM-enabled products exceeded $730 billion in 2012, and is projected to

top $4.4 trillion by 2018 (Lux-Research 2014). While there are clear economic and utility

benefits of enabling products with ENMs, the implications of nanotechnology, in terms of

risk to humans and the environment are poorly understood. Risk arises mainly from our

nascent understanding of the fate, transformation, bioavailability, and potential toxicity of

ENMs in the environment. As suggested by several studies (Nel *et al.* 2006; Klaine *et al.*

2008; Petosa *et al.* 2010; Reinhart *et al.* 2010; Adeleye *et al.* 2013; Keller *et al.* 2013;

Garner & Keller 2014; Richardson & Ternes 2014), engineered nanomaterials have the

potential to become the next important class of contaminants in all major environmental

phases at concentrations that are high enough to affect natural ecosystems (Holden *et al.* 2013; Keller *et al.* 2013; Corsi *et al.* 2014; Garner & Keller 2014; Holden *et al.* 2014; Keller & Lazareva 2014; Garner *et al.* 2015). This is especially true as production and use of engineered nanomaterials are predicted to continue to increase rapidly (Tsuzuki 2013; Lux-Research 2014).

Water bodies cover more than 70% of the total earth surface and are typically polluted to different degrees by human activities such as recreation, agriculture, etc. (Liddle & Scorgie 1980; Ongley 1996). Global release of ENMs into natural waters is currently estimated to exceed 69,000 tons/year (Keller & Lazareva 2014). ENMs may exhibit toxicity towards aquatic organisms (Miller *et al.* 2010; Wang *et al.* 2014), disrupt important ecological functions (Choi & Hu 2008; Zheng *et al.* 2011; Priester *et al.* 2014), and impact water quality (Reinsch *et al.* 2010; Wei *et al.* 2010; Adeleye *et al.* 2013). It is therefore important to understand the fate of commonly used ENMs in aquatic systems in order to predict their implications in natural waters. The fate of ENMs in aquatic systems is mainly determined by the physicochemical properties of both ENMs and media, and the various interactions that occur between particles and the biotic and abiotic factors in aqueous media (Keller *et al.* 2010; Adeleye *et al.* 2013; Adeleye *et al.* 2014; Adeleye & Keller 2014; Conway *et al.* 2015).

1.2. Influence of Physicochemical Properties on Fate of Nanomaterials

Once released into the aquatic environment, the fate of ENMs is largely affected by their colloidal stability (Chen *et al.* 2006; Wang *et al.* 2008; Badawy *et al.* 2010; Stankus *et al.* 2010). The colloidal stability of ENMs in aquatic systems can be predicted by their critical coagulation concentrations (CCC) in relevant electrolyte solutions (Chen *et al.* 2006; He *et al.* 2008; Badawy *et al.* 2010). In general, colloidal stability of ENMs is affected by their

properties such as particle size, surface charge, elemental composition, shape, morphology, presence and type of capping agent, and crystal structure (Elimelech & O'Melia 1990; He *et al.* 2008; Chen & Elimelech 2009; Badawy *et al.* 2010; Keller *et al.* 2010; Stankus *et al.* 2010; Zhou & Keller 2010; Adeleye *et al.* 2013; Zhou & Keller 2013; Adeleye & Keller 2014). These properties can vary considerably among the different ENMs (Figure 1) and may affect their stability in aqueous media to varying extent.
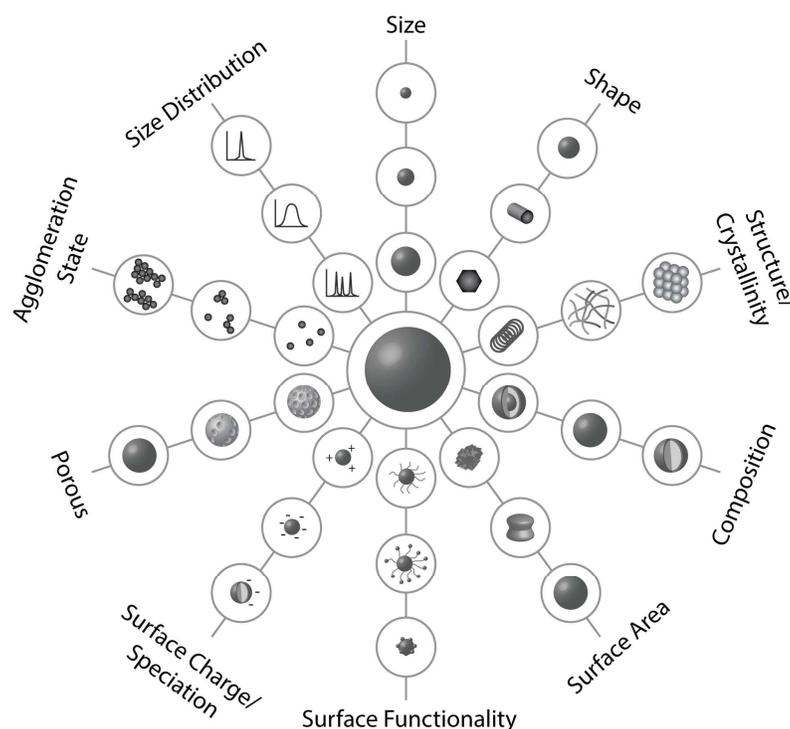
Figure 1. Major physicochemical properties of engineered nanomaterials that affect their colloidal stability in aqueous media

1.2.1. Size and Size Distribution

As particle size decreases, the fraction of surface atoms and specific surface area increase, which may have important effects on particle surface properties, and thus, stability (He *et al.* 2008). Smaller particles have relatively higher surface energy, and are thus more prone to aggregation in order to lower the free energy. The CCC of ENMs, thus, typically

increases with size (He *et al.* 2008; Liu *et al.* 2011; Zhou & Keller 2013). This agrees with Derjaguin-Landau-Verwey- Overbeek (DLVO) theory which predicts that interaction potential between particles decreases as particle size decreases (He *et al.* 2008). According to classical DLVO theory, the agglomeration and stability of particle dispersions are determined by the sum of the attractive (mainly van der Waals) and repulsive forces (mainly electrostatic repulsion) between individual particles (Grasso *et al.* 2002). These controlling forces are inherently dependent on particle size. External forces such as those due to gravitation and hydrodynamic effects are proportional to the cube or square of particle size (Israelachvili & McGuiggan 1988; Elimelech & O'Melia 1990; Elimelech *et al.* 1998a; Elimelech *et al.* 1998b; Grasso *et al.* 2002; Israelachvili 2011). In magnetic ENMs (e.g. nanoscale zerovalent iron or nZVI), the magnetic forces contribute to the net attractive force and are proportional to the sixth power of the particle size (Phenrat *et al.* 2007; Phenrat *et al.* 2008; Phenrat *et al.* 2010).

1.2.2. Surface Charge

Most surfaces (including ENMs and other colloids) in aqueous systems acquire a surface charge through surface dissociation, ion adsorption from solution, or crystal lattice defects (Hunter *et al.* 1987; Israelachvili & McGuiggan 1988; Brant *et al.* 2005; Israelachvili 2011). The net interaction energy between ENMs, or between ENMs and other surfaces in the aquatic system depends on the charges that exist between them (He *et al.* 2008; Jiang *et al.* 2009; Wang & Keller 2009; Zhou *et al.* 2012). ENMs are stable when they possess high surface charge (represented by their zeta potential values) in aqueous media since they can effectively repel each other (Hunter 2013). Zeta potential values more than ± 30 mV are generally considered representative of sufficient electrostatic repulsion to ensure the stability of a colloidal system (Everett 1988).

1.2.3. Capping Agent

Capping/coating agents modify the surface properties of ENMs, and are commonly used to reduce aggregation and/or dissolution (Phenrat et al. 2008; Badawy et al. 2010; Stankus et al. 2010; Huynh & Chen 2011). Capping agents improve stability of ENMs by imparting higher electrostatic repulsion, steric repulsion, or both (electrosteric repulsion) (Phenrat et al. 2009; Stankus et al. 2010; Tejamaya et al. 2012). Electrostatic and electrosteric stabilizations are impacted by anionic, cationic or amphiphilic polyelectrolytes (Phenrat et al. 2009; Jiemvarangkul et al. 2011). In addition, capping agents may also influence the final pH of ENMs in aqueous media (Badawy et al. 2010).

1.2.4. Shape/Morphology

The shapes and morphology of colloids may have effects on their net interaction energy (Vold 1954). According to Zhou and Keller (2010), spherical ZnO nanoparticles were more stable than irregularly-shaped ZnO nanoparticles in aqueous media. Morphology was however not considered as an important factor in aggregation of TiO_2 nanoparticles (Liu *et al.* 2011).

1.2.5. Chemical Composition and Surface Chemistry

ENMs exhibit the properties of their composite elements. For instance, the fate of ZnO is strongly influenced by dissolution, but dissolution does not play any significant role in the fate of TiO_2 (Keller *et al.* 2010; Garner & Keller 2014). In addition, ENMs can undergo different types of chemical transformations that are peculiar to their constituent elements when released into natural aquatic environments. These include oxidation, dissolution, hydrolysis, and biological degradation (Klaine *et al.* 2008; Petosa *et al.* 2010; Levard *et al.* 2012; Lowry *et al.* 2012). The potential for ENMs to undergo these transformations may

however be influenced by modifying their surfaces (George *et al.* 2009; Wiesner *et al.* 2009; Petosa *et al.* 2010; Fairbairn *et al.* 2011; Huynh & Chen 2011; Levard *et al.* 2011).

1.3. Effect of Media Properties on Fate of Nanomaterials

Water chemistry plays an important role in controlling the fate of ENMs by modifying the physicochemical properties and process such as surface charge, hydrodynamic size, aggregation, and transformation.

1.3.1. Ionic Strength

The zeta potential of ENMs reflects the electric potential (Ψ) of the particles at a distance from their surface, which is a function of media's electrolyte concentration (or ionic strength) and valence (Badawy *et al.* 2010; Israelachvili 2011; Hunter 2013). In order words, the concentrations and species of salts in aquatic systems determine the stability and mobility of ENMs (Keller *et al.* 2010; Adeleye & Keller 2014; Conway *et al.* 2015). Cations in water systems screen the electrostatic repulsion of ENMs, thereby decreasing their stability (Chen & Elimelech 2006; Darlington *et al.* 2009).

In the reaction-limited regime, an increase in the electrolyte concentration screens the surface charge of ENMs, and reduces the energy barrier to aggregation, thus leading to faster aggregation. However, at the critical coagulation concentration (CCC), and at electrolyte concentrations above the CCC, the energy barrier is eliminated, leading to diffusion-controlled aggregation (Chen & Elimelech 2006; He *et al.* 2008; Saleh *et al.* 2008b; Zhou & Keller 2013). Since the CCC represents the minimum amount of electrolyte needed to completely destabilize ENMs in aqueous media, it provides a useful metric of colloidal stability for ENMs and can be used in the prediction of their fate and transport in natural waters (Chen & Elimelech 2006; Saleh *et al.* 2008a; Saleh *et al.* 2008b). In water bodies where salt concentrations exceed CCC values of ENMs, rapid aggregation will occur,

leading to sedimentation. In freshwater systems, however, where electrolyte concentrations

may be lower than the CCC of stabilized ENMs, a higher mobility of the particles is

expected (Chen & Elimelech 2006; Keller *et al.* 2010; Huynh & Chen 2011).

1.3.2. pH

The surface charge of ENMs is strongly dependent on pH of the media (Badawy *et al.*

2010; Keller *et al.* 2010; Zhou & Keller 2010; Mohd Omar *et al.* 2014). In the absence of

specific adsorbing ions, ENMs have an isoelectric point (IEP), the pH at which their net

surface charge is zero. At pH lower than the IEP, the ENMs surfaces are positively charged,

while they have negative charges above it (Illés & Tombácz 2006; Badawy *et al.* 2010; Zhou

& Keller 2010; Adeleye *et al.* 2014). In natural waters, aggregation occurs at pH around the

IEP even at low ionic strength, because the charge density is very low at this pH range. In

other words, mobility of ENMs is decreased when the pH of natural water is close to their

IEP. On the contrary, colloid dispersions are stable and far from the pH of IEP, although an

increase in electrolyte concentration can induce the coagulation of the particles at any pH

(Cornell & Schwertmann 2003; Illés & Tombácz 2006).

1.3.3. Natural Organic Matter

Natural organic matter (NOM) stabilizes the ENMs in suspension thereby improving

their mobility (Chen *et al.* 2006; Chen & Elimelech 2007; Hyung & Kim 2008; Keller *et al.*

2010; Petosa *et al.* 2010; Quik *et al.* 2010; Zhou & Keller 2010; Huangfu *et al.* 2013). NOM

such as humic acid, alginate, and fulvic acid contain anionic functional groups with which

they increase the electrostatic repulsion of ENMs. In addition, the presence of

macromolecules in NOM stabilizes ENMs via steric repulsion. Stabilization by NOM is

highly dependent on solution pH (which controls adsorption affinity), and on the presence of

Ca^{2+}, which promotes charge neutralization and inter-particle bridging (Elimelech *et al.*

7

1998a; Mylon *et al.* 2004; Badawy *et al.* 2010). Destabilization of ENM suspensions by humic acid due to charge neutralization at pH < IEP and bridging has been reported (Zhu *et al.* 2014).

1.3.4. Hydrography

This refers to all the factors that influence water movement such as advection, turbulence, upwelling, current, diffusion, and in some places, sea ice and freshwater input (Rysgaard *et al.* 1999; Sutherland 2001; Nybakken & Bertness 2005). For instance, turbulence causes vertical mixing which might re-suspend ENMs that may have settled out or enhance their transport away from the point of release. In addition, mixing may transport ENMs to depths faster than their intrinsic settling rate. The role of hydrography in the fate and transport of ENMs has not received much attention.

1.4. Microorganisms and extracellular polymeric substances

Microorganisms—prokaryotes and eukaryotes—are ubiquitous in natural waters (Whitman *et al.* 1998; Sorokin & Sorokin 1999; Pomeroy *et al.* 2007; Zinger *et al.* 2012). The abundance of microorganisms in natural waters implies that collisions/interactions with ENMs are inevitable upon release of these man-made materials into water. Interaction of microorganisms with ENMs may occur directly between microbial cell membranes and ENMs, or indirectly when ENMs interact with the exudates of microorganisms such as extracellular polymeric substances or EPS (Miao *et al.* 2009; Adeleye & Keller 2014; Kadar *et al.* 2014).

EPS are produced by microorganisms growing in natural as well as artificial environments either as single species, in binary association or in heterogeneous communities (Wilderer & Characklis 1989; Wingender *et al.* 1999; Underwood *et al.* 2004; Alasonati & Slaveykova 2012). EPS are composed of a wide range of organic macromolecules such as

polysaccharides, proteins, glycoproteins, glycolipids, nucleic acids, humic substances, uronic acid, phospholipids, and other polymeric substances excreted by microorganisms (Nielsen & Jahn 1999; Wingender *et al.* 1999; Thornton 2002; Bhaskar & Bhosle 2005; Zhang *et al.* 2008). These macromolecules may be held together by electrostatic interactions, hydrogen bonds, London dispersion forces, ionic interactions, and chain-chain complex networks (Mayer *et al.* 1999; Sutherland 2001; Tian *et al.* 2006). EPS are localized outside the cell surface to which they may either be tightly linked via a covalent or non-covalent association (bound EPS or bEPS), or not linked to membrane, i.e. freely released into the environment (soluble or sEPS) (Al-Halbouni *et al.* 2008; Pal & Paul 2008; Alasonati & Slaveykova 2012). sEPS are abundant in natural waters, constituting a large source of dissolved organic carbon (Fogg 1983; Hoagland *et al.* 1993; Gerbersdorf *et al.* 2009).

The polysaccharides represent the major component, accounting for 40 – 95% of the microbial EPS; while proteins can be up to 60% (Flemming & Wingender 2001). Metabolically, the sEPS are actively secreted by bacteria and are biodegradable, while bEPS remain attached to active and inert biomass (Laspidou & Rittmann 2002). The composition and distribution of EPS may vary spatially and temporally depending on the activities of the extracellular enzymes in biofilm (Wingender *et al.* 1999; Flemming *et al.* 2007), organism species, growth phase, nutritional status, and environmental conditions (Sutherland 2001; Underwood *et al.* 2004; Al-Halbouni *et al.* 2008; Zhang *et al.* 2012a). For instance, Al-Halbouni *et al.* (2008) observed EPS concentrations in activated sludge flocs were as low as 17 mg/g dry matter in the summer and as high as 51 mg/g dry matter in the winter.
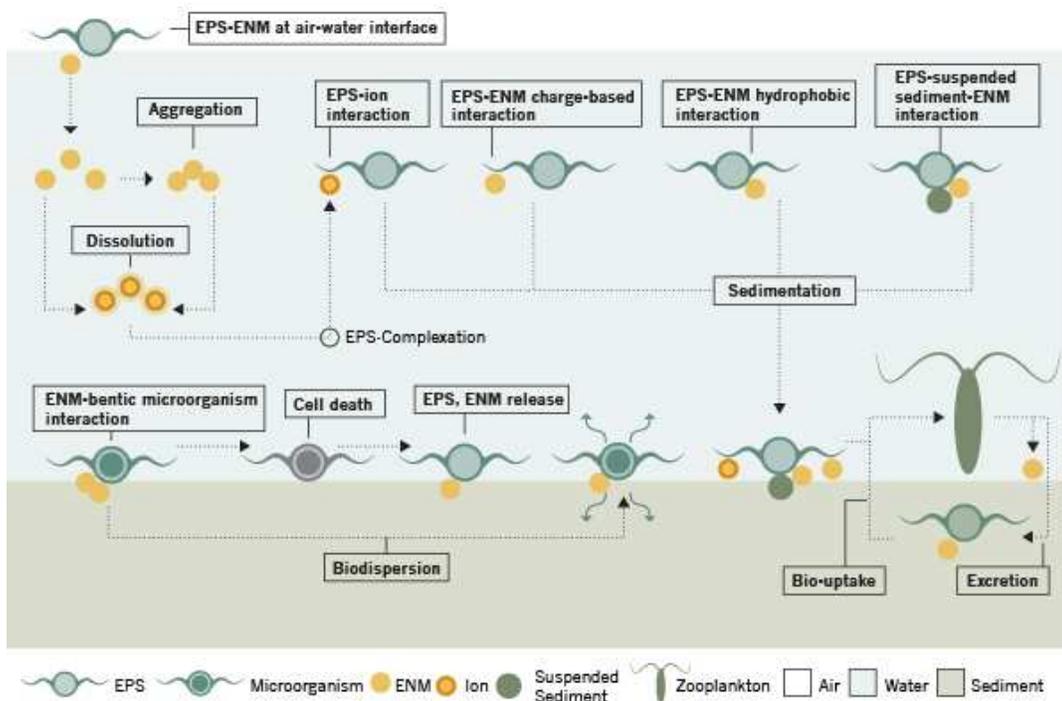
Figure 2. A conceptual diagram showing influence of EPS on fate of ENMs in aquatic systems

Majority of EPS are polyionic due to the presence of functional groups such as uronic acid, phosphoryl groups or carboxylic groups of amino acids (Sutherland 2001; Pal & Paul 2008). EPS of aquatic microbes are polyanions under natural conditions by forming salt bridges with carboxyl groups of acidic polymers or by forming weak electrostatic bonds with hydroxyl groups on polymers containing neutral carbohydrates (Sutherland 2001; Pal & Paul 2008). Proteins rich in acidic amino acids, including aspartic and glutamic acid, also contribute to the anionic properties of EPS (Sutherland 2001; Pal & Paul 2008). Nucleic acids are polyanionic due to the phosphate residues in the nucleotide moiety (Sutherland 2001; Pal & Paul 2008). Polycationic EPS have also been reported (Mack *et al.* 1996). As a result of these charges, EPS can interact with ions and particles with surface charge via

10

electrostatic associations (Pal & Paul 2008). The interactions of EPS with ENMs will affect the fate, transformation, and transport of ENMs in natural systems (Miao *et al.* 2009; Zhang *et al.* 2012b; Quigg *et al.* 2013).

1.5. Organization of the Dissertation

A lot of advances have been made in understanding how ENM and media properties influence the fate of ENMs in aquatic systems. Many of these advances were summarized in sections 1.2 and 1.3. This dissertation focuses on how interactions between sEPS, microorganisms and ENMs can affect the fate and transformation of ENMs in natural waters.

In Chapter 2, interactions between sEPS extracted from *Isochrysis galbana*, a marine phytoplankton, and an insoluble ENM (single wall carbon nanotubes or SWCNTs) were investigated. The effect of interactions between the sEPS and SWCNT on aggregation and sedimentation of the ENMs were examined and compared to treatments in which sEPS were replaced by Suwannee River natural organic matter (SRNOM), a typical proxy for NOM. This Chapter has been published in Water Research; DOI:10.1016/j.watres.2013.11.032 (Adeleye & Keller 2014).

Since several high-use ENMs are metallic, which are often more reactive than carbonaceous materials, it was important to also consider how sEPS affects the fate and transformation of metallic ENMs. In Chapter 3, influence of sEPS isolated from *Isochrysis galbana* on the fate of three copper-based ENMs (which have different levels of solubility) was studied. The copper-based ENMs were CuO (low solubility), Cu (moderate-high solubility), and Kocide 3000, a highly soluble $Cu(OH)_2$-based commercial bactericide/fungicide. Effects of sEPS on aggregation, sedimentation, dissolution,

transformation, and speciation were studied. This Chapter has been published in Environmental Science & Technology; DOI: 10.1021/es5033426 (Adeleye *et al.* 2014).

Apart from solubility, ENMs also present varieties of surface properties: surface charge, hydrophilicity/hydrophobicity, surface coating, etc. More so, the composition of sEPS varies with organism type, nutrient condition, growth phase, etc. In Chapter 4, sEPS were isolated from *Chlamydomonas reinhardtii* (a freshwater phytoplankton) and *Dunaliella tertiolecta* (a marine phytoplankton). sEPS were isolated from D. tertiolecta grown in standard f/2 media and nitrogen-spiked f/2 media to see how nutrient composition will affect sEPS macromolecules and their subsequent impact on ENM fate. In addition, the mechanisms behind interactions between sEPS and three types of TiO_2 nanomaterials were studied at the molecular level.

Chapter 5 focuses on how biopolymers produced by *C. reinhardtii* affect the surface properties, size, and aggregation of modified nanoscale zerovalent iron (named FeSSi). Effects of algal cells and their NOM on the dissolution and transformation of FeSSi were investigated, as well as how the presence of algal NOM affects the toxicity of FeSSi to *C. reinhardtii*.

Lastly, Chapter 6 concludes this doctoral research, and proposes future work.

References

Adeleye, A.S., Conway, J.R., Perez, T., Rutten, P. & Keller, A.A. (2014). Influence of Extracellular Polymeric Substances on the Long-Term Fate, Dissolution, and Speciation of Copper-Based Nanoparticles. *Environ Sci Technol*, 48, 12561-12568.

Adeleye, A.S. & Keller, A.A. (2014). Long-term colloidal stability and metal leaching of single wall carbon nanotubes: effect of temperature and extracellular polymeric substances. *Water research*, 49, 236-250.

Adeleye, A.S., Keller, A.A., Miller, R.J. & Lenihan, H.S. (2013). Persistence of commercial nanoscaled zero-valent iron (nZVI) and by-products. *Journal of Nanoparticle Research*, 15, 1-18.

Al-Halbouni, D., Traber, J., Lyko, S., Wintgens, T., Melin, T., Tacke, D. *et al.* (2008). Correlation of EPS content in activated sludge at different sludge retention times with membrane fouling phenomena. *Water research*, 42, 1475-1488.

Alasonati, E. & Slaveykova, V.I. (2012). Effects of extraction methods on the composition and molar mass distributions of exopolymeric substances of the bacterium Sinorhizobium meliloti. *Bioresource Technology*, 114, 603-609.

Badawy, A.M.E., Luxton, T.P., Silva, R.G., Scheckel, K.G., Suidan, M.T. & Tolaymat, T.M. (2010). Impact of Environmental Conditions (pH, Ionic Strength, and Electrolyte Type) on the Surface Charge and Aggregation of Silver Nanoparticles Suspensions. *Environmental Science & Technology*, 44, 1260-1266.

Bhaskar, P. & Bhosle, N.B. (2005). Microbial extracellular polymeric substances in marine biogeochemical processes. *Current Science*, 88, 45-53.

Brant, J., Lecoanet, H., Hotze, M. & Wiesner, M. (2005). Comparison of Electrokinetic Properties of Colloidal Fullerenes (n-C60) Formed Using Two Procedures†. *Environmental Science & Technology*, 39, 6343-6351.

Chen, K.L. & Elimelech, M. (2006). Aggregation and Deposition Kinetics of Fullerene (C60) Nanoparticles. *Langmuir*, 22, 10994-11001.

Chen, K.L. & Elimelech, M. (2007). Influence of humic acid on the aggregation kinetics of fullerene (C60) nanoparticles in monovalent and divalent electrolyte solutions. *Journal of Colloid and Interface Science*, 309, 126-134.

Chen, K.L. & Elimelech, M. (2009). Relating Colloidal Stability of Fullerene (C60) Nanoparticles to Nanoparticle Charge and Electrokinetic Properties. *Environmental Science & Technology*, 43, 7270-7276.

Chen, K.L., Mylon, S.E. & Elimelech, M. (2006). Aggregation Kinetics of Alginate-Coated Hematite Nanoparticles in Monovalent and Divalent Electrolytes. *Environmental Science & Technology*, 40, 1516-1523.

Choi, O. & Hu, Z. (2008). Size Dependent and Reactive Oxygen Species Related Nanosilver Toxicity to Nitrifying Bacteria. *Environmental Science & Technology*, 42, 4583-4588.

Conway, J.R., Adeleye, A.S., Gardea-Torresdey, J. & Keller, A.A. (2015). Aggregation, Dissolution, and Transformation of Copper Nanoparticles in Natural Waters. *Environmental Science & Technology*, 49, 2749-2756.

Cornell, R.M. & Schwertmann, U. (2003). *The iron oxides : structure, properties, reactions, occurrences, and uses*. Wiley-VCH, Weinheim.

Corsi, I., Cherr, G.N., Lenihan, H.S., Labille, J., Hassellov, M., Canesi, L. *et al.* (2014). Common Strategies and Technologies for the Ecosafety Assessment and Design of Nanomaterials Entering the Marine Environment. *ACS Nano*, 8, 9694-9709.

Darlington, T.K., Neigh, A.M., Spencer, M.T., Guyen, O.T.N. & Oldenburg, S.J. (2009). Nanoparticle characteristics affecting environmental fate and transport through soil. *Environmental Toxicology and Chemistry*, 28, 1191-1199.

Elimelech, M., Jia, X., Gregory, J. & Williams, R. (1998a). *Particle deposition & aggregation: measurement, modelling and simulation*. Butterworth-Heinemann.

Elimelech, M. & O'Melia, C.R. (1990). Effect of particle size on collision efficiency in the deposition of Brownian particles with electrostatic energy barriers. *Langmuir*, 6, 1153-1163.

Elimelech, M., Williams, R., Gregory, J. & X, J. (1998b). *Particle Deposition and Aggregation*. Butterworth-Heinemann, Oxford, UK.

Everett, D. (1988). Basic principles of colloid science. *Royal Society of Chemistry paperbacks*.

Fairbairn, E.A., Keller, A.A., Mädler, L., Zhou, D., Pokhrel, S. & Cherr, G.N. (2011). Metal oxide nanomaterials in seawater: Linking physicochemical characteristics with biological response in sea urchin development. *Journal of Hazardous Materials*, 192, 1565-1571.

Flemming, H. & Wingender, J. (2001). Relevance of microbial extracellular polymeric substances (EPSs)--Part I: Structural and ecological aspects. *Water science and technology: a journal of the International Association on Water Pollution Research*, 43, 1.

Flemming, H.-C., Neu, T.R. & Wozniak, D.J. (2007). The EPS matrix: the "house of biofilm cells". *Journal of Bacteriology*, 189, 7945-7947.

Fogg, G.E. (1983). The Ecological Significance of Extracellular Products of Phytoplankton Photosynthesis. In: *Botanica Marina*, p. 3.

Garner, K.L. & Keller, A.A. (2014). Emerging patterns for engineered nanomaterials in the environment: a review of fate and toxicity studies. *Journal of Nanoparticle Research*, 16, 1-28.

Garner, K.L., Suh, S., Lenihan, H.S. & Keller, A.A. (2015). Species Sensitivity Distributions for Engineered Nanomaterials. *Environmental Science & Technology*.

George, S., Pokhrel, S., Xia, T., Gilbert, B., Ji, Z., Schowalter, M. *et al.* (2009). Use of a rapid cytotoxicity screening approach to engineer a safer zinc oxide nanoparticle through iron doping. *ACS Nano*, 4, 15-29.

Gerbersdorf, S., Westrich, B. & Paterson, D. (2009). Microbial Extracellular Polymeric Substances (EPS) in Fresh Water Sediments. *Microb Ecol*, 58, 334-349.

Grasso, D., Subramaniam, K., Butkus, M., Strevett, K. & Bergendahl, J. (2002). A review of non-DLVO interactions in environmental colloidal systems. *Reviews in Environmental Science and Biotechnology*, 1, 17-38.

He, Y.T., Wan, J. & Tokunaga, T. (2008). Kinetic stability of hematite nanoparticles: the effect of particle sizes. *Journal of Nanoparticle Research*, 10, 321-332.

Hoagland, K.D., Rosowski, J.R., Gretz, M.R. & Roemer, S.C. (1993). Diatom Extracellular Polymeric Substance: Function, Fine Structure, Chemistry, and Physiology. *Journal of Phycology*, 29, 537-566.

Holden, P.A., Klaessig, F., Turco, R.F., Priester, J.H., Rico, C.M., Avila-Arias, H. *et al.* (2014). Evaluation of Exposure Concentrations Used in Assessing Manufactured Nanomaterial Environmental Hazards: Are They Relevant? *Environmental Science & Technology*, 48, 10541-10551.

Holden, P.A., Nisbet, R.M., Lenihan, H.S., Miller, R.J., Cherr, G.N., Schimel, J.P. *et al.* (2013). Ecological Nanotoxicology: Integrating Nanomaterial Hazard Considerations Across the Subcellular, Population, Community, and Ecosystems Levels. *Acc. Chem. Res.*, 46, 813-822.

Huangfu, X., Jiang, J., Ma, J., Yongze, L. & Jing, Y. (2013). Aggregation Kinetics of Manganese Dioxide Colloids in Aqueous Solution: Influence of Humic Substances and Biomacromolecules. *Environmental Science & Technology*.

Hunter, R.J. (2013). *Zeta potential in colloid science: principles and applications*. Academic press.

Hunter, R.J., White, L.R. & Chan, D.Y. (1987). *Foundations of colloid science*. Clarendon Press Oxford.

Huynh, K.A. & Chen, K.L. (2011). Aggregation Kinetics of Citrate and Polyvinylpyrrolidone Coated Silver Nanoparticles in Monovalent and Divalent Electrolyte Solutions. *Environmental Science & Technology*, 45, 5564-5571.

Hyung, H. & Kim, J.-H. (2008). Natural Organic Matter (NOM) Adsorption to Multi-Walled Carbon Nanotubes: Effect of NOM Characteristics and Water Quality Parameters. *Environmental Science & Technology*, 42, 4416-4421.

Illés, E. & Tombácz, E. (2006). The effect of humic acid adsorption on pH-dependent surface charging and aggregation of magnetite nanoparticles. *Journal of Colloid and Interface Science*, 295, 115-123.

Israelachvili, J.N. (2011). *Intermolecular and Surface Forces: Revised Third Edition*. Elsevier Science.

Israelachvili, J.N. & McGuiggan, P.M. (1988). Forces Between Surfaces in Liquids. *Science*, 241, 795-800.

Jiang, J., Oberdörster, G. & Biswas, P. (2009). Characterization of size, surface charge, and agglomeration state of nanoparticle dispersions for toxicological studies. *Journal of Nanoparticle Research*, 11, 77-89.

Jiemvarangkul, P., Zhang, W.-x. & Lien, H.-L. (2011). Enhanced transport of polyelectrolyte stabilized nanoscale zero-valent iron (nZVI) in porous media. *Chemical Engineering Journal*, 170, 482-491.

Kadar, E., Cunliffe, M., Fisher, A., Stolpe, B., Lead, J. & Shi, Z. (2014). Chemical interaction of atmospheric mineral dust-derived nanoparticles with natural seawater — EPS and sunlight-mediated changes. *Science of The Total Environment*, 468–469, 265-271.

Keller, A.A. & Lazareva, A. (2014). Predicted Releases of Engineered Nanomaterials: From Global to Regional to Local. *Environmental Science & Technology Letters*, 1, 65-70.

Keller, A.A., McFerran, S., Lazareva, A. & Suh, S. (2013). Global life cycle releases of engineered nanomaterials. *Journal of Nanoparticle Research*, 15, 1-17.

Keller, A.A., Wang, H., Zhou, D., Lenihan, H.S., Cherr, G., Cardinale, B.J. *et al.* (2010). Stability and Aggregation of Metal Oxide Nanoparticles in Natural Aqueous Matrices. *Environmental Science & Technology*, 44, 1962-1967.

Klaine, S.J., Alvarez, P.J.J., Batley, G.E., Fernandes, T.F., Handy, R.D., Lyon, D.Y. *et al.* (2008). Nanomaterials in the environment: Behavior, fate, bioavailability, and effects. *Environmental Toxicology and Chemistry*, 27, 1825-1851.

Laspidou, C.S. & Rittmann, B.E. (2002). A unified theory for extracellular polymeric substances, soluble microbial products, and active and inert biomass. *Water research*, 36, 2711-2720.

Levard, C., Hotze, E.M., Lowry, G.V. & Brown, G.E. (2012). Environmental Transformations of Silver Nanoparticles: Impact on Stability and Toxicity. *Environmental Science & Technology*, 46, 6900-6914.

Levard, C., Reinsch, B.C., Michel, F.M., Oumahi, C., Lowry, G.V. & Brown, G.E. (2011). Sulfidation Processes of PVP-Coated Silver Nanoparticles in Aqueous Solution: Impact on Dissolution Rate. *Environmental Science & Technology*, 45, 5260-5266.

Liddle, M.J. & Scorgie, H.R.A. (1980). The effects of recreation on freshwater plants and animals: A review. *Biological Conservation*, 17, 183-206.

Liu, X., Chen, G. & Su, C. (2011). Effects of material properties on sedimentation and aggregation of titanium dioxide nanoparticles of anatase and rutile in the aqueous phase. *Journal of Colloid and Interface Science*, 363, 84-91.

Lowry, G.V., Gregory, K.B., Apte, S.C. & Lead, J.R. (2012). Transformations of nanomaterials in the environment. *Environmental Science & Technology*, 46, 6893-6899.

Lux-Research (2014). Nanotechnology Update: Corporations Up Their Spending as Revenues for Nano-enabled Products Increase. Available at: https://portal.luxresearchinc.com/research/report_excerpt/16215 Last accessed December 2014.

Mack, D., Fischer, W., Krokotsch, A., Leopold, K., Hartmann, R., Egge, H. *et al.* (1996). The intercellular adhesin involved in biofilm accumulation of Staphylococcus epidermidis is a linear beta-1,6-linked glucosaminoglycan: Purification and structural analysis. *Journal of Bacteriology*, 178, 175-183.

Mayer, C., Moritz, R., Kirschner, C., Borchard, W., Maibaum, R., Wingender, J. *et al.* (1999). The role of intermolecular interactions: studies on model systems for bacterial biofilms. *International journal of biological macromolecules*, 26, 3-16.

Miao, A.-J., Schwehr, K.A., Xu, C., Zhang, S.-J., Luo, Z., Quigg, A. *et al.* (2009). The algal toxicity of silver engineered nanoparticles and detoxification by exopolymeric substances. *Environmental Pollution*, 157, 3034-3041.

Miller, R.J., Lenihan, H.S., Muller, E.B., Tseng, N., Hanna, S.K. & Keller, A.A. (2010). Impacts of Metal Oxide Nanoparticles on Marine Phytoplankton. *Environmental Science & Technology*, 44, 7329-7334.

Mohd Omar, F., Abdul Aziz, H. & Stoll, S. (2014). Aggregation and disaggregation of ZnO nanoparticles: Influence of pH and adsorption of Suwannee River humic acid. *Science of The Total Environment*, 468–469, 195-201.

Mylon, S.E., Chen, K.L. & Elimelech, M. (2004). Influence of Natural Organic Matter and Ionic Composition on the Kinetics and Structure of Hematite Colloid Aggregation: Implications to Iron Depletion in Estuaries. *Langmuir*, 20, 9000-9006.

Nel, A., Xia, T., Mädler, L. & Li, N. (2006). Toxic Potential of Materials at the Nanolevel. *Science*, 311, 622-627.

Nielsen, P.H. & Jahn, A. (1999). Extraction of EPS. In: *Microbial extracellular polymeric substances*. Springer, pp. 49-72.

Nybakken, J.W. & Bertness, M.D. (2005). *Marine biology: an ecological approach*. Benjamin-Cummings Pub Co.

Ongley, E.D. (1996). *Control of water pollution from agriculture*. Food & Agriculture Org.

Pal, A. & Paul, A. (2008). Microbial extracellular polymeric substances: central elements in heavy metal bioremediation. *Indian journal of microbiology*, 48, 49-64.

PEN (2014). Project on Emerging Nanotechnologies Consumer Products Inventory. Available at: http://www.nanotechproject.org/cpi Last accessed January 2015.

Petosa, A.R., Jaisi, D.P., Quevedo, I.R., Elimelech, M. & Tufenkji, N. (2010). Aggregation and Deposition of Engineered Nanomaterials in Aquatic Environments: Role of Physicochemical Interactions. *Environmental Science & Technology*, 44, 6532-6549.

Phenrat, T., Cihan, A., Kim, H.-J., Mital, M., Illangasekare, T. & Lowry, G.V. (2010). Transport and Deposition of Polymer-Modified Fe0 Nanoparticles in 2-D Heterogeneous Porous Media: Effects of Particle Concentration, Fe0 Content, and Coatings. *Environmental Science & Technology*, 44, 9086-9093.

Phenrat, T., Kim, H.-J., Fagerlund, F., Illangasekare, T., Tilton, R.D. & Lowry, G.V. (2009). Particle Size Distribution, Concentration, and Magnetic Attraction Affect Transport of Polymer-Modified Fe0 Nanoparticles in Sand Columns. *Environmental Science & Technology*, 43, 5079-5085.

Phenrat, T., Saleh, N., Sirk, K., Kim, H.-J., Tilton, R. & Lowry, G. (2008). Stabilization of aqueous nanoscale zerovalent iron dispersions by anionic polyelectrolytes: adsorbed anionic polyelectrolyte layer properties and their effect on aggregation and sedimentation. *Journal of Nanoparticle Research*, 10, 795-814.

Phenrat, T., Saleh, N., Sirk, K., Tilton, R.D. & Lowry, G.V. (2007). Aggregation and Sedimentation of Aqueous Nanoscale Zerovalent Iron Dispersions. *Environmental Science & Technology*, 41, 284-290.

Pomeroy, L.R., Williams, P.J.I., Azam, F. & Hobbie, J.E. (2007). The Microbial Loop. *Oceanography*, 20, 28-33.

Priester, J., Van De Werfhorst, L.C., Ge, Y., Adeleye, A., Tomar, S., Tom, L.M. *et al.* (2014). Effects of TiO2 and Ag Nanoparticles on Polyhydroxybutyrate Biosynthesis By Activated Sludge Bacteria. *Environmental Science & Technology*.

Quigg, A., Chin, W.-C., Chen, C.-S., Zhang, S., Jiang, Y., Miao, A.-J. *et al.* (2013). Direct and indirect toxic effects of engineered nanoparticles on algae: role of natural organic matter. *ACS Sustainable Chemistry & Engineering*.

Quik, J.T.K., Lynch, I., Hoecke, K.V., Miermans, C.J.H., Schamphelaere, K.A.C.D., Janssen, C.R. *et al.* (2010). Effect of natural organic matter on cerium dioxide nanoparticles settling in model fresh water. *Chemosphere*, 81, 711-715.

Reinhart, D.R., Berge, N.D., Santra, S. & Bolyard, S.C. (2010). Emerging contaminants: nanomaterial fate in landfills. *Waste Management*, 30, 2020-2021.

Reinsch, B.C., Forsberg, B., Penn, R.L., Kim, C.S. & Lowry, G.V. (2010). Chemical Transformations during Aging of Zerovalent Iron Nanoparticles in the Presence of Common Groundwater Dissolved Constituents. *Environmental Science & Technology*, 44, 3455-3461.

Richardson, S.D. & Ternes, T.A. (2014). Water Analysis: Emerging Contaminants and Current Issues. *Analytical Chemistry*, 86, 2813-2848.

Roco, M.C., Mirkin, C.A. & Hersam, M.C. (2011). *Nanotechnology research directions for societal needs in 2020: retrospective and outlook*. Springer Science & Business Media.

Rysgaard, S., Nielsen, T.G. & Hansen, B.W. (1999). Seasonal variation in nutrients, pelagic primary production and grazing in a high-Arctic coastal marine ecosystem, Young Sound, Northeast Greenland. *Marine Ecology Progress Series*, 179, 13-25.

Saleh, N., Kim, H.J., Phenrat, T., Matyjaszewski, K., Tilton, R.D. & Lowry, G.V. (2008a). Ionic strength and composition affect the mobility of surface-modified Fe-0 nanoparticles in water-saturated sand columns. *Environmental Science & Technology*, 42, 3349-3355.

Saleh, N.B., Pfefferle, L.D. & Elimelech, M. (2008b). Aggregation Kinetics of Multiwalled Carbon Nanotubes in Aquatic Systems: Measurements and Environmental Implications. *Environmental Science & Technology*, 42, 7963-7969.

Sorokin, Y.I. & Sorokin, P.Y. (1999). Production in the Sea of Okhotsk. *Journal of Plankton Research*, 21, 201-230.

Stankus, D.P., Lohse, S.E., Hutchison, J.E. & Nason, J.A. (2010). Interactions between Natural Organic Matter and Gold Nanoparticles Stabilized with Different Organic Capping Agents. *Environmental Science & Technology*, 45, 3238-3244.

Sutherland, I.W. (2001). Biofilm exopolysaccharides: a strong and sticky framework. *Microbiology*, 147, 3-9.

Tejamaya, M., Römer, I., Merrifield, R.C. & Lead, J.R. (2012). Stability of Citrate, PVP, and PEG Coated Silver Nanoparticles in Ecotoxicology Media. *Environmental Science & Technology*, 46, 7011-7017.

Thornton, D. (2002). Diatom aggregation in the sea: mechanisms and ecological implications. *European Journal of Phycology*, 37, 149-161.

Tian, Y., Zheng, L. & Sun, D.-z. (2006). Functions and behaviors of activated sludge extracellular polymeric substances (EPS): a promising environmental interest. *Journal of Environmental Sciences*, 18, 420-427.

Tsuzuki, T. (2013). *Nanotechnology Commercialization*. Pan Stanford Publishing, Singapore.

Underwood, G.J., Boulcott, M., Raines, C.A. & Waldron, K. (2004). Environmental Effects on Exopolymer Production by Marine Benthic Diatoms: Dynamics, Changes in composition, and Pathways of Production1. *Journal of phycology*, 40, 293-304.

Vold, M.J. (1954). Van der Waals' attraction between anisometric particles. *Journal of Colloid Science*, 9, 451-459.

Wang, H., Ho, K.T., Scheckel, K.G., Wu, F., Cantwell, M.G., Katz, D.R. *et al.* (2014). Toxicity, Bioaccumulation, and Biotransformation of Silver Nanoparticles in Marine Organisms. *Environmental Science & Technology*, 48, 13711-13717.

Wang, P. & Keller, A.A. (2009). Natural and Engineered Nano and Colloidal Transport: Role of Zeta Potential in Prediction of Particle Deposition. *Langmuir*, 25, 6856-6862.

Wang, P., Shi, Q., Liang, H., Steuerman, D.W., Stucky, G.D. & Keller, A.A. (2008). Enhanced Environmental Mobility of Carbon Nanotubes in the Presence of Humic Acid and Their Removal from Aqueous Solution. *Small*, 4, 2166-2170.

Wei, Y.-T., Wu, S.-C., Chou, C.-M., Che, C.-H., Tsai, S.-M. & Lien, H.-L. (2010). Influence of nanoscale zero-valent iron on geochemical properties of groundwater and vinyl chloride degradation: A field case study. *Water research*, 44, 131-140.

Whitman, W., Coleman, D. & Wiebe, W. (1998). Prokaryotes: The unseen majority. *Proceedings of the National Academy of Sciences of the United States of America*, 95, 6578-6583.

Wiesner, M.R., Lowry, G.V., Jones, K.L., Hochella, J.M.F., Di Giulio, R.T., Casman, E. *et al.* (2009). Decreasing Uncertainties in Assessing Environmental Exposure, Risk, and Ecological Implications of Nanomaterials†‡. *Environmental Science & Technology*, 43, 6458-6462.

Wilderer, P. & Characklis, W. (1989). Structure and function of biofilms. *Structure and function of biofilms*, 5-17.

Wingender, J., Neu, T. & Flemming, H. (1999). Microbial Extracellular Polymeric Substances: Characterisation. *Structure and Function, Springer, Berlin*, 123.

Zhang, L., Ren, H. & Ding, L. (2012a). Comparison of extracellular polymeric substances (EPS) extraction from two different activated sludges. *Water Science and Technology*, 66, 1558-1564.

Zhang, S., Jiang, Y., Chen, C.-S., Spurgin, J., Schwehr, K.A., Quigg, A. *et al.* (2012b). Aggregation, dissolution, and stability of quantum dots in marine environments: Importance of extracellular polymeric substances. *Environmental science & technology*, 46, 8764-8772.

Zhang, S., Xu, C. & Santschi, P.H. (2008). Chemical composition and 234Th (IV) binding of extracellular polymeric substances (EPS) produced by the marine diatom Amphora sp. *Marine Chemistry*, 112, 81-92.

Zheng, X., Chen, Y. & Wu, R. (2011). Long-Term Effects of Titanium Dioxide Nanoparticles on Nitrogen and Phosphorus Removal from Wastewater and Bacterial Community Shift in Activated Sludge. *Environmental Science & Technology*, 45, 7284-7290.

Zhou, D., Abdel-Fattah, A.I. & Keller, A.A. (2012). Clay Particles Destabilize Engineered Nanoparticles in Aqueous Environments. *Environmental Science & Technology*, 46, 7520-7526.

Zhou, D. & Keller, A.A. (2010). Role of morphology in the aggregation kinetics of ZnO nanoparticles. *Water research*, 44, 2948-2956.

Zhou, D. & Keller, A.A. (2013). Influence of Material Properties of TiO2 Nanoparticle Agglomeration. *PLOS ONE*, In Press.

Zhu, M., Wang, H., Keller, A.A., Wang, T. & Li, F. (2014). The effect of humic acid on the aggregation of titanium dioxide nanoparticles under different pH and ionic strengths. *Science of The Total Environment*, 487, 375-380.

Zinger, L., Gobet, A. & Pommier, T. (2012). Two decades of describing the unseen majority of aquatic microbial diversity. *Molecular Ecology*, 21, 1878-1896.

Chapter 2. Long-term colloidal stability and metal leaching of single wall carbon nanotubes: Effect of temperature and extracellular polymeric substances[1]

2.1. Introduction

Carbon nanotubes (CNTs) are insoluble and not easily biodegradable (Lam *et al.* 2004), hence, they tend to persist in the environment. In order to assess the long-term impact of CNTs released into surface waters, there is a need to understand how CNTs will partition between surface waters and sediment phases (Schwyzer *et al.* 2012). The hydrophobic surfaces of CNTs makes them interact readily with natural organic matter (NOM), which is abundant in the environment (Saleh *et al.* 2010). Hyung et al. (2007) demonstrated improved CNT stability in the presence of Suwanee River natural organic matter (SRNOM). In water bodies with significant amounts of NOM, such as humic acid, alginate or extracellular polymeric substances (EPS), the stability of CNTs may be enhanced. As such, CNTs may be mobile in natural aquatic systems, and available to pelagic organisms (Schwyzer *et al.* 2012). EPS are composed of a wide range of organic polymers such as polysaccharides, proteins, nucleic acids and phospholipids excreted by microorganisms (Flemming *et al.* 2007); and they may affect the fate and transport of engineered nanomaterials (ENMs) in natural systems (Miao *et al.* 2009).

Colloidal stability of CNTs in aqueous media has been investigated (Lin *et al.* 2010; Schwyzer *et al.* 2011; Schwyzer *et al.* 2012). Schwyzer et al. (2012) investigated the stability of CNTs in aqueous media and concluded that surface functionalization and size correlates with stabilization. Bennett et al. (2013) monitored the dispersability and stability of SWCNTs in freshwaters for 72 hr and found that stability varies widely based on physicochemical properties of SWCNTs. However, long-term stability of CNTs in natural waters has not been examined. More so, the potential effect of temperature and EPS on stability of CNTs has not been reported to date.

As-prepared CNTs usually contain a significant amount of impurities, including metal catalysts (Ge *et al.* 2012; Bennett *et al.* 2013). These impurities are commonly removed in order to obtain purified CNTs. However, some of the metals are protected by graphitic shells, and may remain even after rigorous purification processes (Ge *et al.* 2011). Residual metal impurities may be mobilized upon introduction of CNTs into aquatic systems (Ge *et al.* 2012; Bennett *et al.* 2013). The water chemistry may or may not be favorable for dissolution of metal catalysts attached to CNTs (Ge *et al.* 2012) so leaching of metals may vary widely in different waters. Metal leaching from CNTs when dispersed in natural waters has only been investigated on a short term basis and no significant toxicity to algae was reported within the study period (Bennett *et al.* 2013). However, a 14-day study (Mwangi *et al.* 2012) reported that nickel leached out from CNTs in suspensions at levels that were toxic to amphipods. As such, it is important to quantify the levels of metal impurities that may leach out of CNTs in natural waters over a long period of time.

The goals of this study were to experimentally measure the fate of SWCNT, applied from dry powders to natural waters, and investigate:

1. Long-term stability and partitioning of SWCNTs;

2. Long-term leaching of metals from SWCNTs; and

3. Effect of temperature variations on SWCNT surface characteristics, stability, and metal leaching.

2.2. Materials and Methods

2.2.1. Materials

Five SWCNTs were used for dispersability and stability studies, which include (1) raw (HP-R) and (2) purified (HP-P) forms of high-pressure carbon monoxide SWCNTs (HiPCo, NanoIntegris, IL); (3) raw (P2-R), and (4) purified (P2-P) forms of arc discharge SWCNTs (Carbon Solutions, CA); and (5) SG65, a purified SWCNT prepared using the CoMoCat process (SouthWest NanoTechnologies, OK). All five SWCNTs were used as received. P2-P was selected as a model commercial SWCNT, and was used for all the temperature-dependent and aggregation studies. Some physicochemical properties of these SWCNTs have been described previously (Bennett *et al.* 2013). Additional characterizations done in this study include zeta (ζ) potential analysis (Zetasizer Nano-ZS90, Malvern, UK), transmission electron microscopy (FEI Titan 300 kV FEG TEM), and scanning electron microscopy (FEI XL30 Sirion equipped with an EDAX APOLLO X probe for energy-dispersive X-ray spectroscopy, EDS).

Waters used for this study include NANOpure water with or without 10 mg L^{-1} SRNOM (denoted DI and DINOM respectively), freshwater with 0.1 mg L^{-1} (FW0.1) or 1.0 mg L^{-1} SRNOM (FW1.0), groundwater (GW), lagoon (LW), stormwater (STM), wastewater (WW), and seawater (SEA). Basic characteristics of the waters are shown in Table 1 and additional information is provided in the Supplementary material. Soluble EPS was isolated from an axenic culture of a phytoplankton, *Isochrysis galbana*. Details on EPS isolation are in the

Supplementary material. EPS was characterized by measuring carbohydrate and protein concentrations using anthrone method (Morris 1948), and modified Lowry Protein Assay Kit (Pierce Biotechnology) respectively. Hydrodynamic diameter (HDD) of EPS was determined using the Zetasizer Nano-ZS90.

2.2.2. Effect of Temperature and Natural Organic Materials on Zeta (ζ) Potential

10 mg L^{-1} P2-P suspensions were made in the waters by probe-sonication with a Misonix Sonicator S-4000 (QSonica LLC, Newtown, CT). Sonication was done in ice-bath to reduce defect. ζ potential of an aliquot was then determined from 1-60 °C in DTS 1060 cells (Malvern) using the temperature controlled chamber of the Zetasizer Nano-ZS90. At each temperature, a 120 s equilibration period was allowed before ζ potential data were collected in triplicate measurements—with each measurement reflecting 12-15 runs. Trend experiments were not done in LW, SEA and WW because the ionic strength (IS) of those conditions was too high for the cells to function properly across the temperature range.

To see the effect of NOM on ζ potential, SWCNT stock suspensions were made with SRNOM or EPS or neither (see section 2.3 for details). Aliquots were taken from the three stock suspensions, diluted to make a final [SWCNT] of 10 mg L^{-1}, and analyzed for ζ potential at different NaCl concentrations. All ζ potential measurements were done at pH 7.

2.2.3. Aggregation and Sedimentation Kinetics

Stabilized SWCNT stock suspensions (100 mg L^{-1}) were made by dispersing P2-P in NANOpure water (Barnstead) in ice-bath by probe sonication using the Misonix Sonicator S-4000 in the presence of 3 mg L^{-1} SRNOM. Sonicated SWCNT stock was allowed to stand overnight and stable aqueous phase was removed for characterization and analyses. SWCNT stock was diluted by a factor of 10 for aggregation and sedimentation studies so the final [SWCNT] and [SRNOM] were 10 mg L^{-1} and 0.3 mg L^{-1} respectively. Aggregation kinetics

was studied in (1) increasing concentrations of NaCl solution at pH 7, and (2) natural waters. As shown in Eq. 1, the initial aggregation rate constant (k) of SWCNTs reflects doublet formation and is proportional to the initial rate of increase in the intensity-weighted hydrodynamic radius, $a_h(t)$, with time, t, and the inverse of initial number concentration of SWCNT particles, N_0 (Saleh *et al.* 2008):

$$k \propto \frac{1}{N_0} \left(\frac{da_h(t)}{dt} \right)_{t \to 0}$$

(Eq. 1)

k is obtained from the slope of the best fit line of $(da_h(t)/dt)_{t \to 0}$, which is determined via Dynamic Light Scattering (DLS) using the Zetasizer Nano-ZS90. The analysis requires that the final $a_h(t)$ be approximately 1.3 of initial a_h, where there are sufficient doublets formed and few higher-order aggregates (Zhou & Keller 2010). Attachment efficiencies (α) of SWCNTs in aqueous NaCl were calculated by normalizing the measured k of a given concentration by the diffusion-limited aggregation rate constant $(k)_{fav}$ determined in highly favorable aggregation conditions (Eq. 2) . Attachment efficiencies (α) of SWCNTs in each natural water was calculated by normalizing the measured k of a given natural water by the diffusion-limited aggregation rate constant $(k)_{fav}$ determined in SEA:

$$\alpha = \frac{\left(\dfrac{da_h(t)}{dt} \right)_{t \to 0}}{\left(\dfrac{da_h(t)}{dt} \right)_{t \to 0, fav}}$$

(Eq. 2)

To understand the role of naturally-occurring EPS in SWCNT stability, aggregation kinetics was also studied in SWCNT stock dispersed in 5 mg-C L^{-1} EPS. The final [EPS] in sample was 0.5 mg-C L^{-1}, which is within the range reported for colloidal carbohydrates in natural waters (Hung *et al.* 2001). Finally, an additional aggregation study was conducted in which 0.1 mg-C L^{-1} EPS was added to SWCNT initially stabilized with SRNOM just before

measurements to see whether additional EPS might affect aggregation dynamics of SRNOM-stabilized SWCNTs. Aggregation kinetics was measured using DLS as described elsewhere (Zhou & Keller 2010). In summary a 532 nm laser source and a detection angle of 90° were used to do DLS measurements immediately after adding SWCNT stock and natural waters (or electrolyte, buffer, and NANOpure water). Data were collected until a 50% increase in the initial hydrodynamic radius was observed. The diffusion-limited (DLCA) and reaction-limited (RLCA) clustering aggregation regimes, and thus, CCC, can be identified in a plot of $\log_{10}[NaCl]$ versus $\log_{10} \alpha$. The dynamic aggregation process was monitored using a Biospec 1601 spectrophotometer (Shimadzu, Japan) measuring the sedimentation of the nanoparticles in natural waters and NaCl solution (pH 7) via time-resolved optical absorbency. Optical absorbency was measured every 6 min for 354 min, using aliquots of stabilized SWCNT stock in natural waters or a range of NaCl concentrations.

2.2.4. Stability Experiments

SWCNT dry powder was added to the various waters to obtain concentrations of 10 mg SWCNT L^{-1}. The SWCNT suspensions were bath-sonicated (Branson 8210, Branson Danbury, CT) for 4 hr to enhance dispersion without causing defects on the nanotubes (Islam *et al.* 2003). This form of low-power sonication better mimics naturally-occurring dispersive forces than probe ultrasonication. The sonicated suspensions were kept at 20 °C and monitored for 90 days. To see the effect of temperature on CNT stability, suspensions of the model SWCNT, P2-P, were made in FW1.0 and WW, kept at 4, 20, and 40 °C constant temperatures, and monitored for 30 days. To see how sudden temperature variation may affect stability, three sets of FW1.0 and WW suspensions of P2-P were kept at 20 °C for 7 days, after which a set was moved to 4 °C and another to 40 °C. Stability was monitored at the new temperatures for the next 23 days, and compared with the set that remained at 20 °C.

Stability was monitored as described in previous studies (Schwyzer *et al.* 2011; Bennett *et al.* 2013). In summary, the concentration of suspended SWCNT was determined via absorbance at 550 nm (Biospec 1601). SWCNT concentration was determined by constructing a calibration curve ($R^2 \geq 0.98$) of each SWCNT dispersed in the respective waters.

2.2.5. Metal Leaching

Aliquots of the SWCNT suspensions were filtered with 0.2 µm-sized syringe filters (Millipore) to remove the nanotubes. The dissolved metal content of filtrate was determined as described elsewhere (Adeleye *et al.* 2013). In brief, a measured amount of the filtrate was digested using trace-metal grade nitric acid (Fisher Scientific), diluted with NANOpure water and analyzed via ICP-AES (iCAP 6300, Thermo Scientific) for: (1) nickel (Ni) and yttrium (Y) present in P2-P and P2-R; (2) iron (Fe) present in HP-P and HP-R; and cobalt (Co) and molybdenum (Mo) present in SG65. The temperature-dependent metal leaching study was only done using the model SWCNT, P2-P (at 4 ℃ and 40 ℃). Metal leaching was monitored for 90 days.

2.2.6. Statistical Analysis

Statistical significance between treatments was determined using analysis of variance (ANOVA). Tukey HSD test *post-hoc* was used to determine which treatments significantly differed. A *p* value of <0.05 was considered statistically significant. R statistical software (version 3.0.1) was used for all analyses.

2.3. Results and Discussion

2.3.1. SWCNT and EPS Characterizations

The SWCNTs appeared as closely bound bundles and clusters (Figure 1). This is primarily due to the strong interaction forces that exist in the nanotubes. Tubes of P2-R were

not as densely packed, appearing as thin meshes of nanotubes interspersed with impurities. Morphology of the SWCNTs appeared to be affected by purification as seen in the physical differences between P2-R and P2-P, and HP-R and HP-P. SG65 appeared shorter and thicker compared to arc discharge and HiPCo SWCNTs. The raw forms of SWCNTs contained more non-CNT components than the purified variants. Most of the non-CNT components were metal impurities as confirmed by EDS (Supporting Information, SI Figure S1 in Appendix).

The EPS fraction had an average HDD of 203.95±12.50 nm. Carbohydrate concentration was determined to be 12.19 mg L^{-1} glucose equivalent, while protein concentration was 3.63 mg L^{-1} using a Bovine serum albumin (BSA) standard.

2.3.2. Effect of Temperature and Natural Organic Materials on Zeta Potential

The ζ potential of all the SWCNTs indicated likely instability ($< \pm 30$ mV) in all the waters except in DI, DINOM and the freshwaters, all of which have low IS. ζ potential of the SWCNTs varied widely in different waters, with P2-P exhibiting the highest magnitude in most conditions (Figure 2A). The presence of NOM increased the magnitude of the ζ potential in natural waters, while the presence of salts decreased it. For instance ζ potential of P2-P, in mV, was -39.6±3.0, -32.8±2.2, and -35.5±1.5 in DI, FW0.1, and FW1.0 respectively. Surface charge of carbonaceous ENMs may originate from surface oxidation (Sano *et al.* 2001), accumulation of hydroxides (Chen & Elimelech 2009), defect and mechanochemistry (Saleh *et al.* 2010), or surface electron density distribution (Leys *et al.* 2003).

We observed that ζ potential of P2-P varied significantly with temperature. ζ potential became less negative as temperature increased in all the natural waters (Figure 2B), and even turned positive at 60 °C in some waters. For instance, ζ potential of P2-P in STM increased

in magnitude from -27.3±1.0 mV at 20 °C to -32.7±3.5 mV at 1 °C. At a typical summer temperature in tropical areas (40 °C or 104 °F), however, the ζ potential of the same sample decreased in magnitude to -19.3±0.2 mV. In waters with significant amount of electrolytes (e.g. GW), ζ potentials at high temperature conditions were in the regions of maximum instability. This result suggests that stability of CNTs in natural waters will be influenced by temperature variation. At higher ζ potential induced by lower temperatures, electrostatic repulsion will be more significant and CNTs may have increased mobility in surface waters and groundwater. In hot temperature conditions, electrostatic repulsion will be significantly reduced. In addition, higher temperatures lead to increased evaporation, and thus higher salinity. Decreased surface charge of CNTs, coupled with higher salinity will enhance aggregation at high temperatures and SWCNT sedimentation.

The presence of SRNOM and EPS increased the magnitude of ζ potential of all SWCNTs (Figure 2C, D). For example, ζ potential (in mV) of P2-P in 10 mM NaCl in the presence of EPS, SRNOM, or neither were -49.3±0.4, -44.7±1.7, and -39.1±2.7 respectively. Similarly, in P2-R we observed -42.5±1.3, -35.7±1.5, and -28.2±1.1 in the presence of EPS, NOM, or neither respectively. This suggests that increased electrostatic repulsion is one of the mechanisms by which SRNOM and EPS improve the stability of SWCNTs in aqueous phase, possibly, in addition to steric hindrance. ζ potential values observed in SRNOM were not significantly different from observation in EPS in all the purified SWCNTs. In the raw SWCNT variants however, we observed that ζ potential was significantly higher in the presence of EPS than in SRNOM regardless of IS.

2.3.3. Aggregation and Sedimentation Kinetics

Probe sonication dispersed the SWCNTs which were then stabilized by SRNOM or EPS (Figure 3). HDD (in nm) was 246, and 252 in SRNOM-stabilized, EPS-stabilized SWCNT

respectively, compared to 1.49×10^4 nm with neither stabilizer. SWCNT fractions obtained in the presence of SRNOM and EPS were also monodispersed with average PDI < 0.4 (Figure 3C). Attachment efficiency (α) and aggregation kinetics of P2-P in waters are presented in Figure 4. The smallest α, observed in DINOM, was three orders of magnitude smaller than α in SEA. α in LW was similar to SEA, reflecting similarities in IS. An α of 0.92 was observed in GW, which had lower amounts of electrolytes than SEA and LW. α was an order of magnitude lower in WW and at least two orders of magnitude lower in the rest of the waters.

At low [NaCl] (RLCA region), increased [NaCl] screened the electrostatic repulsion between nanotubes to a higher degree, leading to increase in α. At high [NaCl] (DLCA region), the charge of SWCNT was completely screened and the energy barrier between nanotubes was eliminated. The critical coagulation concentration (CCC) of P2-P stabilized with SRNOM was about 15 mM (Figure 4C). A CCC value of 20 mM was reported in NaCl for a different type of SWCNT that was stabilized via successive sonication (Saleh *et al.* 2010). When EPS was used to stabilize P2-P stock instead of SRNOM, the CCC shifted to about 100 mM in NaCl, suggesting that EPS stabilized the nanotubes better than SRNOM in the conditions of this experiment. Finally, when additional 0.1 mg-C L^{-1} EPS was added to SRNOM-stabilized P2-P just before analysis, a CCC of 54 mM NaCl was obtained. The presence of EPS in aqueous media has been suggested to affect the stability of ENMs (Miao *et al.* 2009). Like other types of NOM, EPS may contain some hydrophobic polysaccharides with vast surface areas with which it can interact with other hydrophobic materials (Flemming *et al.* 2007) like CNTs, thereby creating steric repulsion between nanotubes. More so, the functional groups present in EPS such as hydroxyl, phosphoryl, and carboxylic groups (Pal & Paul 2008) are able to enhance the negative charges on CNT, increasing electrostatic repulsion as indicated by ζ potential data.

32

Sedimentation of stabilized P2-P in natural waters was strongly dependent on the interplay of electrolyte concentration and presence of NOM (Figure 4D). Significant sedimentation was not observed in DI, DINOM, FW0.1, FW1.0, and STM after 6 hr as indicated by their normalized concentrations, C/C_0 (C = concentration and C_0 = initial concentration). In these waters, α was less than 10^{-2}, so P2-P aggregation was unfavorable. Acute exposure of SWCNTs in surface waters with relatively low salt concentrations may therefore be mostly to epipelagic organisms, including phytoplankton, pelagic fish, and birds.

The concentration of suspended P2-P, $[CNT]_{susp}$, detected in GW (Conductivity = 971 µS) after 6 hr ($C/C_0 = 0.12$) was surprisingly lower than in SEA (Conductivity = 49,400 µS) and LW (Conductivity = 50,800 µS). Both SEA and LW had C/C_0 of about 0.20 after 6 hr. Since α of P2-P in GW was lower than SEA and LW, P2-P aggregation in GW was not as fast as in SEA and LW. Decreased sedimentation (despite faster aggregation) of SWCNT in SEA and LW may be due to higher viscosity, and decreased difference in density between particles and medium ($\Delta\rho$) resulting from higher levels of salts compared to GW. Density and viscosity are higher in seawater than freshwater by about 3 % and 10 % respectively (El-Dessouky 2002). In the presence of salts (hydrated ions), water molecules are organized around the ions via ion-dipole interactions, mostly leading to increased viscosity (Chandra & Bagchi 2000). Increased viscosity results from increased ion concentration, especially for ions of higher valence (Chandra & Bagchi 2000), which are abundant in SEA and LW (Table 1). Decreased sedimentation of SWCNTs at high IS conditions was also observed in NaCl solution (Figure 4F). For instance, C/C_0 of EPS-stabilized P2-P suspended in 10 mM NaCl was 0.21 after 6 hr, while in 100 and 1000 mM NaCl, C/C_0 were 0.31 and 0.49 respectively after 6 hr. Salts may also bridge SWCNTs in a network-like manner, decreasing

33

sedimentation temporarily due to low density of network (Schwyzer *et al.* 2013), and/or increased drag from media.

Sedimentation of SWCNT was slower in the presence of EPS than in SRNOM at all [NaCl] studied (Figure 4E, F). C/C_0 for EPS-stabilized P2-P after 6 hr were 0.21 and 0.31 at 10 mM and 100 mM respectively. Meanwhile, at the same salt concentrations and settling time, C/C_0 values were 0.09 and 0.10 for SRNOM-stabilized P2-P.

2.3.4. Stability Experiments

Sedimentation velocity of rod-like particles like SWCNTs depends on particle size, $\Delta\rho$, medium viscosity, and aspect ratio (Herzhaft & Guazzelli 1999). Dispersability and long term stability of SWCNTs in natural waters is also influenced by the presence and concentrations of salts and NOM, wettability of the SWCNTs, and the presence of impurities (Hyung *et al.* 2007; Saleh *et al.* 2008; Li *et al.* 2011). Dispersability is defined as the initial nanomaterial concentration suspended in the media (Bennett *et al.* 2013), and it serves to determine the potential acute exposure of aquatic organisms to ENMs. As shown in Figure 5, P2-R showed the least dispersability (<17% by mass) in all tested waters, as a significant fraction remained aggregated in the air-water interface (AWI) after 4 hr bath sonication. This agrees with our earlier observation of loose clustering of P2-R, compared to dense and compact clustering in all other SWCNTs used in this study. Dispersability of the purified variant, P2-P, was $\geq$ 50% in all the waters, showing that changes in physicochemical properties brought about by purification significantly affect CNT dispersability. GW had the lowest dispersability for all the nanotubes while DINOM suspensions were well-dispersed.

The energy delivered by bath sonication is not expected to overcome the van der Waals attraction between SWCNT pairs, which is estimated at -0.9 eV nm^{-1} (Huang & Terentjev 2012). For the stability studies, however, no additional treatment was performed to increase

the amount of SWCNTs dispersed, since our goal was to understand the fate of dry-powdered SWCNTs in natural aquatic systems. Three distinct layers were identified in the SWCNT suspensions after sonication (Figure 5): In addition to being suspended in the water matrices, some SWCNTs aggregates adhered to the AWI due to low density and hydrophobicity. Density of CNTs is affected by tube diameter, wall structure and the weight fraction of constituent elements (Thostenson & Chou 2003). CNT density is estimated at 1.4-2.0 g cm^{-3} (Huang & Terentjev 2012) with the lower end of the range more likely for SWCNTs, hence, $\Delta\rho$ is usually low compared to other ENMs. Except for P2-R, all the SWCNT had aggregates that also settled out during sonication, forming the third layer at the bottom of the vials. Additional settling was observed within a few minutes after sonication and throughout the study. Based on these observations, the introduction of SWCNTs presents exposure risks to organisms in all the phases of aquatic systems—AWI, water column, and sediment phases.

The stability of SWCNTs in waters over a period of 8 days is shown in Figure 6A-D. Although ζ potential indicated instability in most of waters, some stability was observed in STM and WW on the order of days (Figure 6E), and in DINOM on the order of weeks. The stability observed may be due to steric repulsion from adsorbed NOM (Saleh *et al.* 2008). By Day 8, the order of [CNT]$_{susp}$ of P2-P was DINOM > WW > STM > FW1.0 > DI = SEA > FW0.1 > GW. SWCNTs were expected to be completely unstable in SEA and LW, and sediment out within hours as commonly observed for other ENMs (Keller *et al.* 2010). However, [CNT]$_{susp}$ of 0.78-2.71 mg L^{-1} was observed in SEA by Day 8. Stability of SWCNTs in SEA and LW may be improved by high water density and viscosity and other factors discussed previously.

SWCNTs were only detectable in DINOM (lowest α) by Day 60, as suspended CNTs had fully sedimented in all the other waters by then. Thus, the long term fate of most SWCNTs in aquatic systems is the sediment phase. Fluctuations were observed in $[CNT]_{susp}$, and this may be due to resuspension of sedimented CNTs during sampling, even though considerable care was taken to minimize mixing. Their low density and weak attachment to other CNTs may result in easy resuspension. This may be different in a natural environment where clays and other sediments are present, and the CNTs can mobilize into pore water. Resuspension may still occur though, due to storm events and bioturbation. Settling of nanotubes to the sediment phase of natural waters implies that exposure of benthic organisms may increase significantly over time in the event of a CNT release. This may be a considerable concern as a recent study (Velzeboer *et al.* 2013) demonstrated that the structure of benthic communities in natural systems is sensitive to environmentally relevant levels of CNTs.

2.3.5. Effect of Temperature on Stability

Colloidal stability of P2-P decreased significantly at 40 °C compared to lower temperatures (Figure 7). However, they were either more stable at 20 °C than 4 °C (as observed in WW) or not significantly different (as observed in FW1.0). In WW, 36% of the SWCNT suspended after sonication had settled out after 48 hr at 40 °C, compared to 31% and 24% sedimentation at 4 °C and 20 °C respectively. By Day 30, 81% had sedimented at 20 °C and 86% at 4 °C, while SWCNT was not detectable in the water column at 40 °C. The trend was similar in FW1.0, with C/C_0 of 0.12, 0.29, and 0.32 by Day 30 at 40 °C, 4 °C and 20 °C respectively. Increase in temperature corresponds to energy input into SWCNT suspensions, which may lead to disruption of weak interaction forces (Zhou *et al.* 2012), increased Brownian motion (and collision), and decreased ζ potential. Disagglomeration of

36

ENMs due to disruption of weak forces may improve stability temporarily since smaller particles sediment slower. However, as collision of nanotubes continues due to increased kinetic energy, more nanotubes aggregate due to lower surface charge. As such, high temperature favors aggregation of ENMs in the long run, leading to faster sedimentation.

Changing the temperature of the P2-P suspensions from 20 °C to either 4 °C or 40 °C resulted in faster sedimentation relative to samples that remained at 20 °C (Figure 7C, D). For WW, warming from 20 °C to 40 °C decreased $[CNT]_{susp}$ by 28 % within three days (Day 7-10), but only by 13 % within the same time frame when cooled to 4 °C. In SWCNT suspensions kept at a constant 20 °C, $[CNT]_{susp}$ only decreased by 7 % between Day 7 and Day 10. The initial instability caused by temperature change decreased with time, especially at 4 °C, which shows that acute temperature changes may affect CNT stability more than prolonged temperature variations. By Day 30 C/C_0 was 0.14 in both the constant 4 °C and when cooling from 20 °C to 4 °C for P2-P in WW. Neither 40 °C temperature treatments had detectable SWCNT in WW suspension by Day 30. Similarly, C/C_0 was 0.25 and 0.29 in constant 4 °C, and 20 °C to 4 °C treatments respectively for SWCNTs suspended in FW1.0. These observations imply that stability of CNTs in the natural environment may be affected as ambient temperatures change, especially with rapid temperature fluxes (e.g. those due to sunrise and sunset).

2.3.6. Metal Leaching

2.3.6.1. Effect of CNT Purification

Significant release of metals was found in all conditions (SI Table 1). For arc discharge SWCNTs, the total amount of dissolved metals detected was higher in P2-R than in P2-P (Figure 8A). However, in proportion to the amount of residual metals in each SWCNT, there was more leaching in P2-P than in P2-R. For instance, Day 90 dissolved nickel

37

concentrations, [Ni]$_{diss}$, detected in WW were 158 µg L^{-1} in P2-R (representing 7.0% by mass of residual Ni) and 42 µg L^{-1} (representing 14.3% by mass of residual Ni) in P2-P. Similarly, dissolved yttrium (mass %) by Day 90 in WW was 0.8% in P2-R and 5.6% in P2-P. A similar trend was observed between HP-R and HP-P. Removal of metal impurities from raw CNTs is commonly done by using strong oxidizers, which may weaken the attachment of some residual metals that remain attached. This may make it easier for metal leaching to occur in purified CNTs when exposed to aqueous media. [Ni]$_{diss}$ detected in P2-R increased over time in all waters as more of the residual metal was mobilized with time, but this was not observed in most P2-P suspensions suggesting that most of the leachable Ni in P2-P leached out earlier on. Low amount of metals detected over 90 days (compared to total metals present in the SWCNTs) may be due to 1) re-adsorption of mobilized metals; and 2) the presence of metals in insoluble state. Both possibilities are discussed in later sections.

2.3.6.2. Effect of Water and Metal Chemistries

The concentration of each dissolved metal detected in SWCNT suspensions varied widely in the different waters (Figure 8A, SI Table S1), which shows that water chemistry plays a primary role in leaching and mobilization of metals from CNTs. For instance, observed Day 90 [Ni]$_{diss}$ in P2-R were 130 and 53 µg L^{-1} in GW and LW respectively. Similarly in SWCNTs that contained two types of metals the level of each dissolved metal detected in waters did not follow the same trend, suggesting that the chemistry of individual elements also controlled their leaching. In P2-R for instance, the amount of dissolved Ni released into waters over 90 days ($p < 0.05$) was GW > WW = FW0.1 > DINOM > SEA = STM > FW1.0 > LW > DI. Meanwhile the order detected for Y was GW = SEA > DINOM > STM = LW > WW = FW1.0 = FW0.1 > DI over the same period. The order was also different for Co and Mo that leached out of SG65. Dissolved Co was quite low and not

significantly different in all the waters, except in FW where it was relatively high.

Meanwhile, for Mo we found GW = LW = STM = SEA > FW0.1 = FW1.0 = WW = DI > DINOM. Fe leached from HP-R was not significantly different in all the waters over 90 days. There were similarities in the trend of metal leaching into waters between raw and purified SWCNT variants (SI Table S1). The chemistry of metal ions is dependent on the formation of complexes with ligands present in natural waters (Dries *et al.* 2005; Adeleye *et al.* 2013). Such complexes reduce the concentration of the free metal species in solution and thus affect solubility of metals (Dries *et al.* 2005).

2.3.6.3. Effect of CNT Exposure Time

$[Ni]_{diss}$ from P2-R and $[Mo]_{diss}$ from SG65 increased with time in all waters. However, $[Fe]_{diss}$ from HP-R decreased with time, and there was no clear trend in other metals. In addition to water and metal chemistries, the amount of metals that were mobilized from SWCNTs appeared to also depend on proportion of residual metals that is leachable. For instance, the highest $[Ni]_{diss}$ from P2-R detected (on Day 90) was 183 $\mu g\ L^{-1}$ (in GW) which represents only 8.1% of the total Ni in P2-R. Since $[Ni]_{diss}$ in P2-R increased throughout this study, we may have detected higher levels of $[Ni]_{diss}$ if we continued sampling beyond 90 days. In conditions where metal concentration decreased or remained steady with time, we can assume that total leachable metal from SWCNTs were obtained based on the conditions of this experiment or the solubility limits were reached. The proportion of residual metals that is leachable may also depend on pre-treatment of CNTs, and experimental conditions (e.g. pH, and temperature).

Decreased metal concentration with time may be due to sorption to SWCNT or NOM (Tian *et al.* 2012), and/or precipitation or complexation (Davis 1984). In HP-R the highest levels of dissolved Fe were detected on Day 0, and then $[Fe]_{diss}$ decreased over time in all the

waters. As an example, $[Fe]_{diss}$ in HP-R were 112 µg L^{-1} and 31 µg L^{-1} in GW on Day 0 and

Day 90 respectively. This suggests that leachable Fe from HP-R was released as the

nanotubes were suspended and sonicated, probably due to high amount of loosely held

soluble Fe. With time, released Fe adsorbed to SWCNT and/or NOM in the different waters

or precipitated out. $[Fe]_{diss}$ increased with time in HP-P in some waters as seen in GW where

Day 0 and Day 90 $[Fe]_{diss}$ were 2 µg L^{-1} and 33 µg L^{-1} respectively. This suggests gradual

release of leachable Fe from HP-P suspension since most of the loosely attached Fe had been

removed during purification.

2.3.6.3. Effect of Natural Organic Matter

The presence of NOM appears to have significant effect for certain metals. $[Ni]_{diss}$ from

P2-R in FW1.0 was a factor of 2 or 3 lower than in FW0.1, suggesting that Ni was adsorbed

to NOM or perhaps, SWCNT-adsorbed NOM inhibited dissolution. $[Ni]_{diss}$ detected in P2-R

right after sonication on Day 0 were 114 µg L^{-1} and 39 µg L^{-1} in FW0.1 and FW1.0

respectively. By Day 90 the proportion had not changed significantly with $[Ni]_{diss} = 153$ µg

L^{-1} in FW0.1 and 84 µg L^{-1} in FW1.0. Similarly, $[Ni]_{diss}$ from P2-P released into FW0.1 was

slightly higher than in FW1.0. This is similar to the observation of another study (Tong *et al.*

2012) which recovered less metal species from solutions with higher amount of NOM. Both

dissolved NOM and NOM bound to SWCNT may adsorb metals or precipitate them out via

complexation (Lin *et al.* 2012; Tian *et al.* 2012). Surface-bound NOM with oxygen-

containing functional groups improves metal adsorption onto CNTs (Lin *et al.* 2012). In

addition, metal ions may be electrostatically attracted to the diffuse layer of NOM-CNT

complex (Lin *et al.* 2012), which is more charged at higher levels of NOM. In contrast

$[Ni]_{diss}$ was much lower in DI than in DINOM in both P2-R and P2-P. The lowest metal

concentrations were detected in DI for most of the metals (SI Table S1) perhaps due to lack

of redox-active and/or complexing species. Similar to Ni, higher $[Co]_{diss}$ was detected at lower levels of NOM. However, there was no significant correlation difference between Fe and Mo, and NOM levels. Lin et al. (2012) also detected lower amount of dissolved Co compared to Mo from a CNT in the presence of humic acid. Increased adsorption of metals in the presence of NOM will control their bioavailability when mobilized from CNTs into natural media (Tong *et al.* 2012).

2.3.6.2. Effect of Temperature

We observed no significant difference between $[Ni]_{diss}$ detected over 90 days at 4 ^oC and 40 ^oC in all the waters. However, when $[Ni]_{diss}$ detected over 90 days at 20 ^oC was compared with the levels detected at either 4 ^oC or 40 ^oC we confirmed that more dissolved Ni was present at both 4 ^oC and 40 ^oC in SWCNT suspensions of STM, DINOM, FW1.0. These are conditions with relatively high amount of NOM and low IS. As reported for the 20 ^oC conditions, NOM appeared to result in increased adsorption of dissolved metal, thus leading to detection of lower amount of dissolved metal at FW1.0 relative to the levels detected in FW0.1 over 90 days. In contrast, there was no significant difference in the $[Ni]_{diss}$ detected between FW0.1 and FW1.0 at either 4 ^oC or 40 ^oC. This suggests that the adsorption potential of CNT-NOM complex for Ni is affected by change in temperature, and this effect is more pronounced in waters with relatively high NOM level.

2.4. Conclusion and Environmental Significance

Release of CNTs into water bodies will lead to immediate exposure of organisms in all phases. In the long run however, exposure of benthos will increase as CNTs sediment. In addition to electrolytes and natural organic matter (NOM), sedimentation of CNTs is also controlled by media density and viscosity, and temperature. Elevated temperatures decrease the magnitude of surface charge of CNTs, and may thus favor aggregation. As such, in hot

temperatures, exposure risk of aquatic organisms to CNTs may be higher around the point of release. Temperature variation decreases CNT stability and the effect is less significant with time when the media is cooled down (e.g. from summer to winter temperatures) relative to when it is heated up (e.g. winter to summer temperatures).

This study demonstrated the improved stability of CNTs by EPS compared to SRNOM. EPS is a NOM synthesized by microbes growing under normal conditions and as a response to stress. Exposure of microbes to CNTs may trigger increased synthesis of EPS, a defense mechanism seen with other ENMs (Miao *et al.* 2009), which may further increase CNT stability (and thus organisms' exposure) in water matrix. Accounting for the role of EPS in ENM stability may improve the closeness of ENM fate and transport prediction to what may happen in reality. Also, adsorption of EPS and other types of NOM to CNTs and their leached metals may significantly change their bioavailability to organisms.

Significant leaching of CNT metals may occur in groundwater, seawater, and wastewater. The dynamics of leaching vary widely between the different CNTs and their respective metals. While most dissolved Fe was found right after exposure of a CNT to waters, dissolved [Ni] increased with time in another CNT. 6% of CNTs produced and used globally are currently estimated to end up in wastewater treatment plants (WWTP) and this may increase with novel applications (Keller *et al.* 2013). This represents about 180 t of CNTs or 4-45 t of metals that may potentially enter wastewater streams annually, based on global CNT production of ~3000 t/yr, and 2-25% metal content by weight as found in commercial CNTs. The chemistry of wastewater favors metal leaching from CNTs and this may portend a potential challenge to proper WWTP functioning since biota may be affected. In addition, WWTPs may only be an intermediate step for CNTs and their leached metals as they may transfer into surface waters with effluents, or biosolids.

Table 1. Characteristics of water samples used in this study. ND = non-detect.

Parameter	Unit	DI water[1]	Storm	Groundwater	Freshwater[1]	Seawater	Lagoon	Wastewater
pH		7.1	7.7	7.5	7.3	7.3	6.6	7.6
Conductivity	$\mu S\ cm^{-1}$	0.44×10^1	3.86×10^2	9.71×10^2	0.97×10^2	4.94×10^4	5.08×10^4	2.29×10^3
TOC	$mg\ L^{-1}$	ND	6.49	ND	ND	ND	ND	2.38
UV_{254}		0	0.242	0.002	0.002	0.002	0.041	0.098
UV_{550}		0	0.001	0	0.001	0.007	0.001	0.005
Redox potential	mV	9.68×10^1	1.67×10^2	1.37×10^2	1.60×10^2	1.42×10^2	1.36×10^2	1.24×10^2
Na	$mg\ L^{-1}$	ND	4.93×10^1	1.58×10^2	ND	1.27×10^4	1.28×10^4	3.25×10^2
Ca	$mg\ L^{-1}$	0.03	3.61×10^1	4.95×10^1	0.15×10^1	4.90×10^2	4.93×10^2	1.20×10^2
Mg	$mg\ L^{-1}$	ND	1.0×10^1	2.75×10^1	0.35×10^1	1.65×10^3	1.69×10^1	7.8×10^1
Al	$mg\ L^{-1}$	ND	ND	ND	ND	ND	ND	ND
K	$mg\ L^{-1}$	0.48×10^0	0.75×10^1	0.86×10^1	0.12×10^1	4.61×10^2	4.64×10^2	3.86×10^1
Cu	$mg\ L^{-1}$	0.02	0.16	ND	0.01	ND	ND	0.08
Fe	$mg\ L^{-1}$	ND	0.25	ND	0.06	ND	ND	0.35
Ni	$mg\ L^{-1}$	ND	ND	ND	ND	ND	ND	ND
Y	$mg\ L^{-1}$	ND	ND	ND	ND	ND	ND	ND
Co	$mg\ L^{-1}$	ND	ND	ND	ND	ND	ND	ND
Mo	$mg\ L^{-1}$	ND	0.03	ND	ND	0.08	0.11	0.07

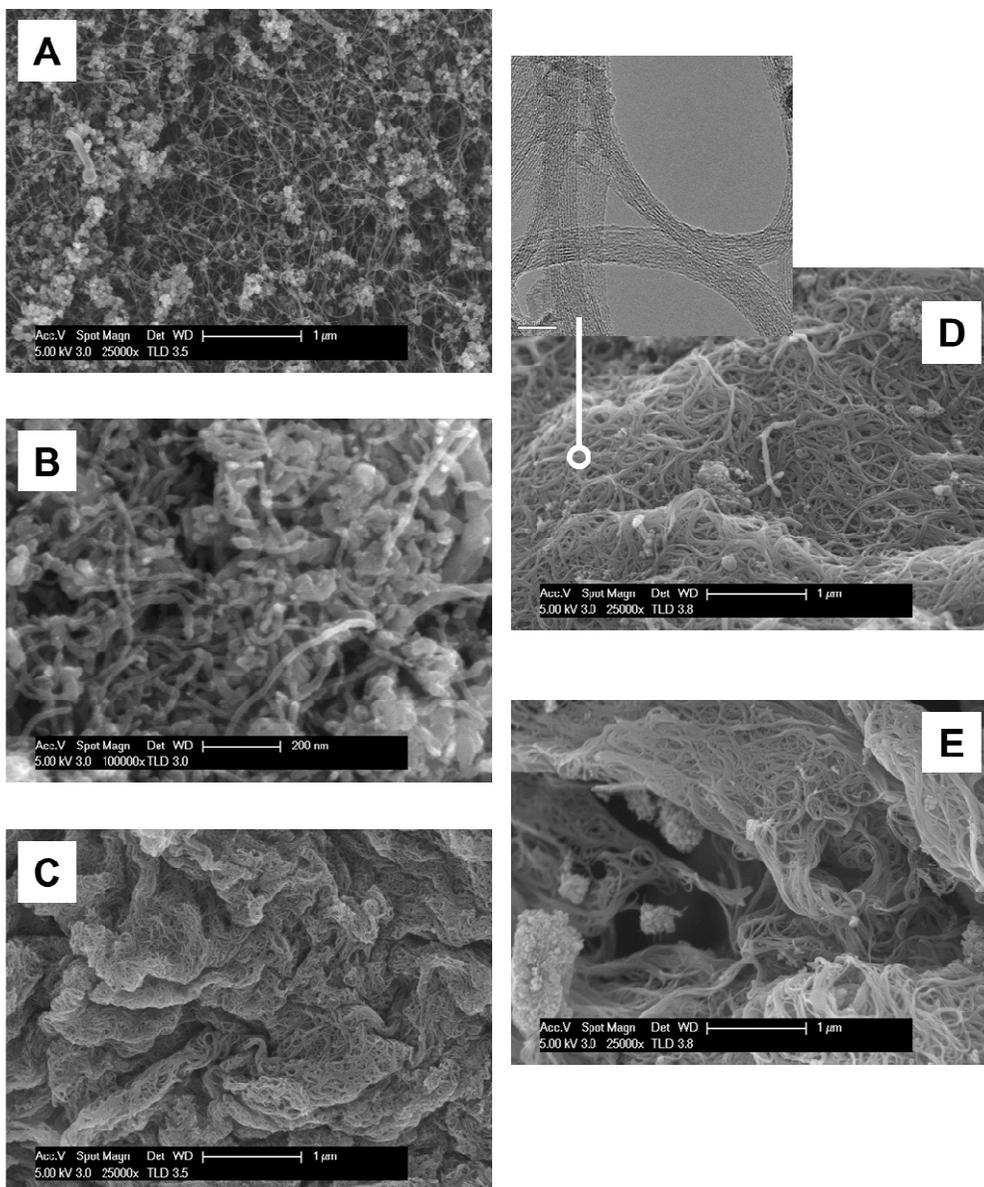[1] Measurements were done before the addition of SRNOM

43

Figure 1. SEM micrographs of (A) P2-R, (B) SG65, (C) HP-R, (D) P2-P with inset showing

a bundle of tightly packed tubes obtained via TEM, and (E) HP-P.
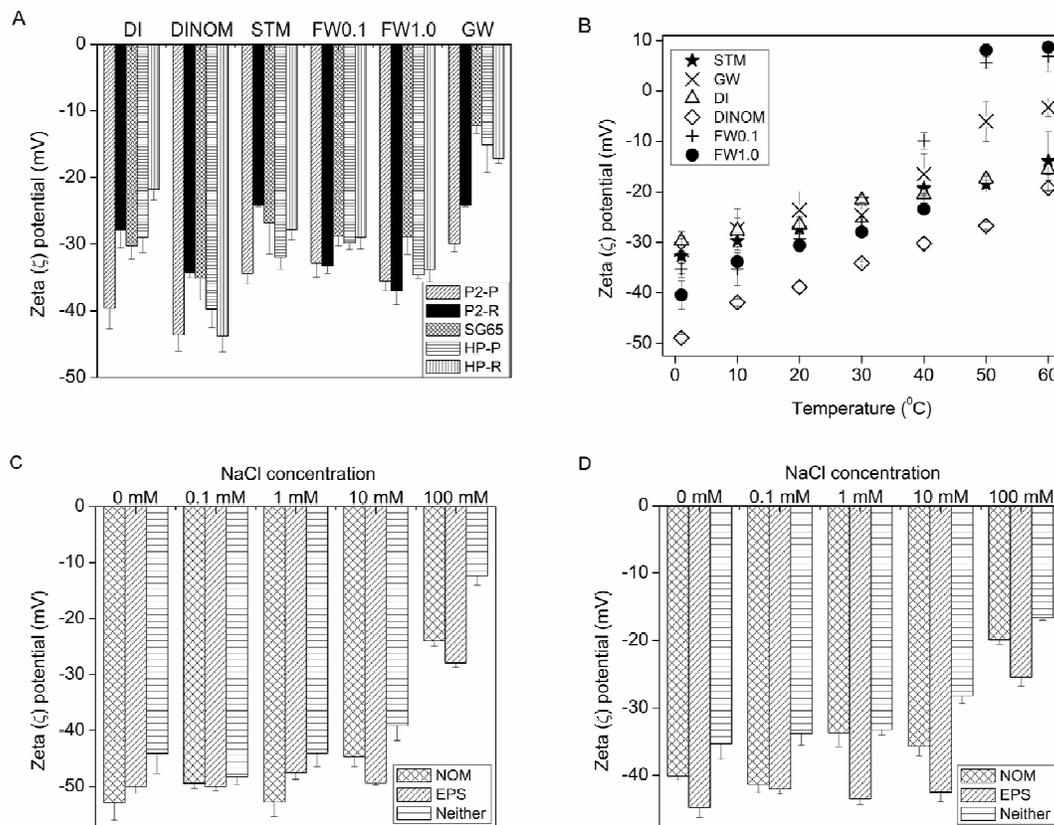
Figure 2. Zeta (ζ) potential of SWCNTs. (A) ζ potential of SWCNTs in selected waters. (B)

ζ potential of P2-P in waters as a function of temperature. ζ potential of (C) P2-P and (D)

P2-R as a function of NaCl concentration at pH 7 and in the presence of NOM, EPS or

neither.
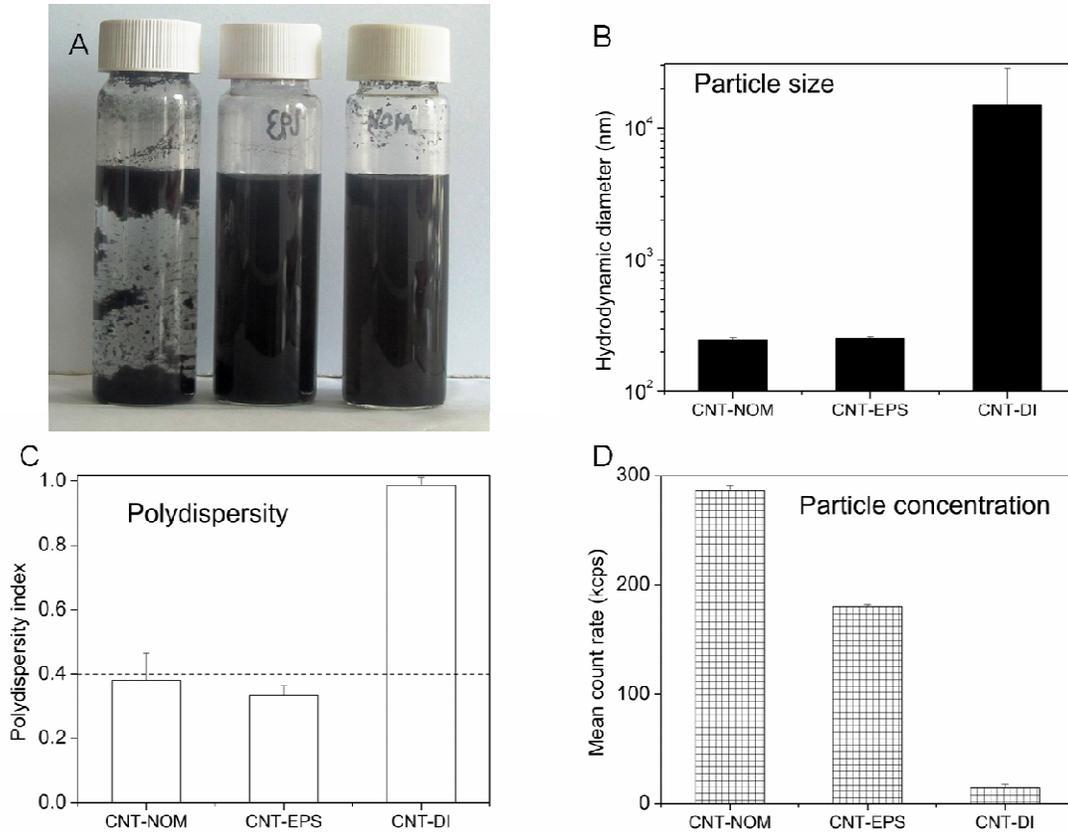
Figure 3. Characterization of SWCNT dispersed via probe-sonication in ice-bath. (A) Front view of stocks after 24 hr settling, (B) Hydrodynamic diameter, (C) Polydispersity, and (D) Mean count rate of aqueous phase of SWCNT dispersed in SRNOM, EPS or neither
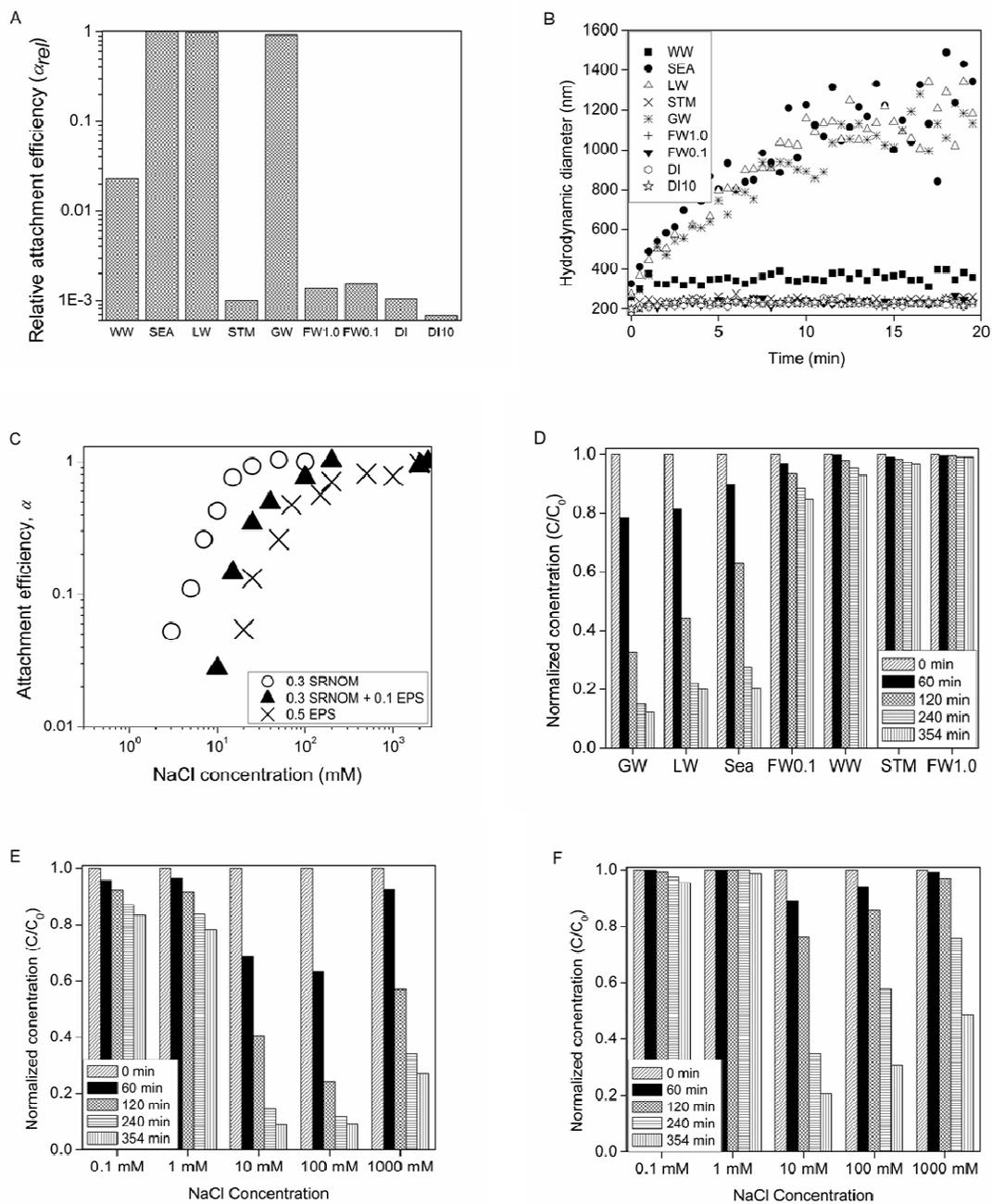
Figure 4. Aggregation kinetics of SWCNT. (A) Attachment efficiencies (α) of P2-P in waters. (B) Aggregation of P2-P in waters as a function of time. (C) Attachment efficiency of P2-P as a function of [NaCl]. Sedimentation of P2-P in (D) natural waters, (E) NaCl + SRNOM, and (F) NaCl + EPS.
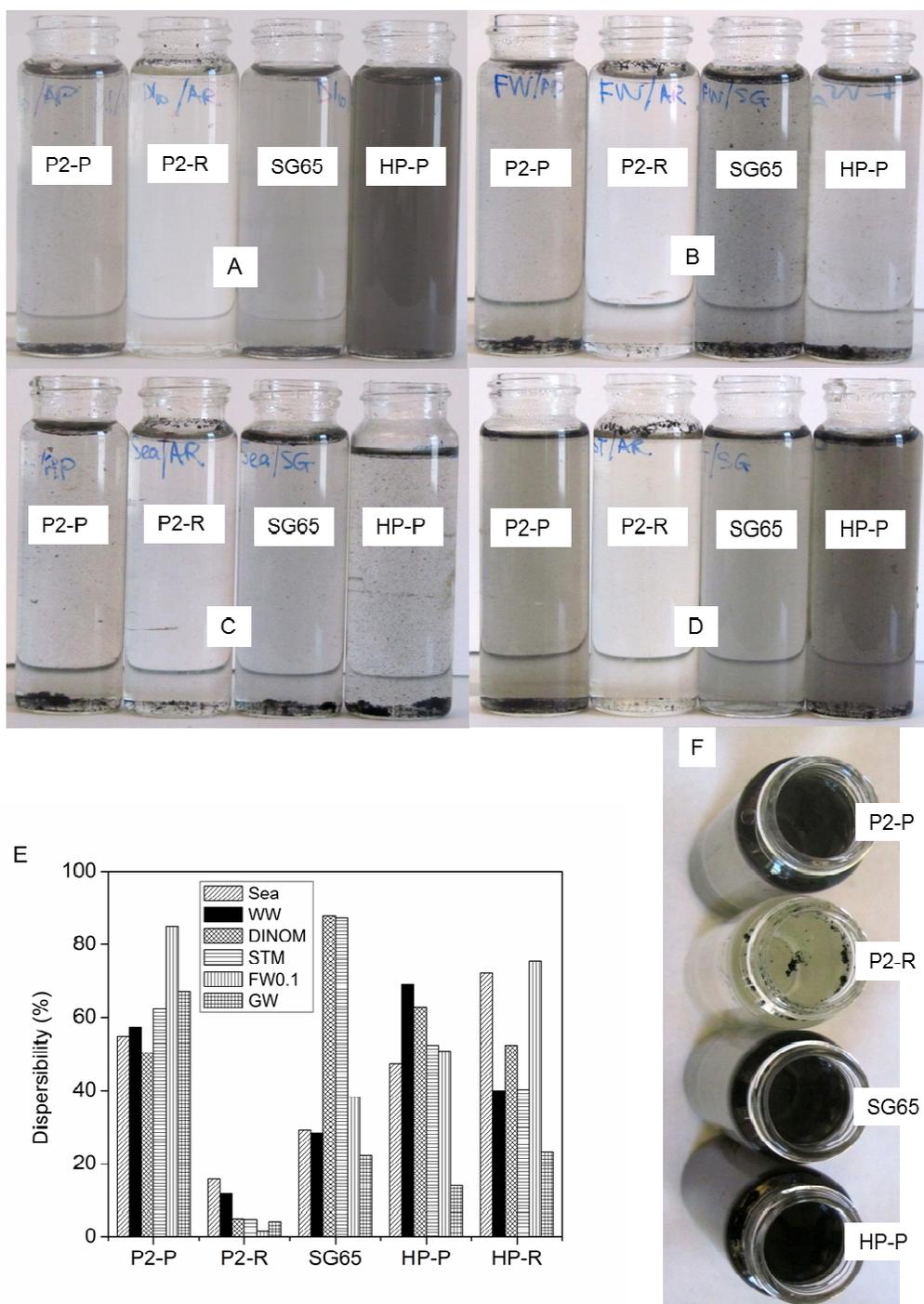
Figure 5. Dispersability of SWCNTs after 4 hr sonication in (A) DINOM, (B) FW1.0, and (C) SEA. (D) and (F) are top and side views of SWCNTs in STM respectively, and (E) mass percent of SWCNTs detected in suspension of selected waters immediately after sonication.
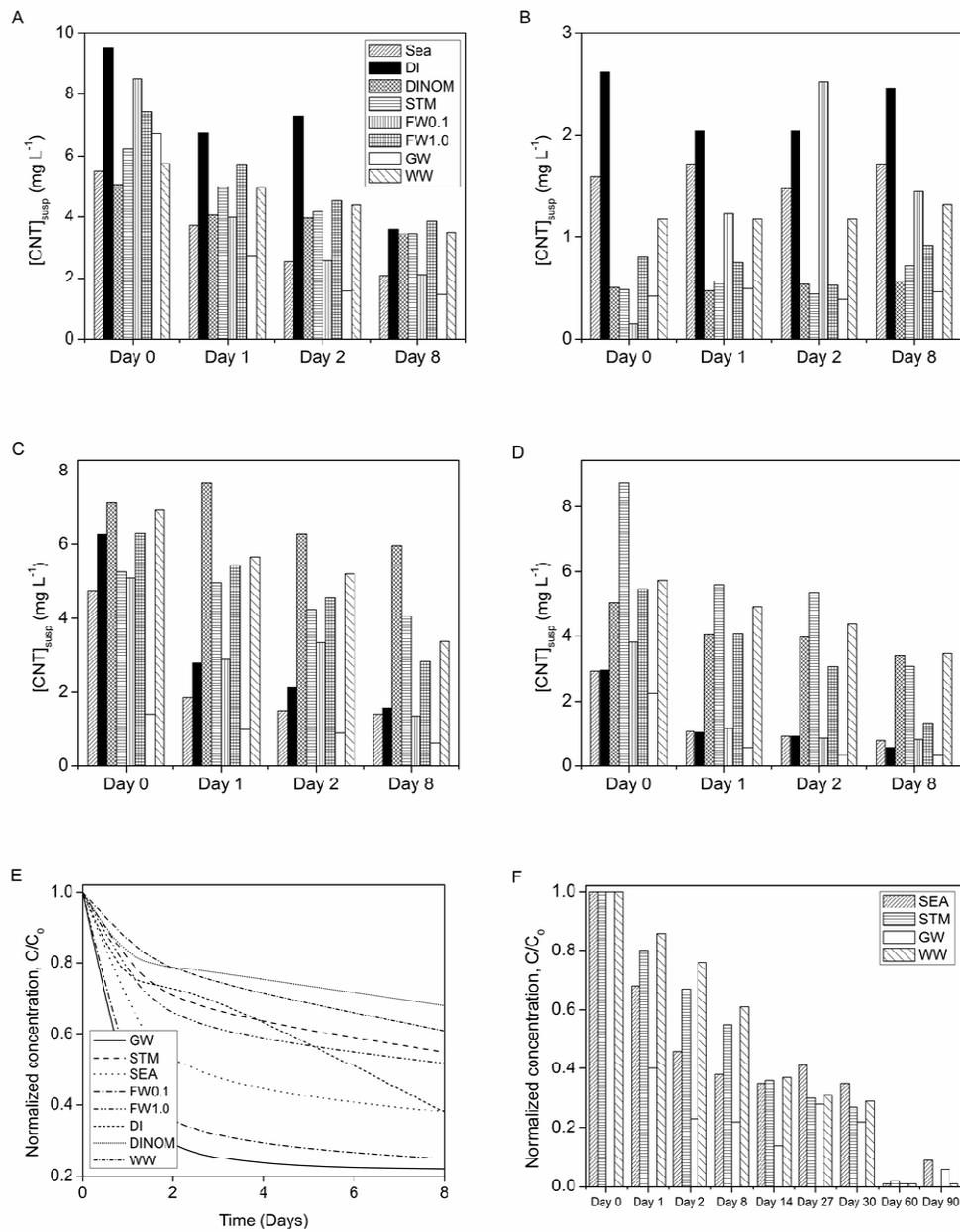
Figure 6. Stability of SWCNTs in waters. Suspended concentrations, [CNT]$_{susp}$, in waters of (A) P2-P, (B) P2-R, (C) HP-P, and (D) SG65 over 8 days. (E) and (F) are normalized concentration of P2-P in waters over 8 days and 90 days respectively.
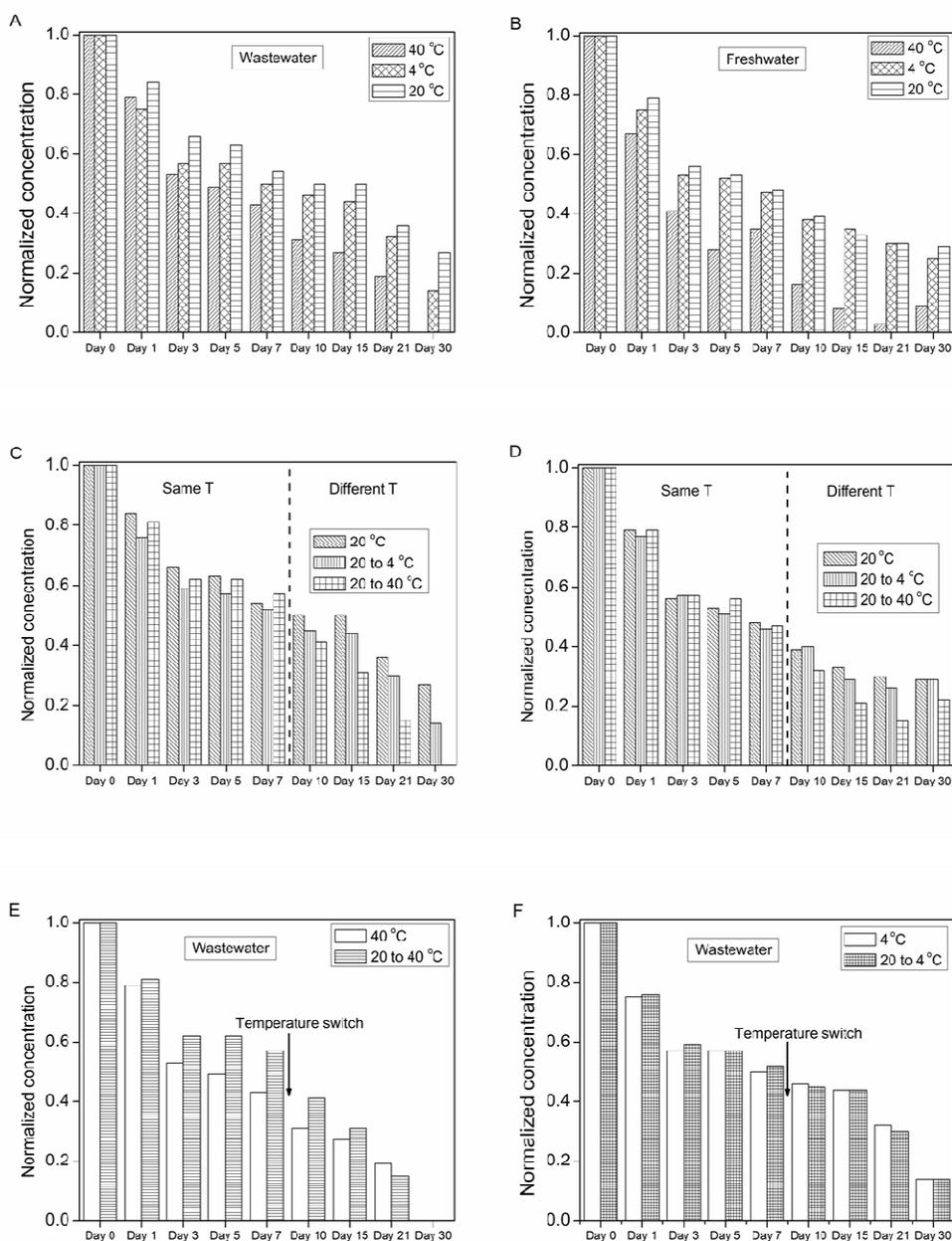
Figure 7. Effect of temperature on SWCNT stability. Stability of P2-P in (A) WW, and (B) FW1.0 at constant temperatures. Comparison of P2-P moved from 20 °C to either 4 °C or 40 °C after 7 days with P2-P kept at 20 °C in (C) WW and (D) FW1.0. Comparison of P2-P in WW kept at constant 4 °C or 40 °C with P2-P in WW moved from 20 °C to either 4 °C, or 40 °C.
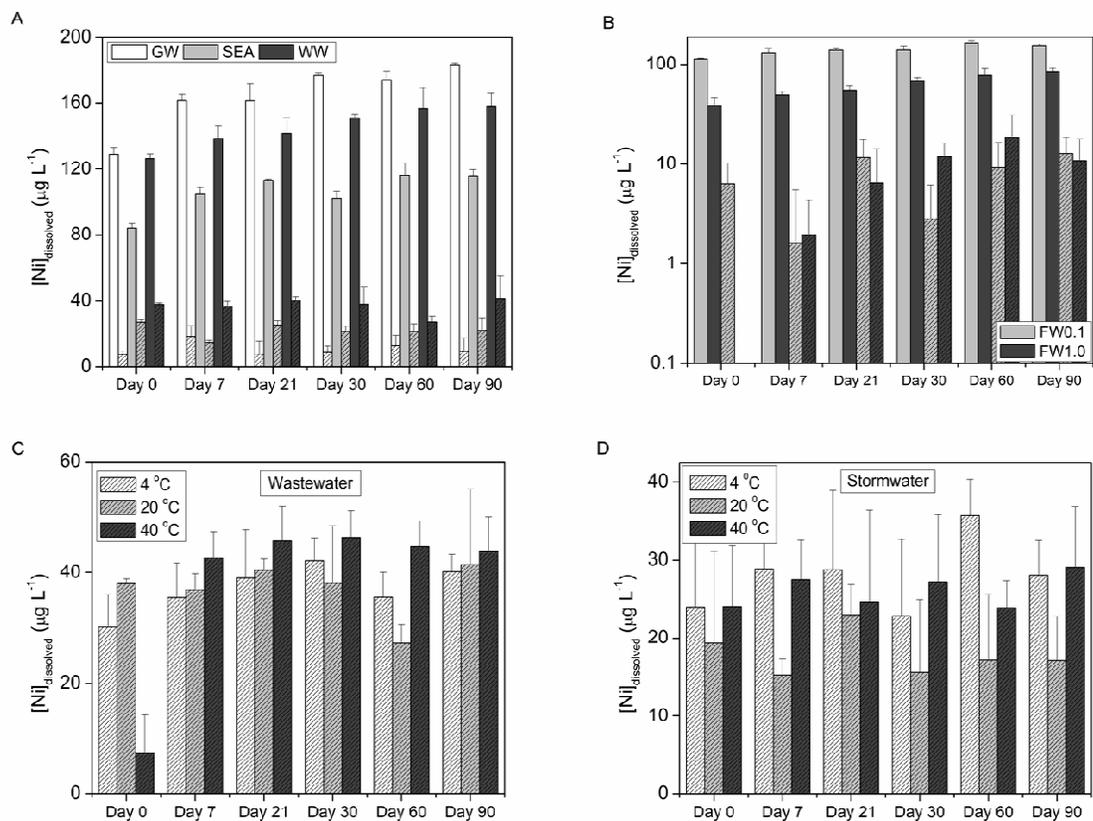
Figure 8. Metal leaching from SWCNTs. Block and patterned bars represent P2-R and P2-P respectively in all plots. (A) Comparison of dissolved Ni leached from P2-R and P2-P in selected waters. (B) Effect of NOM on metal leaching. Effect of temperature on metal leaching in (C) WW, and (D) STM.

Appendix. Supporting Information

Natural waters

Nine waters were used for this study: These include NANOpure water (Barnstead) with and without NOM (designated DINOM and DI respectively). To prepare the water sample with NOM, Suwanee River natural organic matter (SRNOM) isolate (IHSS, St. Paul, MN) was dissolved in NANOpure water and stirred for 24 hr to achieve a stock solution of 500 mg L^{-1}. The stock solution was added to NANOpure water to produce 10 mg SRNOM L^{-1} water. Storm water (STM) was collected from a storm drain destined for a lagoon at University of California, Santa Barbara (UCSB). The lagoon (LW) also periodically receives seawater, and it was used separately in this study. Seawater (SEA) was obtained from UCSB's Marine Science Institute laboratory water system (taken directly from the Pacific Ocean in Santa Barbara, CA). Freshwater growth media was made in accordance with EPA method 1003.0 (EPA 2002) with 0.1 or 1.0 mg SRNOM L^{-1} (FW0.1 and FW1.0 respectively). EDTA was not added to the EPA growth media to avoid potential interference with metal leaching experiments. Wastewater (WW) was collected from the secondary effluent of El Estero Wastewater Treatment Plant (Santa Barbara). Synthetic groundwater (GW) was prepared by adding salts to NANOpure water. (Schnabel *et al.* 1997). All the salts used were ACS grade, and purchased from Fisher Scientific. DI, DINOM, FW1.0, FW0.1, and GW were adjusted to pH 7.0 with HCl and NaOH (Fisher Scientific). All the waters were filtered with 0.1 µm filter (Millipore, Ireland) and stored in 4 °C prior to the experiments.

Water samples were characterized by measuring total organic carbon (TOC) using a Shimadzu TOC 5000 analyzer. The pH and oxidation-reduction (redox) potential were measured using a HACH HQ 40d portable meter. Conductivity was measured with a

Traceable bench conductivity meter (Fisher Scientific). UV_{254} and UV_{550} were obtained

using a Shimadzu Biospec 1601. Metal contents of water samples were quantified via ICP-

AES (iCAP 6300, Thermo Scientific).

EPS production and extraction technique

An axenic culture of *Isochrysis galbana* was obtained from the Provasoli-Guillard

National Center for Culture of Marine Phytoplankton, and was maintained in standard media

(f/2) made with autoclaved filtered natural seawater. Algae were incubated under cool white

fluorescent lights (14:10 light:dark, 100–120 μmol m^{-2} s^{-1}) at 20 °C with aeration until the

stationary phase prevailed (Miller *et al.* 2012). Cell densities were measured using a

fluorometer (Trilogy, Turner Designs), which was converted to cell numbers using a

standard curve based on counts done with a hemacytometer (Reichert, Buffalo NY). When

the cells reached the stationary growth phase they were centrifuged 15 min at 2500g and 4

°C (RC 5B Plus, Sorvall, CT). The supernatant was collected and then filtered with 0.22 μm

PES filters (Thermo Fisher Scientific) under sterile conditions. This fraction contained

soluble (unattached) EPS. To remove the residual salts from the growth medium and low

molecular-weight metabolites, EPS was dialyzed against NANOpure water for 96 hr at 4 °C

using regenerated cellulose tubular membrane of 3500 Da cut-off (Fischer Scientific), which

had been treated with $NaHCO_3$ and Na_2EDTA to remove residues. The dialysis NANOpure

water was renewed daily, and dialyzed EPS were stored in 4 °C until use. EPS was

characterized by measuring carbohydrate and protein concentrations using anthrone method

(Morris 1948), and modified Lowry Protein Assay Kit (Pierce Biotechnology, Rockford, IL)

(Legler *et al.* 1985) respectively. Hydrodynamic diameter of EPS was determined using the
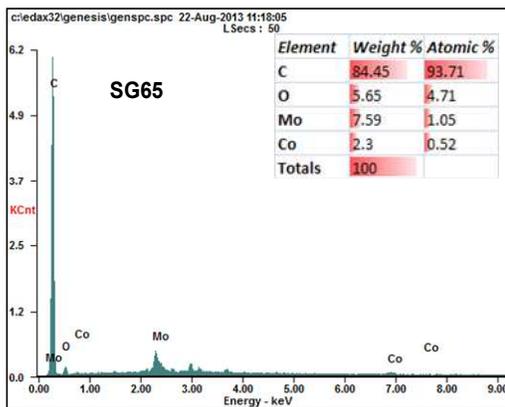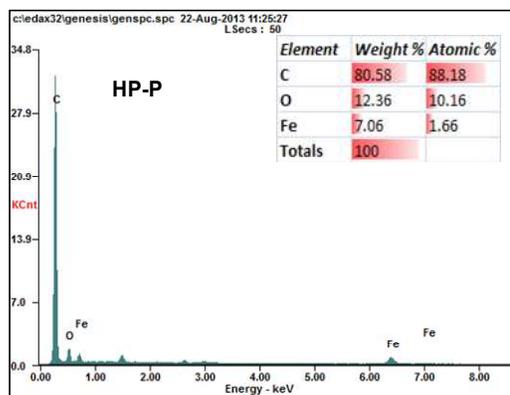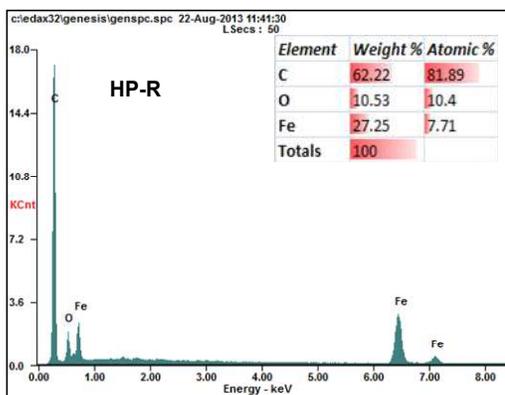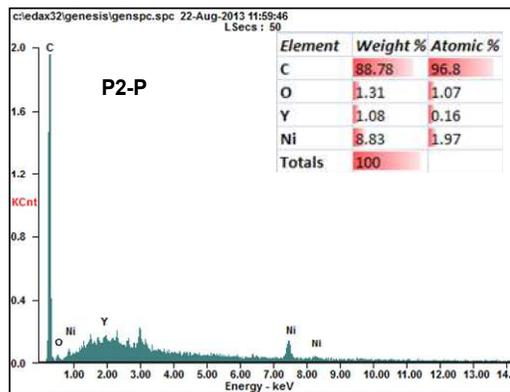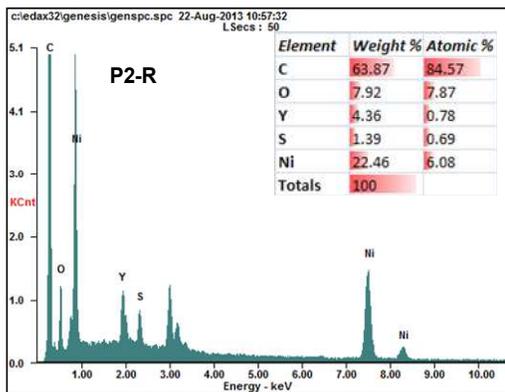
Zetasizer Nano-ZS90.

Figure S1. Energy-dispersive X-ray spectroscopy (EDS) of five carbon nanotubes used in this study

Table S1. Average concentrations of dissolved metal mobilized from five SWCNTs in x 10^2 µg L^{-1}. ND = non-detect.

Natural water	SWCNT	P2-R		P2-P		HP-R	HP-P	SG65	
	[Me] (x 10^2 µg L^{-1})	Ni	Y	Ni	Y	Fe	Fe	Co	Mo
Groundwater	Day 0	1.291	0.180	0.075	0.041	1.116	0.020	ND	0.205
	Day 3	1.572	0.264	0.104	0.001	0.293	0.085	0.044	0.279
	Day 7	1.614	0.280	0.182	0.018	0.047	0.092	ND	0.273
	Day 21	1.613	0.259	0.078	0.011	0.298	0.048	0.023	0.412
	Day 30	1.767	0.286	0.090	0.002	0.009	0.027	0.001	0.437
	Day 60	1.741	0.256	0.128	ND	0.107	0.536	ND	0.488
	Day 90	1.834	0.110	0.096	0.032	0.310	0.328	0.020	0.586
Stormwater	Day 0	0.940	0.098	0.194	0.016	1.245	ND	0.012	0.273
	Day 3	0.957	0.059	0.258	ND	0.163	0.127	0.008	0.293
	Day 7	0.970	0.089	0.152	0.028	0.073	ND	0.012	0.315
	Day 21	1.051	0.066	0.229	0.018	0.297	0.515	0.014	0.439
	Day 30	1.015	0.102	0.156	0.014	0.266	0.434	0.018	0.445
	Day 60	1.161	0.074	0.172	ND	0.398	0.828	ND	0.534
	Day 90	1.064	0.053	0.172	0.031	0.248	0.532	0.008	0.547
Seawater	Day 0	0.842	0.155	0.271	0.038	0.922	0.292	ND	0.248
	Day 3	0.916	0.158	0.168	0.023	0.589	0.532	0.001	0.298
	Day 7	1.046	0.198	0.148	0.039	0.234	0.365	ND	0.286
	Day 21	1.133	0.204	0.255	0.063	0.063	0.103	0.003	0.426
	Day 30	1.023	0.216	0.211	0.052	0.055	0.129	ND	0.406
	Day 60	1.160	0.198	0.212	0.027	0.232	0.296	ND	0.516
	Day 90	1.157	0.257	0.221	0.059	0.094	0.188	ND	0.523
Freshwater + NOM0.1	Day 0	1.137	0.048	0.064	ND	13.574	0.172	0.080	0.172
	Day 3	1.272	0.022	0.121	ND	0.358	0.322	0.068	0.192
	Day 7	1.307	0.017	0.016	0.007	0.161	0.247	0.055	0.183
	Day 21	1.387	0.026	0.117	0.013	0.186	0.278	0.050	0.320
	Day 30	1.392	0.030	0.028	ND	0.146	0.406	0.024	0.293
	Day 60	1.675	0.039	0.093	ND	0.361	0.511	0.024	0.378
	Day 90	1.531	0.016	0.128	0.026	0.112	0.354	0.022	0.381
Freshwater + NOM1.0	Day 0	0.388	0.053	ND	0.025	1.101	0.330	0.033	0.215
	Day 3	0.447	0.037	0.001	0.011	0.402	0.485	0.025	0.212
	Day 7	0.491	0.032	0.020	0.008	0.414	0.296	0.023	0.201
	Day 21	0.555	0.029	0.065	0.037	0.303	0.237	0.029	0.311
	Day 30	0.688	0.064	0.120	0.024	0.217	0.483	0.028	0.310

	Day 60	0.775	0.017	0.186	ND	0.539	0.425	ND	0.395
	Day 90	0.844	0.051	0.109	0.025	0.254	0.544	0.053	0.420
DI	Day 0	0.031	0.028	ND	0.016	0.253	0.336	0.016	0.183
	Day 3	0.106	0.014	0.062	ND	0.193	0.170	0.003	0.213
	Day 7	0.178	ND	0.012	0.019	0.070	0.067	0.019	0.187
	Day 21	0.264	ND	0.001	0.019	0.208	0.033	0.051	0.278
	Day 30	0.045	0.012	0.042	0.007	0.015	ND	ND	0.274
	Day 60	0.244	0.019	0.076	ND	0.350	0.157	0.006	0.392
	Day 90	0.167	0.017	0.051	0.019	0.155	0.321	0.006	0.446
DI + NOM10	Day 0	0.886	0.178	0.120	0.026	0.514	0.916	0.045	0.179
	Day 3	1.027	0.160	0.045	ND	0.679	0.720	0.035	0.217
	Day 7	0.901	0.160	0.123	0.009	0.966	0.475	0.049	0.158
	Day 21	1.081	0.161	0.064	0.028	0.550	1.395	0.023	0.249
	Day 30	0.940	0.192	0.053	0.024	0.467	0.631	ND	0.240
	Day 60	1.134	0.180	0.017	0.027	0.631	0.873	0.017	0.340
	Day 90	1.323	0.146	0.085	0.050	0.577	2.334	ND	0.316
Wastewater	Day 0	1.265	0.081	0.380	0.017	0.327	0.960	0.037	0.223
	Day 3	1.296	0.058	0.348	0.002	0.399	0.588	0.054	0.235
	Day 7	1.385	0.047	0.370	0.028	0.352	0.246	0.024	0.237
	Day 21	1.417	0.055	0.404	0.033	0.256	0.233	0.006	0.348
	Day 30	1.509	0.015	0.382	0.022	0.050	0.056	ND	0.343
	Day 60	1.568	0.026	0.272	0.002	0.290	0.295	ND	0.403
	Day 90	1.580	0.035	0.415	0.031	0.046	0.298	0.001	0.451
Lagoon	Day 0	0.418	0.080	0.087	0.049	0.179	0.735	0.014	0.300
	Day 3	0.443	0.083	0.131	0.003	0.076	0.104	0.053	0.293
	Day 7	0.444	0.086	0.253	0.059	0.055	0.004	0.012	0.339
	Day 21	0.368	0.063	0.145	0.082	ND	0.066	ND	0.511
	Day 30	0.473	0.085	0.045	0.040	ND	ND	ND	0.457
	Day 60	0.588	0.073	0.208	0.005	0.269	4.576	0.010	0.545
	Day 90	0.530	0.123	0.190	0.072	0.118	0.159	ND	0.532

References

Adeleye A.S., Keller A.A., Miller R.J. & Lenihan H.S. (2013). Persistence of commercial nanoscaled zero-valent iron (nZVI) and by-products. *J Nanopart Res*, 15.

Bennett S.W., Adeleye A., Ji Z. & Keller A.A. (2013). Stability, metal leaching, photoactivity and toxicity in freshwater systems of commercial single wall carbon nanotubes. *Water research*, 47, 4074-85.

Chandra A. & Bagchi B. (2000). Beyond the Classical Transport Laws of Electrochemistry: New Microscopic Approach to Ionic Conductance and Viscosity. *J. Phys. Chem. B*, 104, 9067-9080.

Chen K.L. & Elimelech M. (2009). Relating Colloidal Stability of Fullerene (C60) Nanoparticles to Nanoparticle Charge and Electrokinetic Properties. *Environmental Science & Technology*, 43, 7270-7276.

Davis J.A. (1984). Complexation of Trace-Metals by Adsorbed Natural Organic-Matter. *Geochimica Et Cosmochimica Acta*, 48, 679-691.

Dries J., Bastiaens L., Springael D., Kuypers S., Agathos S.N. & Diels L. (2005). Effect of humic acids on heavy metal removal by zero-valent iron in batch and continuous flow column systems. *Water research*, 39, 3531-3540.

El-Dessouky H.T.E.H.M. (2002). *Fundamentals of salt water desalination*. Elsevier, Amsterdam; New York.

EPA U.S. (2002). Method 1003.0 in Short-Term Methods for Estimating the Chronic Toxicity of Effluents and Receiving Waters to Freshwater Organisms. In. US EPA Washington DC.

Flemming H.-C., Neu T.R. & Wozniak D.J. (2007). The EPS matrix: the "house of biofilm cells". *Journal of Bacteriology*, 189, 7945-7947.

Ge C.C., Li W., Li Y.F., Li B., Du J.F., Qiu Y., Liu Y., Gao Y.X., Chai Z.F. & Chen C.Y. (2011). Significance and Systematic Analysis of Metallic Impurities of Carbon Nanotubes Produced by Different Manufacturers. *Journal of Nanoscience and Nanotechnology*, 11, 2389-2397.

Ge C.C., Li Y., Yin J.J., Liu Y., Wang L.M., Zhao Y.L. & Chen C.Y. (2012). The contributions of metal impurities and tube structure to the toxicity of carbon nanotube materials. *Npg Asia Materials*, 4.

Herzhaft B. & Guazzelli E. (1999). Experimental study of the sedimentation of dilute and semi-dilute suspensions of fibres. *Journal of Fluid Mechanics*, 384, 133-158.

Huang Y.Y. & Terentjev E.M. (2012). Dispersion of Carbon Nanotubes: Mixing, Sonication, Stabilization, and Composite Properties. *Polymers*, 4, 275-295.

Hung C.C., Tang D.G., Warnken K.W. & Santschi P.H. (2001). Distributions of carbohydrates, including uronic acids, in estuarine waters of Galveston Bay. *Marine Chemistry*, 73, 305-318.

Hyung H., Fortner J.D., Hughes J.B. & Kim J.-H. (2007). Natural Organic Matter Stabilizes Carbon Nanotubes in the Aqueous Phase. *Environmental Science & Technology*, 41, 179-184.

Islam M.F., Rojas E., Bergey D.M., Johnson A.T. & Yodh A.G. (2003). High Weight Fraction Surfactant Solubilization of Single-Wall Carbon Nanotubes in Water. *Nano Lett.*, 3, 269-273.

Keller A.A., McFerran S., Lazareva A. & Suh S. (2013). Global life cycle releases of engineered nanomaterials. *Journal of Nanoparticle Research*, 15, 1-17.

Keller A.A., Wang H., Zhou D., Lenihan H.S., Cherr G., Cardinale B.J., Miller R. & Ji Z. (2010). Stability and Aggregation of Metal Oxide Nanoparticles in Natural Aqueous Matrices. *Environmental Science & Technology*, 44, 1962-1967.

Lam C., James J., McCluskey R. & Hunter R. (2004). Pulmonary toxicity of single-wall carbon nanotubes in mice 7 and 90 days after intratracheal instillation. *Toxicol. Sci.*, 77, 126-134.

Legler G., Mullerplatz C.M., Mentgeshettkamp M., Pflieger G. & Julich E. (1985). On the Chemical Basis of the Lowry Protein Determination. *Analytical Biochemistry*, 150, 278-287.

Leys F.E., Amovilli C., Howard I.A., March N.H. & Rubio A. (2003). Surface charge model of a carbon nanotube: self-consistent field from Thomas–Fermi theory. *Journal of Physics and Chemistry of Solids*, 64, 1285-1288.

Li Z., Lin W., Moon K.-S., Wilkins S.J., Yao Y., Watkins K., Morato L. & Wong C. (2011). Metal catalyst residues in carbon nanotubes decrease the thermal stability of carbon nanotube/silicone composites. *Carbon*, 49, 4138-4148.

Lin D., Liu N., Yang K., Xing B. & Wu F. (2010). Different stabilities of multiwalled carbon nanotubes in fresh surface water samples. *Environmental Pollution*, 158, 1270-1274.

Lin D.H., Tian X.L., Li T.T., Zhang Z.Y., He X. & Xing B.S. (2012). Surface-bound humic acid increased Pb2+ sorption on carbon nanotubes. *Environmental Pollution*, 167, 138-147.

Miao A.-J., Schwehr K.A., Xu C., Zhang S.-J., Luo Z., Quigg A. & Santschi P.H. (2009). The algal toxicity of silver engineered nanoparticles and detoxification by exopolymeric substances. *Environmental Pollution*, 157, 3034-3041.

Miller R.J., Bennett S., Keller A.A., Pease S. & Lenihan H.S. (2012). TiO2 nanoparticles are phototoxic to marine phytoplankton. *Plos One*, 7, e30321.

Morris D.L. (1948). Quantitative Determination of Carbohydrates with Dreywoods Anthrone Reagent. *Science*, 107, 254-255.

Mwangi J.N., Wang N., Ingersoll C.G., Hardesty D.K., Brunson E.L., Li H. & Deng B.L. (2012). Toxicity of carbon nanotubes to freshwater aquatic invertebrates. *Environmental Toxicology and Chemistry*, 31, 1823-1830.

Pal A. & Paul A. (2008). Microbial extracellular polymeric substances: central elements in heavy metal bioremediation. *Indian journal of microbiology*, 48, 49-64.

Saleh N.B., Pfefferle L.D. & Elimelech M. (2008). Aggregation Kinetics of Multiwalled Carbon Nanotubes in Aquatic Systems: Measurements and Environmental Implications. *Environmental Science & Technology*, 42, 7963-7969.

Saleh N.B., Pfefferle L.D. & Elimelech M. (2010). Influence of Biomacromolecules and Humic Acid on the Aggregation Kinetics of Single-Walled Carbon Nanotubes. *Environmental Science & Technology*, 44, 2412-2418.

Sano M., Okamura J. & Shinkai S. (2001). Colloidal Nature of Single-Walled Carbon Nanotubes in Electrolyte Solution: The Schulze−Hardy Rule. *Langmuir*, 17, 7172-7173.

Schnabel W., Dietz A., Burken J., Schnoor J. & Alvarez P. (1997). Uptake and transformation of trichloroethylene by edible garden plants. *Water research*, 31, 816-824.

Schwyzer I., Kaegi R., Sigg L., Magrez A. & Nowack B. (2011). Influence of the initial state of carbon nanotubes on their colloidal stability under natural conditions. *Environmental Pollution*, 159, 1641-1648.

Schwyzer I., Kaegi R., Sigg L. & Nowack B. (2013). Colloidal stability of suspended and agglomerate structures of settled carbon nanotubes in different aqueous matrices. *Water research*, 47, 3910-3920.

Schwyzer I., Kaegi R., Sigg L., Smajda R., Magrez A. & Nowack B. (2012). Long-term colloidal stability of 10 carbon nanotube types in the absence/presence of humic acid and calcium. *Environmental Pollution*, 169, 64-73.

Thostenson E. & Chou T. (2003). On the elastic properties of carbon nanotube-based composites: modelling and characterization. *Journal of Physics D-Applied Physics*, 36, 573-582.

Tian X.L., Li T.T., Yang K., Xu Y., Lu H.F. & Lin D.H. (2012). Effect of humic acids on physicochemical property and Cd(II) sorption of multiwalled carbon nanotubes. *Chemosphere*, 89, 1316-1322.

Tong Z., Bischoff M., Nies L.F., Myer P., Applegate B. & Turco R.F. (2012). Response of Soil Microorganisms to As-Produced and Functionalized Single-Wall Carbon Nanotubes (SWNTs). *Environmental Science & Technology*, 46, 13471-13479.

Velzeboer I., Peeters E. & Koelmans A.A. (2013). Multiwalled carbon nanotubes at environmentally relevant concentrations affect the composition of benthic communities. *Environmental Science & Technology*.

Zhou D., Bennett S.W. & Keller A.A. (2012). Increased mobility of metal oxide nanoparticles due to photo and thermal induced disagglomeration. *Plos One*, 7, e37363.

Zhou D. & Keller A.A. (2010). Role of morphology in the aggregation kinetics of ZnO nanoparticles. *Water research*, 44, 2948-2956.

Chapter 3. Influence of Extracellular Polymeric Substances on the Long-Term Fate, Dissolution and Speciation of Copper-Based Nanoparticles[1]

3.1. Introduction

Global production of copper-based nanoparticles (CBNPs) was estimated at ~200 metric ton/yr in 2010, and is increasing (Keller *et al.* 2013). CBNPs have found use in cosmetics, pigments, paints and coatings, electronics, and pesticides (Wang *et al.* 1999; Cioffi *et al.* 2005; Ren *et al.* 2009). These applications may lead to direct exposure of CBNPs to the environment due to normal use, product wear-and-tear, and/or end-of-life disposal (Keller *et al.* 2013). Toxicity of CBNPs and composites to organisms has been demonstrated (Tranquada *et al.* 1995; Cioffi *et al.* 2005; Griffitt *et al.* 2007; Shi *et al.* 2011; Hanna *et al.* 2013). It is therefore important to understand the long term fate and transformations of these materials in aquatic systems in order to predict exposure to at-risk organisms.

Stability and dissolution of engineered nanoparticles (ENPs) depend on ionic strength (IS), pH, and natural organic material (NOM) (Flemming & Trevors 1989; Keller *et al.* 2010; Adeleye *et al.* 2013a; Bennett *et al.* 2013). Rapid aggregation of nano-Cu was reported in freshwater (Griffitt *et al.* 2007). The authors also found that less than 0.1% of the nano-Cu dissolved in 48 hr in the freshwater media used (pH 8.2). 98% dissolution of nano-Cu was however reported at pH 6 in "uterine-fluid" after a week (Cai *et al.* 2005), demonstrating the importance of pH and media composition on CBNPs' dissolution. Mudunkotuwa and coworkers reported increased dissolution of aged and new CBNPs in the presence of organic

---

acids (Mudunkotuwa *et al.* 2012). Similarly, Worthington *et al.* showed that the chitosan improved stability and dissolution of nano-Cu.(Worthington *et al.* 2013). To our knowledge, no studies have previously investigated the effects of naturally-occurring NOM such as extracellular polymeric substances (EPS) on the stability and dissolution of CBNPs. EPS are synthesized by microorganisms, which are abundant in natural aquatic systems. EPS are mainly composed of polysaccharides, proteins, nucleic acids, and other polymers; and their composition may vary spatially and temporally even within the same species (Flemming *et al.* 2007). EPS may interact with ENPs, thus affecting their fate and transformation (Adeleye & Keller 2014). Additionally, the long-term fate and transformation of CBNPs in aqueous media has not been reported in the literature.

Studies commonly investigate the aggregation of ENPs in order to predict their environmental fate. In this study however, we also investigated the fate of a commercial $Cu(OH)_2$-based product, Kocide 3000 (denoted Kocide). We introduced Kocide, nano-Cu and nano-CuO to a series of aqueous solutions with the goal of investigating the effect of EPS, pH, and IS on (1) stability; and (2) dissolution and speciation over 90 days. To understand the role of EPS, studies were also conducted in the presence of Suwannee River natural organic matter (SRN).

3.2. Material and Methods

3.2.1. Copper-based Nanoparticles

Nano-CuO (Sigma Aldrich), nano-Cu (US Research Nanomaterials) and Kocide (Dupont) particles were used as received. The size and surface charge were characterized by measuring initial hydrodynamic diameter (HDD) and zeta (ζ) potential using a Malvern

Zetasizer Nano-ZS90. HDD was an average of 7 measurements with each measurement reflecting 3 runs. Isoelectric point (IEP) was determined by titrating CBNP suspensions with dilute HCl and NaOH. Copper content (wt. %) of particles was determined via ICP-AES (iCAP 6300, Thermo Scientific). Further characterizations were done via X-ray diffraction (XRD, Bruker D8 Advance), X-ray photoelectron spectroscopy (XPS, Kratos Axis Ultra), thermogravimetric analysis (Mettler STARe TGA/sDTA851e), Brunau–Emmet–Teller (BET) surface area analysis (Micromeritics TriStar 3000 porosimeter), helium density analysis (Micromeritics AccuPyc II 1340 pycnometer) and scanning electron microscopy (FEI XL30 Sirion equipped with an EDAX APOLLO X probe for energy-dispersive X-ray spectroscopy, EDS).

3.2.2. Stock Suspension Preparation and EPS Characterization

200 mg/L stock suspensions of CBNPs were bath-sonicated (Branson 2510) for 30 min to disperse the particles. 100 mM buffer stocks (pH 4 = acetate, pH 7 and 11 = phosphate) were prepared and passed through 0.1 μm filter prior to use (final buffer concentration was 0.5 mM for all experiments). A SRN stock solution was prepared as described in Supporting Information (SI) in Appendix. Soluble EPS was extracted from a marine phytoplankton, *Isochrysis galbana,* as described in a previous study (Adeleye & Keller 2014) and summarized in SI.

EPS was characterized by measuring carbohydrate and protein concentrations using anthrone method and modified Lowry protein assay respectively (Morris 1948; Legler *et al.* 1985). Total organic carbon (TOC) was determined using a Shimadzu 5000A TOC analyzer. Hydrodynamic diameter of EPS was determined using the Zetasizer. ζ potential of EPS at the conditions of this study and titrimetry were also done using the Zetasizer. Infrared spectroscopy of EPS and SRN was obtained using a Nicolet iS10 FTIR spectrometer with a

diamond ATR crystal. Interferograms were obtained by taking 256 scans with a resolution of 2 cm^{-1}.

3.2.3. Aggregation and Sedimentation Kinetics

Aggregation and sedimentation kinetics were studied using the Zetasizer and time-resolved optical absorbency (Shimadzu 1601 UV-Vis spectrophotometer) respectively (Adeleye & Keller 2014). Detailed information on aggregation, CCC determination and sedimentation experiments are in SI.

3.2.4. Dissolution, Speciation, and Suspended Cu

Dissolution of each particle was investigated at 10 mg/L in 15 conditions (Table S1) at different pH (4, 7, and 11), IS (1, 10, and 100 mM NaCl), and NOM conditions (EPS, SRN or neither). A pH of 11 is not commonly found in the environment but has been observed in arid soils and the corresponding groundwater and lakes (Grant & Jones 2000). Measured aliquots of CBNPs stocks, EPS/SRN/neither, NaCl, and buffer were vortexed to prepare each condition, and transferred directly into Millipore Amicon® Ultra-4 10 kDa centrifugal filter tubes (maximum pore size ~4 nm), which were kept at 20 °C for increasing time periods (0, 1, 7, 14, 21, 30, 60 and 90 days). To determine dissolution and speciation, the ultrafiltration tubes were centrifuged for 40 min (Sorvall RC 5B Plus) with a swinging bucket rotor at 4000 g. A fraction of the filtrate was analyzed for free cupric ion (f-Cu^{2+}) using an ion selective electrode (Cole Parmer). The electrode was calibrated within every hour of use, and lighting was kept constant to minimize the effect of any photoinduced reactions at the electrode probe surface that would cause measurement error. The remaining filtrate fraction was digested and analyzed for total dissolved copper ([Cu]$_{diss}$) via ICP-AES as described previously (Adeleye *et al.* 2013a; Su *et al.* 2014). Complexed cupric ion (c-Cu^{2+}) in CuO and Kocide was determined by mass balance: [Cu]$_{diss}$ – f-Cu^{2+}. Since nano-Cu

may also form some Cu^+, the mass balance yielded non-f-Cu^{2+} species. Further speciation and complexation of Cu at equilibrium were estimated using Visual MINTEQ 3.0, which was downloaded from http://vminteq.lwr.kth.se/ and used without modification. CBNPs were input as finite solids based on their copper content and speciation. Kocide was modeled as $Cu(OH)_2$, nano-Cu was modeled as Cu metal, and nano-CuO was modeled as Tenorite(c). More details about MINTEQ calculations are in the SI.

Additional experiments were set up similar to the dissolution and speciation experiments, but aliquots were not filtered prior to digestion and ICP-AES analyses. In this way, total copper in the supernatant, $[Cu]_{total}$ (dissolved + suspended) could be determined. Suspended copper in the supernatant, $[Cu]_{susp}$, was derived from $[Cu]_{total} - [Cu]_{diss}$. The pH of suspensions was monitored over time.

3.3. Results and Discussion

3.3.1. Nanoparticle and EPS Characterization

Major physicochemical properties of CBNPs are presented in Table 1. Nano-CuO appeared as aggregates of 30-100 nm-size particles, and nano-Cu were nanosized (<100 nm) particles that were mostly aggregated to 500-1000 nm. Kocide particles were 20-200 μm in diameter. SEM images and size distribution histograms of the CBNPs are provided in SI Figures S1- S2, respectively. Despite its large size, Kocide had the largest BET surface area (Table 1) due to surface roughness and porosity. Size distributions of CBNPs in DI at pH 7 are presented in Figure 1. Nanosized particles were detected in the Kocide suspension, suggesting that Kocide particles were broken up in aqueous media. Kocide was negatively charged in the range of pH studied, so its IEP could not be determined. IEP of nano-CuO and nano-Cu was pH 6.3 and 2.1 respectively (Figure 1D). ζ potential of CBNPs in the

65

conditions of this experiment (buffered solution) are shown in Table S2. XPS, TGA, and

XRD data are shown in SI Figures. S3-S5. For TGA, the weight loss in the 50-150 °C

temperature range, which corresponds to adsorbed water and surface hydroxyl group was

high for Kocide (11%) relative to nano-Cu (0.14%) and nano-CuO (0.23%). In addition,

TGA and EDS results (SI Figure S6) suggest high content of carbon (up to 21%) in Kocide,

possibly a binder for the particles.

The carbohydrate/protein ratio of *I. galbana*-derived EPS was 3.36. Average HDD and $\square$

potential of EPS at pH 7 were 204 nm and -24 mV respectively. The net surface charge of

EPS and SRN was negative across the range of pH studied (Figure 2A) with SRN being

more negative. The FTIR spectra of EPS and SRN are shown in Figure 2B.

3.3.2. Effects of EPS on HDD and Zeta (ζ) Potential

HDD of nano-Cu and Kocide indicated micron-sized particles with broad size

distribution as indicated by polydispersity index (PDI) > 0.7 (SI Figure S7). High

polydispersity limits the reliability of nanoparticle HDD values (Malvern 2008, 2011), so

HDD of nano-Cu and Kocide were not used for further analyses. Nano-CuO was relatively

stable in water, with an average HDD of 280 nm. Nano-CuO was however not overly

monodisperse as indicated by a PDI in the range from 0.1 to 0.4 (Malvern 2008; Nidhin *et

al.* 2008; Malvern 2011). HDD of nano-CuO increased significantly (t = 2.929, *p* = 0.01)

from 280 nm to 308 nm in the presence of EPS (SI Figure S7), probably due to EPS coating

the particles. There was however no significant change in size of nano-CuO in the presence

of SRN (t = 0.199, *p* = 0.85). EDS confirmed the presence of carbon on nano-CuO in the

presence of both EPS and SRN, and the absence of carbon when neither was present.

At pH 7 (buffered solution) ζ potential (in mV) of nano-CuO decreased in magnitude

from -34 to -25 in the presence of EPS (ζ potential$_{EPS}$ = -24), and increased in magnitude to -

41 in the presence of SRN (ζ potential$_{SRN}$ = -44). ζ potential (mV) of nano-CuO at pH 4 changed from +43 in buffered solution to -22 and -26 when EPS and SRN were present, respectively. A similar but weaker trend was observed for nano-Cu and Kocide (Figure 3). Patterns in HDD and ζ potential of nano-CuO suggest that 5 mg-C/L EPS effectively coated the surface of the particles, which imparted steric stabilization in addition to influencing the surface charge (electrosteric stabilization). To confirm this, measurement of nano-CuO ζ potential at pH 7 in increasing amounts of EPS (0-5 mg-C/L) showed a gradual change from -34 to -25, which is approximately equal to the ζ potential of EPS. Similar analyses suggest that nano-Cu and Kocide were not completely coated by the amount of EPS used in this study (probably due to their large size in aqueous media) and that SRN mainly imparted electrostatic stabilization at the concentration used (5 mg/L).

3.3.3. Effects of EPS on Aggregation and Sedimentation Kinetics

Aggregation kinetics and CCC were not determined for nano-Cu and Kocide due to the high polydispersity of the particles. The CCC of nano-CuO was ~40 mM NaCl at pH 7 in the absence of NOM (SI Figure S8). CCC increased to ~75 mM in the presence of 0.25 mg/L SRN but could not be determined in the presence of EPS due to steric stabilization (which typically does not follow the classical DLVO theory (Grasso *et al.* 2002)). Similarly, nano-CuO was relatively stable up to 10 mM at pH 11 in the absence of NOM. Stability decreased at pH 4 as nano-CuO aggregated rapidly at IS $\geq$ 10 mM (SI Figure S9), probably due to rapid dissolution (Cu^{2+} ions released from dissolving particles may have subtle effects on electrostatic double layer/repulsion). Similarly, particles sedimented faster at pH 4 than pH 7 or 11: We observed 64%, 40%, and 39% sedimentation after 6 hr when nano-CuO was suspended in 10 mM NaCl at pH 4, 7, and 11 respectively (SI Figure S9). The HDD at pH 7

was not significantly different from the HDD at pH 4 (t = 2.139, p = 0.05), and pH 11 (t = 0.085, p = 0.93) as seen in SI Figure S10.

Among the three particles Kocide showed the slowest sedimentation (SI Figure S11), probably due to higher surface charge (Figure 3, SI Table S2) and high content of stabilizer. In addition, Kocide also has a relatively low density and very rough surface, both of which may have improved its buoyancy. Normalized absorbance (A/A$_0$, where A = absorbance and A$_0$ = initial absorbance) after 6 hr in 10 mM IS at pH 7 was 0.60, 0.25, and 0.74 for nano-CuO, nano-Cu, and Kocide respectively. Rapid dissolution of nano-Cu at low pH and high IS obscured accurate measurement of sedimentation at those conditions—the dissolution products (mostly pale blue Cu^{2+}) absorb more strongly than the dark-brown nano-Cu particles.

I. galbana EPS decreased aggregation of nano-CuO to a much greater extent than SRN (Figure 4). Decreased aggregate size resulted in decreased sedimentation, especially at high IS. A similar but weaker pattern was observed for Kocide and nano-Cu. Complete sedimentation data for CBNPs are presented in SI Figure S12.

3.3.4. Effects of EPS on Dissolution and Speciation

3.3.4.1. Total Dissolved Cu

In general, dissolution rate was Kocide > nano-Cu >> nano-CuO. In terms of pH, dissolution was pH 4 >> pH 7 > pH 11 for the three CBNPs. At pH 4 [Cu]$_{diss}$ peaked for Kocide, nano-Cu, and nano-CuO around 2-24 hr (100%), Day 1-7 (100%), and Day 21-30 (98%) respectively. Unlike nano-Cu and nano-CuO however, we observed a decreasing [Cu]$_{diss}$ in Kocide at pH 4 from Day 21 (Figure 5), probably due to precipitation of Cu-containing species like $Cu(OH)_2$ and CuO (Hidmi & Edwards 1999). We observed an increase in pH over time in all pH 4 samples (pH 5-6 by Day 90), while pH decreased over

time at pH 11 (pH 7-8 by Day 90). There was only a slight decrease in pH at pH 7. Rapid dissolution of Kocide is beneficial for its use as a pesticide but may have important influence on susceptible aquatic organisms if released into natural waters—from excess pesticide application or accidental release.

EPS and SRN slowed down dissolution of CBNPs at pH 4: $[Cu]_{diss}$ from nano-CuO decreased from over 21% without NOM after 2 hr to about 2.3% and 4.0% in the presence of EPS and SRN respectively (Figure 5). $[Cu]_{diss}$ from nano-Cu at pH 4 after 2 hr was 34%, 17% and 37% in the presence of SRN, EPS, or neither, but the effect of NOM decreased over time. Similarly, EPS decreased dissolution of Kocide from 96% to 77% after 2 hr at pH 4, but SRN did not have an obvious effect. The weaker effect of EPS on dissolution of nano-Cu and Kocide may be due to the large size of these particles, which may result in incomplete coating by EPS. Decreased $[Cu]_{diss}$ in the presence of EPS and SRN may have been caused by (1) steric exclusion of water from the surface of the particles by NOM aggregates, (2) reduced availability of H^+ which may bind to NOM molecules, and/or (3) adsorption of dissolved Cu by NOM aggregates. NOM tend to be protonated and insoluble at low pH (Balnois *et al.* 1999), and their adsorption onto the CBNPs surface may exclude water to some degree. Due to NOM's insolubility at low pH, they have been shown to sorb more metal ions in acidic conditions, while sorbing less metal ions at basic conditions because they form soluble metal-NOM complexes (Zhao *et al.* 2011). Protonation of NOM at acidic pH will also reduce the amount of H^+ available to drive dissolution.

$[Cu]_{diss}$ from nano-CuO at pH 4 peaked around Day 21-30 in the absence of NOM, but in the presence of EPS and SRN the highest $[Cu]_{diss}$ were detected on Day 7. $[Cu]_{diss}$ then decreased by about 20% and 14% by Day 14 in the presence of EPS and SRN respectively, and stabilized. The decrease in $[Cu]_{diss}$ after reaching the peak concentration was probably

due to binding of Cu ions to the functional groups of EPS and SRN. Carboxyl and phosphate groups present in EPS participate in sorption of Cu^{2+} (Fang *et al.* 2011). Binding of Cu ions to NOM must have occurred fast (much less than 7 days) but we did not observe it until we sampled on Day 14. Decrease in $[Cu]_{diss}$ was also observed for Kocide with and without NOM, but the rate and magnitude of decrease were greater in the presence of EPS and SRN.

In contrast to the results seen at pH 4, the presence of EPS and SRN correlated with increased $[Cu]_{diss}$ at pH 7 and 11 in all CBNPs (Figure 5). This observation may be adduced to improved stability, solubility of NOM-Cu complexes, and the strength of interactions between NOM and CBNPs. Higher ζ potential obtained at higher pH in the presence of NOM (Figure 3) typically correlated with slower aggregation (SI Figure S13). Smaller aggregate sizes at pH 7 and 11 (relative to pH 4) may thus have contributed to enhanced dissolution. Unlike at acidic conditions where NOM (and thus associated Cu species) may be insoluble, NOM typically forms soluble metal complexes at neutral and alkaline pH conditions. As such we detected the dissolved Cu associated with NOM at pH 7 and 11, but not at pH 4. Increased dissolution may also be explained by the strength of interactions between NOM and particles: Figure 2A and SI Table S2 suggest that electrostatic interactions between NOM and CBNPs will be least at pH 11 and highest at pH 4. This implies that binding of NOM to CBNPs, and thus steric exclusion of water, is not as strong at pH 7 and 11 compared to pH 4.

Dissolution of CBNPs increased with IS under most conditions (SI Figure S14) due to formation of soluble Cl⁻complexes; more so in the presence of NOM. For instance, average dissolution of Kocide at pH 7 over 90 days increased from 7.0%, 10.9%, and 17.4% at 1, 10, and 100 mM respectively to 12.7%, 13.5%, and 20.7% in the presence of EPS; and 8.4%, 13.2, and 18.8% in the presence of SRN. These results imply that rapid sedimentation of

CBNPs in natural waters with high IS may not necessarily decrease the exposure to pelagic organisms, as NOM may increase the release of Cu ions, but probably in complexed forms. Additional information on effect of pH and IS on dissolution is in SI.

3.3.4.2. Speciation

The ratio of free Cu^{2+} to total dissolved Cu, $f\text{-}Cu^{2+}/ [Cu]_{diss}$, was determined in order to understand how different solution chemistries may influence speciation of dissolved Cu. $f\text{-}Cu^{2+}$ species are more bioavailable (Sunda & Guillard 1976), hence, $[Cu]_{diss}$ and $f\text{-}Cu^{2+}$ levels may be useful for predicting the availability and toxicity of CBNPs in natural waters. A prediction of pH-dependent speciation obtained using MINTEQ is shown in SI Figure S15, and the trend in $f\text{-}Cu^{2+}$ agreed well with experimental findings. Experimentally, $f\text{-}Cu^{2+}/ [Cu]_{diss}$ decreased in the presence of NOM, and with increasing pH and IS (Figure 6, SI Figure S16). At pH 7 $f\text{-}Cu^{2+}$ accounted for 0-55% of $[Cu]_{diss}$ detected in CBNPs over 90 days. At pH 4, $f\text{-}Cu^{2+}$ varied with time from 60 to 100%. The lowest concentration of $f\text{-}Cu^{2+}$ in the Kocide/NaCl/H_2O system at pH 4 was 1.10 mg/L (observed on Day 90) but still accounted for 63% of the $[Cu]_{diss}$ detected. Although nano-Cu was expected to release Cu^{+} (Cai *et al.* 2005; Mudunkotuwa *et al.* 2012), we found that $f\text{-}Cu^{2+}$ accounted for $\geq 72\%$ of $[Cu]_{diss}$ during the 90 days at pH 4. Cu^{+} may oxidize or disproportionate to form Cu^{2+} ions. The most prominent forms of $c\text{-}Cu^{+}$ and $c\text{-}Cu^{2+}$ predicted by MINTEQ at pH 4 are $CuCl_2^{-}$ and $CuCl^{+}$, respectively. In contrast to pH 4 and 7, $f\text{-}Cu^{2+}$ was non-detect at pH 11 both via direct measurements and modelling. Hydrolysis of Cu^{2+} occurs at alkaline pH so it exists mostly as $Cu(OH)_4^{2-}$, $Cu(OH)^{+}$, $Cu(OH)_2$, and $Cu(OH)_3^{-}$. In general, Kocide had higher amounts of dissolved and suspended Cu than nano-Cu and nano-CuO at pH 7 on Cu mass basis. Nano-Cu, however, had the highest fraction of $f\text{-}Cu^{2+}$. Based on this, we predict that

exposure to pelagic organisms of these three particles will be nano-Cu $\geq$ Kocide $\gg$ nano-CuO.

The ratio f-Cu^{2+}/ $[Cu]_{diss}$ differed based on the presence and type of NOM (Figure 6). For instance, at pH 4 the amount of f-Cu^{2+} and $[Cu]_{diss}$ from nano-CuO decreased in the presence of EPS and SRN. However, while f-Cu^{2+} accounted for most of $[Cu]_{diss}$ in the presence of SRN, significant amounts of c-Cu^{2+} were observed in the presence of EPS suggesting that EPS may be a better Cu-complexing agent than SRN at acidic conditions. A similar observation was made in nano-Cu systems at the same pH, as f-Cu^{2+}/$[Cu]_{diss}$ increased in the presence of SRN compared to EPS. Differences in f-Cu^{2+}/$[Cu]_{diss}$ between EPS and SRN at acidic pH may be due to differences in competitive sorption affinity of f-Cu^{2+} and H^+ for NOM binding sites (Cabaniss & Shuman 1988). Higher complexation of Cu^{2+} by EPS at pH 4 was confirmed by measuring f-Cu^{2+} in $CuCl_2$ solution over time in the presence of EPS, SRN or neither (data not shown).

Complexing agents in the conditions of this study were mainly Cl^-, OH^- and NOM, and results obtained at pH 7 suggest that dissolution of CBNPs was driven by both $[H^+]$ and the formation of complexes. Some complexing could occur from buffer components but this is not expected to be significant due to low concentrations of buffer used (0.5 mM). In nano-Cu, for instance, the total amount of f-Cu^{2+} increased slightly within the first 24 hr but in that same period f-Cu^{2+}/$[Cu]_{diss}$ decreased from 1.28 to 0.32 (-75%), 3.06 to 0.26 (-92%), and 1.20 to 0.46 (-62%) in the presence of EPS, SRN, and neither respectively. As such, NOM appears to contribute somewhat to complexation, but Cl^- and OH^- were the primary complexing agents. Inorganic dissolved Cu in natural waters exists mostly as complexes of carbonate (e.g. $CuCO_3$ and $Cu(CO_3)_2^{2-}$), hydroxide (e.g. $Cu(OH)_2$, $Cu(OH)^+$, and $Cu_2(OH)_2^{2+}$), and NOM (Flemming & Trevors 1989). The predominant species is highly

dependent on the concentrations of OH^- and CO_3^{2-} (i.e., pH and water hardness) (Flemming & Trevors 1989). As we showed in this study, organic ligands from biota in aquatic systems may play an important role in Cu-complexation, and thus, its bioavailability and toxicity to organisms (Wang *et al.* 2002).

3.3.4.3. Suspended and Total Cu in Supernatant

The total amount of copper in the supernatant, $[Cu]_{total}$, represents the level of Cu to which pelagic organisms are exposed; and it is composed of dissolved ($[Cu]_{diss}$) and suspended species ($[Cu]_{susp}$). $[Cu]_{susp}$ may include suspended undissolved CBNPs and recrystallized particles, as well as Cu ions adsorbed to suspended particles. In general, $[Cu]_{susp}$ was highest on Day 0 at all pH conditions, then decreased by about 1-2 orders of magnitude within a day due to sedimentation and dissolution (SI Figure S17). $[Cu]_{total}$ decreased rapidly at pH 7 and 11 due to sedimentation and slow dissolution, but generally increased at pH 4 due to rapid dissolution. $[Cu]_{total}$ decreased faster at lower IS since there was more dissolution at high IS (SI Figure S18).

$[Cu]_{susp}$ was higher in the presence of EPS and SRN in all CBNPs at pH 7 and in most conditions at pH 4 and 11. For example, after a week of dissolution and settling, $[Cu]_{susp}$ in nano-CuO system (pH 7, 10 mM) was 0.48, 0.32, and 0.10 mg/L in the presence of EPS, SRN, and neither respectively. The trend was similar in nano-Cu and Kocide (SI Figure S19). Increased $[Cu]_{susp}$ in the presence of NOMs resulted mainly from improved stability of undissolved particles, and binding of Cu ions to suspended particles—including NOMs (mostly at acidic pH) and undissolved/precipitated particles. MINTEQ was unable to model Cu ions adsorbed to EPS and SRN separately but estimated Cu^{2+} bound to DOC as 0.8 mg/L at pH 4 in the nano-CuO system. Experimentally for nano-CuO we detected average $[Cu]_{susp}$ of 1.59, 2.36, and 0.28 mg/L in the presence of EPS, SRN, and neither respectively between

Day 30 and 90 at pH 4. At the same pH and time in nano-Cu system, $[Cu]_{susp}$ was 0.36, 0.17, and 0.14 mg/L in the presence of EPS, SRN, and neither respectively. For Kocide we found 1.21, 1.18, and 1.0 mg/L in the presence of EPS, SRN, and neither respectively. Increased suspended CBNPs in the presence of EPS may result in additional toxicity to sensitive species (in addition to toxicity from ions) (Shi *et al.* 2011). Effective regulation of CBNPs may therefore require particle-specific toxicological information; e.g. (Shi *et al.* 2011) in addition to widely used data for copper ions and salts. Overall, results suggest that the long-term fate of CBNPs is the sediment phase, where they will persist. Exposure of benthic organism to CBNPs is therefore likely to be chronic.

At pH 7 and 11, $[Cu]_{total}$ was higher in the presence of NOM for all CBNPs due to improved stability and dissolution. Average $[Cu]_{total}$ (Day 0-90) in nano-Cu system was 1.80, 1.86, and 1.44 mg/L at pH 7 in the presence of EPS, SRN, and neither respectively. Average $[Cu]_{total}$ in nano-CuO was 1.41, 1.28, and 1.02 mg/L in the presence of EPS, SRN, and neither respectively. In Kocide we detected average $[Cu]_{total}$ of 1.20, 1.19, and 1.03 mg/L in the presence of EPS, SRN, and neither respectively. Hence, similar to $[Cu]_{susp}$, $[Cu]_{total}$ at pH 7 was EPS > SRN > neither. These results suggest that exposure of pelagic organisms to Cu species, if there is a release into natural waters, may increase at higher organic material content, particularly EPS. The additional Cu may be complexed with NOM (if ionic) or coated with NOM (if particulate), which may influence bioavailability.

Table 1. Physicochemical properties of particles used in this study

Property	Nano-CuO	Nano-Cu	Kocide
Primary particle size (nm)	50^1	40^1	$50 \times 10^{3\ 2}$
Hydrodynamic diameter[3] (nm)	280 ± 15	2590 ± 1138	1532 ± 580
Copper content (wt. %)	74.3 ± 1.2	83.3 ± 2.1	26.5 ± 0.9
Main copper phase	Monoclinic CuO	Cubic Cu and Cu_2O	Orthorhombic$Cu(OH)_2$
Helium density (g/cm³)	6.349	6.578	2.399
Other elements present	O	C, O	C, O, Na, Al, Si, S, Zn
BET surface area (m²/g)	12.31 ± 0.05	4.86 ± 0.03	15.71 ± 0.16
Isoelectric point (IEP)	6.3	2.1	<3.0
CCC at pH 7 (mM NaCl)	40	ND	ND
Estimated water content (wt. %)[4]	0.23	0.14	10.84

ND = Non-detect

---

[1] As reported by the manufacturer
[2] Determined via electron microscopy
[3] Measurement was done in DI water at pH 7
[4] Estimated by mass lost at 50-150 °C under nitrogen atmosphere
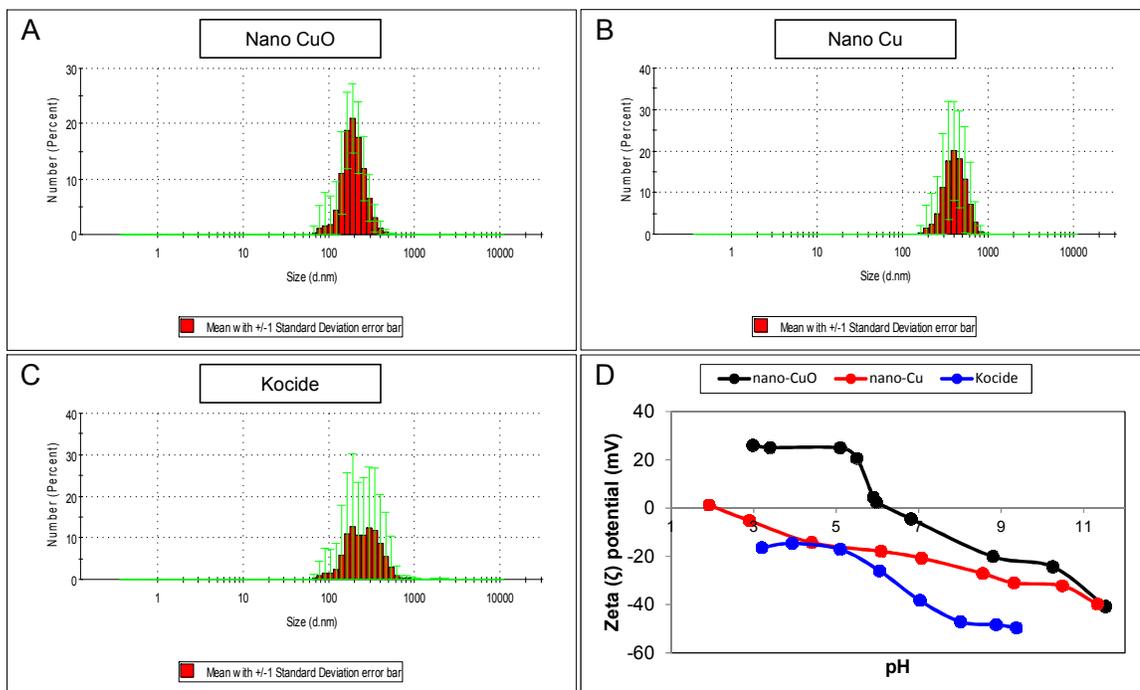
Figure 1. Size distribution of (A) nano-CuO, (B) nano-Cu, and (C) Kocide in DI at pH 7; and

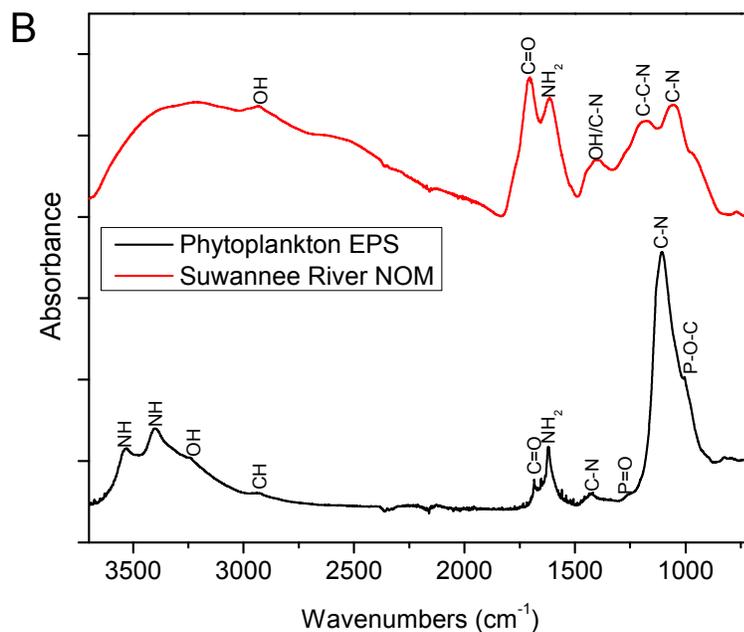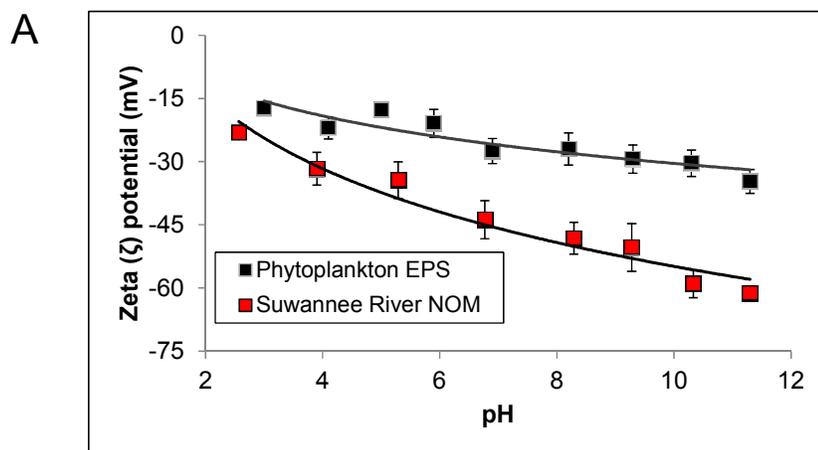surface charge characterization of the three particles across a range of pH, (D)

Figure 2. (A) Zeta (ζ) potential (mV) of Suwannee River NOM (SRN) and soluble EPS

derived from *Isochrysis galbana* (EPS) as a function of pH. (B) FTIR spectrum of SRN and

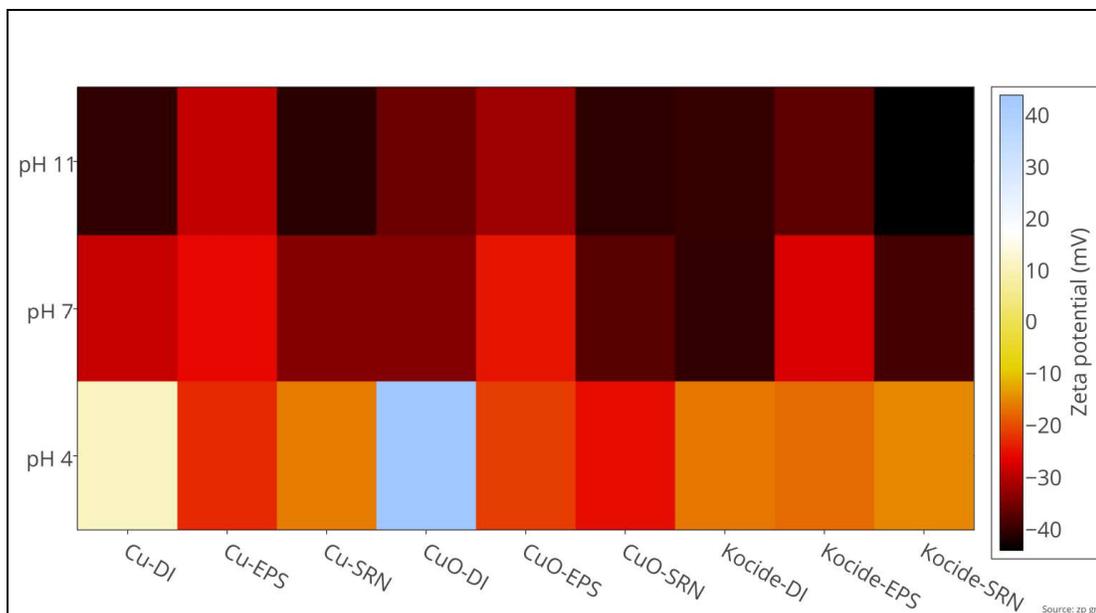EPS. Detailed band assignments are provided in Table S3.

Figure 3. Effect of EPS, SRN and pH on zeta potential of nano-CuO, nano-Cu, and Kocide. Relative standard deviations (RSD) for zeta potential obtained in the presence of EPS were $\leq$ 6% except in Kocide where we saw an RSD of 12.5%.
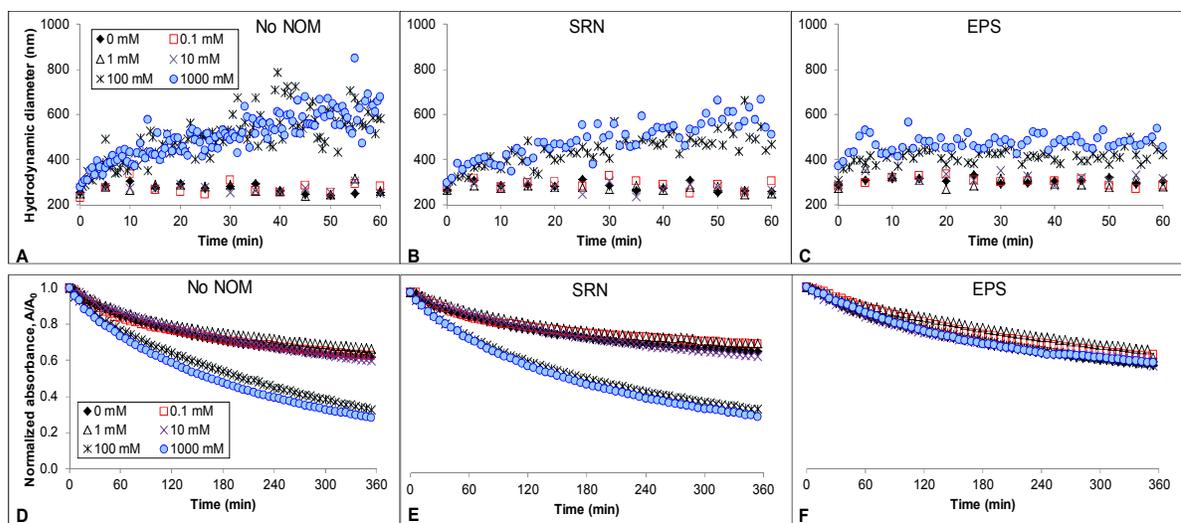
Figure 4. Aggregation kinetics of nano-CuO at pH 7 in (A) absence of NOM, (B) 5 mg/L SRN, (C) 5 mg-C/L EPS, and sedimentation kinetics of nano-CuO in (D) absence of NOM, (E) 5 mg/L SRN, (F) 5 mg-C/L EPS. Relative standard deviation < 4.5%
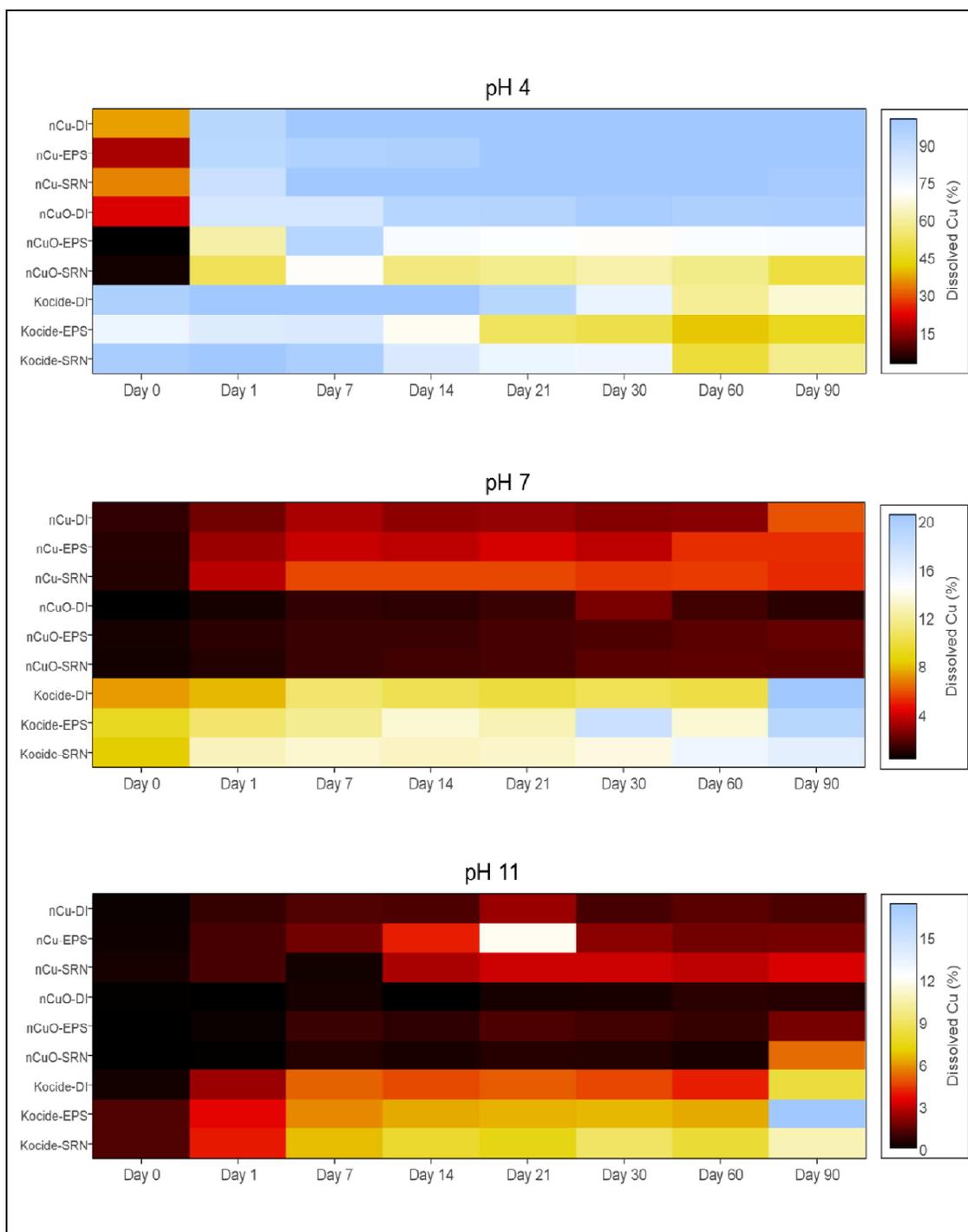
Figure 5. Effect of NOM and pH on 90-day [Cu]$_{diss}$ from nano-Cu, nano-CuO, and Kocide.
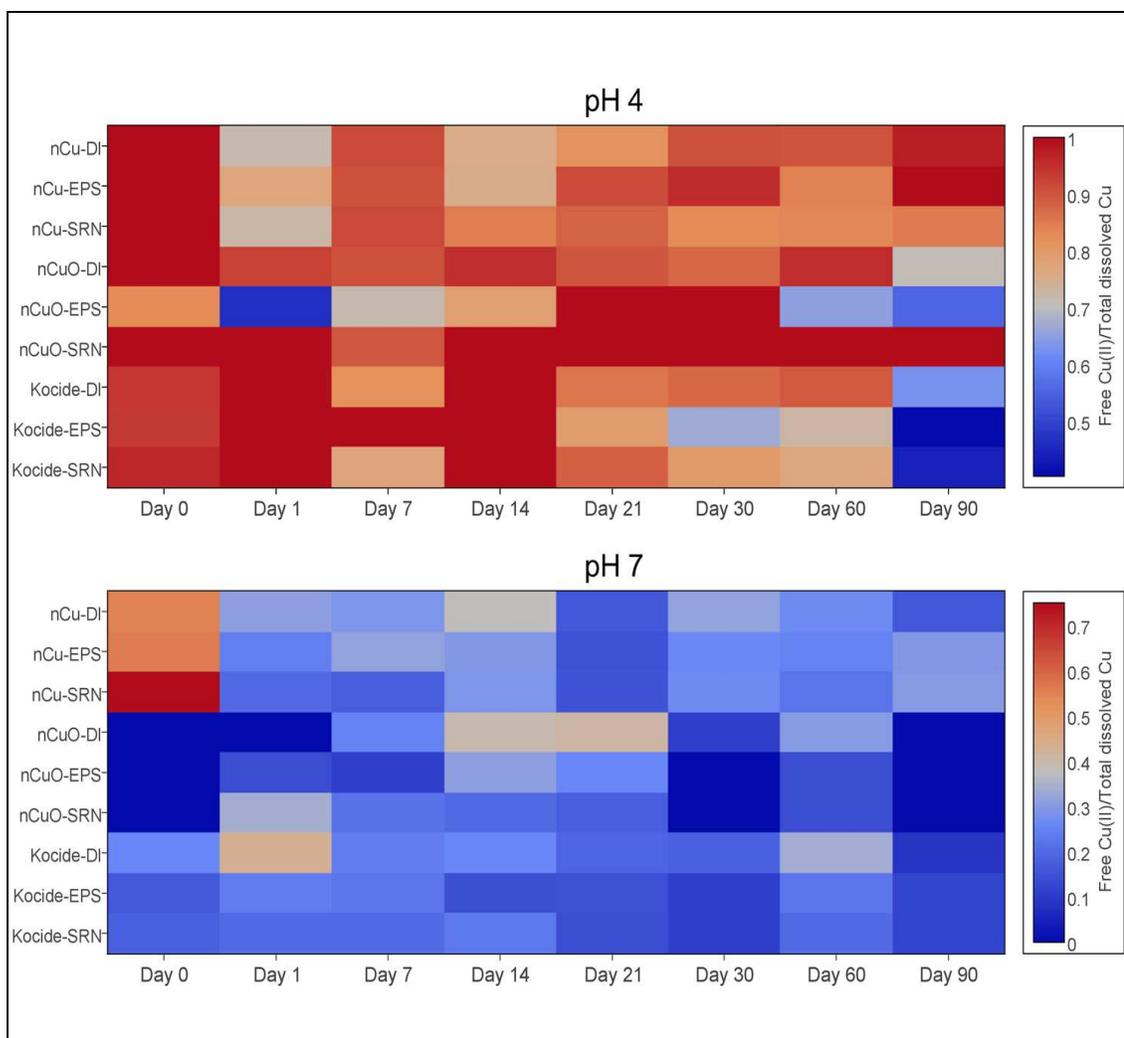
IS = 10 mM NaCl

Figure 6. Ratio of Free Cu^{2+} relative to total dissolved Cu at pH 4 and 7. Ratio = 0 for all

CBNPs at pH 11 (data not shown)

Appendix. Supporting Information

Suwanee River natural organic matter (SRNOM) stock preparation

SRNOM stock was prepared according to (Zhou & Keller 2010). A known amount of SRNOM powder (International Humic Substances Society IHSS, St. Paul, MN) was mixed with NANOpure water to achieve 500 mg/L concentration. pH was adjusted to 8 to facilitate dissolution, and stirred overnight. Stock was kept in the dark at 4 °C until use.

EPS production and extraction technique

The method was adopted from (Adeleye & Keller 2014) An axenic culture of *Isochrysis galbana*, obtained from the Provasoli-Guillard National Center for Culture of Marine Phytoplankton, was maintained in standard (f/2) media made with autoclaved filtered natural seawater collected from the Pacific Ocean in Santa Barbara. Algae were incubated under cool white fluorescent lights (14:10 light:dark, 100–120 μmol m^{-2} s^{-1}) at 20 °C with aeration until stationary phase. Cell densities were measured using a fluorometer (Trilogy, Turner Designs), which was converted to cell numbers using a standard curve based on counts done with a hemacytometer (Reichert, Buffalo NY). Soluble EPS fraction was harvested at the stationary growth phase via centrifugation of culture for 30 min at 4000 x *g* and 4 °C (RC 5B Plus, Sorvall, CT). The supernatant was collected and filtered with 0.22 μm PES filters (Thermo Fisher Scientific) under sterile conditions. This fraction contained soluble (unattached) EPS. To remove the residual salts from the growth medium and low molecular-weight metabolites, EPS was dialyzed against NANOpure water for 96 hr at 4 °C using regenerated cellulose tubular membrane of 3500 Da cut-off (Fischer Scientific), which had been treated with $NaHCO_3$ and Na_2EDTA to remove residues. The dialysis NANOpure water was renewed daily, and dialyzed EPS were stored in 4 °C until use.

Aggregation and sedimentation kinetics

Measured aliquots of nanoparticle stock suspensions, NaCl, and buffer were pipetted into a cuvette with or without 5 mg-C/L EPS or 5 mg/L SRN (~3.54 mg-C/L), and diluted with DI to achieve 50 mg-CBNP/L. This exceeds predicted average concentrations in surface waters (Keller *et al.* 2013), but may represent the levels of CBNPs at the point of release (e.g. from antifouling paint or pesticide use). In addition, nanoparticle concentration affects the frequency of collision, but not the attachment efficiency (α). Final concentration of buffer for each condition was 0.5 mM. Mixing was done via 2 or 5 s probe sonication with a Misonix Sonicator S-4000 (QSonica LLC). Aggregation was studied at 20 °C via time-resolved dynamic light scattering (DLS) using the Zetasizer. Data were collected in triplicates at 30 s intervals for 1 hr. α and critical coagulation concentration (CCC) in NaCl were determined as described previously (Adeleye & Keller 2014). Sedimentation was studied via time-resolved optical absorbency (Shimadzu 1601 UV-Vis spectrophotometer).

CCC determination and sedimentation kinetics

Aggregation kinetics was studied in increasing concentrations of NaCl solution at pH 7 and 20 °C. Critical coagulation concentration (CCC) was determined only in nano-CuO due to wide distribution in size of nano-Cu and Kocide. As shown in SI Eq. S1, the initial aggregation rate constant (k) reflects doublet formation and is proportional to the initial rate of increase in the intensity-weighted hydrodynamic radius, $a_h(t)$, with time, t, and the inverse of initial number concentration of nanoparticles, N_0: (Saleh *et al.* 2008; Adeleye & Keller 2014)

$$k \propto \frac{1}{N_0}\left(\frac{da_h(t)}{dt}\right)_{t \to 0}$$

(Eq. S1)

k is obtained from the slope of the best fit line of $(da_h(t)/dt)_{t\to 0}$, which is determined via

Dynamic Light Scattering (DLS) using the Zetasizer Nano-ZS90. The analysis requires that

the final $a_h(t)$ be approximately 1.3 of initial a_h, where there are sufficient doublets formed

and few higher-order aggregates (Zhou & Keller 2010). Attachment efficiencies (α) of nano-

CuO in aqueous NaCl were calculated by normalizing the measured *k* of a given

concentration by the diffusion-limited aggregation rate constant $(k)_{fav}$ determined in highly

favorable aggregation conditions (SI Eq. S2):

$$\alpha = \frac{\left(\dfrac{da_h(t)}{dt}\right)_{t\to 0}}{\left(\dfrac{da_h(t)}{dt}\right)_{t\to 0, fav}}$$

(Eq. S2)

To examine the influence of natural organic materials (NOM) on CCC of nano-CuO,

experiments were repeated in the presence of 0.25 mg-C/L *Isochrysis galbana*-derived EPS

or 0.25 mg/L SRN. Aggregation kinetics was monitored immediately after adding

appropriate fractions of nano-CuO stock, NaCl, buffer, DI, and NOM (as appropriate). Data

were collected until a 50% increase in the initial hydrodynamic radius was observed. The

diffusion-limited (DLCA) and reaction-limited (RLCA) clustering aggregation regimes, and

thus, CCC, can be identified in a plot of $\log_{10}[\text{NaCl}]$ versus $\log_{10} \alpha$.

Sedimentation was monitored using a Biospec 1601 spectrophotometer (Shimadzu,

Japan), measuring the sedimentation of the nanoparticles in buffered NaCl solution via time-

resolved optical absorbency at 390 nm (nano-CuO), 990 nm (nano-Cu), and 302 nm

(Kocide). These wavelengths were selected based on regions where peak differences were

observed between the spectra of the nanoparticle suspension and blank (buffered solution

without CBNP). Optical absorbency was measured every 6 min for 354 min, using aliquots

of CBNP stock in a range of NaCl concentrations.

Table S1. Experimental conditions of dissolution and speciation experiments

Condition #	pH	[NaCl] (mM)	NOM (5 mg/L)	EPS (5 mg-C/L)
1	4	10	Yes	-
2	4	10	-	-
3	4	10	-	Yes
4	7	1	Yes	-
5	7	1	-	-
6	7	1	-	Yes
7	7	10	Yes	-
8	7	10	-	-
9	7	10	-	Yes
10	7	100	Yes	-
11	7	100	-	-
12	7	100	-	Yes
13	10	10	Yes	-
14	10	10	-	-
15	10	10	-	Yes

Equilibrium concentration of copper speciation using MINTEQ 3.0

The parameters were set as follows: pH was fixed at 4, 7, or 11; temperature was 20 °C

(similar to the temperature of our study); ionic strength was to be calculated depending on

components added (e.g. 10 mM Na^+ and 10 mM Cl^-, and 0.5 mM phosphate buffer);

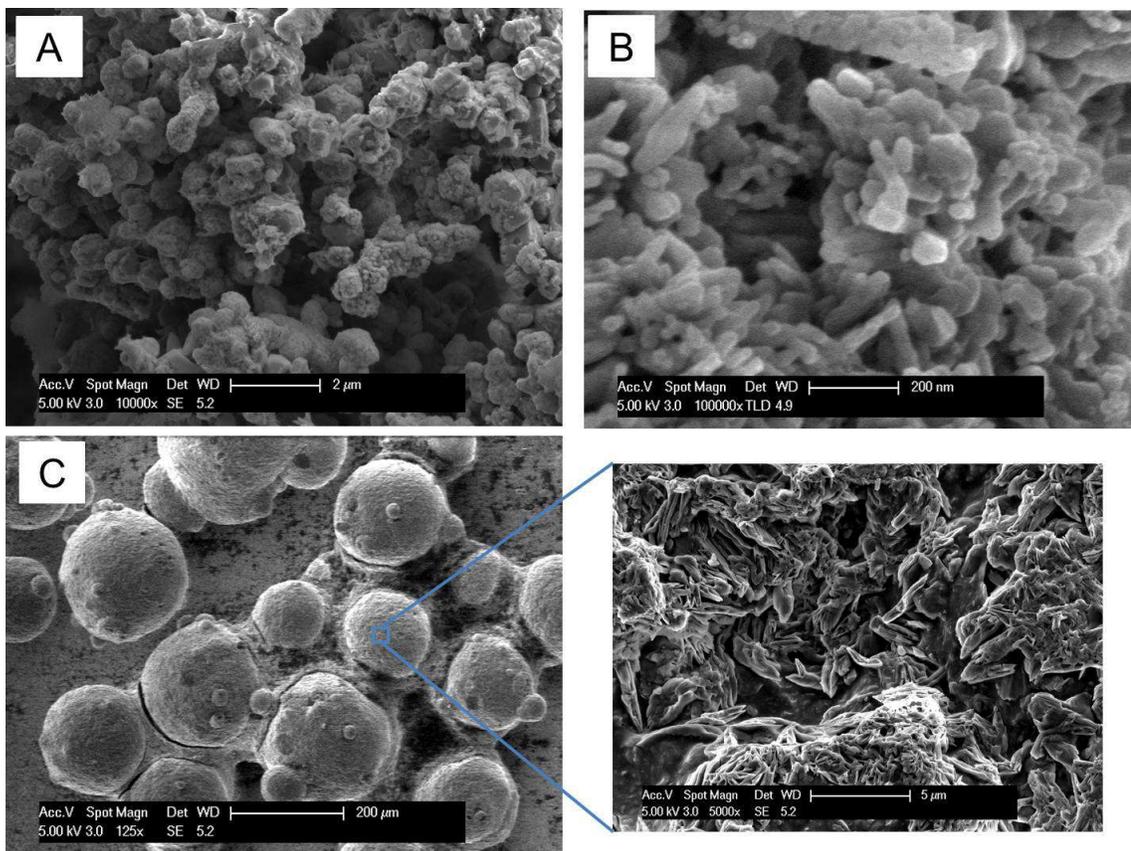nanoparticles were specified as finite solid phase.

Figure S1. SEM micrographs of (A) nano-Cu, (B) nano-CuO, and (C) Kocide with inset showing close-up of surface
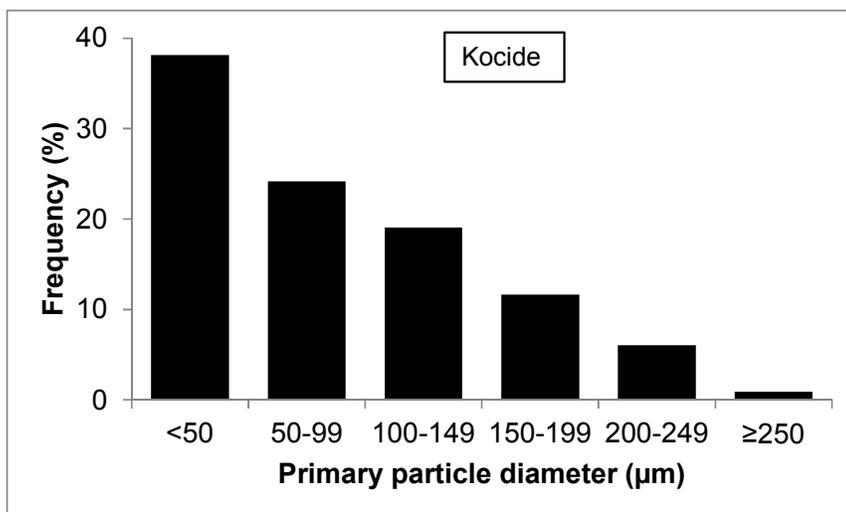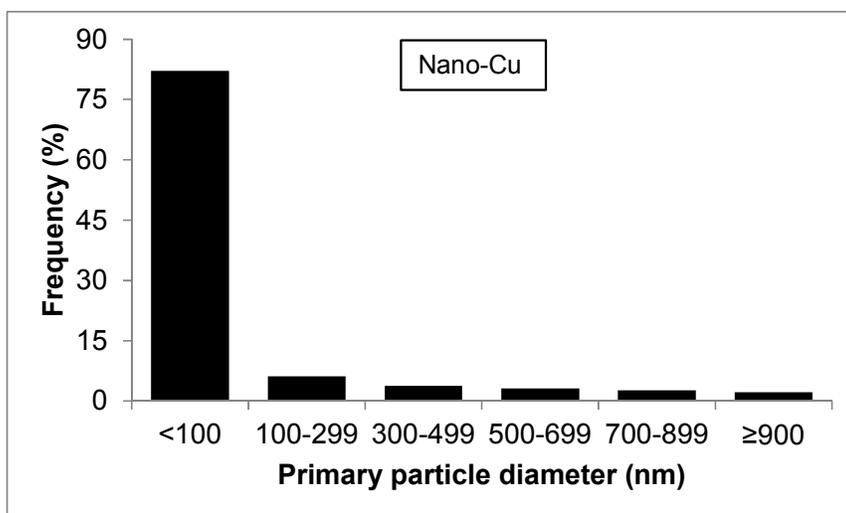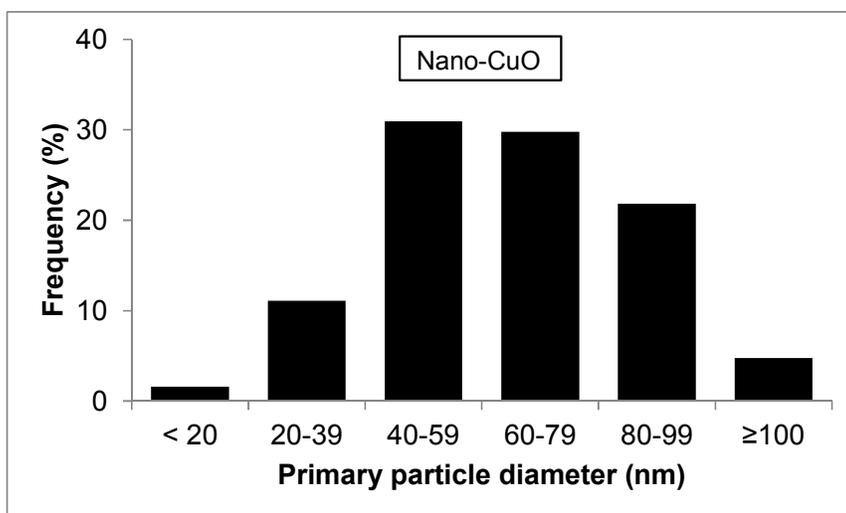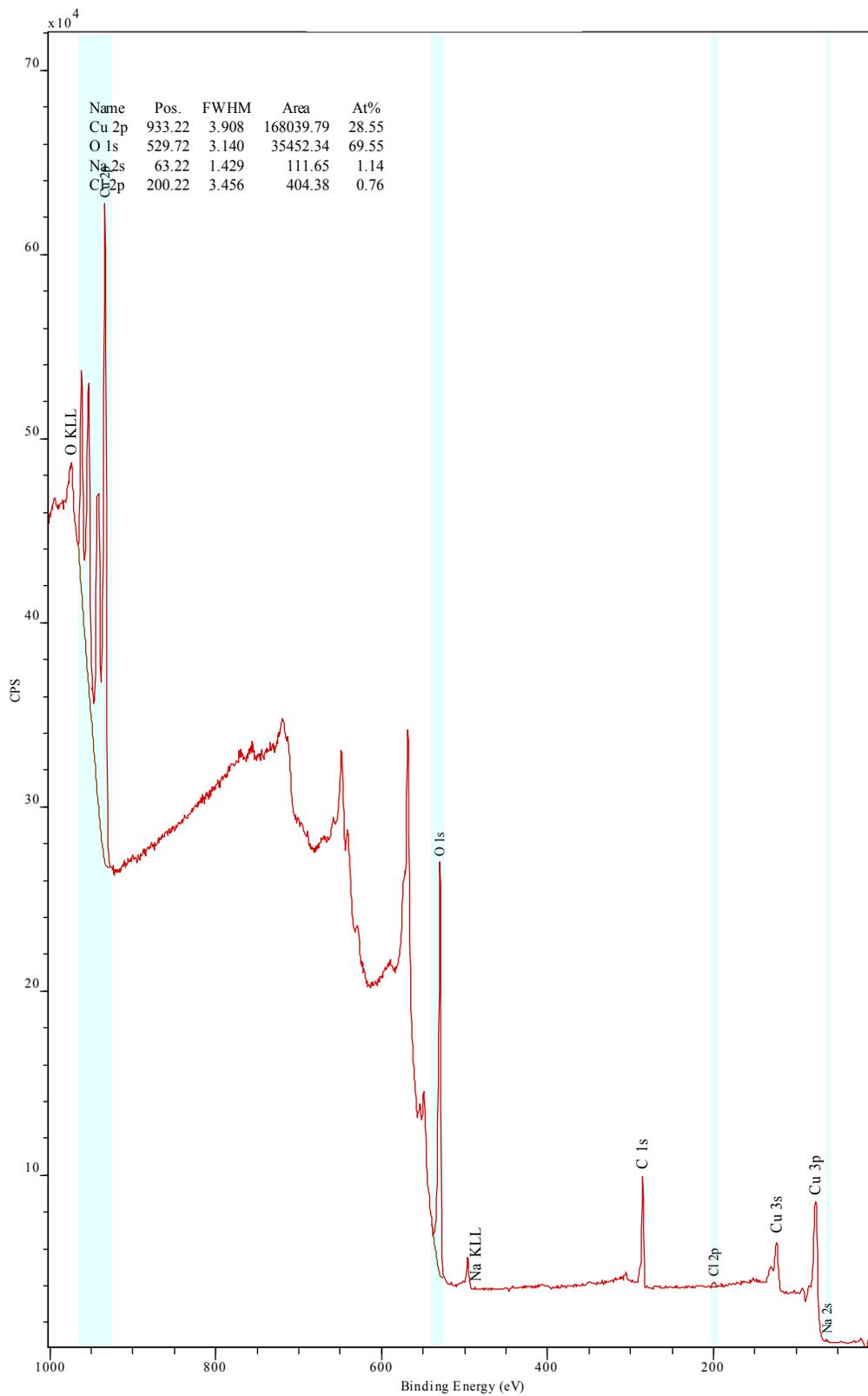
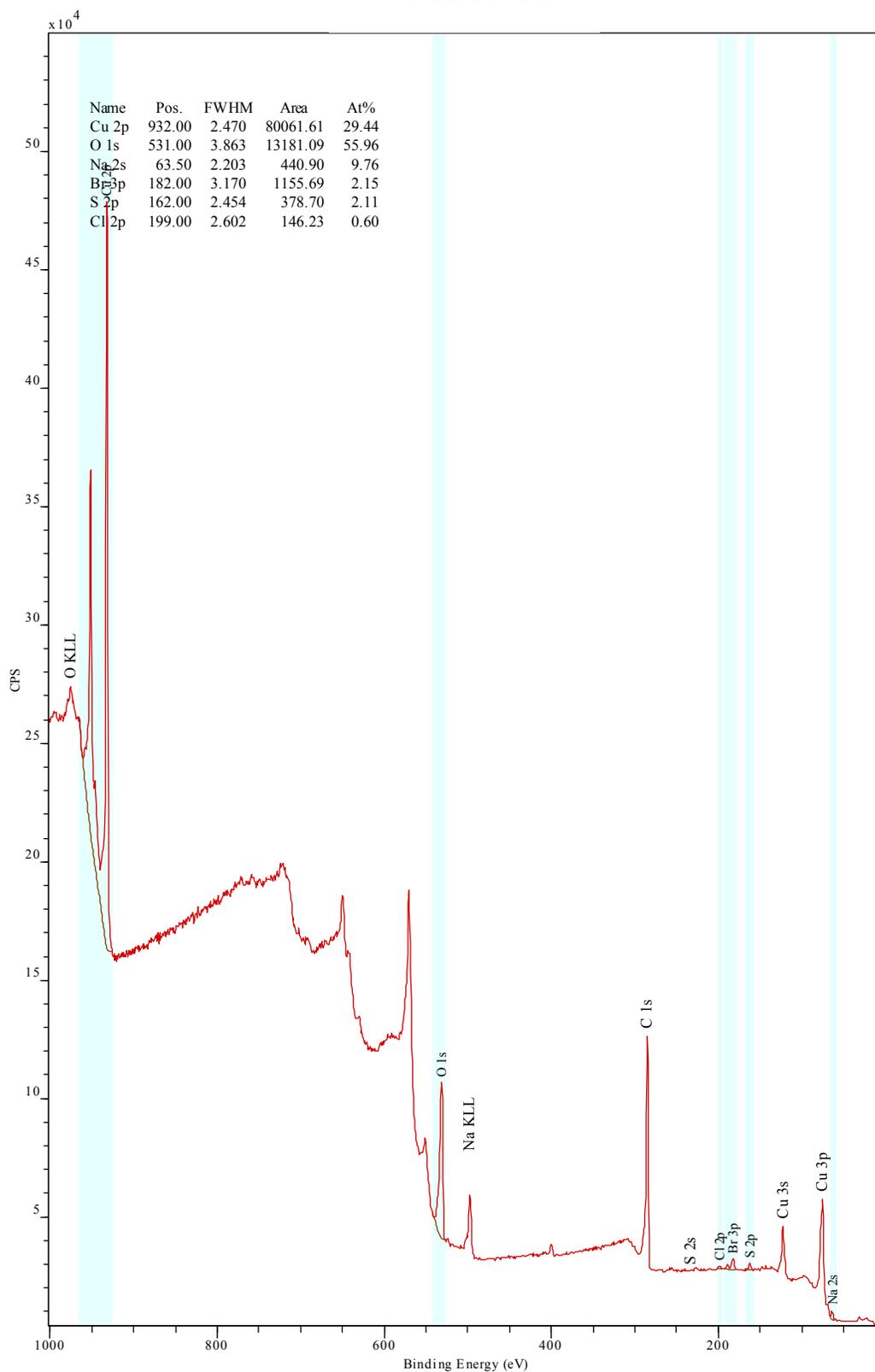Figure S2. Size distribution of nano-CuO, nano-Cu, and Kocide primary particles

Table S2. Zeta (ζ) potential of CBNPs at the conditions of this experiment (buffered solutions)

pH	Nano-CuO	Nano-Cu	Kocide
4	+43.3±1.1	+10.9±4.0	-16.8±1.6
7	-34.4±0.5	-29.4±0.8	-40.9±2.7
11	-36.3±0.6	-40.8±1.7	-40.4±2.0

Nano-CuO

Name	Pos.	FWHM	Area	At%
Cu 2p	933.22	3.908	168039.79	28.55
O 1s	529.72	3.140	35452.34	69.55
Na 2s	63.22	1.429	111.65	1.14
Cl 2p	200.22	3.456	404.38	0.76

Nano-Cu

Name	Pos.	FWHM	Area	At%
Cu 2p	932.00	2.470	80061.61	29.44
O 1s	531.00	3.863	13181.09	55.96
Na 2s	63.50	2.203	440.90	9.76
Br 3p	182.00	3.170	1155.69	2.15
S 2p	162.00	2.454	378.70	2.11
Cl 2p	199.00	2.602	146.23	0.60

CPS

O KLL

O 1s

Na KLL

C 1s

S 2s

Cl 2p

Br 3p

S 2p

Cu 3s

Cu 3p

Na 2s

Binding Energy (eV)

Kocide

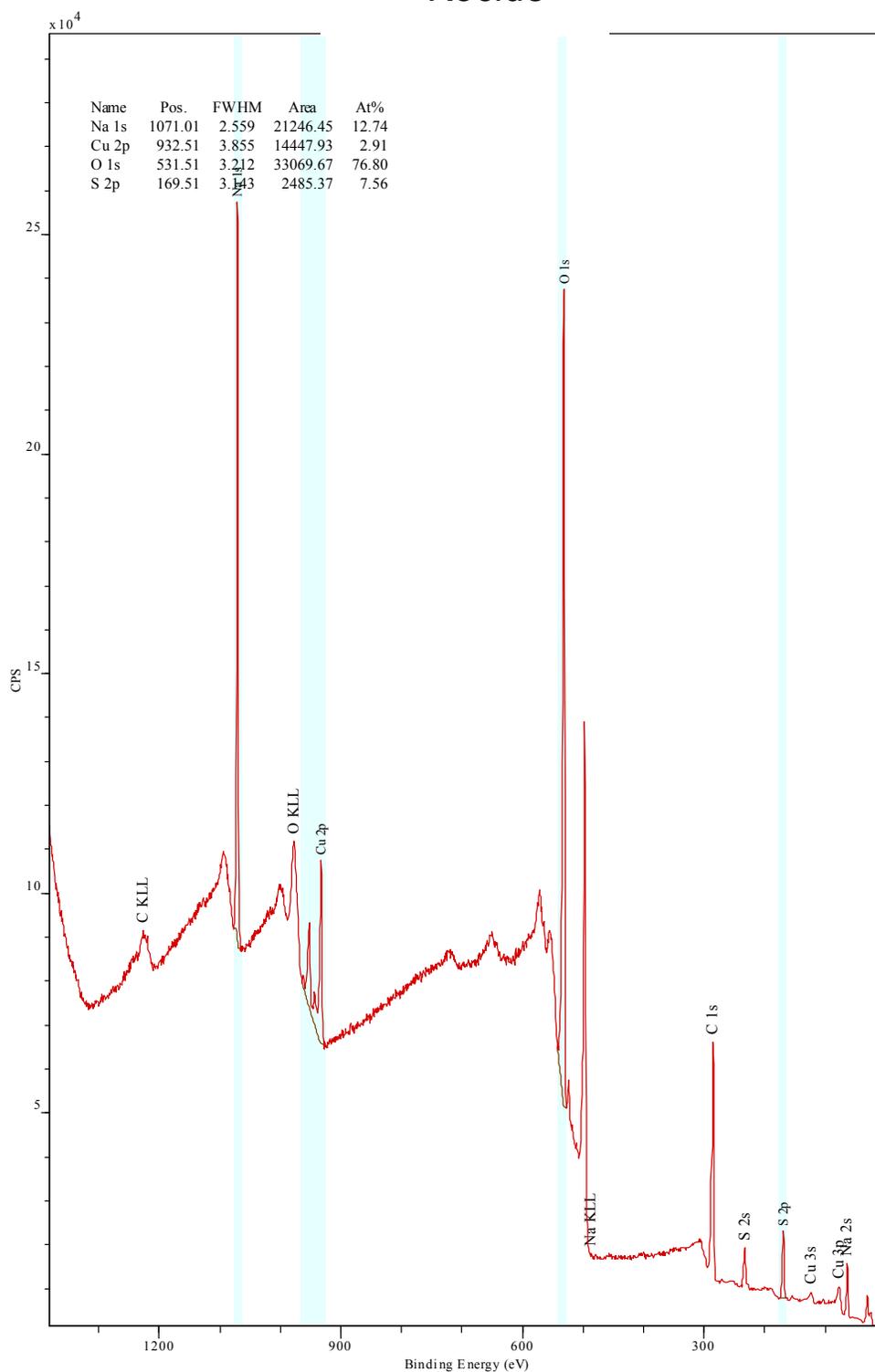| Name	Pos.	FWHM	Area	At%
Na 1s	1071.01	2.559	21246.45	12.74
Cu 2p	932.51	3.855	14447.93	2.91
O 1s	531.51	3.212	33069.67	76.80
S 2p	169.51	3.143	2485.37	7.56

Figure S3. XPS spectra of nano-CuO, nano-Cu, and Kocide. The spectra of nano-CuO and

Kocide showed two strong satellite peaks (~943 eV and 963 eV) expected of Cu(II)
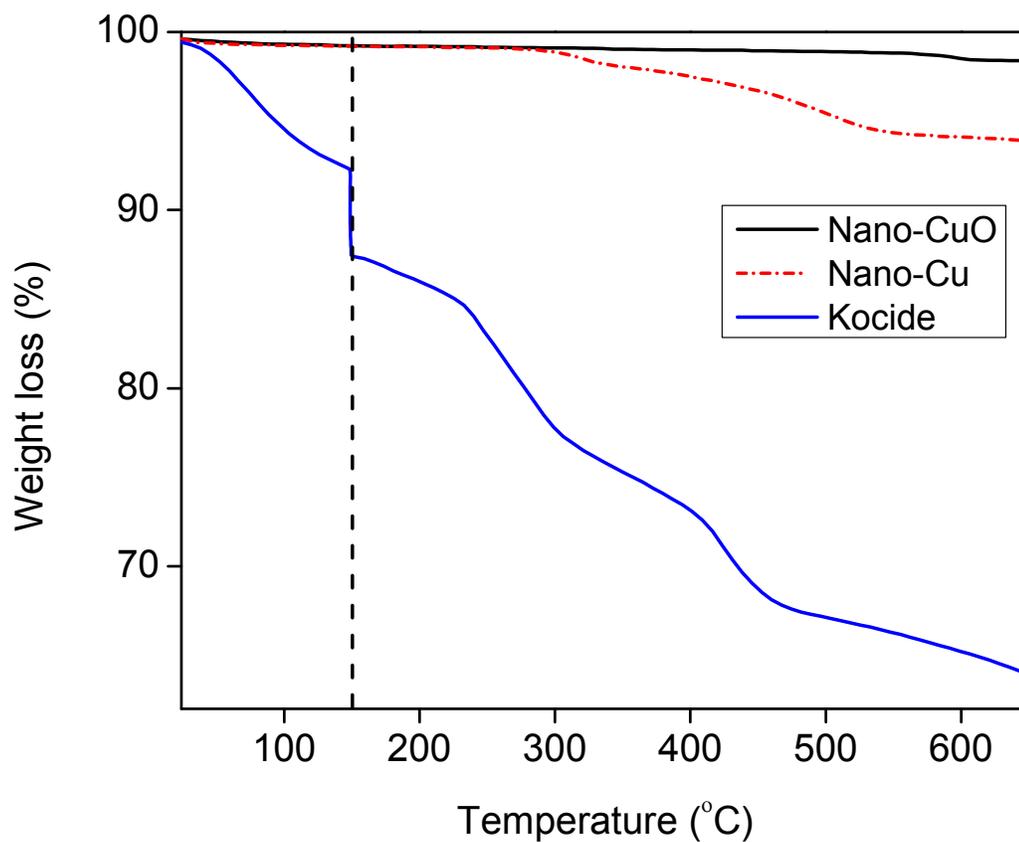
Figure S4. Thermogravimetric analysis of nano-CuO, nano-Cu, and Kocide done in nitrogen atmosphere. The weight loss in the 50-150 °C temperature range, which corresponds to adsorb water and surface hydroxyl group was relatively high for Kocide relative to nano-Cu and nano-CuO
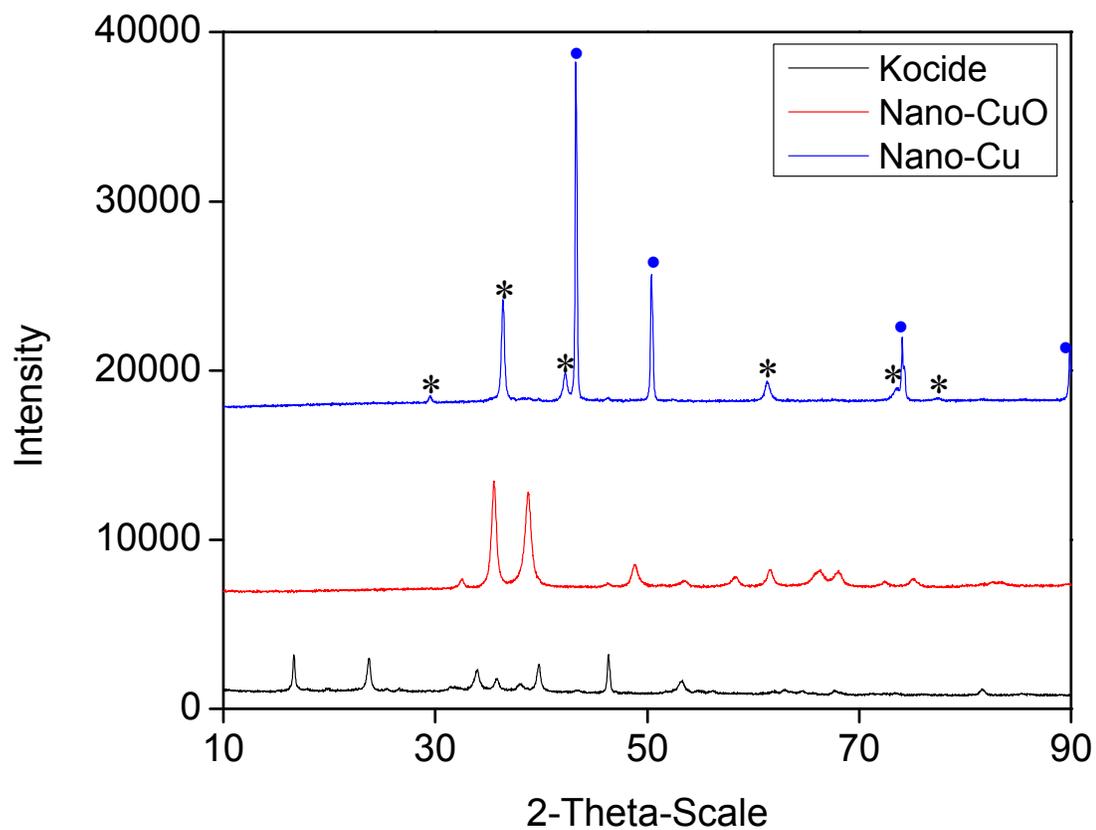
Figure S5. X-ray diffractograms of nano-CuO (monoclinic CuO phase), Kocide (orthorhombic Cu(OH)$_2$ phase), and nano-Cu (* denotes cubic Cu$_2$O, and • denotes cubic Cu)

Kocide

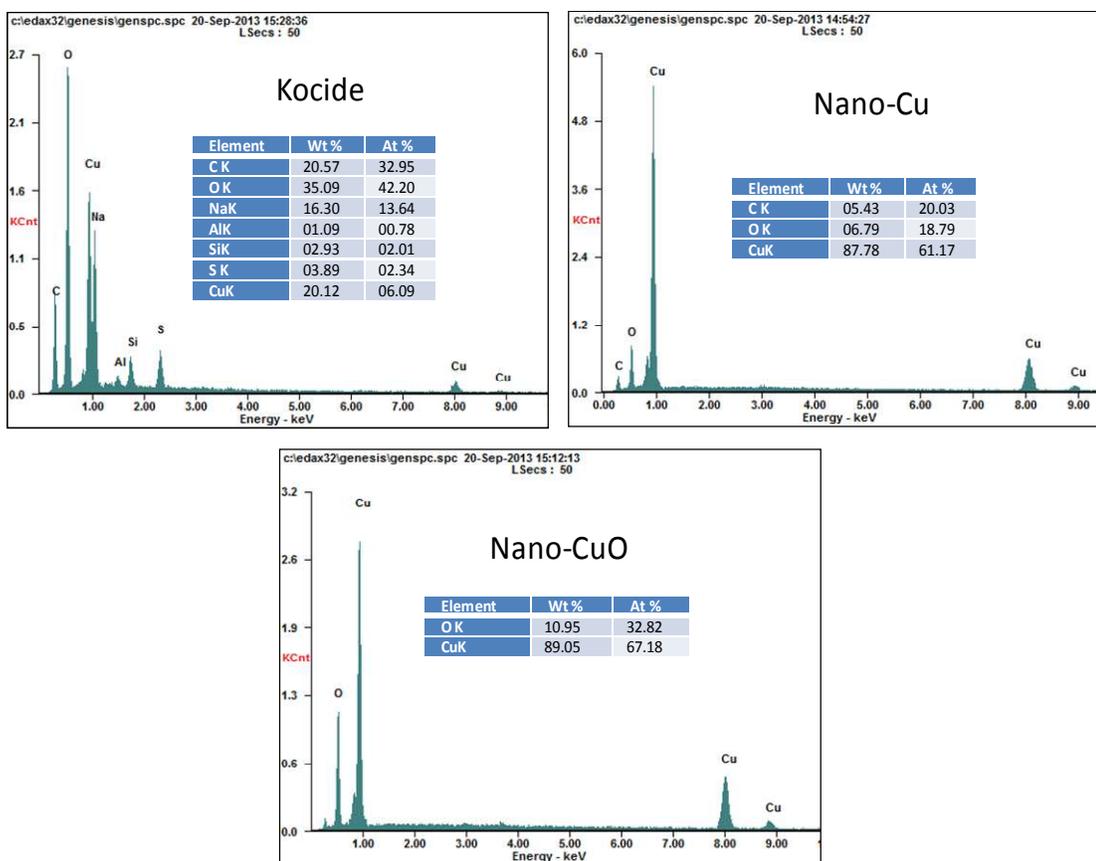| Element	Wt %	At %
C K	20.57	32.95
O K	35.09	42.20
NaK	16.30	13.64
AlK	01.09	00.78
SiK	02.93	02.01
S K	03.89	02.34
CuK	20.12	06.09

Nano-Cu

Element	Wt %	At %
C K	05.43	20.03
O K	06.79	18.79
CuK	87.78	61.17

Nano-CuO

Element	Wt %	At %
O K	10.95	32.82
CuK	89.05	67.18

Figure S6. Energy-dispersive X-ray spectroscopy (EDS) of copper-based particle

Table S3. Band assignments for FTIR spectrum of (A) soluble EPS of *Isochrysis galbana*, and (B) Suwannee River NOM (Lambert *et al.* 1987; Omoike & Chorover 2004; Cao *et al.* 2011).

A

Wavenumber (cm^{-1})	Functional groups in *Isochrysis galbana* EPS
3528	NH stretch in primary amines
3398	NH stretch in primary amines
3250	OH stretch in polysaccharide and proteins
2930	CH asymmetric stretch in membrane lipids and fatty acids
1684	C=O stretch in primary amides of proteins
1620	NH$_2$ deformation in primary amines of proteins
1419	C-N stretch in proteins' primary amide and symmetric stretch of carboxylic acid groups
1241	P=O stretch in phosphodiester backbone of nucleic acid or phosphorylated proteins
1107	C-N stretch in primary aliphatic amines in proteins
1007	P-O-C asymmetric stretch from nucleic acids
824	NH$_2$ wag in primary amines

B

Wavenumber (cm^{-1})	Functional groups in Suwannee River NOM
3214	NH$_3^+$ asymmetric stretch in primary amides
2933	H-bonded OH-stretch in carboxylic acids
2349	P-H stretch in organophosphorus compounds
1704	C=O stretch in carboxylic acid
1616	NH$_2$ deformation in primary amines
1404	OH bending in carboxylic acid or C-N stretch in primary amide
1174	C-C-N bending in amines
1057	C-N stretch in primary aliphatic amines
944	P-O-C asymmetric stretch in organophosphorus compounds
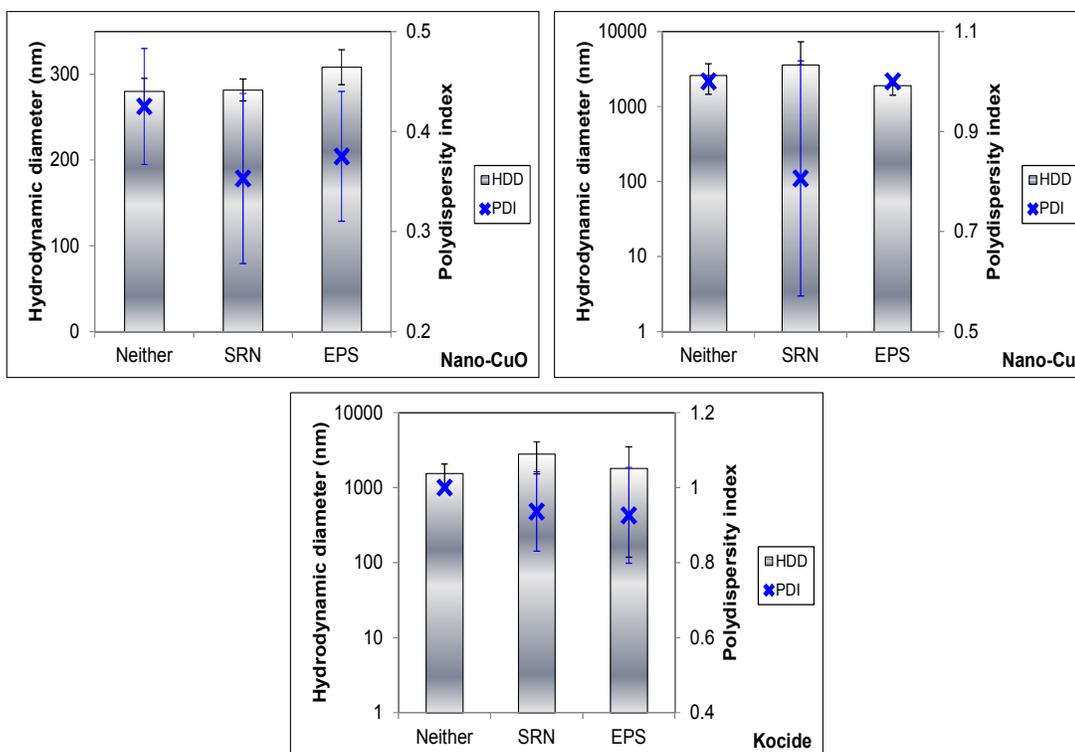
Figure S7. HDD and PDI of nano-CuO, nano-Cu, and Kocide in DI at pH 7. Polydispersity index shown in blue within the bar graph
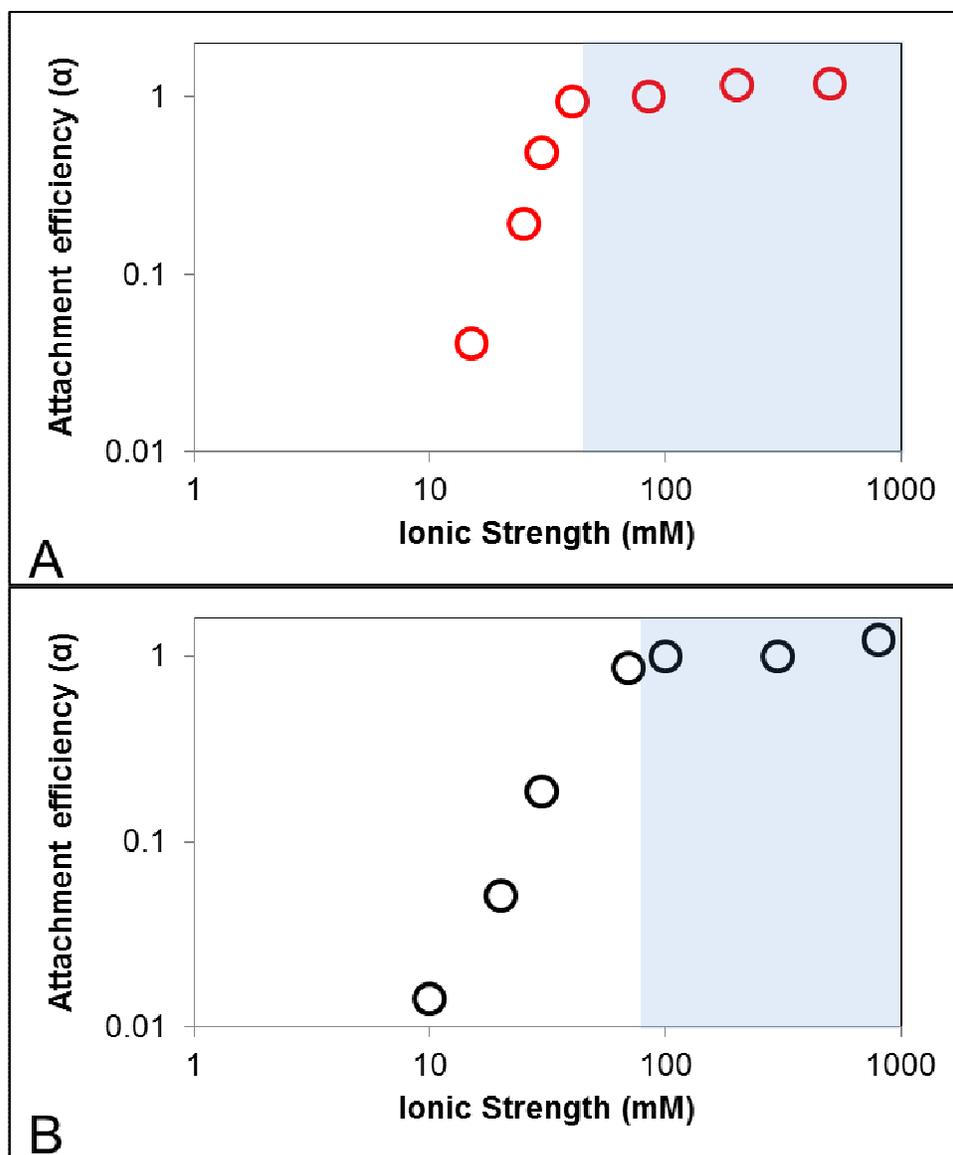
Figure S8. Attachment efficiency of nano-CuO as a function of IS at pH 7 in (A) absence of NOM (CCC ~ 40 mM NaCl), and (B) presence of SRN (CCC ~ 75 mM NaCl)
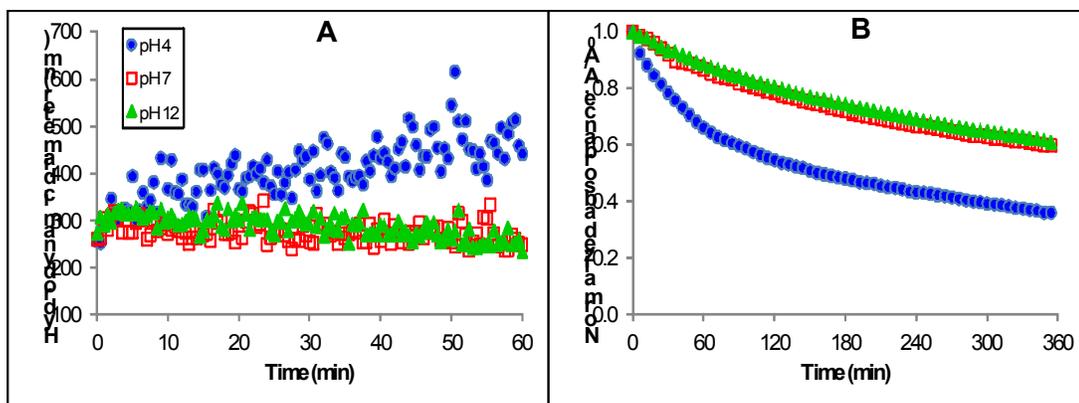
Figure S9. pH-dependent aggregation dynamics of nano-CuO. (A) Aggregation and (B)

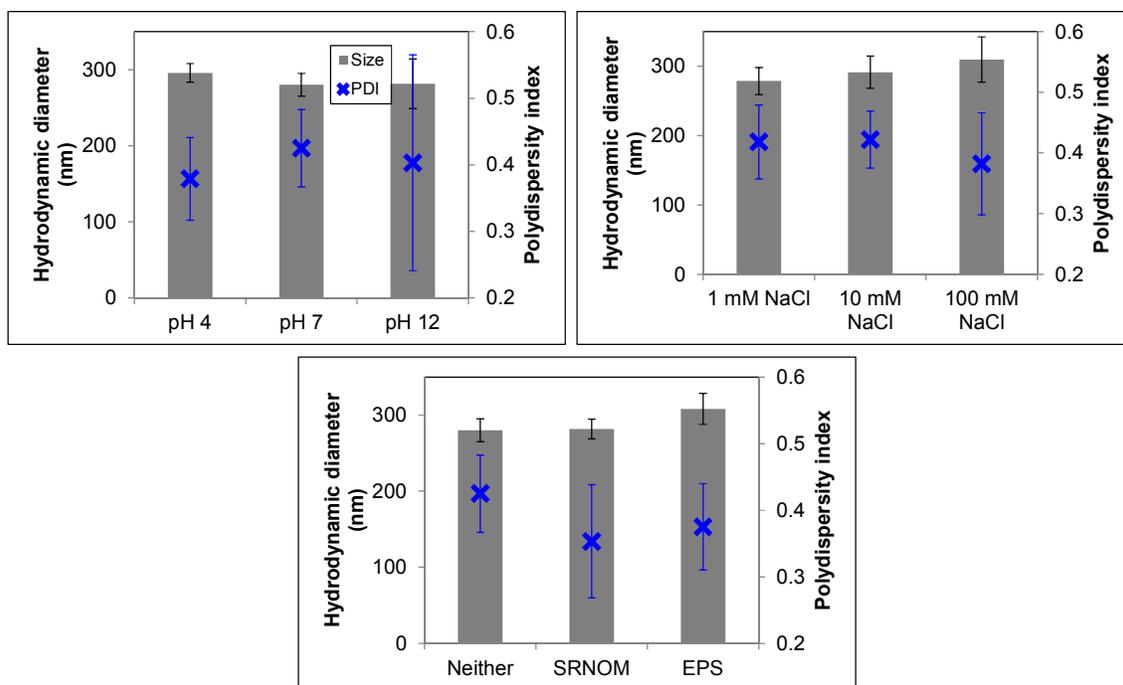Sedimentation kinetics in 10 mM NaCl at pH 4, 7, and 11

Figure S10. Effect of pH, IS, and NOM on initial hydrodynamic diameter of nano-CuO. * = statistical significance at $\square = 0.05$ ($p = 0.01$). Polydispersity index shown in blue within the bar graph
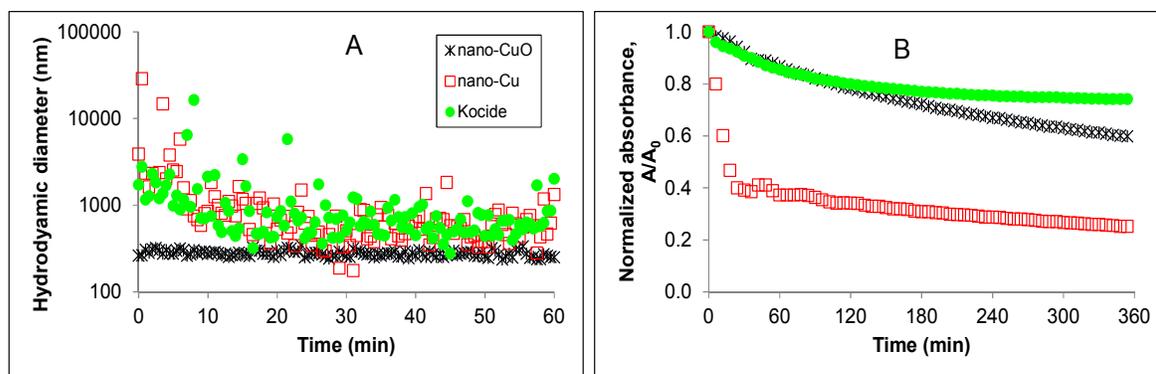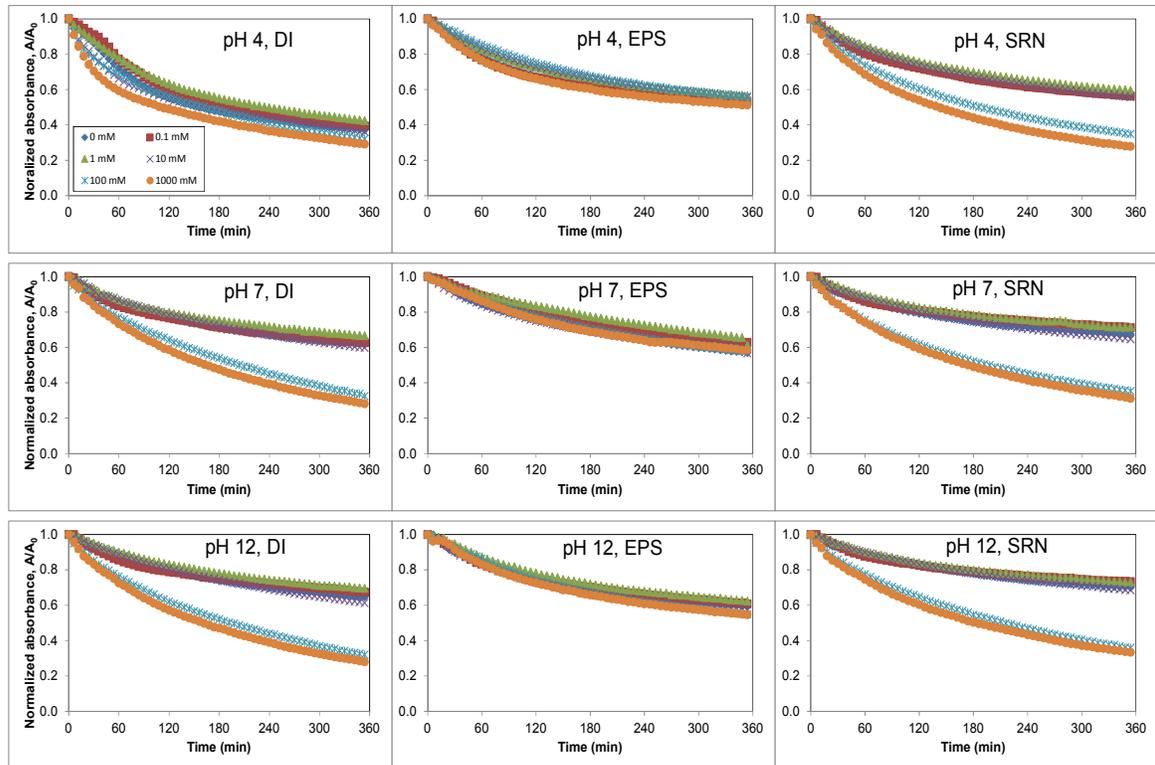
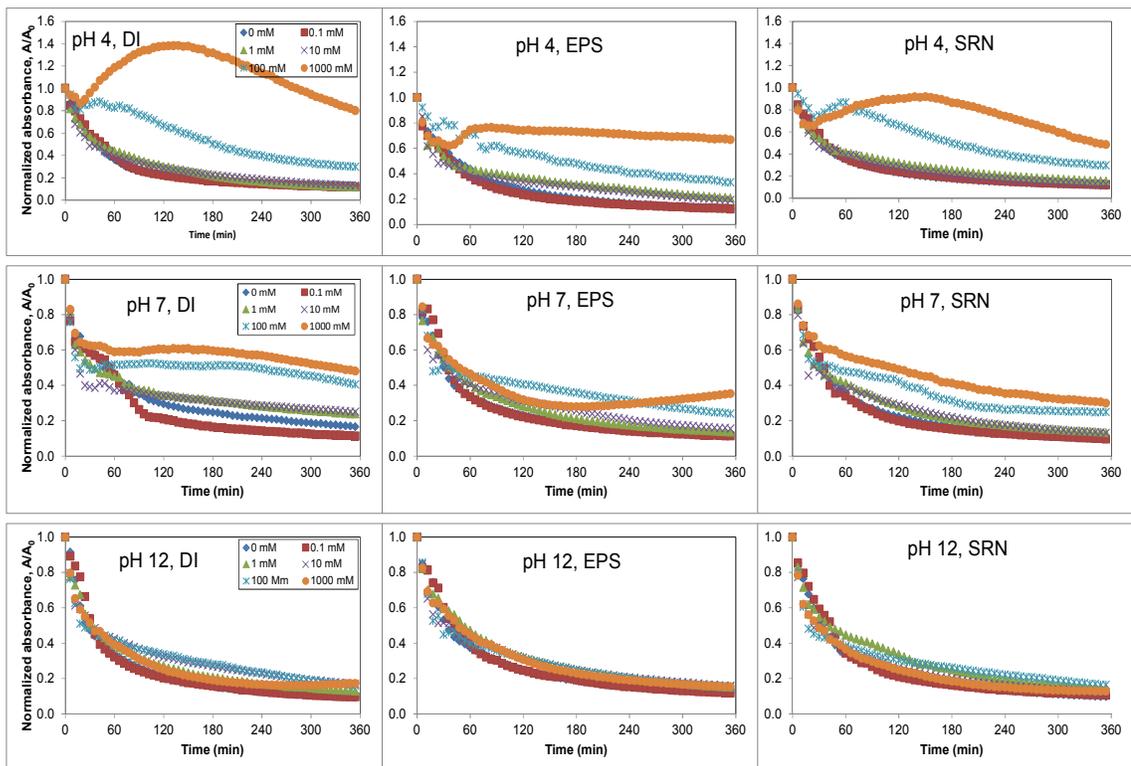Figure S11. (A) Aggregation and (B) Sedimentation kinetics of CBNPs in 10 mM NaCl at pH 7

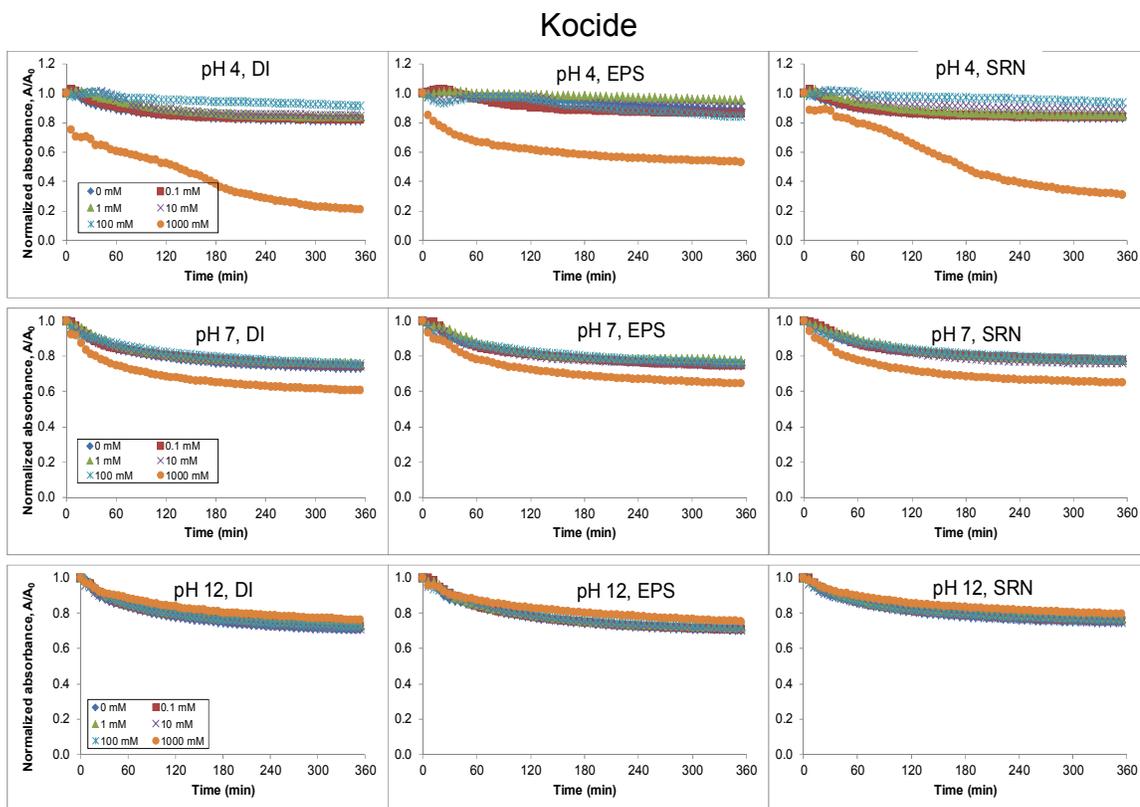# Nano-

Nano-Cu

Kocide

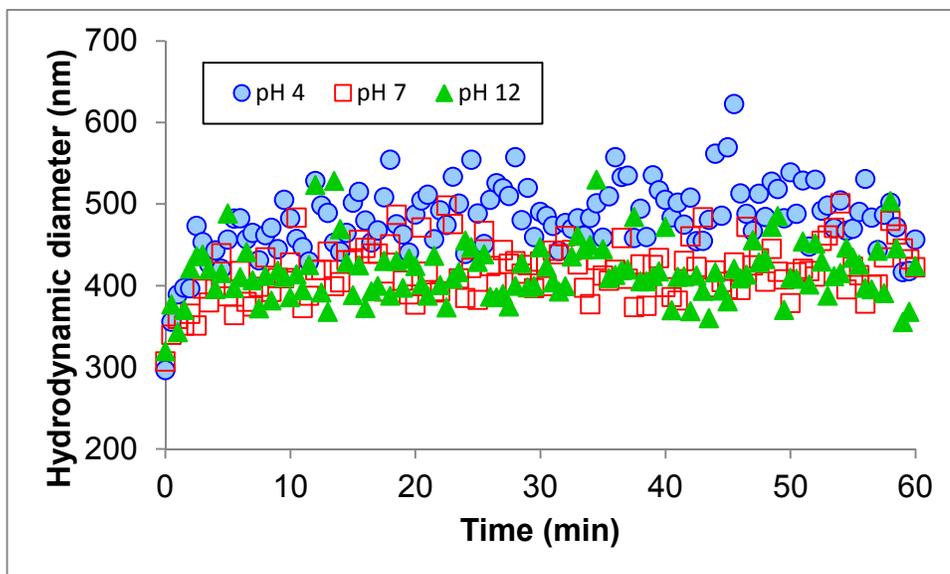Figure S12. Sedimentation kinetics of nano-CuO, nano-Cu, and Kocide: Effect of pH, ionic strength and NOM

Figure S13. Aggregation kinetics of nano-CuO in the presence of 5 mg-C/L EPS. IS = 100 mM NaCl
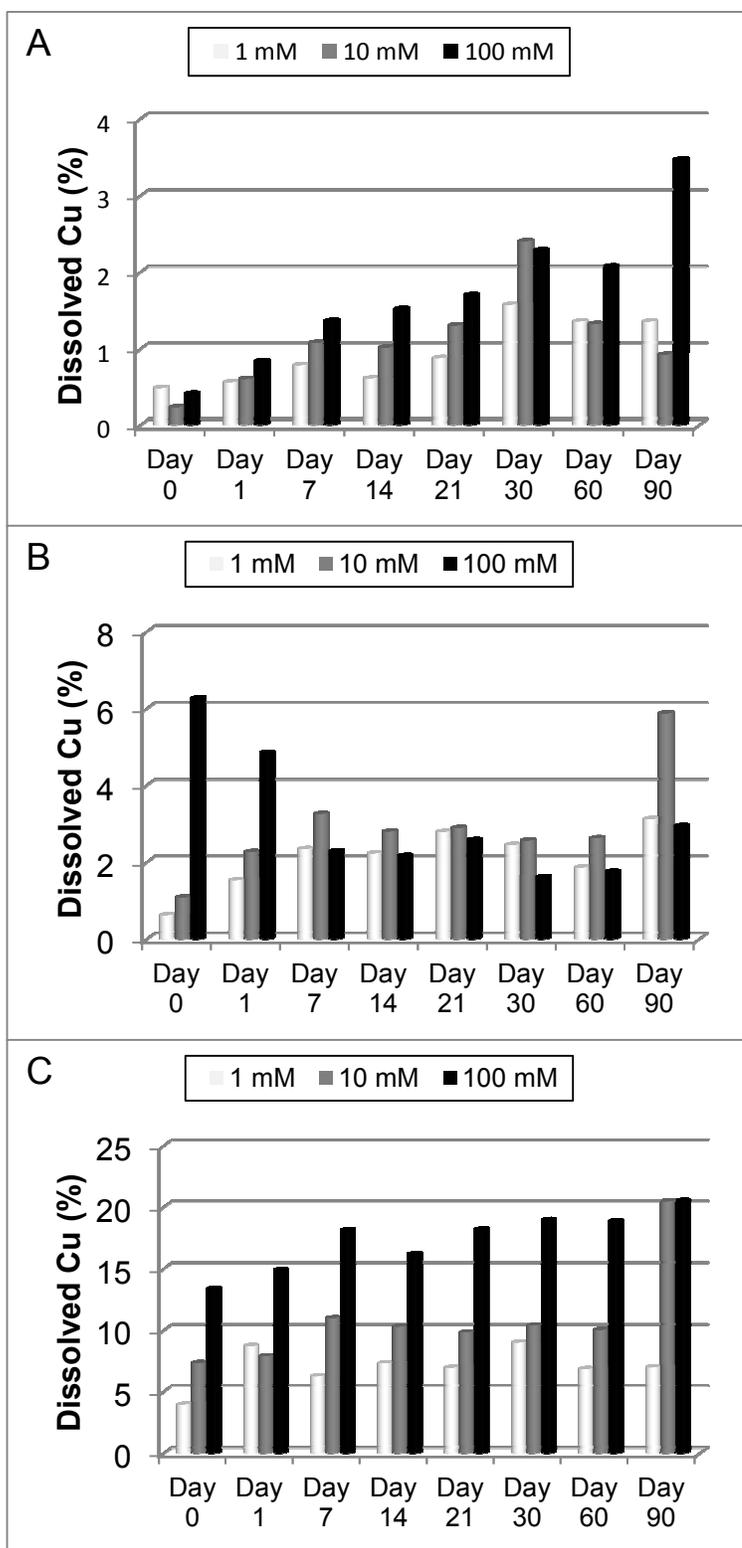
Figure S14. Effect of ionic strength on dissolution of (A) nano-CuO, (B) nano-Cu, and (C)

Kocide at pH 7
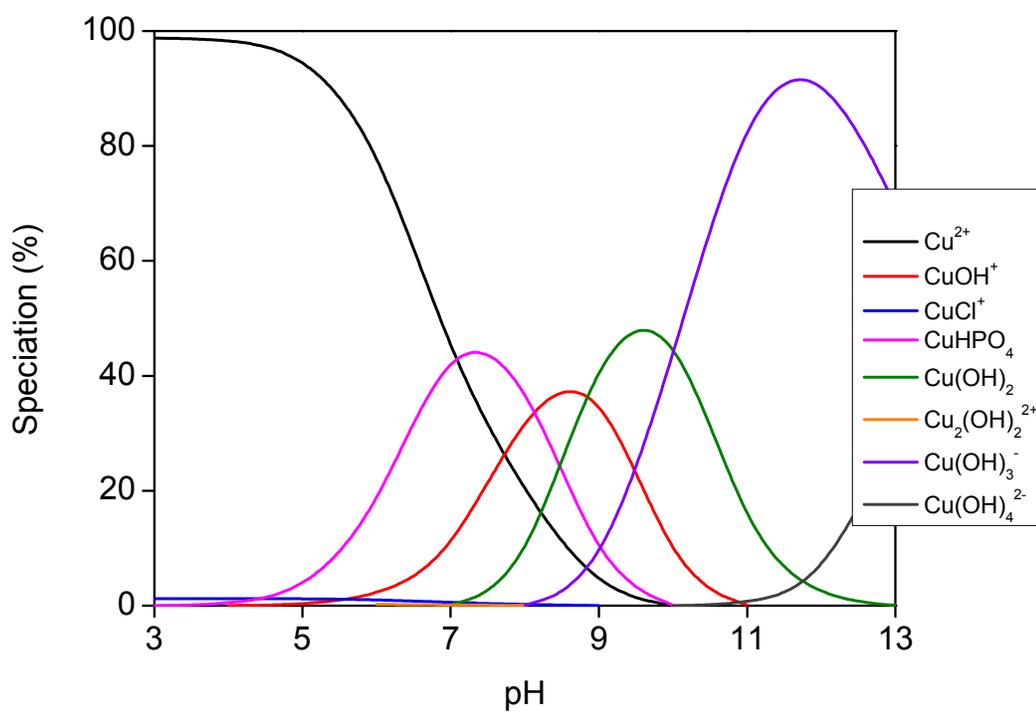
Figure S15. pH-dependent speciation of cuprous ion in aqueous media containing 10 mM NaCl and 0.5 mM phosphate predicted by Visual MINTEQ
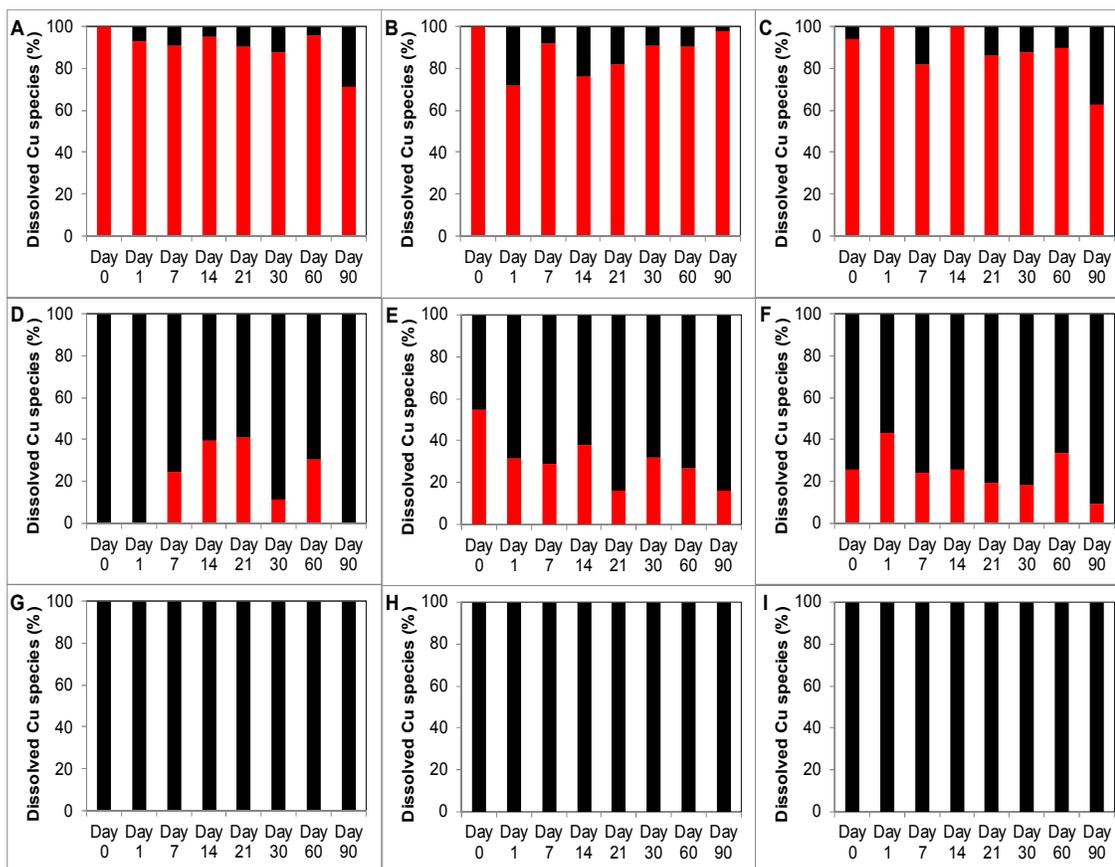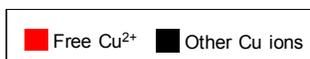
Figure S16. Speciation of dissolved Cu species. f-Cu^{2+}/ [Cu]$_{diss}$ from nano-CuO at (A) pH 4, (D) pH 7, and (G) pH 11; nano-Cu at (B) pH 4, (E) pH 7, and (H) pH 11; and Kocide at (C) pH 4, (F) pH 7, and (I) pH 11. Ionic strength = 10 mM NaCl with no NOM
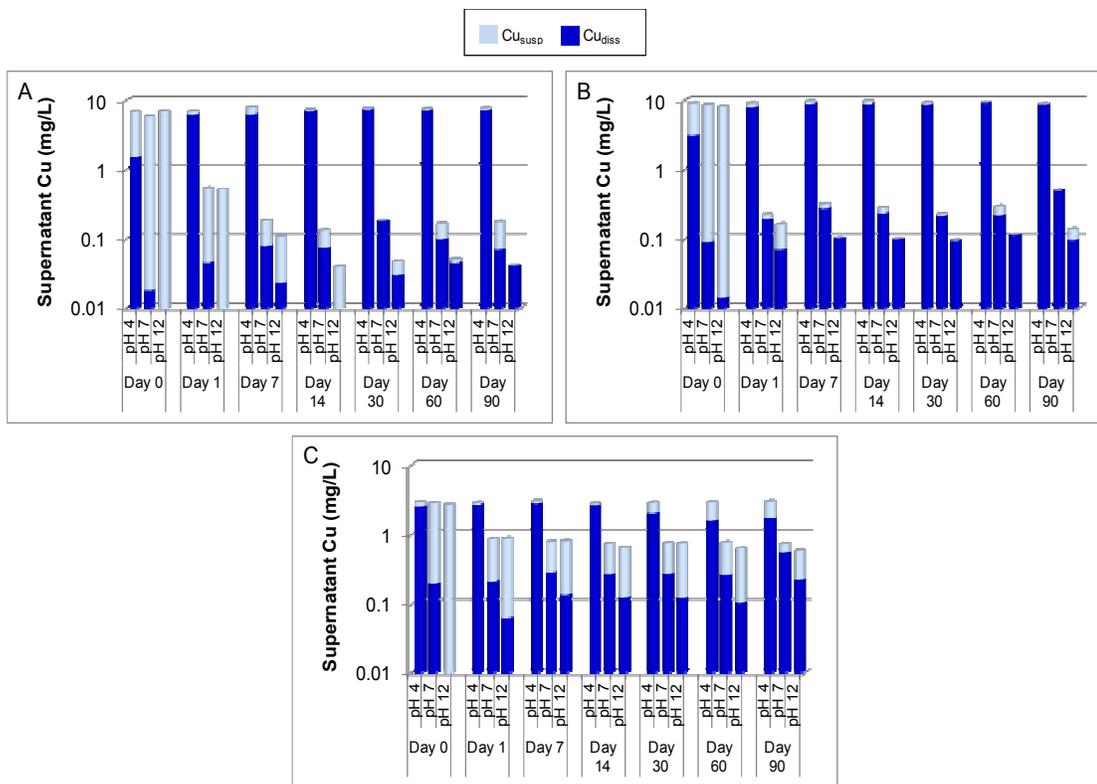
Figure S17. Effect of pH on distribution of Cu in supernatant of (A) nano-CuO, (B) nano-Cu, and (C) Kocide. All studies at 10 mM NaCl and no NOM
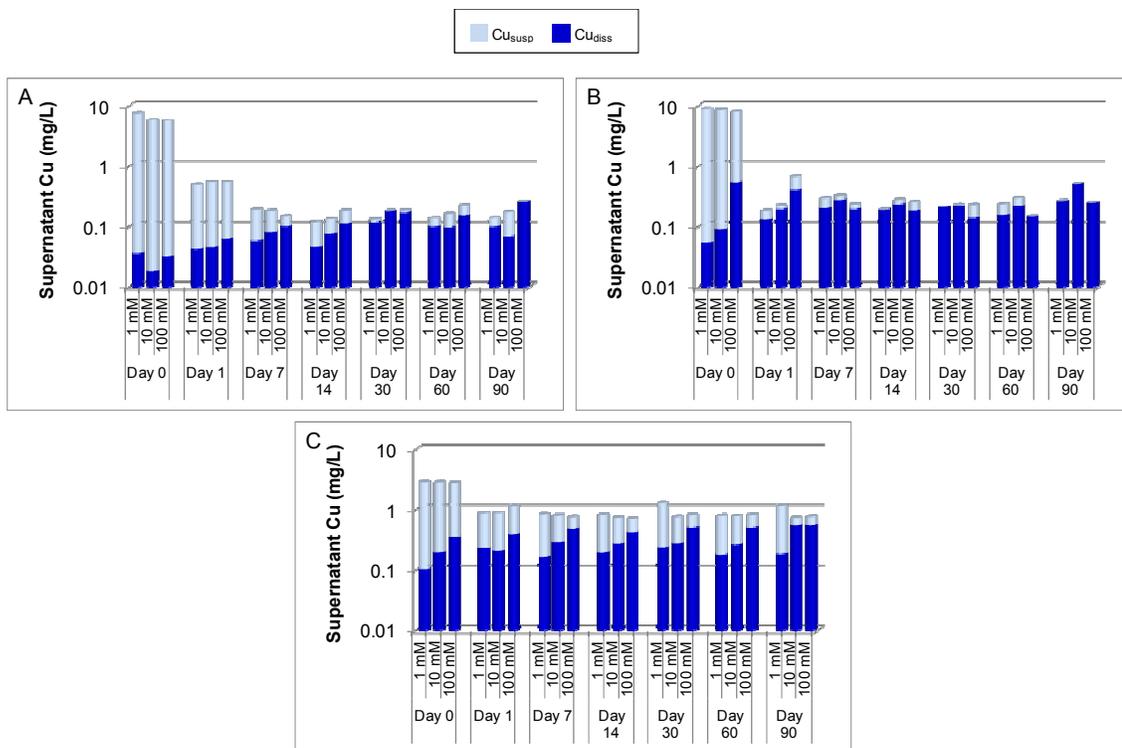
Figure S18. Effect of ionic strength on distribution of Cu in supernatant of (A) nano-CuO, (B) nano-Cu, and (C) Kocide. pH = 7 and no NOM
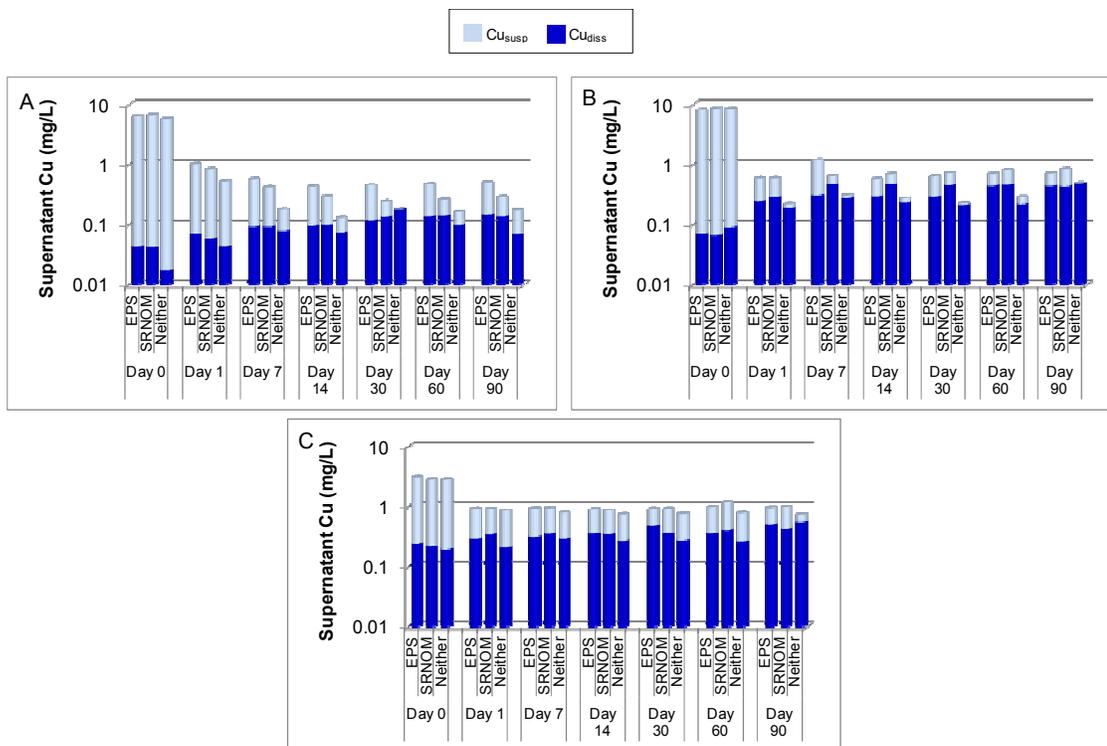
Figure S19. Effect of EPS and SRN on distribution of Cu in supernatant of (A) nano-CuO, (B) nano-Cu, and (C) Kocide. pH = 7

Additional information on effect of pH on dissolution and speciation

Total dissolved Cu

Within 2 hr of dispersal of nano-CuO into the aqueous phase at pH 4, about 21% of the particles were dissolved, compared to 0.2% at pH 7 and 0.1% at pH 11 (Figure 6). Dissolution of nano-Cu was even faster: 37% at pH 4, 1.1% at pH 7, and 0.2% at pH 11 within 2 hr. Kocide dissolved fastest, with 96% at pH 4, 7.3% at pH 7, and 0.3% at pH 11 within 2 hr. In 24 hr, over 80% of nano-CuO and 90% of nano-Cu were dissolved at pH 4.

Dissolution of nano-CuO reached equilibrium after about 21-30 days under most conditions at 10 mM, but dissolution of nano-Cu and Kocide continued at pH 7 and 11 beyond Day 90. At pH 4, nano-Cu was 100% dissolved after 7 days. Similarly, $Cu(OH)_2$ in Kocide dissolved fully at pH 4 within 24 hr, but we observed a decreasing $[Cu]_{diss}$ from Day 21 (Fig. 6), suggesting removal of dissolved Cu^{2+} due to precipitation of Cu-containing species. For Kocide at pH 7 $[Cu]_{diss}$ increased from 10% to 21% between Day 14 and 90. At pH 11, dissolution reached 8.3% in Kocide by Day 90 but remained below 1% in nano-CuO. At pH 11 the amount of $[Cu]_{diss}$ from nano-Cu was higher than from nano-CuO by 1-2 orders of magnitude.

Acidic environments will enhance dissolution of CBNPs studied, while a larger fraction of the Cu particles will end up in the sediment phase in neutral and alkaline conditions where they may continue to release ions over a long period of time. Dissolution rate was Kocide > nano-Cu >> nano-CuO at all pH conditions. As such, the release of Kocide or nano-Cu into natural waters may portend a higher acute exposure of organisms to dissolved Cu than nano-CuO. The surface of nano-Cu may be oxidized in the natural waters to Cu_2O and/or CuO, which do not dissolve at fast as Cu (Cai *et al.* 2005; Mudunkotuwa *et al.* 2012). However, gradual dissolution of the oxidized particles may continue to occur depending on

112

water pH as shown here. Once dissolution has occurred natural purification processes in natural waters, such as adsorption to NOM and suspended particles, complexation, and precipitation, may remove dissolved Cu from the water column into sediment where Cu may accumulate to higher concentrations.(Flemming & Trevors 1989) Thus, long-term fate of CBNPs in natural waters is sediment phase, where they may accumulate and exhibit toxicity to benthic organisms (Hanna *et al.* 2013).

Speciation

F-Cu^{2+} was dominant at pH 4 in all CBNPs. Although nano-Cu was expected to release Cu^+ (Cai *et al.* 2005; Mudunkotuwa *et al.* 2012) we found that f-Cu^{2+} accounted for $\geq 72\%$ of $[Cu]_{diss}$ during the 90 days at pH 4. Cu^+ may oxidize or disproportionate to form Cu^{2+} ions (SI Eq. S3) (Ciavatta *et al.* 1980). The most prominent forms of c-Cu^+ and c-Cu^{2+} predicted by Visual MINTEQ at pH 4 are $CuCl_2^-$ and $CuCl^+$, respectively.

$$2Cu^+ \leftrightarrow Cu^{2+} + Cu_{(s)}$$

Eq. S3

At pH 7, complexed forms of copper dominated for all CBNPs, but with a fraction of f-Cu^{2+}, which varied with time from around 0 to 55%. For nano-Cu, f-Cu^{2+}/$[Cu]_{diss}$ decreased over time, suggesting that either complexation-based dissolution of nano-Cu dominated over time, or f-Cu^{2+} was rapidly complexed as it was formed. On average, f-Cu^{2+} composed 25% of $[Cu]_{diss}$ in Kocide detected at each sampling point over the 90 day period. No f-Cu^{2+} was detected in nano-CuO on Day 0, 1, and 90. Variation of f-Cu^{2+}/$[Cu]_{diss}$ is likely due to cyclical complex formation and decomposition (Cai *et al.* 2005). f-Cu^{2+} was undetected in all pH 11 treatments, which agrees with modeling results.

Total Cu in Supernatant

In nano-CuO $[Cu]_{susp}$ was 5.20, 5.81 and 6.91 mg/L at pH 4, 7, and 11 respectively on Day 0, and decreased to 0.60, 0.49, and 0.51 mg/L at the respective pH conditions 24 hr later. Similarly observations were made in nano-Cu and Kocide. In general, $[Cu]_{susp}$ continued to decrease in all conditions over 90 days as more particles dissolved or sedimented out. However, for Kocide $[Cu]_{susp}$ increased after Day 14 at pH 4, likely due to precipitation of Cu or Cu-based compounds as discussed earlier.

$[Cu]_{total}$ decreased rapidly at pH 7 and 11 due to sedimentation and low dissolution, but generally increased at pH 4 due to rapid dissolution. For nano-Cu, for instance, $[Cu]_{total}$ increased from 3.11 to 7.79 mg/L within 24 hr at pH 4, and decreased from 8.48 to 0.22 mg/L and 8.02 to 0.16 mg/L at pH 7 and 11 respectively. $[Cu]_{total}$ was relatively stable at pH 4 in Kocide since dissolution was rapid. These results show that sedimentation of CBNPs may not completely reduce exposure of pelagic and benthic organisms to Cu species as sedimented particles may release potentially toxic ions.

Additional information on effect of ionic strength on dissolution and speciation

Total dissolved Cu

The effects of IS on CBNP dissolution and speciation were only studied at pH 7. Higher IS is generally associated with increased aggregation of ENPs due to ionic shielding and weakening of the repulsive charges on nanoparticle surfaces (Keller *et al.* 2010; Adeleye *et al.* 2013b; Adeleye & Keller 2014), which in turn decreases dissolution as less total surface area is exposed to the surrounding media (Cai *et al.* 2005). However, 24 hr after introducing Kocide into aqueous phase 9.3%, 11.0%, and 16.6% dissolution was observed in 1, 10, and 100 mM conditions respectively. Similar trend was observed in nano-Cu and Kocide (SI Figure S12). $[Cu]_{diss}$ increased gradually over time in all IS conditions, except in nano-Cu at

114

100 mM, where $[Cu]_{diss}$ was highest on Day 0 and then decreased steadily, probably due to saturation and precipitation.

Assuming equilibrium on Day 30 in nano-CuO systems, average dissolution was 1.43%, 1.55%, and 2.61% at 1, 10, and 100 mM respectively. This agreed reasonably well with the prediction of Visual MINTEQ: 1.91%, 1.93%, and 2.25% for the respective conditions. Average dissolution in Kocide, over 90 days, was 7.0%, 10.9%, and 17.4% which corroborates our earlier observation of higher dissolution in the pesticide. Dissolution occurs partly via complexation at neutral pH, suggesting that increased concentrations of anions (i.e., Cl^-) lead to an increased rate and/or magnitude of dissolution of CBNPs, which has also been observed in other ENPs (Huynh & Chen 2011). In this study, we found evidence for this in the levels of $c\text{-}Cu^{2+}$ detected in CBNPs. For instance, in nano-CuO average $c\text{-}Cu^{2+}$ was 84%, 86%, and 96% at 1, 10, and 100 mM over 90 days.

Speciation

$F\text{-}Cu^{2+}/[Cu]_{diss}$ decreased with increased IS in all CBNPs. This indicates either increased complexation-based dissolution at higher $[Cl^-]$, or increased complexation of $f\text{-}Cu^{2+}$. In nano-CuO $f\text{-}Cu^{2+}$ was not detected in any IS condition until Day 7 (although $[Cu]_{diss}$ was detected); and on Day 30 $f\text{-}Cu^{2+}/c\text{-}Cu^{2+}$ was 0.18, 0.16 and 0.05 at 1, 10, and 100 mM NaCl respectively. In nano-Cu, $f\text{-}Cu^{2+}$ was the most dominant Cu species on Day 0 at 1 and 10 mM, representing 75% and 55% respectively. At 100 mM however, $f\text{-}Cu^{2+}$ was only 8% even though $[Cu]_{diss}$ was 0.53 mg/L at 100 mM compared to 0.053 and 0.092 mg/L detected at 1 and 10 mM respectively. $[Cu]_{diss}$ increased from 0.053 and 0.092 mg/L to 0.13 and 0.19 mg/L at 1 and 10 mM respectively between Day 0 and 1, but $f\text{-}Cu^{2+}/[Cu]_{diss}$ decreased by 45% and 23% at the two IS respectively. Since there was no corresponding decrease in $f\text{-}Cu^{2+}$ within this period, increased $[Cu]_{diss}$ was probably due to complexation-based

dissolution rather than complexation of f-Cu^{2+}. By Day 90 f-Cu^{2+}/[Cu]$_{diss}$ in nano-Cu was

27%, 16% and 8% at 1, 10, and 100 mM respectively. In Kocide, average f-Cu^{2+} over 90

days was 26%, 25%, and 11% at 1, 10, and 100 mM respectively. The maximum f-Cu^{2+}

detected in Kocide at 100 mM was 18%, on Day 1. Days 0 and 90 ratio of f-Cu^{2+}/c-Cu^{2+} in

Kocide were 0.40 and 0.28, 0.35 and 0.10, and 0.09 and 0.06 at 1, 10, and 100 mM

respectively showing that c-Cu^{2+} increased significantly over time.

   Total Cu in Supernatant

[Cu]$_{susp}$ was not detected on Day 90 at 100 mM condition of nano-CuO and all the

conditions of nano-Cu. In Kocide however, [Cu]$_{susp}$ accounted for a significant portion of

[Cu]$_{total}$ at pH 7 (and 11) throughout the study. [Cu]$_{susp}$ was about 80% of [Cu]$_{total}$ on Day 90

in Kocide at 1 mM; and about 30% at 10 and 100 mM respectively (SI Figure S16). This

agrees with our previous observation of slow sedimentation in Kocide due to high surface

charge and low density. Thus, although the % Cu in Kocide is lower than nano-CuO or

nano-Cu by several factors, both [Cu]$_{diss}$ and [Cu]$_{susp}$ were significantly higher in Kocide at

pH 7. This implies that the release of Kocide into natural waters may result in a larger total

release of Cu species in the water matrix than equivalent bulk masses of nano-CuO and

nano-Cu.

References

Adeleye A., Keller A., Miller R. & Lenihan H. (2013a). Persistence of commercial nanoscaled zero-valent iron (nZVI) and by-products. *Journal of Nanoparticle Research*, 15, 1-18.

Adeleye A.S. & Keller A.A. (2014). Long-term colloidal stability and metal leaching of single wall carbon nanotubes: effect of temperature and extracellular polymeric substances. *Water research*, 49, 236-50.

Adeleye A.S., Keller A.A., Miller R.J. & Lenihan H.S. (2013b). Persistence of commercial nanoscaled zero-valent iron (nZVI) and by-products. *Journal of Nanoparticle Research*, 15.

Balnois E., Wilkinson K.J., Lead J.R. & Buffle J. (1999). Atomic Force Microscopy of Humic Substances: Effects of pH and Ionic Strength. *Environmental Science & Technology*, 33, 3911-3917.

Bennett S.W., Adeleye A., Ji Z. & Keller A.A. (2013). Stability, metal leaching, photoactivity and toxicity in freshwater systems of commercial single wall carbon nanotubes. *Water research*.

Cabaniss S.E. & Shuman M.S. (1988). Copper binding by dissolved organic matter: I. Suwannee River fulvic acid equilibria. *Geochimica et Cosmochimica Acta*, 52, 185-193.

Cai S., Xia X. & Xie C. (2005). Research on Cu2+ transformations of Cu and its oxides particles with different sizes in the simulated uterine solution. *Corrosion Science*, 47, 1039-1047.

Cao B., Shi L., Brown R., Xiong Y., Fredrickson J., Romine M., Marshall M., Lipton M. & Beyenal H. (2011). Extracellular polymeric substances from Shewanella sp HRCR-1 biofilms: characterization by infrared spectroscopy and proteomics. *Environmental Microbiology*, 13, 1018-1031.

Ciavatta L., Ferri D. & Palombari R. (1980). On the equilibrium Cu2+ + Cu(s) ⇄2Cu+. *Journal of Inorganic and Nuclear Chemistry*, 42, 593-598.

Cioffi N., Torsi L., Ditaranto N., Tantillo G., Ghibelli L., Sabbatini L., Bleve-Zacheo T., D'Alessio M., Zambonin P.G. & Traversa E. (2005). Copper Nanoparticle/Polymer Composites with Antifungal and Bacteriostatic Properties. *Chem. Mater.*, 17, 5255-5262.

Fang L., Wei X., Cai P., Huang Q., Chen H., Liang W. & Rong X. (2011). Role of extracellular polymeric substances in Cu (II) adsorption on< i> Bacillus subtilis</i> and< i> Pseudomonas putida</i>. *Bioresource technology*, 102, 1137-1141.

117

Flemming C.A. & Trevors J.T. (1989). Copper Toxicity and Chemistry in the Environment - a Review. *Water Air and Soil Pollution*, 44, 143-158.

Flemming H.-C., Neu T.R. & Wozniak D.J. (2007). The EPS matrix: the "house of biofilm cells". *Journal of Bacteriology*, 189, 7945-7947.

Grant W. & Jones B. (2000). Alkaline environments. *Encyclopaedia of microbiology*, 1, 126-133.

Grasso D., Subramaniam K., Butkus M., Strevett K. & Bergendahl J. (2002). A review of non-DLVO interactions in environmental colloidal systems. *Reviews in Environmental Science and Biotechnology*, 1, 17-38.

Griffitt R.J., Weil R., Hyndman K.A., Denslow N.D., Powers K., Taylor D. & Barber D.S. (2007). Exposure to Copper Nanoparticles Causes Gill Injury and Acute Lethality in Zebrafish (Danio rerio). *Environmental Science & Technology*, 41, 8178-8186.

Hanna S.K., Miller R.J., Zhou D.X., Keller A.A. & Lenihan H.S. (2013). Accumulation and toxicity of metal oxide nanoparticles in a soft-sediment estuarine amphipod. *Aquat. Toxicol.*, 142, 441-446.

Hidmi L. & Edwards M. (1999). Role of Temperature and pH in Cu(OH)2 Solubility. *Environmental Science & Technology*, 33, 2607-2610.

Huynh K.A. & Chen K.L. (2011). Aggregation Kinetics of Citrate and Polyvinylpyrrolidone Coated Silver Nanoparticles in Monovalent and Divalent Electrolyte Solutions. *Environmental Science & Technology*, 45, 5564-5571.

Keller A.A., McFerran S., Lazareva A. & Suh S. (2013). Global life cycle releases of engineered nanomaterials. *Journal of Nanoparticle Research*, 15, 1-17.

Keller A.A., Wang H., Zhou D., Lenihan H.S., Cherr G., Cardinale B.J., Miller R. & Ji Z. (2010). Stability and Aggregation of Metal Oxide Nanoparticles in Natural Aqueous Matrices. *Environmental Science & Technology*, 44, 1962-1967.

Lambert J.B., Shurvell H.F., Lightner D.A. & Cooks R.G. (1987). *Introduction to organic spectroscopy*. Macmillan New York.

Legler G., Mullerplatz C.M., Mentgeshettkamp M., Pflieger G. & Julich E. (1985). On the Chemical Basis of the Lowry Protein Determination. *Analytical Biochemistry*, 150, 278-287.

Malvern (2008). *Zetasizer nano series user manual*, UK.

Malvern (2011). Dynamic Light Scattering: Common Terms Defined. In. Malvern Instruments Limited Worcestershire, UK.

Morris D.L. (1948). Quantitative Determination of Carbohydrates with Dreywoods Anthrone Reagent. *Science*, 107, 254-255.

Mudunkotuwa I.A., Pettibone J.M. & Grassian V.H. (2012). Environmental Implications of Nanoparticle Aging in the Processing and Fate of Copper-Based Nanomaterials. *Environmental Science & Technology*, 46, 7001-7010.

Nidhin M., Indumathy R., Sreeram K.J. & Nair B. (2008). Synthesis of iron oxide nanoparticles of narrow size distribution on polysaccharide templates. *Bull Mater Sci*, 31, 93-96.

Omoike A. & Chorover J. (2004). Spectroscopic Study of Extracellular Polymeric Substances from Bacillus s ubtilis: Aqueous Chemistry and Adsorption Effects. *Biomacromolecules*, 5, 1219-1230.

Ren G.G., Hu D.W., Cheng E.W.C., Vargas-Reus M.A., Reip P. & Allaker R.P. (2009). Characterisation of copper oxide nanoparticles for antimicrobial applications. *International Journal of Antimicrobial Agents*, 33, 587-590.

Saleh N.B., Pfefferle L.D. & Elimelech M. (2008). Aggregation Kinetics of Multiwalled Carbon Nanotubes in Aquatic Systems: Measurements and Environmental Implications. *Environmental Science & Technology*, 42, 7963-7969.

Shi J., Abid A.D., Kennedy I.M., Hristova K.R. & Silk W.K. (2011). To duckweeds (Landoltia punctata), nanoparticulate copper oxide is more inhibitory than the soluble copper in the bulk solution. *Environmental Pollution*, 159, 1277-1282.

Su Y., Adeleye A.S., Huang Y., Sun X., Dai C., Zhou X., Zhang Y. & Keller A.A. (2014). Simultaneous removal of cadmium and nitrate in aqueous media by nanoscale zerovalent iron (nZVI) and Au doped nZVI particles. *Water research*, 63, 102-11.

Sunda W.G. & Guillard R.R.L. (1976). Relationship between Cupric Ion Activity and Toxicity of Copper to Phytoplankton. *J Mar Res*, 34, 511-529.

Tranquada J., Sternlieb B., Axe J., Nakamura Y. & Uchida S. (1995). Evidence for stripe correlations of spins and holes in copper oxide superconductors. *Nature*, 375, 561-563.

Wang X.W., Xu X.F. & Choi S.U.S. (1999). Thermal conductivity of nanoparticle-fluid mixture. *Journal of Thermophysics and Heat Transfer*, 13, 474-480.

Wang Z., Huang S. & Liu Q. (2002). Use of anodic stripping voltammetry in predicting toxicity of copper in river water. *Environmental Toxicology and Chemistry*, 21, 1788-1795.

Worthington K.L., Adamcakova-Dodd A., Wongrakpanich A., Mudunkotuwa I.A., Mapuskar K.A., Joshi V.B., Guymon C.A., Spitz D.R., Grassian V.H. & Thorne P.S.

(2013). Chitosan coating of copper nanoparticles reduces in vitro toxicity and increases inflammation in the lung. *Nanotechnology*, 24, 395101.

Zhao G., Li J., Ren X., Chen C. & Wang X. (2011). Few-Layered Graphene Oxide Nanosheets As Superior Sorbents for Heavy Metal Ion Pollution Management. *Environmental Science & Technology*, 45, 10454-10462.

Zhou D. & Keller A.A. (2010). Role of morphology in the aggregation kinetics of ZnO nanoparticles. *Water research*, 44, 2948-2956.

Chapter 4. Interactions between algal extracellular polymeric substances and TiO₂ nanoparticles in aqueous media

4.1. Introduction

Nanosized titanium dioxide (nTiO$_2$) is one of the most-manufactured and used engineered nanomaterials or ENMs (Keller *et al.* 2013). Common uses of nTiO$_2$—such as in personal care products, paints and coatings, and cleaning products, etc.—will likely lead to direct release of the ENMs into the environment. For instance, Gondikas *et al*. recently reported increase in titanium ratio of suspended particles in a lake during the summer months when recreational activities peak (Gondikas *et al.* 2014). The spike in colloidal titanium was attributed to release of nTiO$_2$ from the matrix of sunscreen used by swimmers. A thorough understanding of the fate of nTiO$_2$ in aquatic systems is necessary for reliable environmental risk assessment of these particles in natural waters.

The fate and effect of ENMs in natural waters depend on the physicochemical properties of particles as well as their interactions with other factors present in media (Keller *et al.* 2010; Adeleye *et al.* 2013; Adeleye & Keller 2014). Homoaggregation, and more importantly, heteroaggregation between ENMs and other naturally-occurring colloids will determine the fate of nanomaterials in aquatic systems (Quik *et al.* 2012; Praetorius *et al.* 2013; Quik *et al.* 2014). Natural organic matter (NOM) is also expected to affect the stability of ENMs via direct interactions as well as influencing heteroaggregation of nTiO$_2$ with natural colloids. The effect of commonly used proxies of NOM such as humic acid, fulvic acid, alginate, etc. on the stability of nTiO$_2$ is well understood (Thio *et al.* 2011; Erhayem & Sohn 2014). The influence of a different type of NOM solely produced by microorganisms,

known as extracellular polymeric substances or EPS, on the stability of nTiO$_2$ in aquatic systems is however largely uninvestigated.

About 50% of phytoplankton photosynthetic products are released as EPS (Kadar *et al.* 2014), which is mainly composed of polysaccharides, proteins, lipids, nucleic acids, and other polymeric substances excreted by microorganisms (Nielsen & Jahn 1999; Wingender *et al.* 1999; Flemming *et al.* 2007). EPS can interact with other charged particles via the functional groups in the macromolecules (Pal & Paul 2008; Adeleye *et al.* 2014; Adeleye & Keller 2014; Kadar *et al.* 2014). More so, the hydrophobic fractions of EPS polysaccharides can interact with other hydrophobic surfaces (Flemming *et al.* 2007). EPS derived from marine organisms were shown to affect the fate and effects of carbon nanotubes (Adeleye & Keller 2014), copper nanoparticles (Adeleye *et al.* 2014), and ferrihydrite (Kadar *et al.* 2014). In this study, we investigated the potential for interactions between three types of nTiO$_2$ and EPS extracted from both freshwater and marine phytoplankton. The mechanisms behind interactions as well as the effects on the stability of the ENMs were also probed.

4.2. Materials and Methods

4.2.1. Engineered TiO$_2$ Nanomaterials

Hombikat UV 100 (denoted UV100), UV-Titan M212 (denoted M212), and UV Titan M262 (denoted M262) were obtained as dry ENM powder from Sachtleben, Germany. According to the manufacturer, UV100 is uncoated, while M212 and M262 had hydrophilic and hydrophobic coatings, respectively. The three nTiO$_2$ were used as received. We determined the primary particle size, morphology, and surface elemental distribution of each nTiO$_2$ via electron microscopy using a FEI Titan 300 kV FEG transmission electron microscope (TEM) with an Oxford INCA x-sight probe for energy-dispersive X-ray

spectroscopy (EDS) and a FEI XL30 Sirion scanning electron microscope (SEM) equipped with an EDAX APOLLO X probe EDS. Hydrodynamic diameter (HDD) and zeta (ζ) potential of the particles were determined in deionized water (DI, 18.2 MΩ.cm, Barnstead nanopure diamond) using a Zetasizer Nano-ZS90 (Adeleye *et al.* 2014; Adeleye & Keller 2014). The isoeletric point (IEP) of the particles was determined by adjusting pH with dilute HCl and NaOH (Fisher Scientific) and measuring ζ potential using the Zetasizer. Brunauer–Emmett–Teller (BET) surface areas were determined using a Micromeritics TriStar 3000 porosimeter while phase and crystal structures of particles were determined using a Bruker D8 Advance X-ray diffractometer (Adeleye *et al.* 2013).

4.2.2. Extracellular Polymeric Substances

Soluble extracellular polymeric substances (sEPS) were extracted from axenic cultures of two algal species—*Chlamydomonas reinhardtii* (a freshwater phytoplankton) and *Dunaliella tertiolecta* (a seawater phytoplankton). *C. reinhardtii* was cultured in COMBO media according to Stevenson *et al.* (2013) while *D. tertiolecta* was cultured in f/2 media made with natural seawater collected from the Pacific Ocean (Santa Barbara, CA) according to Miller et al. (2012). . sEPS were extracted via centrifugation (2,500 *g*, 15 min, and 4 °C using a Sorvall RC 5B Plus) when the cells reached stationary growth phase (Adeleye & Keller 2014). The supernatants, which contained sEPS, were aseptically filtered with 0.2 μm PES membrane filters (Thermo Fisher Scientific). To remove residual salts from the growth media and low molecular-weight metabolites, sEPS were dialyzed against DI water (renewed twice daily) for 96 h at 4 °C using a 3.5 kDa cut-off regenerated cellulose tubular membrane (Fischer Scientific). The membranes were treated with $NaHCO_3$ and Na_2EDTA to remove residues before use. sEPS were characterized by measuring dissolved organic carbon (DOC) and total dissolved nitrogen (TDN) using a Shimadzu TOC-V with an attached TNM1 unit.

123

In addition, carbohydrate and protein concentrations were determined using the anthrone method (with glucose as standard) (Morris 1948), and modified Lowry Protein Assay (with bovine serum albumin as standards) (Legler *et al.* 1985), respectively. ζ potentials of sEPS were determined using the Zetasizer. Infrared spectroscopy of freeze-dried (Labconco 7754042) sEPS was done using a Nicolet iS10 spectrometer with a diamond ATR crystal (Adeleye *et al.* 2014). Interferograms were collected by taking 256 scans in the range 4000 – 400 cm^{-1} at 2 cm^{-1}.

4.2.3. Effect of sEPS on Surface Charge of nTiO$_2$

The effect of sEPS on the surface charge of nTiO$_2$ was determined by measuring the ζ potential of the particles (50 mg/L) in aqueous media (pH 7, 0.5 mM carbonate buffer) in the presence of sEPS (0 – 0.5 mg-C/L) using the Zetasizer. The influence of carbonate buffer on ζ potential of the particles was also determined in order to clearly quantify the contributions of sEPS to changes in the ENM physicochemical property.

4.2.4. Effect of sEPS on Aggregation of nTiO$_2$

The effects of sEPS (0 – 0.5 mg-C/L) on the aggregation kinetics of UV100, M212, and M262 were studied via dynamic light scattering (DLS) as described previously (Saleh *et al.* 2008; Adeleye *et al.* 2014; Adeleye & Keller 2014). A measured mass of each nTiO$_2$ was added into DI containing aliquots of sEPS stock and then bath-sonicated (Branson 2510) for 30 min to prepare nTiO$_2$ stock solutions (200 mg/L). Aliquots were taken from the prepared stock (to make a final nTiO$_2$ concentration of 50 mg/L), and added to NaCl (varying concentrations), buffer (0.5 mM), and DI (to make up the volume to 1 mL) for DLS analyses. The initial aggregation rate constant (k) reflects doublet formation and is proportional to the initial rate of increase in the intensity-weighted hydrodynamic

124

radius, $a_h(t)$, with time, t, and the inverse of initial number concentration of nanoparticles, N_0 (Eq. 1) (Saleh *et al.* 2008; Adeleye & Keller 2014):

$$k \propto \frac{1}{N_0} \left(\frac{da_h(t)}{dt} \right)_{t \to 0}$$

(1)

k is obtained from the slope of the best fit line of $(da_h(t)/dt)_{t \to 0}$, which is determined via DLS using the Zetasizer. Attachment efficiencies (α) of nTiO$_2$-sEPS suspensions were derived by normalizing the measured k by the diffusion-limited aggregation rate constant $(k)_{fav}$ (Eq. 2). $(k)_{fav}$ may be calculated from Smoluchowski's equation for diffusion-limited aggregation or determined in highly favorable aggregation conditions (done in this study). The diffusion-limited and reaction-limited clustering aggregation regimes and critical coagulation concentrations (CCC) were identified in a plot of $\log_{10}$[Ionic strength] versus $\log_{10}\alpha$.

$$\alpha = \frac{\left(\dfrac{da_h(t)}{dt} \right)_{t \to 0}}{\left(\dfrac{da_h(t)}{dt} \right)_{t \to 0, fav}}$$

(2)

4.2.4.1. Role of sEPS Concentration

Concentrations of EPS in natural waters is expected to vary temporally and spatially based on water productivity and nutrient availability, among other factors. To study the role of sEPS concentration, we prepared nTiO$_2$ stocks with 0.5, 1, and 2 mg-C/L *C. reinhardtii* sEPS. All the studies were done at pH 7 and final concentration of sEPS in the samples measured was 0.125, 0.25, and 0.5 mg-C/L, respectively.

4.2.4.2. Role of sEPS Type

The composition of EPS varies widely with growth stage, nature of habitat, microbial species, etc (Nielsen & Jahn 1999; Wingender *et al.* 1999; Flemming *et al.* 2007). To

investigate if the source of sEPS influenced its effect on nTiO$_2$ aggregation dynamics, we compared the effects of both sEPS isolated from *C. reinhardtii* and *D. tertiolecta*. nTiO$_2$ stocks were made with 0.5 – 2 mg-C/L of sEPS from either organism and the suspensions were kept at pH 7.

4.2.4.3. Role of Algal Media Nutrient Level

To see how variation in algal nutrient level may affect sEPS composition and its influence on nTiO$_2$ aggregation, we cultured *D. tertiolecta* in f/2 media with (1) normal nutrient levels and (2) with spiked nitrogen (twice the normal level or 17.64×10^{-4} M NaNO$_3$). Aggregation kinetics was compared using nTiO$_2$ stocks made with 1 mg-C/L of sEPS isolated from both sets of organisms.

sEPS isolated from *C. reinhardtii* is hereafter referred to as sEPS-Chl. sEPS isolated from *D. tertiolecta* grown in normal f/2 media and f/2 media with spiked N are hereafter denoted as sEPS-Dun1 and sEPS-Dun2, respectively.

4.2.5. Interactions of sEPS with nTiO$_2$

To confirm the adsorption of sEPS unto nTiO$_2$, and to investigate the sEPS groups that are responsible for interactions with nTiO$_2$, we added 5 mg of nTiO$_2$ to DI or sEPS stock solutions. The suspensions were sonicated for 1 h (Branson 2510) to allow for interactions after which they were centrifuged (12,000 g, 30 min). The aqueous phase (containing sEPS that are not adsorbed to nTiO$_2$) was decanted. The solid fractions obtained were lyophilized and then analyzed using the Nicolet FTIR spectrometer in absorbance mode (256 scans in the range 4000 – 400 cm^{-1} at a resolution of 2 cm^{-1}). The spectra obtained from DI-suspended solids were subtracted from the spectra obtained from samples suspended in sEPS in order to remove signals due to nTiO$_2$. The spectra obtained after the subtraction were then compared with that from pristine sEPS.

126

4.3. Results and Discussions

4.3.1 nTiO$_2$ and sEPS Characterizations

TEM analyses showed that the primary particles of UV100 are about an order of magnitude smaller than those of M212 and M262 (Figure 1, Table 1). This is in agreement with BET data shown in Table 1. The sizes were determined from the average size of 30 – 60 particles and distributions of particle sizes are presented in Supporting Information (SI) Figure S1. EDS analyses (SI Figure S2) revealed the presence of aluminum (less than 4% wt.) in M212 and M262, while M262 also contained some silicon (~1% wt.). This agrees with the information provided by the manufacturer, which reports that M212 is coated with alumina and glycerol while M262 is coated with alumina and dimethicone, (C$_2$H$_6$OSi)n.

Despite its small primary particle size, UV100 formed the largest aggregates in water— with HDD more than twice that of M212 and M262 (Table 1). The instability of UV100 is probably due to its low surface charge in suspension as indicated by a ζ potential of 3 mV in DI. The ζ potential of M212 and M262 exceeded 30 mV, a typical threshold of colloidal stability (Everett 1988). The suspensions of the three nTiO$_2$ measured pH ~ 5.8 in DI, which is below their respective IEPs (Table 1, SI Figure S3).

Table 2 shows the major properties of the three sEPS used in this study. The three sEPS had net negative charges both in DI and in buffered solutions (Table 2, SI Figure S4). However, sEPS from *D. tertiolecta* were more negatively-charged, and more sensitive to pH than sEPS from *C. reinhardtii*. Increased negative charges of sEPS with pH is typically due to deprotonation of carboxyl (pH 2.0-6.0), phospholipids (pH 2.4-7.2), phosphodiester (pH 3.2-3.5), amine (pH 9.0-11.0), and hydroxyl (pH ≥ 10) groups (Martinez *et al.* 2002; Jiang *et al.* 2004; Fang *et al.* 2012). Although polysaccharides are generally considered as the major

127

fraction of EPS, we observed a carbohydrate:protein mass ratio ranging from 0.8 (in *C. reinhardtii*) to 6.1 (in *D. tertiolecta*).

FTIR is useful for identifying functional groups of macromolecules, including those of biological origins (Naumann *et al.* 1991; Jiang *et al.* 2004; Fang *et al.* 2012). The FTIR spectra of the sEPS are presented in Figure 2. The three spectra are quite similar as have also been observed in other studies (Jiang *et al.* 2004).

4.3.2 Effect of sEPS on Surface Charge of nTiO$_2$

The stability of ENMs in aqueous media can be predicted from their surface charge (as indicated by their ζ potential). In addition, the adsorption of other materials (such as ions, polymers, colloids, etc.) onto the surface of ENMs often reflects on the particles' ζ potentials. In this study we measured the ζ potential of UV100, M212, and M262 in the presence of sEPS (0 – 0.5 mg-C/L) at pH 7. As shown in Figure 3, sEPS affected the ζ potential of the three nTiO$_2$. For instance, carbonate buffer reduced the ζ potential of M262 from 32.4 to 21.6 mV, probably due to the attachment of carbonate ions on the surface of the particles. ζ potential was reduced even further to -2.99, -10.7, and -11.5 in the presence of 0.125, 0.25, and 0.5 mg-C/L sEPS-Chl, respectively. The values of ζ potential at 0.25 and 0.5 mg-C/L suggest that the surface of M212 was mostly coated with the algal polymers whose ζ potential was measured at -12.7 mV (Table 2). Similar observations were made with sEPS-Dun1 and sEPS-Dun2 when present in the stock of both M262 and M212 (i.e. ζ potential of particles shifted towards that of the respective sEPS at increasing sEPS concentrations, and was reasonably close at 0.5 mg-C/L sEPS concentration). Unlike M212 and M262, UV100 is expected to be negatively charged at pH 7 (IEP = pH 6.2; SI Figure S3) and we found its ζ potential to be -25.0 mV in the presence of carbonate buffer (pH 7). The addition of sEPS-Chl (up to 0.5 mg-C/L) only slightly increased its ζ potential to -23.7 mV.

Thus, unlike in M212 and M262, 0.5 mg-C/L of sEPS did not sufficiently coat the surface of UV100. This may be partly due to low electrostatic attraction between UV100 and sEPS, since both had net negative charges at pH 7. (Although the net charges on the sEPS were negative, they do contain some positively charged moieties, such as amino groups in proteins, with which sEPS can interact electrostatically with negatively charged surfaces.) In addition, aggregates of UV100 are considerably larger than those of M212 and M262 in aqueous media, which may require more EPS to coat effectively.

These results suggest that sEPS can interact with both positively and negatively charge nTiO$_2$ (and possibly other ENMs) in aqueous media. However, they may coat positively (or neutrally) charged particles more effectively due to electrical attractions. Such coating may lead to a reversal of surface charge as seen in M212 and M262 at concentrations of sEPS that are environmentally-relevant (up to 3.7 mg-C/L has been reported) (Hung $et\ al.$ 2001). In addition, the strong influence of sEPS on the surface charge of nTiO$_2$ suggests the formation of anionic negatively charged surface complexes. In other words, sEPS formed negatively-charged inner-sphere complexes on nTiO$_2$ (Fang $et\ al.$ 2012). Like most charged surfaces, ionic strength and pH can affect the surface charge of sEPS (Martinez $et\ al.$ 2002), which can affect the strength of their attractive interactions with nTiO$_2$.

4.3.3 Effect of sEPS on Aggregation of nTiO$_2$

The stability of ENMs in aquatic systems can be reasonably predicted from their experimental CCC values obtained in relevant aqueous media since it represents the ionic strength at which attachment efficiency of ENMs reaches unity and aggregation is diffusion-limited. We investigated how CCC of nTiO$_2$ responded to change in pH (4 – 11) in the presence of NaCl. As shown in Figure 4, the CCC of all three particles decreased as pH approached their respective IEPs (which are very close to the base of the broken lines joining

the data points). Although M212 and M262 are essentially the same core particle, M262 was much less stable in aqueous media across the range of pH studied. This is probably due to surface hydrophobicity resulting from its coating. Of the three nTiO$_2$, M212 was the most stable in acidic conditions while UV100 was the most stable in alkaline conditions.

sEPS-Chl generally increased the CCC of the three nTiO$_2$ (Figure 5a). For instance, the CCC of M262 at pH 7 increased by an order of magnitude from 5.5 mM NaCl in the absence of sEPS-Chl to 63 mM NaCl in the presence of 0.5 mg-C/L sEPS-Chl. The adsorption of sEPS on M262 therefore increased the stability of the nTiO$_2$ in aqueous media, which may lead to an increase in the exposure of pelagic organisms to an otherwise relatively unstable ENM (Figure 5a). Increased stability of the nTiO$_2$ by sEPS is due to steric hindrance between particle aggregates imparted by the algal macromolecules. The charged groups on EPS can also impart some electrostatic stabilization on the ENMs they adsorb onto as we reported in the previous section and other studies (Adeleye *et al.* 2014; Adeleye & Keller 2014).

The effect on stability of nTiO$_2$ by sEPS-Dun1, extracted from a marine phytoplankton, compared reasonably well with that of sEPS-Chl, which was extracted from a freshwater phytoplankton (Figure 5b). However, stronger influence on stability (i.e. increased CCC) of all three ENMs was observed in the presence of sEPS-Dun2, isolated from D. *tertiolecta* that was cultured in N-spiked media. The mechanism behind the higher stabilizing potential of sEPS-Dun2 is not very clear: Although sEPS-Dun2 had a higher DOC than sEPS-Dun1 and sEPS-Chl (Table 2) this may not account for increased stability since the DOC of all three types of sEPS was normalized for the entire study.

The conformation of sEPS macromolecules attached to all the nTiO$_2$ particles is expected to differ based on the charge, and perhaps hydrophobicity, of the ENMs surfaces.

At pH 7 for instance (where M212 and M262 are positively charged, and UV100 is negatively charged), one would expect sEPS to be less tightly bound to UV100 than to M212 and M262. Particles with looser binding/conformation may experience fewer collisions since a relatively larger fraction of sEPS polymers is free to exert steric effects than in particles where sEPS is tightly bound (Scheme 1). However, at higher sEPS concentrations particles with tightly bound sEPS may experience higher stability since a higher collision may not necessarily result in increased attachment (since their surface will be completely covered). This may explain why sEPS appeared to have more stabilizing effects on UV100 than M262 and M212, except at the highest concentration of sEPS-Chl (Figure 5a).

4.3.4 Analyses of nTiO$_2$-sEPS Complexes

We compared the FTIR spectra of pristine sEPS to those collected after allowing the biopolymers to interact with nTiO$_2$ in order to identify the functional groups that are responsible for interactions with the ENMs. Two typical spectra obtained from nTiO$_2$-sEPS interactions are shown in Figure 6. Adsorption on sEPS onto nTiO$_2$ modified the spectra of the macromolecules. In Figure 6a for instance, the bands around 3270 and 3387 cm^{-1}, (symmetric and asymmetric stretch of NH$_2$ in primary amides, respectively) decreased in intensity and shifted to higher wavenumbers after sEPS interacted with nTiO$_2$. Similarly, the C=O out-of-plane band in amides at around 598 cm^{-1} disappeared. The bands around 1439 and 1220 cm^{-1} (OH bending in carboxylic acids and P=O stretching of phospholipids or nucleic acids, respectively) shifted to 1450 and 1260 cm^{-1}, respectively. The band for O—C=O bending in carboxylic acid around 667 cm^{-1} disappeared. Band shifts and disappearance after interactions indicate the functional groups that are involved in adsorption/complexation (Ojamäe $et\ al.$ 2006; Bouhekka & Bürgi 2012; Fang $et\ al.$ 2012). A new band emerged around 1376 cm^{-1} which is consistent with the symmetric stretch of COO$^-$ group in

131

carboxylic acid salts (Lambert *et al.* 1987), suggesting the formation of a chemical bond between the carboxylic group and the surface of nTiO$_2$ (Ojamäe *et al.* 2006; Parikh *et al.* 2011; Beaussart *et al.* 2012; Fang *et al.* 2012). The corresponding asymmetric stretch of COO$^-$ band was probably masked by the carboxylic acid OH bending band around 1460 cm^{-1}.

These results indicate that interactions/attachments between sEPS and nTiO$_2$ occurred via amide, hydroxyl, and carboxylic groups of sEPS proteins, as well as phosphate groups in phospholipids or nucleic acids. Emergence of a new COO$^-$ band and the disappearance of a O—C=O group are consistent with inner sphere complexation of sEPS on the surface hydroxyl groups of nTiO$_2$ (Parikh *et al.* 2011; Fang *et al.* 2012). Our findings agree to some extent with other studies that have probed the interactions between metallic oxides and microbial macromolecules. For instance, Fang *et al.* found that bacterial EPS proteins adsorbed onto goethite but phosphate groups were responsible for the formation of chemical bonds (Fang *et al.* 2012). Proteinaceous components of EPS were also involved in the adsorption of the biopolymer to natural colloids, montmorillonite and kaolinite (Cao *et al.* 2011).

Although the strength of adsorption of sEPS on nTiO$_2$ via electrostatic interactions depends on media chemistry such as pH and ionic strength, the existence of chemical bonding between sEPS macromolecules and nTiO$_2$ will make the association strong and possibly long-lived. As a result, the modification of the surface properties of nTiO$_2$ brought about by associated sEPS may persist (although sEPS may be liable to biodegradation or catalytic degradation). More so, this surface-modified nTiO$_2$ (and possibly other metallic ENMs) is probably the form that aquatic organisms will be exposed to on the long term and

an understanding of their effects—as different from those of pristine ENMs—is imperative for reasonable environmental risk assessment of the ENMs.

4.4. Environmental Implications

In natural waters, ENMs will interact with other biogenic and geogenic matter that are present, including sEPS. These interactions may lead to physisorption and/or chemisorption of sEPS on the surface of the ENMs, which may change the particles' physicochemical properties and fate. sEPS may lead to charge reversal of positively charged nTiO$_2$ ENMs, which will play an important role in the bioavailability of ENMs to organisms, their interactions with other charged surfaces (e.g. membranes of bacteria), and their overall effect on biota.

Chemisorption of sEPS to nTiO$_2$ implies that the biomacromolecules may not be easily desorbed from the nanomaterials. As a result, the effects of sEPS on nTiO$_2$ properties, fate, and effects in natural waters may not be short-lived. Degradation of sEPS or their utilization as nutrient sources by heterotrophs may however interfere with the sEPS-ENM association. For instance, the catalytic properties of ENMs such as nTiO$_2$ can degrade biopolymers such as sEPS, similar to their effect on cellular membranes (Kiwi & Nadtochenko 2005). sEPS are also used by heterotrophs as carbon source, although one would expect the availability of sEPS associated to nTiO$_2$ to be somewhat different.

Surface coating of ENMs clearly plays an important role in their stability, fate and exposure. In this study for instance, poor stability of M262 in aqueous media (compared to M212 which has a similar core) due to its hydrophobic surface coating implies that pelagic organisms will be less exposed to M262 relative to M212 if both nTiO$_2$ are released into water (e.g. from the matrix of sunscreen). Attachment of sEPS onto the surface of ENMs

with low stability (like M262) may however improve their stability in water such that the fate and effects of the ENMs cannot be simply predicted based on the particles' intrinsic physicochemical properties.

Table 1. Major physicochemical properties of nanoparticles used in this study

Property	UV100	M212	M262
Hydrodynamic diameter (nm)[1]	526	212	257
Zeta potential (mV) [1]	3.3	31.9	32.4
Average primary particle size (nm)	3.6	23	24
Isoelectric point (pH)	6.2	9.3	9.2
Phase	Anatase	Rutile	Rutile
Crystal structure	Tetragonal	Tetragonal	Tetragonal
BET surface area (m^2/g)	320	56.2	47.7

[1] Measurements were taken in DI (pH ~ 5.8)

Table 2. Major characteristics of soluble EPS used in this study

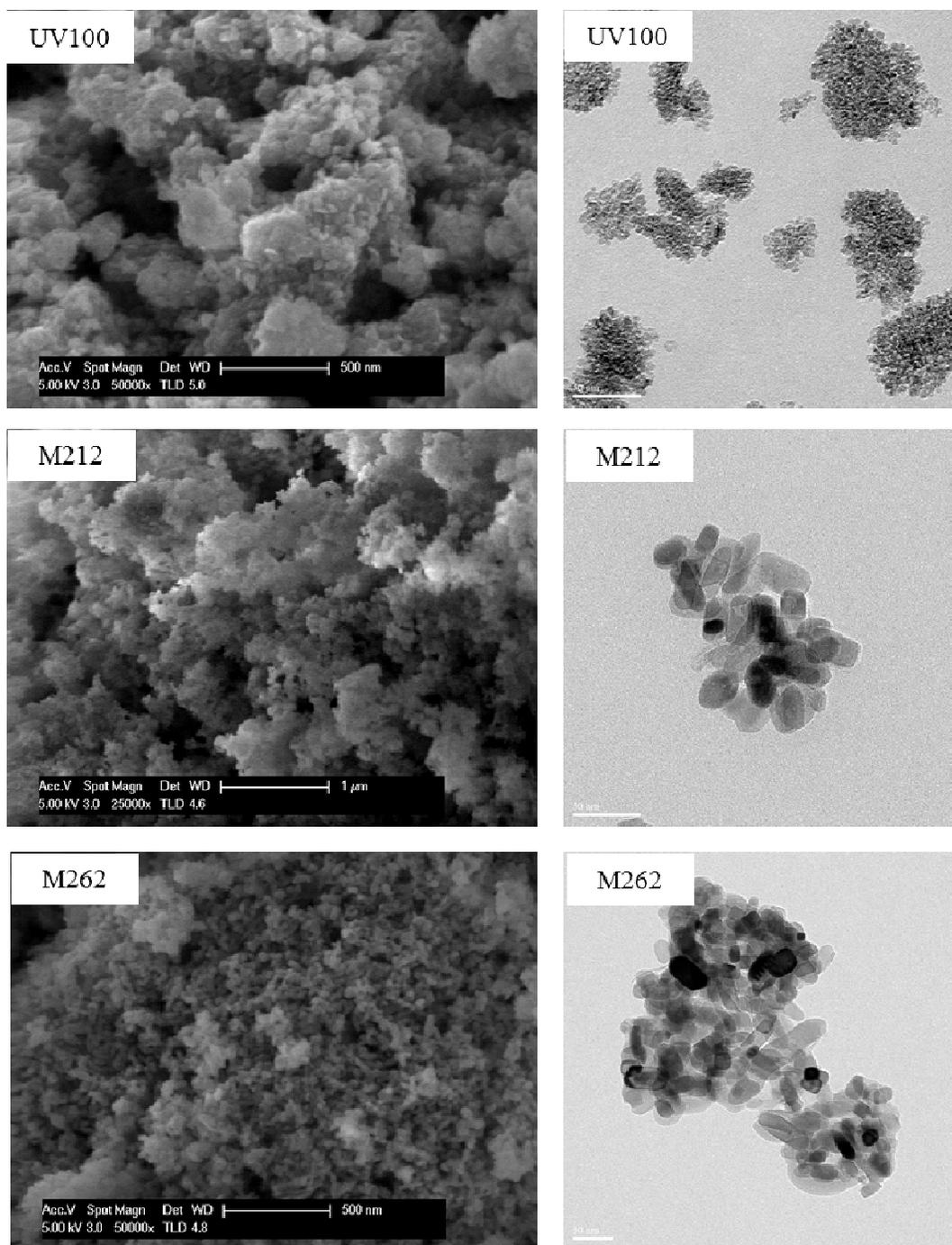| Property	sEPS-Chl	sEPS-Dun1	sEPS-Dun2
Dissolved organic carbon (mg-C/L)	8.46	14.3	16.9
Total dissolved nitrogen (mg/L)	2.59	0.81	1.39
Carbohydrate (mg/L-glucose equiv.)	15.8	11.6	15.6
Protein (mg/L-BSA equiv.)	20.3	1.91	6.62
Zeta potential (mV)	-12.7	-25.2	-22.1

Figure 1. Scanning (left) and transmission (right) electron micrographs of UV100, M212, and M262 nTiO$_2$. The scale bars of the three TEM micrographs represent 50 nm
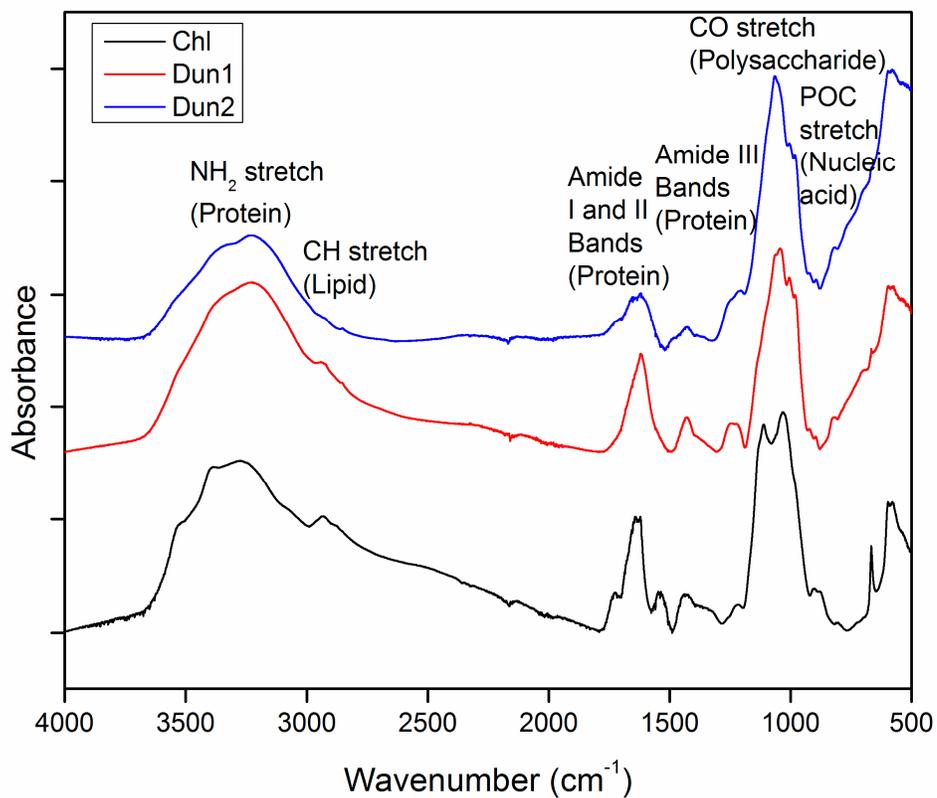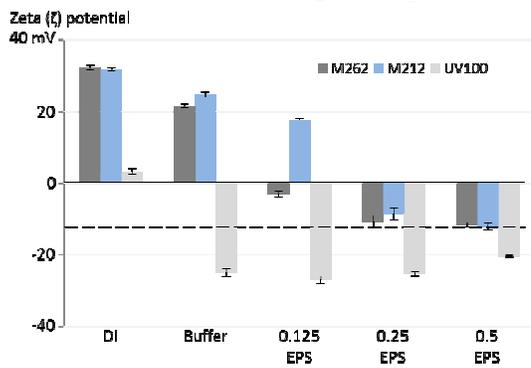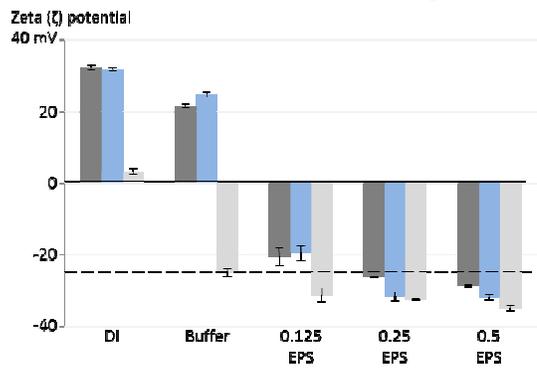
Figure 2. FTIR spectra of EPS isolated from *C. reinhardtii* (Chl), *D. tertiolecta* grown in normal f/2 media (Dun1), and *D. tertiolecta* grown in nitrogen-spiked f/2 media (Dun2). Detailed band assignments are shown in SI Table S1a-c

Effect of sEPS-Chl on surface charge of *n*TiO₂

Effect of sEPS-Dun1 on surface charge of *n*TiO₂
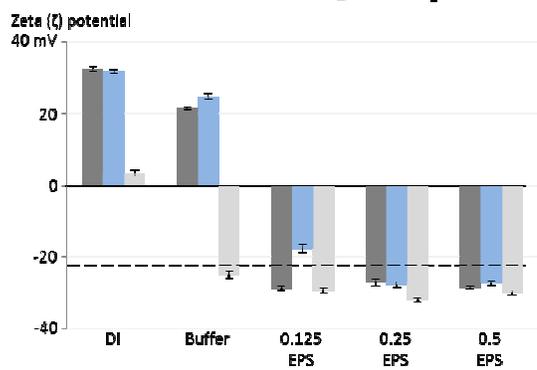
Effect of sEPS-Dun2 on surface charge of *n*TiO₂

Figure 3. Effect of sEPS on the ζ potentials of *n*TiO₂. Broken lines represent the ζ potentials of sEPS. pH = 7 except in DI (pH ~ 5.8).

Effect of pH on nTiO2 stability

Critical coagulation concentration, CCC
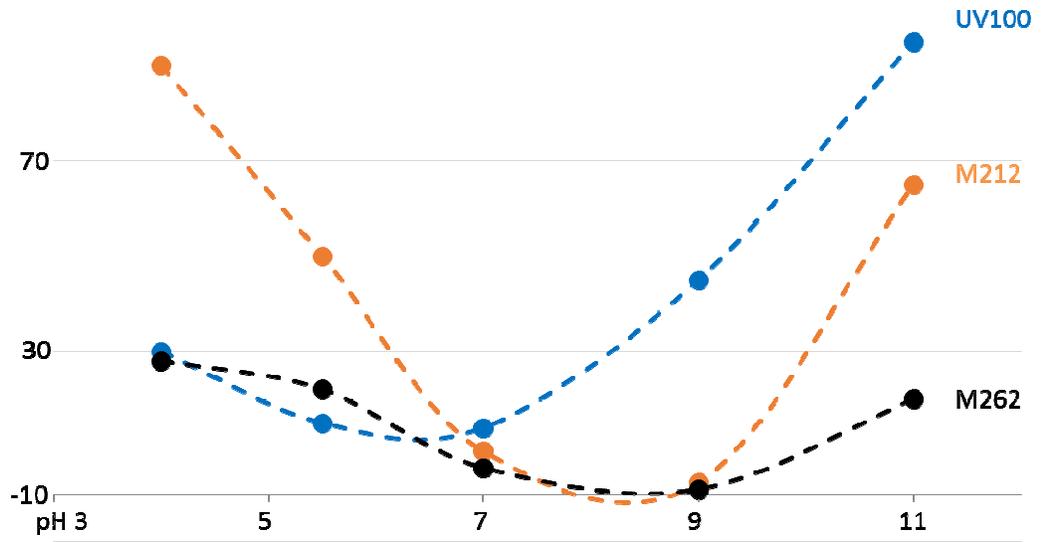
Figure 4. Effect of pH on CCC of nTiO$_2$ in NaCl

Effect of sEPS-Chl on stability of nTiO$_2$

Critical coagulation concentration, CCC
80 mM

Effect of sEPS source on stability of nTiO$_2$

Critical coagulation concentration, CCC
180 mM
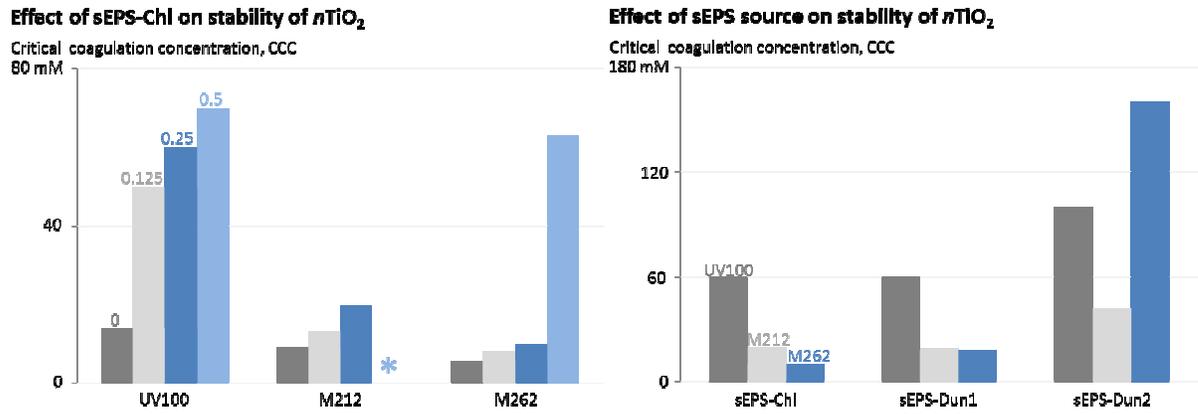
Figure 5. (A) Effect of sEPS-Chl (0.125 – 0.5 mg-C/L) on CCC of nTiO$_2$ in NaCl at pH 7. *M212 was completely stable in the presence of 0.5 mg-C/L sEPS-Chl, hence CCC could not be determined. (B) Comparison of CCC (in NaCl) of nTiO$_2$ in the presence of 0.25 mg-C/L sEPS-Chl, sEPS-Dun1, and sEPS-Dun2 at pH 7

141
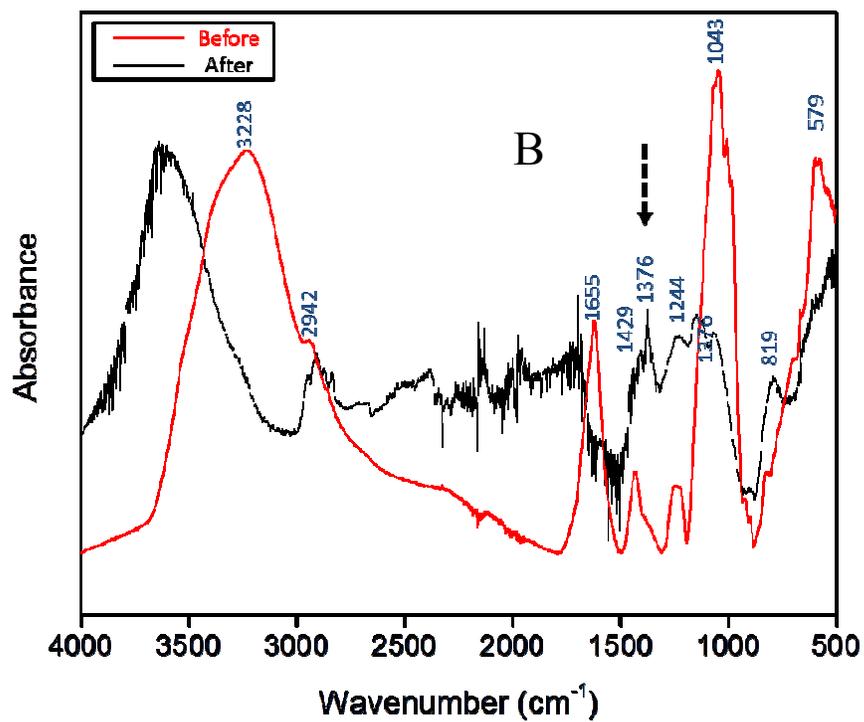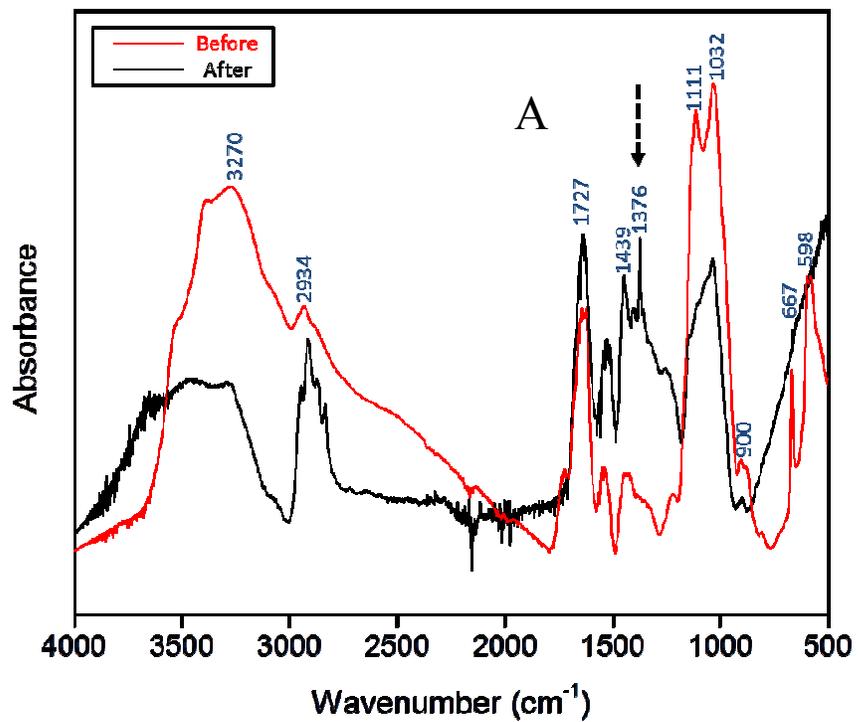
Figure 6. FTIR spectra of sEPS isolated from (A) *C. reinhardtii* and (B) *D. tertiolecta* before and after interactions with UV100 nTiO$_2$
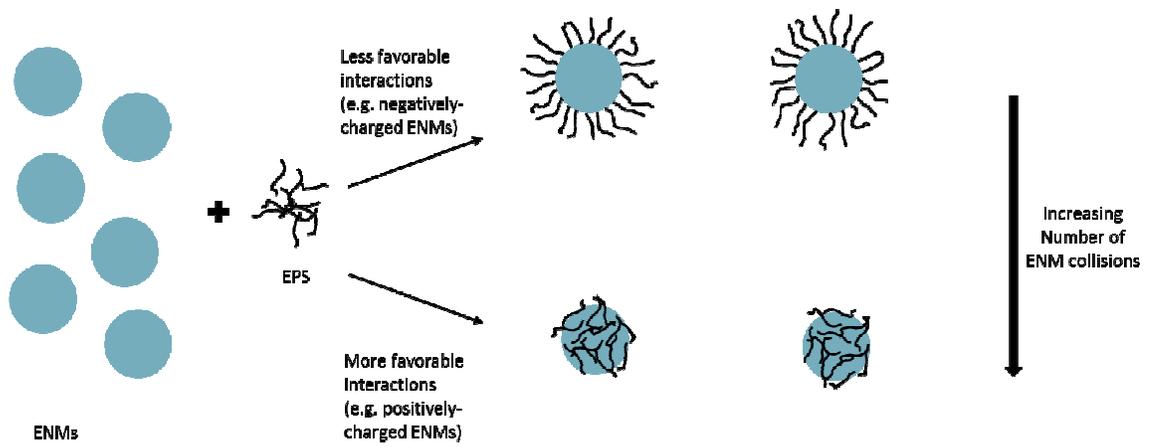
Scheme 1. Effect of ENM surface charge on conformation and influence of sEPS
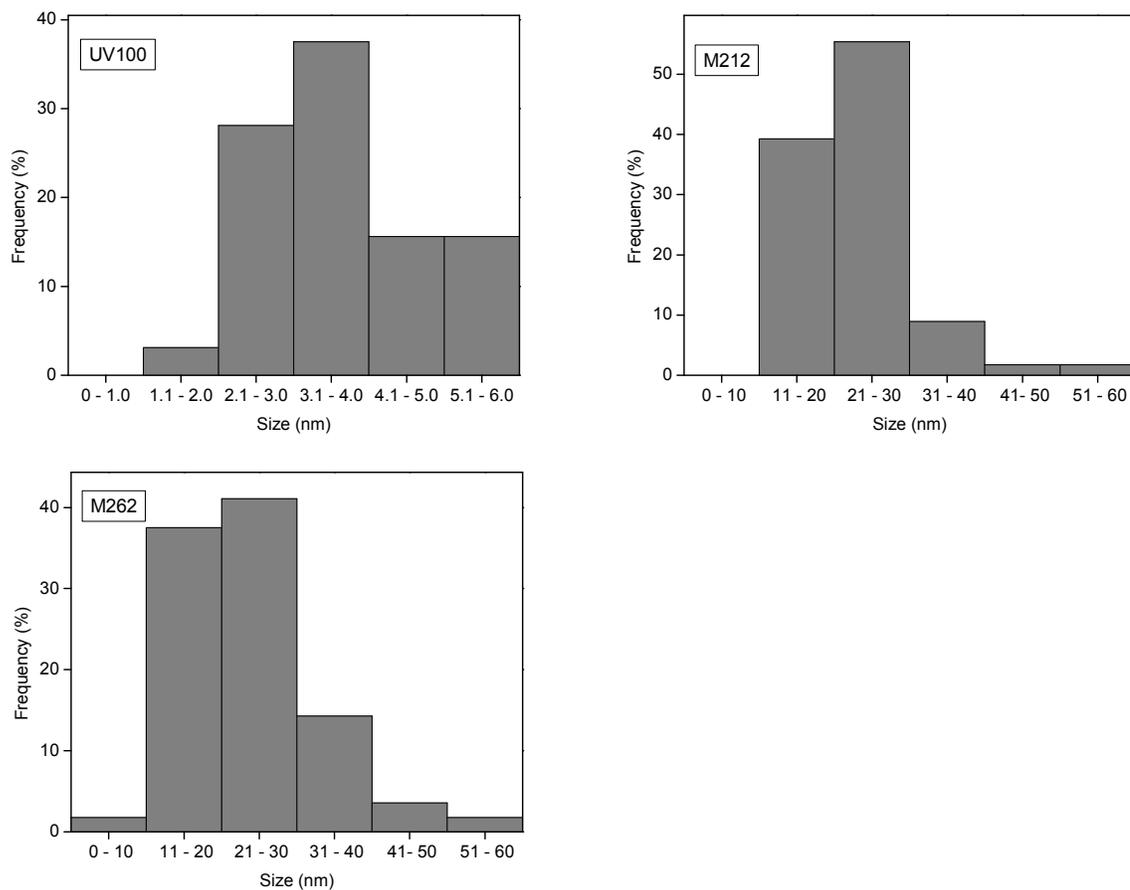
Figure S1. Primary particle size distribution of UV100, M212, and M262 nTiO$_2$
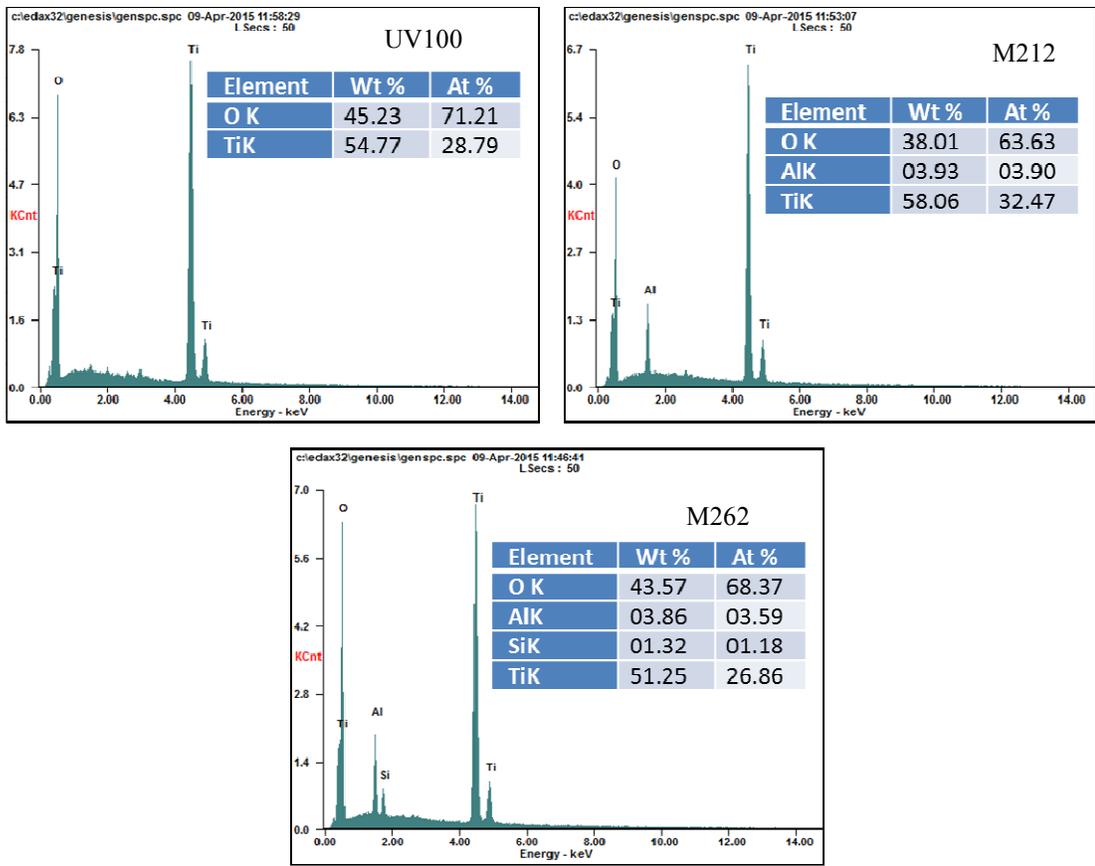
Figure S2. Energy dispersive spectroscopy (EDS) spectra of nTiO$_2$
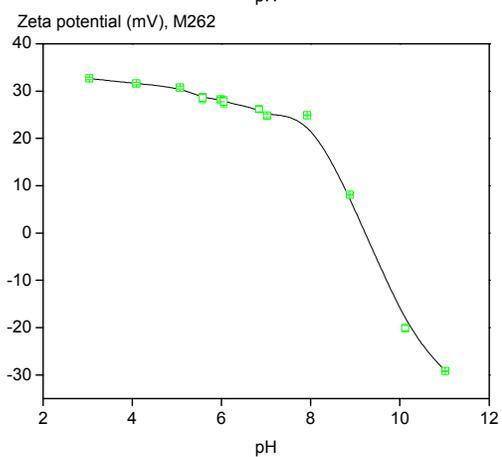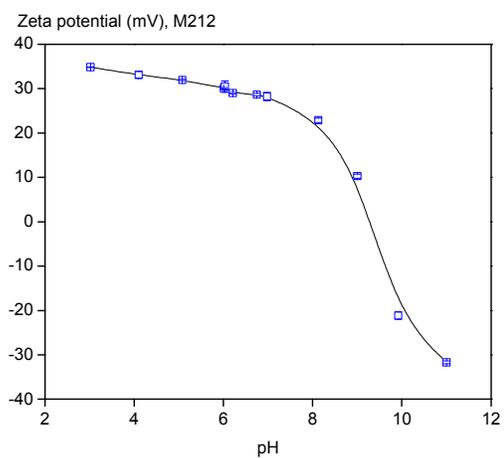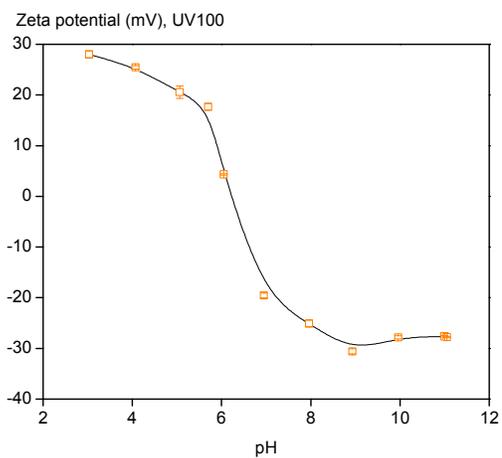
Figure S3. Effect of pH on zeta potential of UV100, M212, and M262 nTiO$_2$
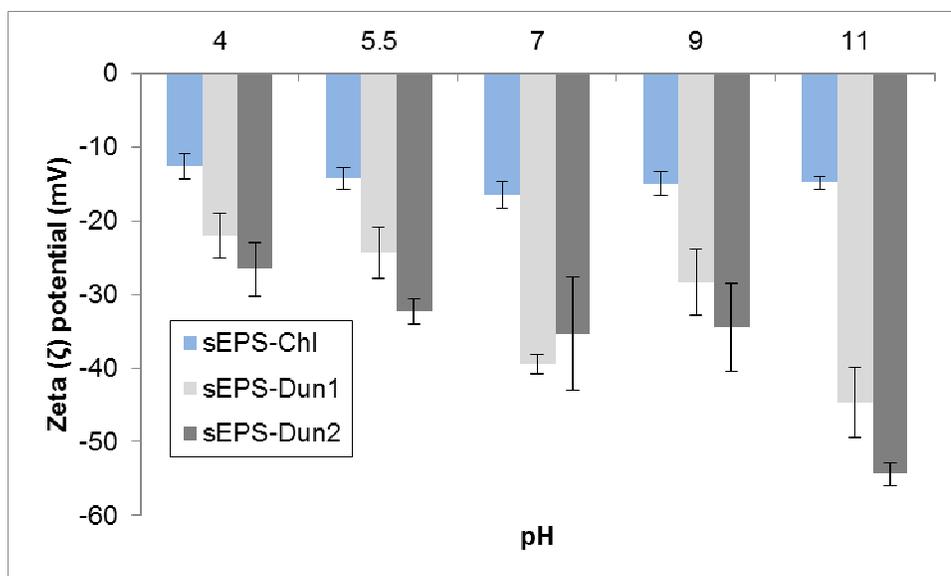
Figure S4. Zeta potential of sEPS in 0.5 mM buffer solutions

Table S1. Band assignment of sEPS isolated from (a) *Chlamydomonas reinhardtii* or sEPS-Chl, (B) *Dunaniella tertiolecta* grown in normal f/2 media or sEPS-Dun1, and (C) *Dunaniella tertiolecta* grown in N-spiked f/2 media or sEPS-Dun2 (Susi 1972; Lambert *et al.* 1987; Jiang *et al.* 2004; Parikh & Madamwar 2006; Fang *et al.* 2012; Lembre *et al.* 2012).

| A	
Wavenumber (cm^{-1})	**Band assignment**
580	C=O out-of-plane bend in amides of proteins
598	C=O out-of-plane bend in amides of proteins
667	O—C=O bending in carboxylic acids
804	NH$_2$ wag in primary amines of proteins
900	P-O-C antisym stretch in organophosphorus compounds
1032	C-O stretching of polysaccharides
1111	C-O, C-O-C stretching of polysaccharides
1217	P=O stretching of phospholipids or nucleic acids
1439	OH bending in carboxylic acids
1547	N-H deformation Amide II of proteins
1642	NH$_2$ deformation in primary amines from proteins
1655	C=O stretching of Amide I from proteins
1712	C=O stretch in lipids/phospholipids
1727	C=O stretch in lipids/phospholipids
2876, 2934	CH antisym and sym stretching in lipids
3270	NH$_2$ sym stretch in primary amides of proteins
3387	NH$_2$ antisym stretch in primary amides of proteins

B	
Wavenumber (cm^{-1})	**Band assignment**
579	C=O out-of-plane bend in amides of proteins
596	C=O out-of-plane bend in amides of proteins
667	O—C=O bending in carboxylic acids
819	NH$_2$ wag in amines of proteins
897	NH$_2$ wag in amines of proteins
923	P-O-C antisym stretch in organophosphorus compounds
983	P-O-C antisym stretch in organophosphorus compounds
1005	C-O stretching of polysaccharides
1043	C-O, C-O-C stretching of polysaccharides
1222	P=O stretching of phospholipids or nucleic acids
1244	P=O stretching of phospholipids or nucleic acids
1429	OH bending in carboxylic acids
1619	NH$_2$ deformation in primary amines from proteins
1655	C=O stretching of Amide I from proteins
2857, 2942	CH antisym and sym stretching in lipids
3228	NH$_2$ sym stretch in primary amides of proteins
3386	NH$_2$ antisym stretch in primary amides of proteins

C	
Wavenumber(cm^{-1})	**Band assignment**
581	C=O out-of-plane bend in amides of proteins
596	C=O out-of-plane bend in amides of proteins
669	O—C=O bending in carboxylic acids
816	NH$_2$ wag in amines of proteins
895	NH$_2$ wag in amines of proteins
922	P-O-C antisym stretch in organophosphorus compounds
982	P-O-C antisym stretch in organophosphorus compounds
1005	C-O stretching of polysaccharides
1066	C-O, C-O-C stretching of polysaccharides
1207	P=O stretching of phospholipids or nucleic acids
1242	P=O stretching of phospholipids or nucleic acids
1427	OH bending in carboxylic acids
1620	NH$_2$ deformation in primary amines from proteins
1655	C=O stretching of Amide I from proteins
2857, 2927	CH antisym and sym stretching in lipids
3230	NH$_2$ sym stretch in primary amides of proteins
3338	NH$_2$ antisym stretch in primary amides of proteins

References

Adeleye A.S., Conway J.R., Perez T., Rutten P. & Keller A.A. (2014). Influence of Extracellular Polymeric Substances on the Long-Term Fate, Dissolution, and Speciation of Copper-Based Nanoparticles. *Environ Sci Technol*, 48, 12561-12568.

Adeleye A.S. & Keller A.A. (2014). Long-term colloidal stability and metal leaching of single wall carbon nanotubes: effect of temperature and extracellular polymeric substances. *Water research*, 49, 236-50.

Adeleye A.S., Keller A.A., Miller R.J. & Lenihan H.S. (2013). Persistence of commercial nanoscaled zero-valent iron (nZVI) and by-products. *Journal of Nanoparticle Research*, 15, 1-18.

Beaussart A., Petrone L., Mierczynska-Vasilev A., McQuillan A.J. & Beattie D.A. (2012). In Situ ATR FTIR Study of Dextrin Adsorption on Anatase TiO2. *Langmuir*, 28, 4233-4240.

Bouhekka A. & Bürgi T. (2012). In situ ATR-IR spectroscopy study of adsorbed protein: Visible light denaturation of bovine serum albumin on TiO2. *Applied Surface Science*, 261, 369-374.

Cao Y., Wei X., Cai P., Huang Q., Rong X. & Liang W. (2011). Preferential adsorption of extracellular polymeric substances from bacteria on clay minerals and iron oxide. *Colloids and Surfaces B: Biointerfaces*, 83, 122-127.

Erhayem M. & Sohn M. (2014). Stability studies for titanium dioxide nanoparticles upon adsorption of Suwannee River humic and fulvic acids and natural organic matter. *Science of The Total Environment*, 468–469, 249-257.

Everett D. (1988). Basic principles of colloid science. *Royal Society of Chemistry paperbacks*.

Fang L., Cao Y., Huang Q., Walker S.L. & Cai P. (2012). Reactions between bacterial exopolymers and goethite: A combined macroscopic and spectroscopic investigation. *Water Research*, 46, 5613-5620.

Flemming H.-C., Neu T.R. & Wozniak D.J. (2007). The EPS matrix: the "house of biofilm cells". *Journal of Bacteriology*, 189, 7945-7947.

Gondikas A.P., Kammer F.v.d., Reed R.B., Wagner S., Ranville J.F. & Hofmann T. (2014). Release of TiO2 Nanoparticles from Sunscreens into Surface Waters: A One-Year Survey at the Old Danube Recreational Lake. *Environmental Science & Technology*, 48, 5415-5422.

Hung C.C., Tang D.G., Warnken K.W. & Santschi P.H. (2001). Distributions of carbohydrates, including uronic acids, in estuarine waters of Galveston Bay. *Marine Chemistry*, 73, 305-318.

Jiang W., Saxena A., Song B., Ward B.B., Beveridge T.J. & Myneni S.C.B. (2004). Elucidation of Functional Groups on Gram-Positive and Gram-Negative Bacterial Surfaces Using Infrared Spectroscopy. *Langmuir*, 20, 11433-11442.

Kadar E., Cunliffe M., Fisher A., Stolpe B., Lead J. & Shi Z. (2014). Chemical interaction of atmospheric mineral dust-derived nanoparticles with natural seawater — EPS and sunlight-mediated changes. *Science of The Total Environment*, 468–469, 265-271.

Keller A.A., McFerran S., Lazareva A. & Suh S. (2013). Global life cycle releases of engineered nanomaterials. *Journal of Nanoparticle Research*, 15, 1-17.

Keller A.A., Wang H., Zhou D., Lenihan H.S., Cherr G., Cardinale B.J., Miller R. & Ji Z. (2010). Stability and Aggregation of Metal Oxide Nanoparticles in Natural Aqueous Matrices. *Environmental Science & Technology*, 44, 1962-1967.

Kiwi J. & Nadtochenko V. (2005). Evidence for the Mechanism of Photocatalytic Degradation of the Bacterial Wall Membrane at the TiO2 Interface by ATR-FTIR and Laser Kinetic Spectroscopy. *Langmuir*, 21, 4631-4641.

Lambert J.B., Shurvell H.F., Lightner D.A. & Cooks R.G. (1987). *Introduction to organic spectroscopy*. Macmillan New York.

Legler G., Mullerplatz C.M., Mentgeshettkamp M., Pflieger G. & Julich E. (1985). On the Chemical Basis of the Lowry Protein Determination. *Analytical Biochemistry*, 150, 278-287.

Lembre P., Lorentz C. & Martino P.D. (2012). *Exopolysaccharides of the Biofilm Matrix: A Complex Biophysical World*.

Martinez R.E., Smith D.S., Kulczycki E. & Ferris F.G. (2002). Determination of Intrinsic Bacterial Surface Acidity Constants using a Donnan Shell Model and a Continuous pKa Distribution Method. *Journal of Colloid and Interface Science*, 253, 130-139.

Morris D.L. (1948). Quantitative Determination of Carbohydrates with Dreywoods Anthrone Reagent. *Science*, 107, 254-255.

Naumann D., Helm D. & Labischinski H. (1991). Microbiological characterizations by FT-IR spectroscopy. *Nature*, 351, 81-82.

Nielsen P.H. & Jahn A. (1999). Extraction of EPS. In: *Microbial extracellular polymeric substances*. Springer, pp. 49-72.

Ojamäe L., Aulin C., Pedersen H. & Käll P.-O. (2006). IR and quantum-chemical studies of carboxylic acid and glycine adsorption on rutile TiO2 nanoparticles. *Journal of Colloid and Interface Science*, 296, 71-78.

Pal A. & Paul A. (2008). Microbial extracellular polymeric substances: central elements in heavy metal bioremediation. *Indian journal of microbiology*, 48, 49-64.

Parikh A. & Madamwar D. (2006). Partial characterization of extracellular polysaccharides from cyanobacteria. *Bioresource Technology*, 97, 1822-1827.

Parikh S.J., Kubicki J.D., Jonsson C.M., Jonsson C.L., Hazen R.M., Sverjensky D.A. & Sparks D.L. (2011). Evaluating Glutamate and Aspartate Binding Mechanisms to Rutile (α-TiO2) via ATR-FTIR Spectroscopy and Quantum Chemical Calculations. *Langmuir*, 27, 1778-1787.

Praetorius A., Arvidsson R., Molander S. & Scheringer M. (2013). Facing complexity through informed simplifications: a research agenda for aquatic exposure assessment of nanoparticles. *Environmental Science: Processes & Impacts*, 15.

Quik J.T.K., Stuart M.C., Wouterse M., Peijnenburg W., Hendriks A.J. & van de Meent D. (2012). Natural colloids are the dominant factor in the sedimentation of nanoparticles. *Environmental Toxicology and Chemistry*, 31, 1019-1022.

Quik J.T.K., Velzeboer I., Wouterse M., Koelmans A.A. & van de Meent D. (2014). Heteroaggregation and sedimentation rates for nanomaterials in natural waters. *Water research*, 48, 269-279.

Saleh N.B., Pfefferle L.D. & Elimelech M. (2008). Aggregation Kinetics of Multiwalled Carbon Nanotubes in Aquatic Systems: Measurements and Environmental Implications. *Environmental Science & Technology*, 42, 7963-7969.

Susi H. (1972). [22] Infrared spectroscopy—Conformation. *Methods in enzymology*, 26, 455-472.

Thio B.J.R., Zhou D. & Keller A.A. (2011). Influence of natural organic matter on the aggregation and deposition of titanium dioxide nanoparticles. *Journal of Hazardous Materials*, 189, 556-563.

Wingender J., Neu T. & Flemming H. (1999). Microbial Extracellular Polymeric Substances: Characterisation. *Structure and Function, Springer, Berlin*, 123.

Chapter 5. Influence of phytoplankton on fate and effects of modified zero-valent iron nanoparticles

5.1. Introduction

Nanoscale zerovalent iron (nZVI) and its derivatives are emerging as an effective option for in situ treatment of important contaminants such as heavy metals and chlorinated organic compounds in soil, groundwater and wastewater (O'Carroll *et al.* 2013; Fu *et al.* 2014; Su *et al.* 2014b). Effective remediation of pollutants using nZVI in benchscale (O'Carroll *et al.* 2013; Crane *et al.* 2015) and (mostly pilot) field studies (Comba *et al.* 2011; Mueller *et al.* 2012; Su *et al.* 2012) has been widely reported in the literature. However, our understanding of the environmental implications of these engineered nanomaterials (ENMs) drastically lags what we know about their potential applications.

nZVI aggregates in aqueous media due to low electrostatic repulsion and magnetic attraction between the particles (Phenrat *et al.* 2008; Adeleye *et al.* 2013), limiting their mobility in the subsurface. Advances in nZVI-based technology include modifying the particles to prevent them from aggregating rapidly and improving reactivity with target pollutants. Such modifications are done via surface-coating (Phenrat *et al.* 2008; Kim *et al.* 2009; Jiemvarangkul *et al.* 2011), supporting them on other materials (Shi *et al.* 2011; Lv *et al.* 2014), and doping them with other elements (Koutsospyros *et al.* 2012; Su *et al.* 2014a; Su *et al.* 2015a). Improved mobility of nZVI increases their chances of reaching target contaminants as well as their migration outside the treatment zone where they may have undesirable effects (Jiemvarangkul *et al.* 2011; Ševců *et al.* 2011; Keller *et al.* 2012; Kocur *et al.* 2014). The removal capacity of some of these modified nZVI for certain pollutants is

considerably higher than that of pristine particles (Kim *et al.* 2013; Su *et al.* 2015a). Therefore, it is our belief that the use of modified nZVI will continue to increase.

The fate and effect of ENMs depend strongly on their stability in the natural environment, which are controlled by media properties such as ionic strength, pH, and natural organic matter (Keller *et al.* 2010; Adeleye *et al.* 2013; Adeleye & Keller 2014). However, natural waters also contain numerous microorganisms (bacteria and algae) that may interact with nanomaterials directly (through membrane-ENM interactions) or indirectly (e.g. via interactions between ENMs and microbial exudates like extracellular polymeric substances, EPS) (Adeleye *et al.* 2014; Ma *et al.* 2014; Rhiem *et al.* 2015). It is still unclear how microorganisms and their exudates may influence the fate and effects of nZVI in natural waters. In this study, a modified nZVI was introduced into *Chlamydomonas reinhardtii* cultures of different ages with the goal of investigating the impact of cells and/or their organic materials on physicochemical properties, stability, transformation, and toxicity of the nanomaterials.

5.2. Materials and Methods

5.2.1. Synthesis of Modified nZVI

nZVI modified with sulfur and silica (FeSSi) was synthesized as described in Su *et al*. Briefly, 250 ml mixture containing 7.6 g sodium borohydride (Oakwood Chemical), 1.5 g dithionite (Sigma-Aldrich), and 0.2 mL of colloidal silica (30 wt.% in water) was titrated into 250 ml solution containing 4.9 g $FeCl_3$ (Fisher Scientific). After reduction, nanoparticles were collected and triple-washed with nitrogen-purged deionized (DI) water (18.2 MΩ.cm, Barnstead Nanopure Diamond). A neodymium-iron-boron magnet was used to separate solids and liquids. Fresh FeSSi particles were stored in 30 % ethanol at 4 °C until

155

use. Major physicochemical properties of FeSSi were described in Su *et al*. Additional

characterizations done in this study include measurement of initial hydrodynamic size

(HDD) and zeta potential at pH 7.5 using a Malvern Zetatasizer Nano-ZS90 (Adeleye *et al*.

2014), as well as scanning electron microscopy (SEM, FEI XL30 Sirion).

5.2.2. Test Organism Cultures

Batch cultures of *C. reinhardtii* were grown in COMBO media as described previously

(Kilham *et al.* 1998; Stevenson *et al.* 2013). The composition of COMBO media is provided

in Supporting Information (SI) Table S1. Fresh cultures were inoculated to achieve a cell

density of 10^6 cells/mL and incubated at 20 °C (12:12 light:dark). To distinguish the effect

of culture age on fate and effects of FeSSi, cultures of different ages (and/or their media)

were used for the experiments. Day 1 (young) and Day 10 (old) cultures were obtained by

starting new batch cultures 1 or 10 days prior to the start of the experiment, and kept

undisturbed in the experimental setup used for the study itself. Day 0 (fresh) cultures were

inoculated with *C. reinhardtii* on the day the experiment started. Fresh and young cultures

were in fast growth phase while old cultures were in slowing growth phase (Stevenson *et al.*

2013).

5.2.3. Test Organism Media and Characterization

To obtain media with algal natural organic matter (algal NOM), batches of young and

old cultures were centrifuged (7500 *g*, 15 min, 4 °C, Sorvall RC-5B Plus) and then filtered

(0.2 μm PES membrane, Thermo Scientific) in aseptic conditions to produce young and old

media, respectively. Sterile COMBO media was used as fresh media. The media were

characterized by measuring dissolved organic carbon (DOC) and total dissolved nitrogen

(TDN) using a Shimadzu TOC-V with an attached TNM1 unit, pH (Oakton EW-35811-71,

Cole Parmer), conductivity (HACH IntelliCAL CDC401), and dissolved oxygen (HACH

156

LDO Model 2). Functional groups present in EPS were characterized by analyzing freeze-dried old media (Labconco 7754042) via infrared spectroscopy using a Nicolet iS10 spectrometer with a diamond ATR crystal (Adeleye *et al.* 2014). Interferograms were obtained by taking 256 scans (resolution = 2 cm^{-1}).

5.2.4. Effect of Algal NOM on Stability of FeSSi

The initial hydrodynamic diameter (HDD) and zeta (ζ) potential of FeSSi (50 mg/L) were measured in fresh, young, and old media using the Zetasizer. Aggregation kinetics was also studied in the three media via dynamic light scattering (DLS) as described previously (Adeleye *et al.* 2014; Adeleye & Keller 2014). The initial aggregation rate constant (k) reflects doublet formation and is proportional to the initial rate of increase in the intensity-weighted hydrodynamic radius, $a_h(t)$, with time, t, and the inverse of initial number concentration of nanoparticles, N_0 (Eq. 1) (Saleh *et al.* 2008; Adeleye & Keller 2014):

$$k \propto \frac{1}{N_0}\left(\frac{da_h(t)}{dt}\right)_{t \to 0}$$

(1)

k is obtained from the slope of the best fit line of $(da_h(t)/dt)_{t \to 0}$, which is determined via DLS using the Zetasizer. Attachment efficiencies (α) of FeSSi in fresh, young, and old media were derived by normalizing the measured k by the diffusion-limited aggregation rate constant $(k)_{fav}$ (Eq. 2). $(k)_{fav}$ may be calculated from Smoluchowski's equation for diffusion-limited aggregation or determined in highly favorable aggregation conditions (done in this study).

$$\alpha = \frac{\left(\dfrac{da_h(t)}{dt}\right)_{t \to 0}}{\left(\dfrac{da_h(t)}{dt}\right)_{t \to 0, fav}}$$

(2)

5.2.5. Influence of Algae on Dissolution and Effect of FeSSi

To study transformation and effects of FeSSi in freshwater environments, stock suspensions of the nanoparticles were added to fresh and old media (without the organisms) and mixed thoroughly for 1 h (80 rpm, Dayton-6Z412A parallel shaft roller-mixer). Each mixed stock was respectively used to dose fresh or old cultures (with the organisms) in triplicates to achieve final FeSSi concentrations of 1.8, 18, and 180 mg/L. We intentionally used concentrations lower than what is typically injected into the subsurface (1-30 g/L) (Mueller *et al.* 2012) in order to account for mass loss during transport from points of injection into nearby natural waters. To monitor dissolution/transformation, aliquots were carefully taken at time points from the supernatant, filtered (0.45 μm SFCA membrane, Thermo Scientific) to remove cells and particles, digested with trace-metal grade HNO_3 (Fisher Scientific), and analyzed for iron (Fe), silicon (Si), and sulfur (S) via ICP-AES (Thermo Scientific iCAP 6300). FeSSi particles aggregate in algal media to sizes greater than 0.45 μm within 3 min and are thus not expected to pass through the filter. Effect of FeSSi on algal population density over time was monitored by measuring concentrations of chlorophyll a (Gemini XPS Fluorescence Microplate Reader, Modular Devices). Fluorescence was converted to concentrations of chlorophyll a (μg/L) using a standard curve made with Turner Designs Liquid Primary Chlorophyll a Standards (Stevenson *et al.* 2013).

5.2.6. Environmental Scanning Electron Microscopy (ESEM)

At the end of the experiments, 1 mL of *C. reinhardtii* cultures dosed with 180 mg/L of FeSSi was fixed with formalin (5%). The suspension was allowed to mix, deposited on a JEOL aluminum specimen mount, and then imaged using a Phillips FEI XL30 FEG ESEM equipped with a Bruker XFlash 6160 energy dispersive spectrometer (EDS). Imaging was

done in wet mode at 3 Torr, 4°C, and an accelerating voltage of 10 kV without gold sputtering.

5.2.7. Transformation of Undissolved FeSSi

To study particle transformation, stock of FeSSi suspension in fresh and old media (mixed for 1 h) was added to fresh and old cultures, respectively, to achieve 180 mg/L. Undissolved particles were analyzed after 1, 10, and 30 d via X-ray diffraction (XRD, fluorescence mode, Bruker D8 Advance) and X-ray photoelectron spectroscopy (XPS, Kratos Axis Ultra). To prepare sample, undissolved particles were separated from suspension via centrifugation (10,000 g, 30 min). Particles were immediately dried under vacuum (Yamato ADP-21) after decanting the supernatant.

5.3. Results and Discussions

5.3.1 Particle and Media Characterization

A representative SEM image of FeSSi is shown in SI Figure S1. The isoelectric point (IEP) of FeSSi was determined as ~pH 7.4 (SI Figure S2). The HDD of FeSSi in DI water at pH 7.5 (phosphate buffer), which is an average of DLS data collected over 2 min, was 341 nm. In the same conditions, ζ potential of FeSSi was -38.0 mV, which is much higher than one would expect at a pH ≈ IEP. The high negative charge under these conditions is probably due to the adsorption of phosphate ions from the buffer by FeSSi. A similar observation was recently made in nano-CuO/phosphate systems (Conway *et al.* 2015). Although the ζ potential value suggests stability, FeSSi particles aggregated to ~470 nm within 6 min after which they were relatively stable.

Major properties of the media used in this study are presented in Table 1. Dissolved organic carbon (DOC, which is a proxy for algal NOM) and dissolved oxygen (DO) in media

increased with culture age while nitrogen and phosphorus decreased over time as they were used up by cells. We also observed that pH increased from 7.6 to ~10 in old media because COMBO media is typically not buffered. In fact, pH > 10 has been previously reported in fresh COMBO media (Urabe *et al.* 1997). The major functional groups in algal NOM are shown in Figure 1.

5.3.2 Effect of Algal Organic Matter on Stability of FeSSi

The initial size of FeSSi was slightly larger in fresh media (pH 7.6, HDD = 369 nm) than in buffered DI with similar pH (pH 7.5, HDD = 341 nm). This suggests a slightly faster aggregation of FeSSi in fresh algal media than in DI. The ionic strength (IS) of fresh media, calculated from the chemical composition of media to be ~5.41 mM, is much lower than the IS of DI due to phosphate buffer (~13.4 mM). One reason for a lower stability in fresh media is lower surface charge (ζ potential = -17.0 mV) compared to DI (ζ potential = -38.0 mV). Fresh media contained only 0.05 mM phosphate, and multivalent ions such as Ca^{2+}, Mg^{2+}, and Fe^{3+}, which are able to screen the electrostatic layer of colloids more strongly than the monovalent cations (Na^+) in buffered DI.

In old media, the initial size of FeSSi was even much bigger (HDD = 390 nm); however, aggregation kinetics showed that FeSSi did not aggregate as fast in this condition relative to fresh and young media (Table 2, SI Figure S3). Such relative increase in initial size of nanoparticle in media that cannot be attributed to relatively faster aggregation is indicative of coating of the particles in the media (Adeleye *et al.* 2014), which will be discussed further later in this section. The ζ potential of FeSSi was much less negative in old culture media (-11.4 mV) compared to DI and fresh media. Despite this low surface charge in old media (which suggests colloidal instability), the attachment efficiency of FeSSi was comparable to what we found in DI, and much lower than in fresh and young media (Table 2).

160

Slower aggregation of FeSSi in old media could not be attributed to lower ionic content as conductivity was slightly higher in old media compared to fresh and young media (Table 1). We therefore hypothesized that slower aggregation of FeSSi in old media was due to high pH and/or steric stabilization by algal NOM. As reported earlier, old media had a pH of ~10 compared to pH ~7.6 found in fresh and young media. nZVI, and ENMs in general, are typically more negatively charged at higher pH which may improve their stability in aqueous media via increased electrostatic repulsion (Zhang & Elliott 2006; Su *et al.* 2015b). To confirm the contribution of pH to improved stability of FeSSi in old media, the aggregation kinetics of FeSSi was also studied in old media with its pH adjusted to 7.6 using dilute HCl (Fisher Scientific). The mean HDD of FeSSi over 1 h was 649 in pristine media and 627 nm in pH-adjusted old media. Maximum hydrodynamic diameter of FeSSi found in pH-adjusted old media over 1 h was 790 nm compared to 930 nm in pristine old media. (Figure 2) In addition, attachment efficiency was slightly lower in adjusted old media ($\alpha = 0.08$) than in pristine old media ($\alpha = 0.09$). This implies that higher pH did not contribute to improved stability of FeSSi in old media. Based on (1) this insensitivity of FeSSi stability to pH in old media, (2) improved stability of FeSSi in old media compared to fresh and young media despite having a much less-negative ζ potential, and (3) increase in the initial size of FeSSi in old media which was not due to increased aggregation, we concluded that slower aggregation of the nanoparticles in old media was due to their coating by algal NOM, which provided steric stabilization.

The organic materials of microorganisms are mostly composed of extracellular polymeric substances or EPS, and are abundant in natural environments (Nielsen & Jahn 1999; Wingender *et al.* 1999; Kadar *et al.* 2014). EPS are made up of a wide range of macromolecules such as polysaccharides, proteins, glycoproteins, glycolipids, nucleic acids,

161

phospholipids, and other polymeric substances excreted by microorganisms (Nielsen & Jahn 1999; Wingender *et al.* 1999; Flemming *et al.* 2007), which may be held together by electrostatic interactions, hydrogen bonds, London dispersion forces, ionic interactions, and chain-chain complex networks (Mayer *et al.* 1999; Sutherland 2001; Tian *et al.* 2006), These polymers contain charged functional groups such as carboxyl, carbonyl, amine, and phosphate, etc. (Figure 1) with which they can interact with other charged surfaces in aqueous media, including ENMs (Sutherland 2001; Pal & Paul 2008; Adeleye *et al.* 2014; Adeleye & Keller 2014), In addition, EPS contain hydrophobic polysaccharides (Flemming *et al.* 2007) with which they can interact with other hydrophobic surfaces. The interactions of EPS with nanomaterials were shown to impart stability in carbon nanotubes (Adeleye & Keller 2014), copper-based nanoparticles (Adeleye *et al.* 2014), ferrihydrite (Kadar *et al.* 2014), and Fe-containing dust nanoparticles (Kadar *et al.* 2014).

5.3.3 Influence of Algae on Transformation of FeSSi

nZVI reacts with oxygen in water to produce soluble ferrous ions (Fe^{2+}), which may undergo oxidation to form ferric ions (Fe^{3+}). Fe^{3+} tends to precipitate on the surface of particles to form ferric oxide or oxohydroxide, especially at high pH (Zhang & Elliott 2006; Adeleye *et al.* 2013). FeSSi, which is black in its pristine state, had turned rusty brown within 1 h of mixing in fresh media while still mostly black in old media (SI Figure S4). This clearly shows that FeSSi is transformed in these aqueous systems, much more in the fresh media conditions. In order to determine how the presence of algae affects dissolution of FeSSi in freshwater systems, we monitored concentrations of dissolved iron ($[Fe]_{diss}$), silicon ($[Si]_{diss}$), and sulfur ($[S]_{diss}$), all components of FeSSi, in fresh and old *C. reinhardtii* cultures. $[Fe]_{diss}$ detected in the aqueous phase was relatively low in all conditions (< 0.3 mg/L) when compared to the concentrations of FeSSi introduced (Figure 3), which is

162

probably due to oxidation of Fe^{2+} to insoluble Fe^{3+} species (Adeleye *et al.* 2013).

Nevertheless, the ratio of $[Fe]_{diss}$ in fresh cultures with FeSSi to $[Fe]_{diss}$ in control conditions (measured 2 h after adding nanoparticles to cultures) was 1.86, 4.19, and 19.0 in treatments with 1.8, 18, and 180 mg-FeSSi/L, respectively. This ratio could not be determined for old culture because $[Fe]_{diss}$ was non-detect in control cultures by Day 7.

$[Fe]_{diss}$ in old culture treatments was an order of magnitude lower relative to the corresponding fresh culture conditions (Figure 3) which suggests a slower rate of Fe^0 oxidation in old cultures despite the presence of a higher amount of DO (Table 1). Slower oxidation in old cultures is due to the presence of higher algae populations whose adsorption to FeSSi is hypothesized to reduce surface available for oxidation. A representative ESEM micrograph showing heteroaggregation between *C. reinhardtii* and FeSSi particles is shown in Figure 4. Slower dissolution in old media may also be attributed to algal NOM coating on particles. The coating of NOM on Fe nanoparticles does not only exclude some water, which is needed for dissolution, but also reduces reactivity on particle surface (Dries *et al.* 2005; Giasuddin *et al.* 2007; Adeleye *et al.* 2013). In a previous study we showed that soluble EPS isolated from *Isochrysis galbana*, a marine phytoplankton, had a pH-dependent influence on dissolution of copper-based nanoparticles (Adeleye *et al.* 2014).

Oxidation of Fe^{2+} is typically faster at higher pH (Keenan & Sedlak 2008; González *et al.* 2014) but we observed that $[Fe]_{diss}$ decreased in fresh culture at a much faster rate than in old cultures, whose pH was much higher. For instance, at initial FeSSi concentration of 180 mg/L, $[Fe]_{diss}$ decreased by 170 and 7.26 (x 10^{-5} mg/L-h) within the first 96 h in fresh and old cultures, respectively. Slower oxidation of Fe^{2+} is due to the presence of higher amounts algal NOM in old cultures (SI Figure S5), which bound to the ions and retarded their oxidation. Gonzalez *et al*. recently reported slower rates of Fe^{2+} oxidation with increasing

163

amounts of algal exudates isolated from *Dunaliela tertiolecta* (González *et al.* 2014). After

14 d, however, there was no obvious difference in the [Fe]$_{diss}$ levels in all the conditions.

The levels of [S]$_{diss}$ detected 2 h after adding FeSSi suspension were higher in all but one

(that is, 1.8 mg-FeSSi/L in old culture) FeSSi treatments compared to their respective

control conditions. The most initial increase in [S]$_{diss}$ was observed in the 180 mg-FeSSi/L

conditions (48 – 52%). These results suggest leaching of S into cultures from FeSSi

particles. [S]$_{diss}$ decreased with time in control and FeSSi treatment cultures except at the

highest FeSSi concentrations where we saw increase in [S]$_{diss}$ over time (Figure 3). In

contrast, [Si]$_{diss}$ detected 2 h after exposure of cultures to FeSSi was 1.8 > 18 > 180 mg-

FeSSi/L in both fresh and old cultures; and lower than in control conditions in most cases. In

fact, [Si]$_{diss}$ in fresh and old cultures exposed to 180 mg-FeSSi/L was lower by a factor of

2.9 and 3.5 relative to their respective control conditions. This trend suggests that FeSSi

removed dissolved background Si from the aqueous phase. Fe^0 is known to have affinity for

dissolved Si (Reardon *et al.* 2008) and this may have important consequences in natural

waters where the ENMs may also adsorb to important nutrients like phosphate and nitrate.

Undissolved FeSSi particles in fresh and old *C. reinhardtii* cultures were collected on

Days 2, 10, and 30 for analyses via XRD and XPS. We found peaks representing oxides of

Fe in both fresh and old cultures in samples analyzed from 2 to 30 d (Figure 5). The major

oxide peaks were assigned to Fe_2O_3, γ-Fe_2O_3, $Fe(OH)_3$, δ-FeOOH, and Fe_2SiO_4. However,

while Fe^0 was detected in aged culture (corresponding to $2\Theta = 44.5°$ (Adeleye *et al.* 2013;

Su *et al.* 2014a)) up to a month after exposing *C. reinhardtii* to FeSSi, we did not detect Fe^0

in fresh culture even after 24 h post-exposure. This implies that transformation (oxidation)

of FeSSi was much faster in fresh media relative to the older cultures that contained a higher

amount of algal NOM. This supports our findings in the previous section where we reported

that $[Fe]_{diss}$ was an order of magnitude higher in fresh cultures than in old cultures. We previously reported slower oxidation of nZVI in natural groundwater compared to synthetic salt solutions and adduced the phenomenon to the presence of NOM in groundwater (Adeleye *et al.* 2013).

Our observation of slower oxidation in old media is somewhat counterintuitive as one would expect a faster oxidation of Fe^0 in the older cultures, which have a higher amount of DO (Table 1) (Reinsch *et al.* 2010). The detection of Fe^0 up to one month after exposure of FeSSi into old cultures suggests that the influence of algal NOM on Fe^0 oxidation is probably more important than the presence of DO in freshwater. Reinsch and coworkers had previously found that the presence of DO in aqueous media was probably more important in Fe^0 oxidation than dissolved anions (which tend to inhibit oxidation) (Reinsch *et al.* 2010). Therefore, FeSSi (and other nZVI derivatives) may persist longer in productive natural waters.

5.3.4 Influence of Algae on Effects of FeSSi

In order to see if FeSSi had an effect on population growth of *C. reinhardtii* we monitored concentrations of chlorophyll a (chl a) over time in all treatments and controls. In fresh cultures, we observed a clear dose-response effect of FeSSi on cells (Figure 6). The chl a concentration (in μg/L), detected 2 h after dosing fresh cultures with FeSSi was 0.34, 0.29, 0.14, and non-detect in control, 1.8, 18, and 180 mg-FeSSi/L, respectively. The detection limit of the fluorescence reader corresponds to 10^{-3} μg/L or 10^2 cells. At 180 mg/L of FeSSi, chl a remained non-detect in fresh cultures until Day 7, after which cells grew exponentially although population density was still much below what we observed at lower levels of FeSSi in fresh cultures. In an acute toxicity study, FeSSi would have been said to have lethal effects on *C. reinhardtii* at 180 mg/L, which underscores the importance of (sub)chronic

165

toxicity studies in order to understand the long term effects of ENMs in the environment. The response of fresh *C. reinhardtii* cultures to FeSSi suggests that (1) the initial amount of toxicant increased with FeSSi concentration, and (2) the amount of toxicant reduced with time, which allowed cells to recover. The possibility of cells becoming better adapted to the toxicant over time is also not ruled out. In old cultures we only observed a negative effect of FeSSi on growth in the 180 mg/L condition, in which biomass was slightly less than control over the course of the study (Figure 6). At FeSSi concentrations of 1.8 and 18 mg/L in old cultures, we observed a positive effect of FeSSi on algal growth, especially on and after 21 d.

Although iron is generally not considered to be very toxic (Kirschling *et al.* 2010; Keller *et al.* 2012; Pádrová *et al.* 2014), nZVI and iron oxides have demonstrated toxicity in organisms, including algae (Kadar *et al.* 2012; Keller *et al.* 2012). Redox-active Fe species can produce reactive oxygen species (ROS) such as hydroxyl radical (OH·) and ferryl ion (Fe(IV)) via Fenton-type chemistry (Keenan & Sedlak 2008; Szivák *et al.* 2009; Ševců *et al.* 2011). This is probably the major toxicity mechanism of FeSSi to *C. reinhardtii* in this study although other toxicity mechanisms are very likely and are discussed later. As we previously mentioned, Fe^0 in FeSSi was more reactive in fresh media, which led to production of aqueous Fe (mostly Fe^{2+}) at concentrations an order of magnitude higher than in old media. Both species (Fe^0 and Fe^{2+}), which are the most redox-active forms of iron (Ševců *et al.* 2011; Keller *et al.* 2012), must have produced ROS at levels that were toxic to algae. In old cultures however, reactivity of FeSSi was suppressed by algal NOM, which may have also chelated some of the Fe^{2+} produced as previously shown for other metals (García-Meza *et al.* 2005) In addition, NOM is known to effectively scavenge ROS, especially the non-selective ones like OH· (Keenan & Sedlak 2008; Chen *et al.* 2011). As such, less ROS was produced

in old media, and algae were better protected from ROS produced by redox-active Fe species in old media than in fresh media. Algal NOM-chelated Fe^{2+} was probably bioavailable (as a source of Fe), which might explain higher biomass of old *C. reinhardtii* at 1.8 and 18 mg-FeSSi/L over time compared to control conditions where Fe was non-detect after 7 d.

The recovery of fresh culture in the 180 mg-FeSSi/L condition after 7 d suggests that the level of toxicant present was not completely lethal but high enough to suppress growth. Oxidative stress typically affects algal growth and impairs photosynthesis via several mechanisms that have been discussed in the literature (Ševců *et al.* 2011; Kadar *et al.* 2012; Keller *et al.* 2012). By Day 7 $[Fe]_{diss}$ in fresh culture with 180 mg-FeSSi/L had decreased to levels similar to the initial $[Fe]_{diss}$ (i.e. Day 0) we found in fresh culture with 18 mg-FeSSi/L (< 0.1 mg/L). Cells were probably able to recover as the amount of redox-active Fe species in aqueous phase decreased with time. Also, the growth of algae after 7 d must have led to production of more NOM, which protected the cells as in the other conditions. We doubt that the increase in aqueous S found in the presence of FeSSi had any negative impact on algae as concentrations similar to what we detected are at times used in preparing algal culture media (Mosulén *et al.* 2003). Decreased levels of Si from aqueous phase, especially in the presence of high amounts of FeSSi, did not have an effect in this study since Si is not an essential nutrient for *C. reinhardtii*. However, this is expected to negatively impact diatoms and other pelagic organisms that require it.

We also believe that FeSSi must have shaded some *C. reinhardtii* cells from light needed for photosynthesis, especially at high concentration where we saw clear effects on growth in both fresh and old cultures. As we showed in Figure 4, heteroaggregation occurred between algae and FeSSi particles in freshwater medium. In fact, aggregates of FeSSi were found to bridge *C. reinhardtii* cells. Shading due to ENMs was found to inhibit growth of freshwater

167

algae, *Chlorella vulgaris* and *Pseudokirchneriella subcapitata* (Schwab *et al.* 2011). In addition, the attachments can lead to direct release of ROS to cell membrane, decrease in cell mobility, membrane lipid by-layer disruption, and decrease in nutrient flow between the cell and the external environment (Navarro *et al.* 2008).

5.3. Environmental Implications

The presence of natural organic materials secreted by freshwater microorganisms will affect the stability of FeSSi (and possibly other derivatives of nZVI). Once coated by the microbial extracellular polymers, their surface properties (mainly surface charge) will change and their aggregation will be slowed via steric stabilization. The nanoparticles will thus not settle out the water matrix as fast as one would expect from particles with high attraction forces (van der Waals and magnetic interactions), which may lead to longer exposure of pelagic organisms.

In agreement with several previous studies we found that FeSSi tends to oxidize rapidly in well-mixed natural waters. But here, we show that in productive waters, which tend to have a lot of microorganisms, and hence microbial organic matter, these nanoparticles may persist longer due to slower oxidation resulting from organic matter coating. Coating of FeSSi by NOM will also have effect on its reactivity, adsorption properties, and toxicity. FeSSi can release some of their components (e.g. Fe and S) into water and also remove other chemical groups (mostly negatively charged groups such as silicate, phosphate and nitrate) since they have isoelectric point of 7.4 – 8.5 (Zhang & Elliott 2006; Adeleye *et al.* 2013). These groups may be transformed on the surface of the particles to other forms that may or may not be available to organisms, or be released back into water as the particles transform further.

Table 1. Properties of media with and without *C. reinhardtii* cells

Property	Fresh (Day 0) media	Young (Day 1) media		Old (Day 10) media	
		With cells	Without[a] cells	With cells	Without[a] cells
Dissolved organic carbon (mg/L)	1.83	nd	2.19	nd	5.58
Total dissolved nitrogen (mg/L)	18.8	nd	16.3	nd	6.30
Dissolved oxygen (mg/L)	8.43	8.98	8.47	9.42	8.92
Phosphorus (mg/L)	4.50	nd	4.10	nd	0.07
pH	7.6	7.8	7.7	10.5	10.4
Conductivity (µS/cm)	272	284	283	284	298

[a] Cells were removed by centrifugation followed by 0.2 µm filtration under sterile conditions

nd = Not determined

Table 2. Hydrodynamic size, zeta potential, and attachment efficiency of FeSSi in media

Media	Hydrodynamic size (nm)	Zeta potential (mV)	Attachment efficiency, α
DI water[a]	341	-38.0	0.07
Fresh media	369	-17.0	0.18
Young media	392	-17.3	0.21
Old media	390	-11.4	0.09

[a] Contained pH 7.5 phosphate buffer (Ionic strength = 13.4 mM)
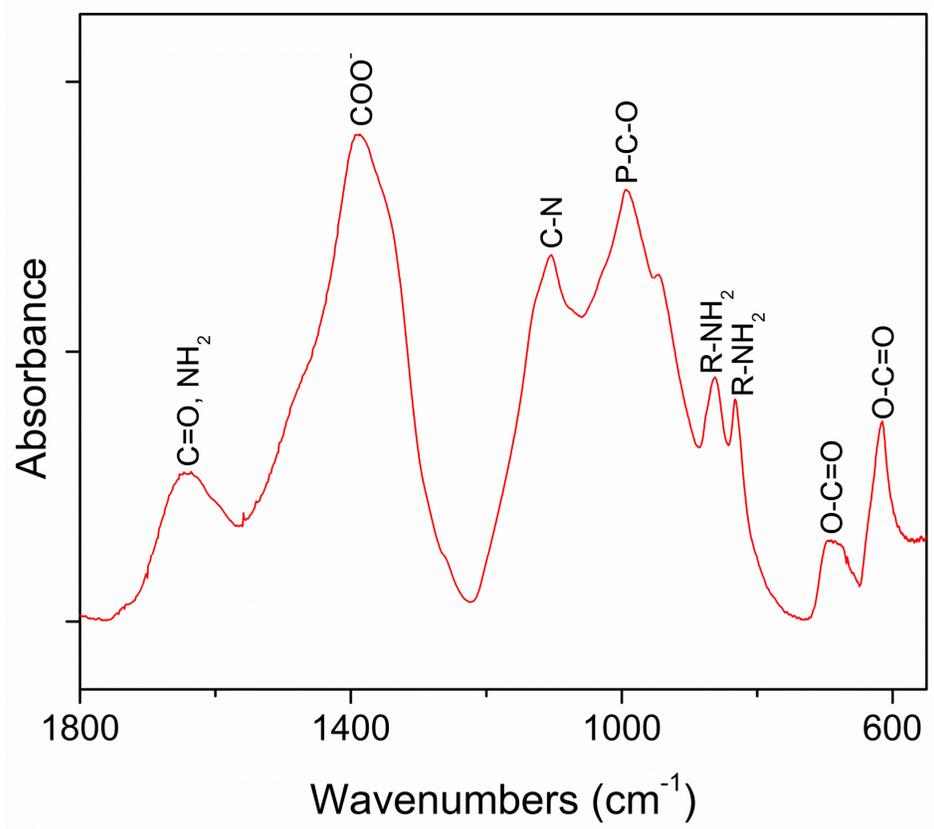
Figure 1. FTIR spectrum of natural organic matter produced by *Chlamydomonas reinhardtii*.
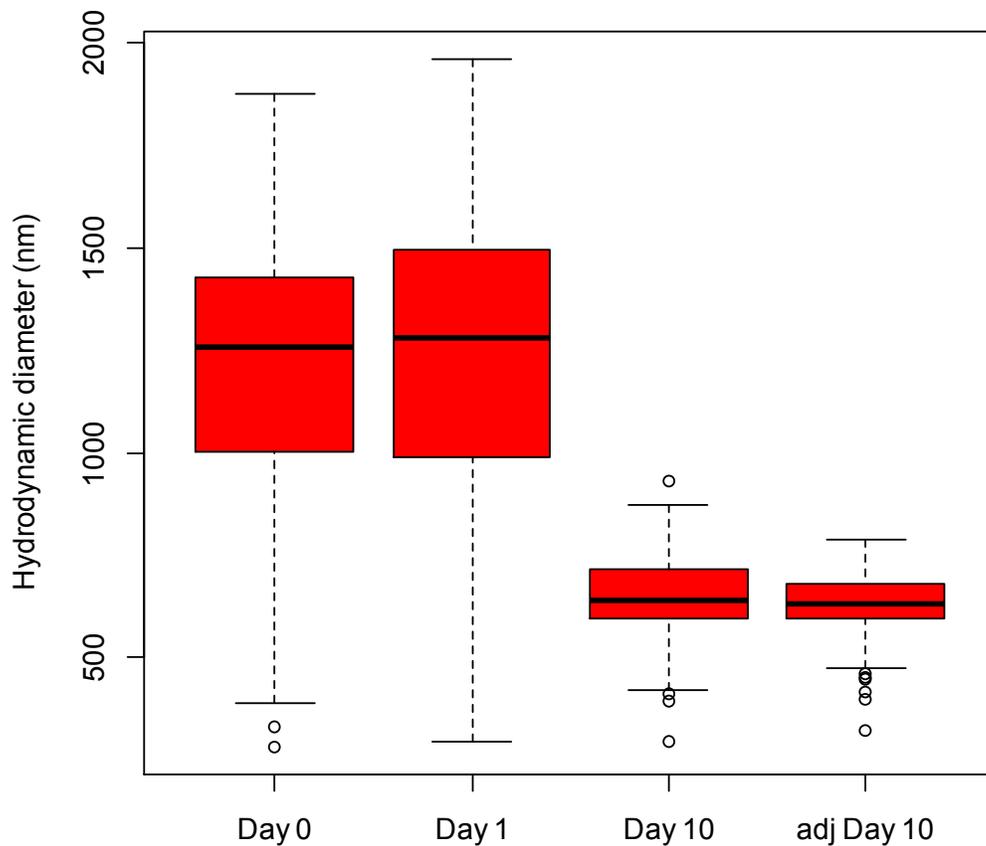
Detailed band assignments are provided in SI Table S2.

Figure 2. Tukey boxplot of hydrodynamic size of FeSSi in fresh (Day 0), young (Day 1), old (Day 10) and pH adjusted old (adj Day 10) media over 1 h. the horizontal line within the box represents the second quartile (median hydrodynamic diameter).
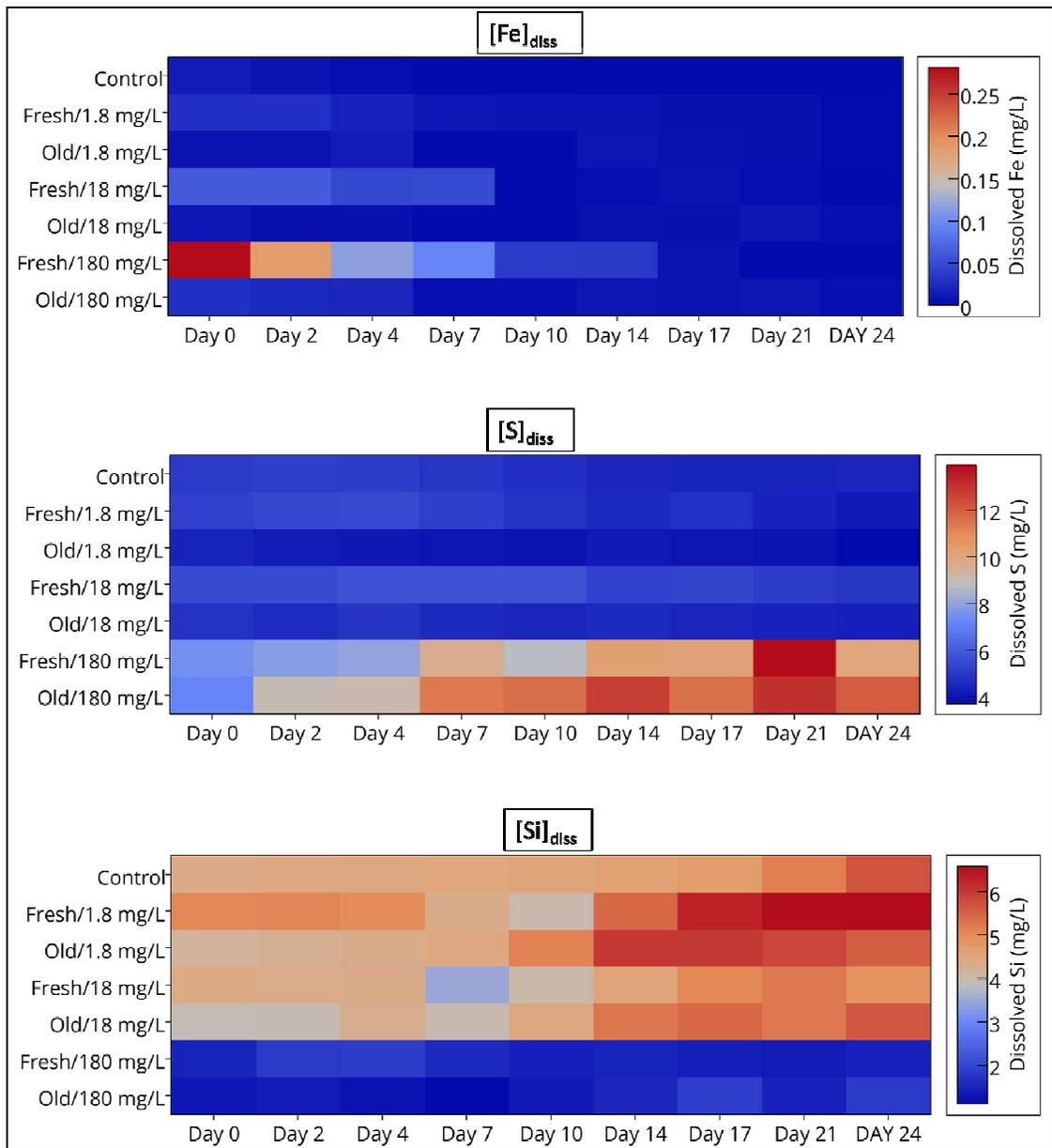
Figure 3. Concentrations of dissolved Fe, S, and Si detected in fresh and young cultures of *C. reinhardtii* in the presence of 1.8, 18, and 180 mg/L of FeSSi particles.
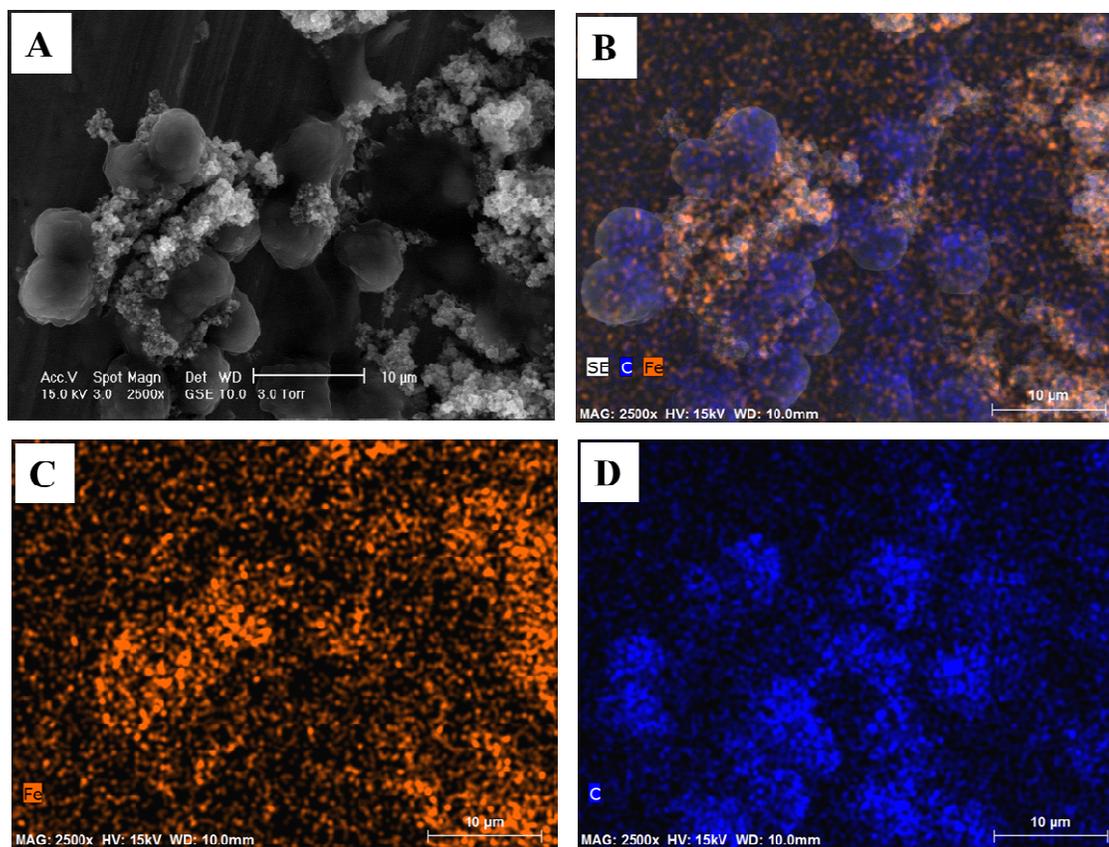
Figure 4. Representative ESEM with EDS hypermaps of culture with FeSSi particles. (A) Heteroaggregation between nanoparticle aggregates and *C. reinhardtii* cells, with (B) showing an overlay of carbon (C) and iron (Fe) distribution on micrograph. Individual distribution of Fe (orange) and C (blue) are shown in (C) and (D), respectively.
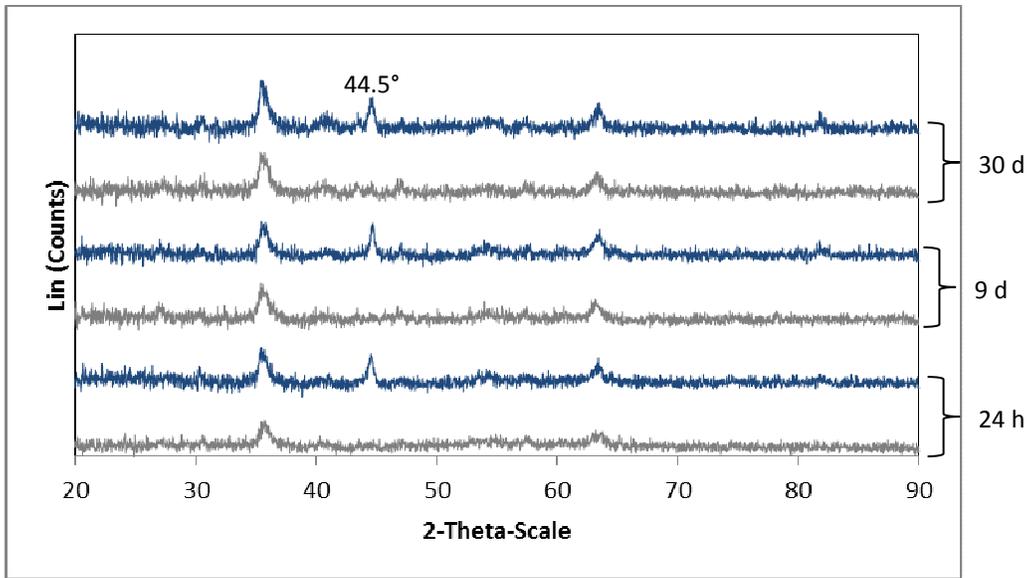
Figure 5. X-ray diffractograms of undissolved FeSSi (180 mg/L) in fresh (grey) and old (blue) algal media over 30 d.
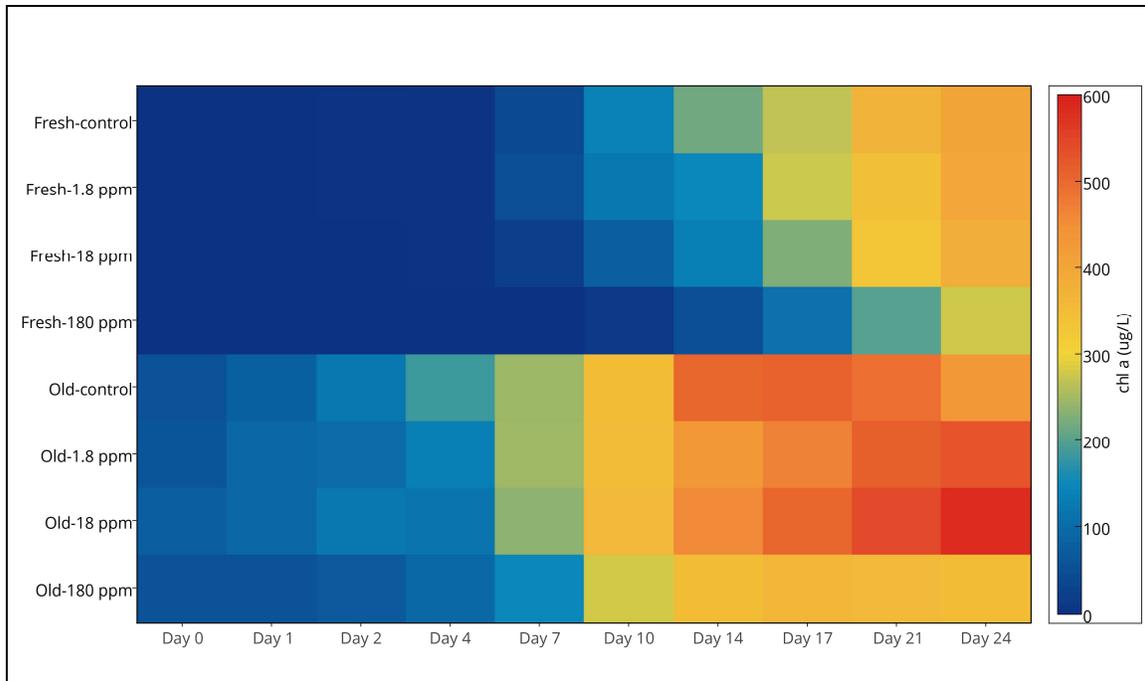
Figure 6. Concentration of chl a (µg/L) in fresh and old cultures with and without FeSSi

Table S1. Composition of COMBO media (Adapted from Kilham *et al*.1998)

Compound	Concentration	
	(mg/L)	(µmol/L)
$CaCl_2.2H_2O$	36.76	250
$MgSO_4.7H_2O$	36.97	150
K_2HPO_4	8.71	50
$NaNO_3$	85.01	1000
$NaHCO_3$	12.60	150
$Na_2SiO_3.9H_2O$	24.42	100
H_3BO_3	24.00	388
KCl	7.45	100
$Na_2EDTA.2H_2O$	4.36	11.7
$FeCl_3.6H_2O$	1.00	3.7
$MnCl_2.4H_2O$	0.18	0.9
$CuSO_4.5H_2O$	0.001	0.004
$ZnSO_4.7H_2O$	0.022	0.08
$CoCl_2.6H_2O$	0.012	0.05
$Na_2MoO_4.2H_2O$	0.022	0.09
H_2SeO_3	0.0016	0.012
Na_3VO_4	0.0018	0.01
LiCl	0.31	7.3
RbCl	0.07	0.6
$SrCl_2.6H_2O$	0.15	0.57
NaBr	0.016	0.16

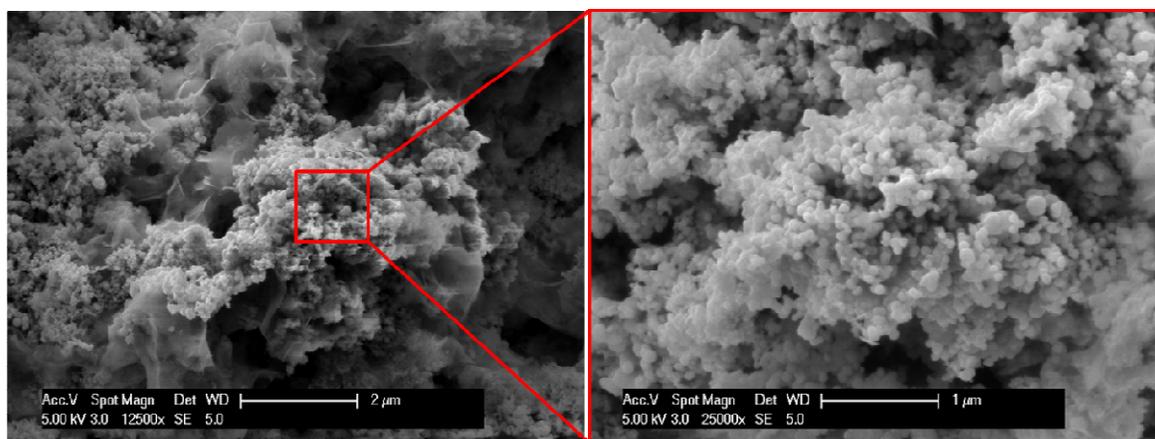|		
KI	0.0033	0.02
Vitamin B_{12}	0.00055	0.0004
Biotin	0.0005	0.002
Thiamin	0.1	0.3

Figure S1. Scanning electron micrograph of FeSSi
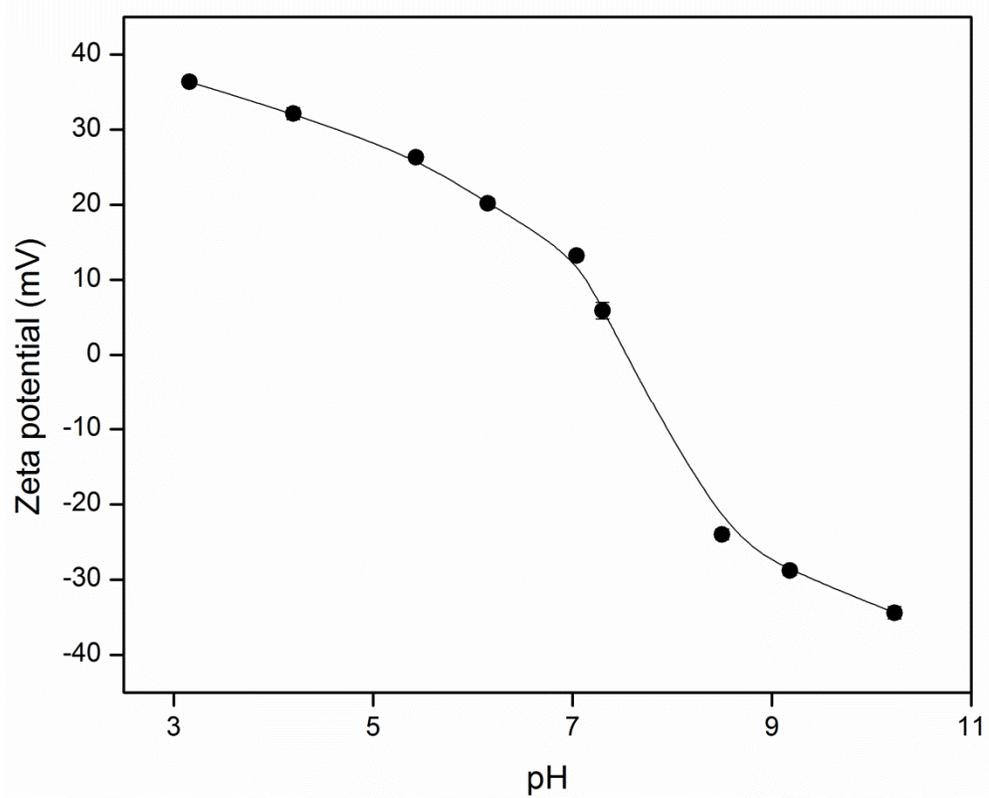
Figure S2. Effect of pH on zeta potential of FeSSi. Isoelectric point (IEP) ≈ pH 7.4

Table S2. Band assignments for FTIR spectrum of organic matter from 10-day old

Chlamydomonas reinhardtii

Wavenumber (cm^{-1})	Functional group/assignment
530	NO_2 deformation
615	C=O out-of-plane bend in amides
690	O-C=O bending in carboxylic acids
833	NH_2 wag primary amines
862	NH_2 wag primary amines
945	P-O-C antisym stretch in organophosphorus compounds
993	P-O-C antisym stretch in organophosphorus compounds
1104	C-O, C-O-C stretching of polysaccharides
1387	COO- symmetric stretch
1636	C=O stretch and NH_2 deformation in primary amides

Figure S3. Aggregation kinetics of FeSSi in DI, Day 0, Day 1, and Day 10 media

Figure S4. FeSSi in Day 0 and Day 10 *C. reinhardtii* media right after dosing with
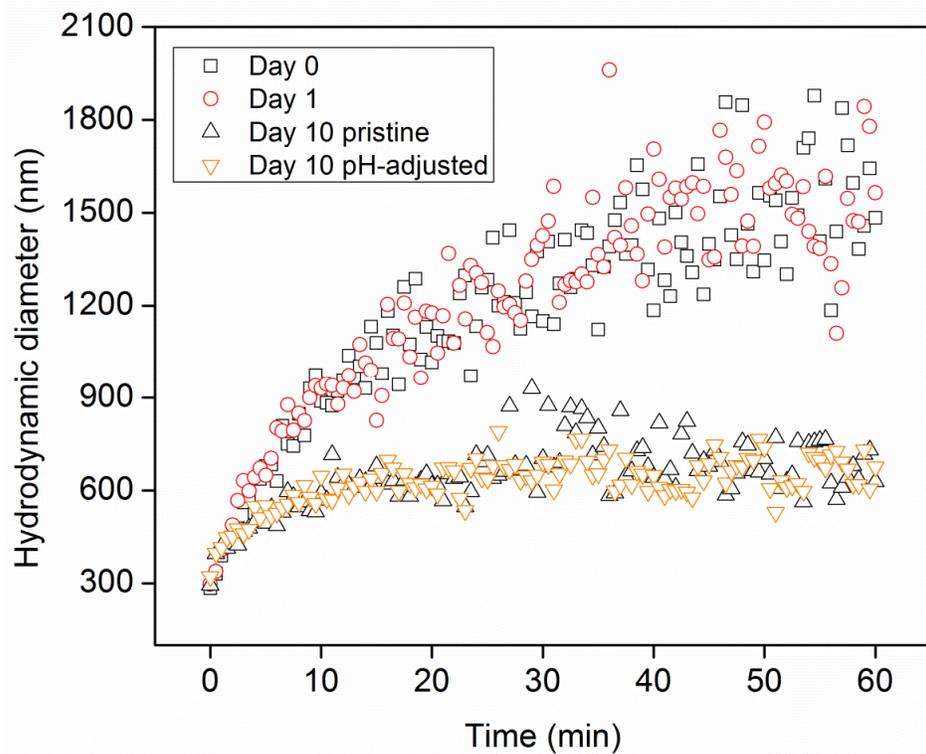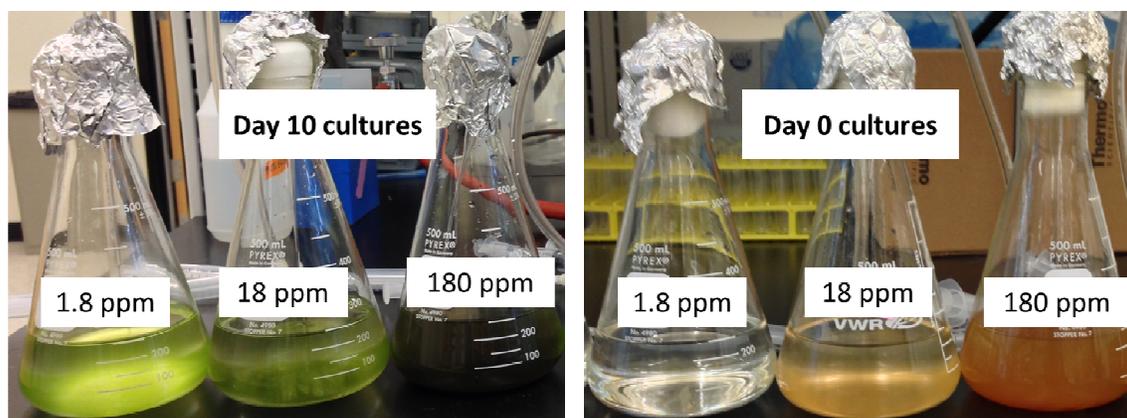
nanoparticles. FeSSi stock was stirred in either Day 0 or Day 10 media before dosing
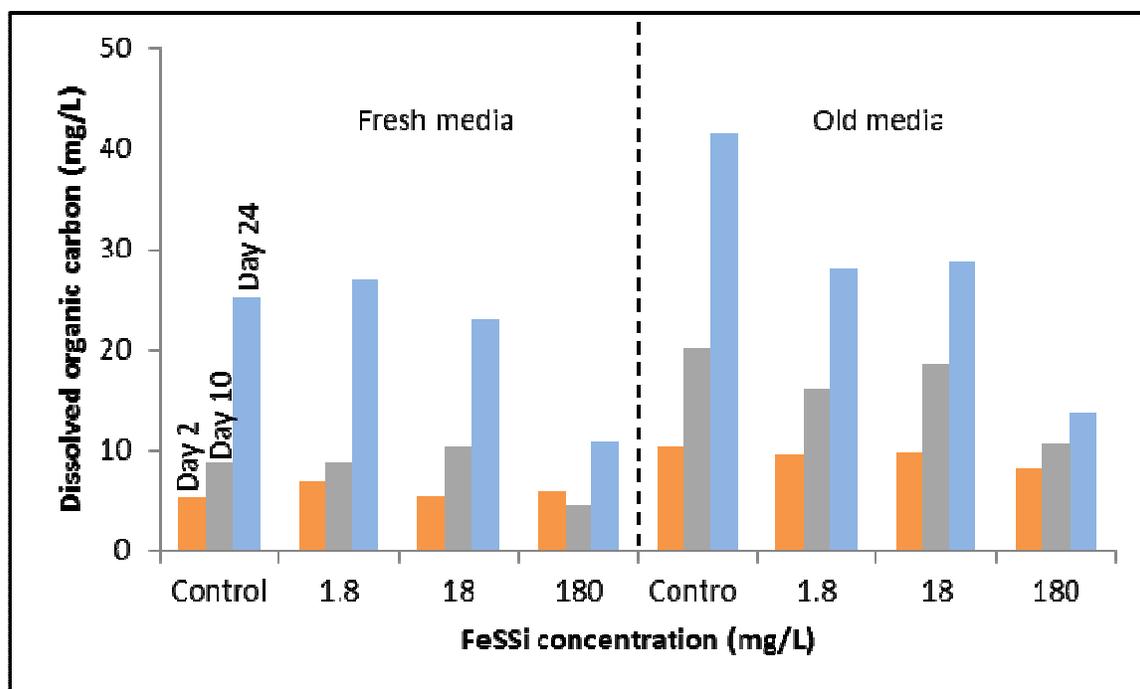
Figure S5. Dissolved organic carbon (DOC) in aqueous phase of *C. reinhardtii* cultures

References

Adeleye A.S., Conway J.R., Perez T., Rutten P. & Keller A.A. (2014). Influence of Extracellular Polymeric Substances on the Long-Term Fate, Dissolution, and Speciation of Copper-Based Nanoparticles. *Environ Sci Technol*, 48, 12561-12568.

Adeleye A.S. & Keller A.A. (2014). Long-term colloidal stability and metal leaching of single wall carbon nanotubes: effect of temperature and extracellular polymeric substances. *Water research*, 49, 236-50.

Adeleye A.S., Keller A.A., Miller R.J. & Lenihan H.S. (2013). Persistence of commercial nanoscaled zero-valent iron (nZVI) and by-products. *Journal of Nanoparticle Research*, 15, 1-18.

Chen J., Xiu Z., Lowry G.V. & Alvarez P.J.J. (2011). Effect of natural organic matter on toxicity and reactivity of nano-scale zero-valent iron. *Water research*, 45, 1995-2001.

Comba S., Di Molfetta A. & Sethi R. (2011). A Comparison Between Field Applications of Nano-, Micro-, and Millimetric Zero-Valent Iron for the Remediation of Contaminated Aquifers. *Water, Air, & Soil Pollution*, 215, 595-607.

Conway J.R., Adeleye A.S., Gardea-Torresdey J. & Keller A.A. (2015). Aggregation, Dissolution, and Transformation of Copper Nanoparticles in Natural Waters. *Environmental Science & Technology*, 49, 2749-2756.

Crane R.A., Dickinson M. & Scott T.B. (2015). Nanoscale zero-valent iron particles for the remediation of plutonium and uranium contaminated solutions. *Chemical Engineering Journal*, 262, 319-325.

Dries J., Bastiaens L., Springael D., Kuypers S., Agathos S.N. & Diels L. (2005). Effect of humic acids on heavy metal removal by zero-valent iron in batch and continuous flow column systems. *Water research*, 39, 3531-3540.

Flemming H.-C., Neu T.R. & Wozniak D.J. (2007). The EPS matrix: the "house of biofilm cells". *Journal of Bacteriology*, 189, 7945-7947.

Fu F., Dionysiou D.D. & Liu H. (2014). The use of zero-valent iron for groundwater remediation and wastewater treatment: A review. *Journal of Hazardous Materials*, 267, 194-205.

García-Meza J.V., Barrangue C. & Admiraal W. (2005). Biofilm formation by algae as a mechanism for surviving on mine tailings. *Environmental Toxicology and Chemistry*, 24, 573-581.

Giasuddin A., Kanel S. & Choi H. (2007). Adsorption of humic acid onto nanoscale zerovalent iron and its effect on arsenic removal. *Environmental Science & Technology*, 41, 2022-2027.

González A.G., Santana-Casiano J.M., González-Dávila M., Pérez-Almeida N. & Suárez de Tangil M. (2014). Effect of Dunaliella tertiolecta Organic Exudates on the Fe(II) Oxidation Kinetics in Seawater. *Environmental Science & Technology*, 48, 7933-7941.

Jiemvarangkul P., Zhang W.-x. & Lien H.-L. (2011). Enhanced transport of polyelectrolyte stabilized nanoscale zero-valent iron (nZVI) in porous media. *Chemical Engineering Journal*, 170, 482-491.

Kadar E., Cunliffe M., Fisher A., Stolpe B., Lead J. & Shi Z. (2014). Chemical interaction of atmospheric mineral dust-derived nanoparticles with natural seawater — EPS and sunlight-mediated changes. *Science of The Total Environment*, 468–469, 265-271.

Kadar E., Rooks P., Lakey C. & White D.A. (2012). The effect of engineered iron nanoparticles on growth and metabolic status of marine microalgae cultures. *Science of The Total Environment*, 439, 8-17.

Keenan C.R. & Sedlak D.L. (2008). Factors Affecting the Yield of Oxidants from the Reaction of Nanoparticulate Zero-Valent Iron and Oxygen. *Environmental Science & Technology*, 42, 1262-1267.

Keller A.A., Garner K., Miller R.J. & Lenihan H.S. (2012). Toxicity of Nano-Zero Valent Iron to Freshwater and Marine Organisms. *PLOS ONE*, 7, e43983.

Keller A.A., Wang H., Zhou D., Lenihan H.S., Cherr G., Cardinale B.J., Miller R. & Ji Z. (2010). Stability and Aggregation of Metal Oxide Nanoparticles in Natural Aqueous Matrices. *Environmental Science & Technology*, 44, 1962-1967.

Kilham S., Kreeger D., Lynn S., Goulden C. & Herrera L. (1998). COMBO: a defined freshwater culture medium for algae and zooplankton. *Hydrobiologia*, 377, 147-159.

Kim E.-J., Murugesan K., Kim J.-H., Tratnyek P.G. & Chang Y.-S. (2013). Remediation of Trichloroethylene by FeS-Coated Iron Nanoparticles in Simulated and Real Groundwater: Effects of Water Chemistry. *Ind. Eng. Chem. Res.*, 52, 9343-9350.

Kim H.-J., Phenrat T., Tilton R.D. & Lowry G.V. (2009). Fe0 Nanoparticles Remain Mobile in Porous Media after Aging Due to Slow Desorption of Polymeric Surface Modifiers. *Environmental Science & Technology*, 43, 3824-3830.

Kirschling T.L., Gregory K.B., Minkley E.G., Lowry G.V. & Tilton R.D. (2010). Impact of Nanoscale Zero Valent Iron on Geochemistry and Microbial Populations in Trichloroethylene Contaminated Aquifer Materials. *Environmental Science & Technology*, 44, 3474-3480.

Kocur C.M., Chowdhury A.I., Sakulchaicharoen N., Boparai H.K., Weber K.P., Sharma P., Krol M.M., Austrins L., Peace C., Sleep B.E. & O'Carroll D.M. (2014).

Characterization of nZVI Mobility in a Field Scale Test. *Environmental Science & Technology*, 48, 2862-2869.

Koutsospyros A., Pavlov J., Fawcett J., Strickland D., Smolinski B. & Braida W. (2012). Degradation of high energetic and insensitive munitions compounds by Fe/Cu bimetal reduction. *Journal of Hazardous Materials*, 219–220, 75-81.

Lv X., Xue X., Jiang G., Wu D., Sheng T., Zhou H. & Xu X. (2014). Nanoscale Zero-Valent Iron (nZVI) assembled on magnetic Fe3O4/graphene for Chromium (VI) removal from aqueous solution. *Journal of Colloid and Interface Science*, 417, 51-59.

Ma S., Zhou K., Yang K. & Lin D. (2014). Heteroagglomeration of Oxide Nanoparticles with Algal Cells: Effects of Particle Type, Ionic Strength and pH. *Environmental Science & Technology*, 49, 932-939.

Mayer C., Moritz R., Kirschner C., Borchard W., Maibaum R., Wingender J. & Flemming H.-C. (1999). The role of intermolecular interactions: studies on model systems for bacterial biofilms. *International journal of biological macromolecules*, 26, 3-16.

Mosulén S., Domı, amp, x, nguez M.J., Vigara J., Vı, lchez C., Guiraum A. & Vega J.M. (2003). Metal toxicity in Chlamydomonas reinhardtii. Effect on sulfate and nitrate assimilation. *Biomolecular Engineering*, 20, 199-203.

Mueller N., Braun J., Bruns J., Cernik M., Rissing P., Rickerby D. & Nowack B. (2012). Application of nanoscale zero valent iron (NZVI) for groundwater remediation in Europe. *Env Sci Poll Res Int*, 19, 550-558.

Navarro E., Baun A., Behra R., Hartmann N.B., Filser J., Miao A.-J., Quigg A., Santschi P.H. & Sigg L. (2008). Environmental behavior and ecotoxicity of engineered nanoparticles to algae, plants, and fungi. *Ecotoxicology*, 17, 372-386.

Nielsen P.H. & Jahn A. (1999). Extraction of EPS. In: *Microbial extracellular polymeric substances*. Springer, pp. 49-72.

O'Carroll D., Sleep B., Krol M., Boparai H. & Kocur C. (2013). Nanoscale zero valent iron and bimetallic particles for contaminated site remediation. *Advances in Water Resources*, 51, 104-122.

Pádrová K., Lukavský J., Nedbalová L., Čejková A., Cajthaml T., Sigler K., Vítová M. & Řezanka T. (2014). Trace concentrations of iron nanoparticles cause overproduction of biomass and lipids during cultivation of cyanobacteria and microalgae. *J Appl Phycol*, 1-9.

Pal A. & Paul A. (2008). Microbial extracellular polymeric substances: central elements in heavy metal bioremediation. *Indian journal of microbiology*, 48, 49-64.

187

Phenrat T., Saleh N., Sirk K., Kim H.-J., Tilton R. & Lowry G. (2008). Stabilization of aqueous nanoscale zerovalent iron dispersions by anionic polyelectrolytes: adsorbed anionic polyelectrolyte layer properties and their effect on aggregation and sedimentation. *Journal of Nanoparticle Research*, 10, 795-814.

Reardon E.J., Fagan R., Vogan J.L. & Przepiora A. (2008). Anaerobic Corrosion Reaction Kinetics of Nanosized Iron. *Environmental Science & Technology*, 42, 2420-2425.

Reinsch B.C., Forsberg B., Penn R.L., Kim C.S. & Lowry G.V. (2010). Chemical Transformations during Aging of Zerovalent Iron Nanoparticles in the Presence of Common Groundwater Dissolved Constituents. *Environmental Science & Technology*, 44, 3455-3461.

Rhiem S., Riding M.J., Baumgartner W., Martin F.L., Semple K.T., Jones K.C., Schäffer A. & Maes H.M. (2015). Interactions of multiwalled carbon nanotubes with algal cells: Quantification of association, visualization of uptake, and measurement of alterations in the composition of cells. *Environmental Pollution*, 196, 431-439.

Saleh N.B., Pfefferle L.D. & Elimelech M. (2008). Aggregation Kinetics of Multiwalled Carbon Nanotubes in Aquatic Systems: Measurements and Environmental Implications. *Environmental Science & Technology*, 42, 7963-7969.

Schwab F., Bucheli T.D., Lukhele L.P., Magrez A., Nowack B., Sigg L. & Knauer K. (2011). Are Carbon Nanotube Effects on Green Algae Caused by Shading and Agglomeration? *Environmental Science & Technology*, 45, 6136-6144.

Ševců A., El-Temsah Y.S., Joner E.J. & Černík M. (2011). Oxidative stress induced in microorganisms by zero-valent iron nanoparticles. *Microbes and Environments*, 26, 271-281.

Shi L.-n., Zhang X. & Chen Z.-l. (2011). Removal of Chromium (VI) from wastewater using bentonite-supported nanoscale zero-valent iron. *Water research*, 45, 886-892.

Stevenson L.M., Dickson H., Klanjscek T., Keller A.A., McCauley E. & Nisbet R.M. (2013). Environmental Feedbacks and Engineered Nanoparticles: Mitigation of Silver Nanoparticle Toxicity to <italic>Chlamydomonas reinhardtii</italic> by Algal-Produced Organic Compounds. *PLOS ONE*, 8, e74456.

Su C., Puls R.W., Krug T.A., Watling M.T., O'Hara S.K., Quinn J.W. & Ruiz N.E. (2012). A two and half-year-performance evaluation of a field test on treatment of source zone tetrachloroethene and its chlorinated daughter products using emulsified zero valent iron nanoparticles. *Water research*, 46, 5071-5084.

Su Y., Adeleye A.S., Huang Y., Sun X., Dai C., Zhou X., Zhang Y. & Keller A.A. (2014a). Simultaneous removal of cadmium and nitrate in aqueous media by nanoscale zerovalent iron (nZVI) and Au doped nZVI particles. *Water research*, 63, 102-111.

188

Su Y., Adeleye A.S., Keller A.A., Huang Y., Dai C., Zhou X. & Zhang Y. (2015a). Magnetic sulfide-modified nanoscale zerovalent iron (S-nZVI) for dissolved metal ion removal. *Water research*, 74, 47-57.

Su Y., Adeleye A.S., Keller A.A., Huang Y., Dai C., Zhou X. & Zhang Y. (2015b). Magnetic sulfide-modified nanoscale zerovalent iron (S-nZVI) for dissolved metal ion removal. *Water Research*, 74, 47-57.

Su Y., Adeleye A.S., Zhou X., Dai C., Zhang W., Keller A.A. & Zhang Y. (2014b). Effects of nitrate on the treatment of lead contaminated groundwater by nanoscale zerovalent iron. *Journal of Hazardous Materials*, 280, 504-513.

Sutherland I.W. (2001). Biofilm exopolysaccharides: a strong and sticky framework. *Microbiology*, 147, 3-9.

Szivák I., Behra R. & Sigg L. (2009). Metal-induced reactive oxygen species production in Chlamydomonas reinhardtii (Chlorophyceae)1. *Journal of Phycology*, 45, 427-435.

Tian Y., Zheng L. & Sun D.-z. (2006). Functions and behaviors of activated sludge extracellular polymeric substances (EPS): a promising environmental interest. *Journal of Environmental Sciences*, 18, 420-427.

Urabe J., Clasen J. & Sterner R.W. (1997). Phosphorus limitation of Daphnia growth: Is it real? *Limnology and Oceanography*, 42, 1436-1443.

Wingender J., Neu T. & Flemming H. (1999). Microbial Extracellular Polymeric Substances: Characterisation. *Structure and Function, Springer, Berlin*, 123.

Zhang W.-x. & Elliott D.W. (2006). Applications of iron nanoparticles for groundwater remediation. *Remediation Journal*, 16, 7-21.

Chapter 6. Conclusions and Future Works

6.1. Conclusions

This doctoral research has improved our understanding of how microorganisms directly and indirectly influence the fate and transformations of a number of engineered nanomaterials (ENMs) in natural aquatic systems. The role of (1) other important environmental factors such as pH, ionic strength, and temperature; and (2) intrinsic physicochemical properties of the ENMs were also considered, as well as how they combine with algal soluble extracellular polymeric substances (sEPS) to determine ENM fate.

In the first research, interaction between sEPS extracted from *Isochrysis galbana* and single wall carbon nanotubes (SWCNTs) was investigated. Interactions between sEPS and SWCNTs were confirmed by change in the surface charge of the nanomaterials: the magnitude of zeta potential increased in the presence of sEPS due to the anionic functional groups in the biopolymers. In addition, effect of sEPS on the stability of SWCNTs was probed, and compared to stability imparted by Suwannee River natural organic matter (SRNOM), a known stabilizer of SWCNTs. There was no significant difference in the hydrodynamic size of SWCNTs in the presence of either SRNOM or sEPS, but polydispersity index was slightly lower in the SWCTs-sEPS system. Aggregation and sedimentation of SWCNTs was slowed down by SRNOM but a stronger suppression of aggregation and sedimentation was found in the presence of sEPS, probably due to stronger impact of sEPS on the surface charge of SWCNTs compared to SRNOM.

The second project followed up on the first one by investigating whether sEPS from *I. galbana* had a similar impact on a different class of ENMs. Nanoparticulate copper (Cu) and

cuprous oxide (CuO) were selected for this project, as well as Kocide 3000—a commercial

bactericide/fungicide that mainly contains copper hydroxide ($CuOH_2$). In addition to

studying effects of sEPS on surface charge and aggregation of these particles, the impact of

the biomacromolecules on dissolution and speciation of the copper-based ENMs were also

investigated. Unlike in SWCNTs where we saw an increase, the surface charge (zeta

potential) of CuO decreased in magnitude in the presence of sEPS. In contrast, the zeta

potential of CuO increased in the presence of SRNOM. Although decrease in surface

charges typically leads to less stability, CuO was most stable in the presence of sEPS than

when SRNOM or neither was used. These results suggest that improved stability of CuO by

sEPS was due to steric repulsion (rather than electrostatic stabilization in SWCNTs), which

was confirmed by increased hydrodynamic diameter of CuO in the presence of sEPS due to

particle coating by the sEPS macromolecules. The hydrodynamic diameter of Cu and Kocide

3000 was in the micron-range and their Polydispersity index was ~1, hence, aggregation

kinetics of those two particles was not studied.

sEPS slowed down dissolution of the three copper-based ENMs at pH 4, and also

complexed their released ions. The influence was strongest in CuO, which had the smallest

size in water (hydrodynamic diameter). Reduced dissolution resulted from steric exclusion

of water due to particle coating by the EPS biomacromolecules. Increased dissolution was

observed at pH 7 and 11 in the presence of sEPS and this was attributed to availability of

higher surface area for dissolution due to improved stability at higher pH. Also electrostatic

interactions between the particles and EPS were weaker compared to pH 4 so particle

coating may not have been as strong. Similar to stability studies, the effect of sEPS on

dissolution was more pronounce in CuO than in Cu and Kocide 3000. In general, lower

amounts of free cupric ion were found in the presence of EPS due to complexation. This

study thus showed that effect of sEPS can be limited by size of particles in water as well as concentrations of sEPS present.

In the third study the effects of sEPS isolated from (1) *Chlamydomonas reinhardtii*, a freshwater phytoplankton; and (2) *Dunaliella tertiolecta*, a marine phytoplankton, on surface charge and aggregation of three types of TiO_2 were investigated. A third sEPS treatment, in which the marine phytoplankton was grown in media spiked with high levels of nitrogen, was also studied. The three sEPS were negatively charged across the range of pH studied. Also, the sEPS had similar macromolecules as shown by Fourier transform infrared spectroscopy but the proportions of each macromolecule varied. For instance, carbohydrate:protein mass ratio ranged from 0.8 in *C. reinhardtii* to 6.1 in *D. tertiolecta*.

At higher concentrations of sEPS, the surface charge of TiO_2 increasingly became more like that of sEPS. In fact, sEPS (0.25 mg-C/L) reversed the surface charge of M212 and M262 TiO_2 from positive to negative at pH 7. A weaker interaction between UV100 and sEPS was observed and this was due to the negatively charged surface of the TiO_2 at pH 7, and possibly, its large hydrodynamic diameter compared to M212 and M262. Differences in the surface charge of the particles also affected the conformation of sEPS on their surfaces, as well as the overall effect of sEPS on their stability. In general the three sEPS increased the stability of the three TiO_2, measured by increased critical coagulation concentrations of particles at increasing amounts of sEPS.

In addition to electrostatic interactions, the occurrence of chemical bonding between the carboxylic group of sEPS and the surface hydroxyl groups of TiO_2 was confirmed by infrared spectroscopy. Interactions between sEPS and TiO_2 were mainly mediated carboxylic function groups in sEPS proteins and phosphate groups in phospholipids or nucleic acids.

The last study focused on direct effects of *C. reinhardtii* cells and their organic matter on the stability, dissolution, and transformation of modified iron nanoparticles, FeSSi. Similar to CuO and TiO_2, the organic materials from algae coated FeSSi and imparted steric stabilization. Direct attachment between algal cells and aggregates of TiO_2 (heteroaggregation) was observed using an environmental scanning electron microscope. Algae-FeSSi heteroaggregation, as well as coating of FeSSi by algal organic materials decreased the surface area available for dissolution and transformation of the ENMs.

The effect of FeSSi on algae, which is mainly via reactive oxygen species produced during iron dissolution, was suppressed in the presence of old *C. reinhardtii* cells and high content of organic matter. In fact, FeSSi stimulated the growth of cells (when compared to control conditions). However, a dose-response relationship was observed when young cells (which also had very low amounts of organic matter) were exposed to FeSSi.

6.2. Future Works

The primary goal of this research was to investigate how microorganisms and their extracellular polymers influence the fate and transformations of ENMs. This work has generated some other vital questions which may need to be answered by future studies for continuous development of tools necessary for carrying out realistic environmental risk assessment of ENMs. These questions include:

6.2.1. How does sEPS coating affect bioavailability and toxicity of ENMs?

Toxicity studies are often done using pristine ENMs over a few days, which generate important fundamental data. However, ENMs are often transformed in the natural environment via chemical reactions and/or interactions with other materials present in water. Chapter 4 of this dissertation showed that binding between sEPS and TiO_2 (and potentially

193

other ENMs) may occur via formation of chemical bonds, leading to strong, long-lasting attachments. As a result, the forms of ENMs that organisms may be exposed to in the long term may be these forms that are coated by different levels by sEPS. Since sEPS mostly have significant influence on the physicochemical properties (size and surface charge) and aggregation behavior of ENMs, the bioavailability and toxicity of sEPS-coated ENMs may be different from those of pristine ENMs. How bioavailability and toxicity of ENMs are changed by association with EPS is largely uninvestigated, and requires some attention.

6.2.2. Competitive interactions with ENMs between sEPS and other forms of NOM?

sEPS is only one type of dissolved NOM in natural waters. Other organic compounds from remains of plants and animals such as humic acid, fulvic acid, alginic acid, etc. and geological sources are also present in natural waters at reasonable amounts. The interactions of some of these other NOM with ENMs have been studied; and as shown in chapters 2–4, they may affect ENMs' fate in ways that are somewhat different from sEPS. Hence, the fate of ENMs in waters will be determined by the type of NOM that actually adsorb on it. It is therefore important to understand the relative affinities of these different types of NOM for the surfaces of ENMs in order to more accurately predict particles' environmental fate and toxicity.